Development of *in vitro* skeletal disease models using CRISPR/Cas9 genome editing in immortalised mesenchymal stem cells

Alice Elizabeth Carstairs

Doctor of Philosophy

University of York

Biology

March 2017

Abstract

The emergence of engineered nucleases for genome editing has allowed for greater understanding of human biology in health and disease, particularly through combination with stem cells and differentiation protocols. Mesenchymal stem cells (MSCs) are a multipotent adult stem cell able to differentiate into osteoblasts, chondrocytes and adipocytes. Early mesoderm differentiation pathways are relatively well understood, yet the understanding of how mesoderm transcription factors drive post-natal differentiation is less well studied. Additionally, the impact of skeletal disease on MSCs is often neglected in the furthering of our understanding of pathophysiology and disease phenotypes. To this end, this PhD project aimed to use an immortalised MSC cell line (hTERT MSCs) to develop a methodology suitable for the generation of genetically modified MSCs (GM-hTERT MSCs). Firstly, the effects of serum in *in vitro* cell culture was considered by reducing serum in hTERT MSC culture. This demonstrated in the absence of a nutrient-rich environment hTERT MSCs shift towards a lipid-based metabolism with a consequential increase in osteogenic capabilities. The initial targets of CRISPR/Cas9 were Runx2 and Sox9, two critical transcription factors in the onset of osteogenesis and chondrogenesis respectively. The methodology developed used a fluorescent sorting strategy to maximise the possibility of generating GM-hTERT MSCs and in this way, successful genome editing was demonstrated. Genome editing of Runx2 did not appear to absolve osteogenic potential in the hTERT MSCs and targeting of Sox9 via the CRISPR/Cas9 technology demonstrated an apparent increase in adipogenesis. To demonstrate the disease modelling capabilities of GM-hTERT MSCs, a human disease relevant mutation was created in the FGFR3 gene mimicking the genotype of CATSHL syndrome resulting in a striking phenotype, where cells showed a decreased differentiation ability but an increased proliferative and migratory capacity. These data were developed further through the use of a 3D spheroid model allowing for the study of differentiated MSCs, including GM hTERT-MSCs, in a more *in vivo* like setting. Together these results demonstrate the potential for expanding our understanding of MSC biology in physiologically relevant *in vitro* conditions.

Table of Contents

Abstract....2
Table of Contents....3
List of Figures....13
List of Tables....18
List of Accompanying Material....19
Acknowledgements....20
Declaration....21
Chapter 1 : Introduction....22
1.1 The study of human disease....22
1.2 Classical gene targeting technology – animal models for human disease....22
1.3 Limitations of current approaches in modelling diseases....23
1.4 Genome editing using engineered nucleases....24
1.4.1 Mechanisms shared by engineered nucleases....24
1.4.2 Zinc finger nucleases....26
1.4.3 Transcription activator-like effector nucleases (TALENs)....28
1.4.4 Clustered regularly interspaced short palindromic repeats (CRISPR)....30
1.5 Stem cells....33
1.5.1 Embryonic Stem Cells....33
1.5.2 Adult Stem Cells....34
1.5.3 Mesenchymal Stem Cells....35
1.5.3.1 MSC sources and isolation....36
1.5.3.2 MSC differentiation....37
1.5.3.3 MSCs as a cellular therapy....40

1.6 Isogenic human model systems – combining engineered nucleases and stem cells 41
1.7 Modelling skeletal disease 42
1.7.1 Skeletal dysplasias resultant from FGFR3 mutations 43
1.7.2 Osteogenesis Imperfecta 44
1.7.3 Fibrodysplasia ossificans progressive 44
1.8 Project Aims 45
Chapter 2 : Methods and Materials 46
2.1.1 Cell Culture 46
2.1.1.1 hTERT MSCs 46
2.1.1.2 Human Embryonic Kidney 293FT cells 46
2.1.1.3 Cell Passage 46
2.1.1.4 Cryopreservation 46
2.1.1.5 Colony forming unit assay 47
2.1.2 Quantitative Real-Time PCR 47
2.1.2.1 Trizol Extraction 47
2.1.2.2 DNAse Treatment of Samples 47
2.1.2.3 cDNA Synthesis 48
2.1.3 Differentiation Assays 48
2.1.3.1 Adipogenic Differentiation 48
2.1.3.2 Oil Red O Staining 48
2.1.3.3 Osteogenic Differentiation 48
2.1.3.4 Alizarin Red Staining 49
2.1.3.5 Alkaline Phosphatase and Von Kossa Staining 49
2.1.3.6 p-Nitrophenyl Phosphate Phosphatase Assay 49
2.1.4 RNA-seq analysis 49
2.1.4.1 RNA isolation, cDNA library preparation and sequencing 49
2.1.4.2 Read mapping 50

2.1.4.3 Quantitation and differential expression analysis 50
2.1.4.4 Pathway analysis 50
Chapter 3 : Reduction of serum in mesenchymal stem cell *in vitro* culture conditions for a controlled proliferation and differentiation environment 52
3.1 Introduction 52
3.2 Aims 54
3.3 Methods and Materials 55
3.3.1 Reduction of serum from MSC maintenance media 55
3.3.2 Population Doublings 55
3.3.3 Analysis of hTERT MSC differentiation 55
3.3.4 Raybiotech Antibody Array 55
3.3.4.1 hTERT Survival Assay 56
3.3.4.2 Supernatant collection and protein preparation 56
3.3.4.3 Array hybridisation 56
3.3.4.4 Interpretation of results 56
3.3.5 Free fatty acid uptake 57
3.3.6 RNA-seq analysis 57
3.4 Results 58
3.4.1 Reduction of serum in Y101 and Y201 hTERT MSCs results in altered morphology and reduced growth rates 58
3.4.2 Y101.5 and Y201.5 cells have a reduced propensity for adipogenic differentiation 61
3.4.3 Y101.5 and Y201.5 hTERT MSCs have an increased osteogenic potential 64
3.4.4 Mechanistic analyses of increased osteogenic potential in reduced serum hTERT MSCs 69
3.4.5 Transcriptome analysis shows Y101.5 hTERT MSCs to have increased lipogenic metabolism and alterations in secretome 71
3.4.6 Y101.5 hTERT MSCs secrete pro-osteogenic factors that aid osteogenesis 77
3.5 Discussion 90

3.5.1 Reduced serum hTERT MSCs increase osteogenic capacity at the expense of adipogenic differentiation potential....90
3.5.2 RNA-seq analysis indicates hTERT MSCs alter metabolism as a response to low serum culture 91
3.5.3 Transcripts upregulated in reduced serum hTERT MSCs are predominantly expressed extracellularly 91
3.5.4 Concluding Remarks....92
Chapter 4 : Establishing the CRISPR/Cas9 system in hTERT MSCs by targeting master differentiation transcription regulators 93
4.1 Introduction 93
4.1.1 Runx2 94
4.1.2 Sox9....94
4.1.3 hTERT MSC CRISPR/Cas9 transfection and fluorescent sorting strategy....95
4.2 Aims....97
4.3 Methods and Materials....98
4.3.1 Generating Knockout Cell Lines 98
4.3.1.1 Single Guide RNA and Single Stranded Oligonucleotide Design 98
4.3.1.2 CRISPR Cloning 98
4.3.1.3 Transformation of DH5α chemically competent E. coli 99
4.3.1.4 Construct Evaluation and DNA extraction 99
4.3.1.5 Lipid Transfection....99
4.3.1.6 Neon Electroporation....101
4.3.1.7 Fluorescent Activated Cell Sorting (FACS)....101
4.3.1.8 Clonal Selection....101
4.3.1.9 Genomic DNA Isolation 102
4.3.1.10 Transgenomic SURVEYOR Mutation Detection Assay....102
4.3.1.11 Sequencing....102
4.3.2 qPCR Primers....103

4.3.3 Analysis of GM-hTERT osteogenic and adipogenic differentiation.....103
4.4 Results.....104
4.4.1 sgRNA template construction.....104
4.4.2 Detectable eGFP fluorescence is produced upon transfecting HEK293FT cells with CRISPR/Cas9.....108
4.4.3 Optimising CRISPR/Cas9 delivery into hTERT MSCs – comparison of lipid transfection and electroporation.....110
4.4.3.1 Delivering CRISPR/Cas9 into hTERT MSCs by lipid transfection results in poor transfection efficiency.....110
4.4.3.2 Electroporation of hTERT MSCs with CRISPR/Cas9 results in viable fluorescent cells 114
4.4.4 Mixed populations of CRISPR/Cas9 mutations can be identified by sequencing but not by SURVEYOR assay.....118
4.4.5 Isolation of clonal lines by serial dilution results in individual mutations in relevant gene targeted by CRISPR/Cas9.....129
4.4.6 Genotypic analysis of clonal GM Runx2 hTERT MSC lines.....129
4.4.7 Genetic modification of Runx2 impacts colony forming capabilities of hTERT MSCs but does not appear to affect morphology or viability.....133
4.4.8 Runx2-GM hTERT MSCs retain osteogenic differentiation and show increased capacity for adipogenic differentiation.....136
4.4.9 Analysis of GM Sox9 hTERT MSCs indicated reduced adipogenic capacity.....141
4.5 Discussion.....93
4.5.1 Generation and identification of genetically modified hTERT MSCs.....148
4.5.2 Osteogenesis does not appear to be disrupted in hTERT MSCs where Runx2 was targeted with CRISPR/Cas9.....149
4.5.3 Phenotypic analysis of Runx2-GM hTERT MSCs demonstrates increase in adipogenesis and increase in viable cell numbers.....149
4.5.4 Early analysis of Sox9-MP hTERT MSCs indicates genetic modification results in negative impacts to proliferation and adipogenesis.....150

4.5.5 Concluding Remarks....151
Chapter 5 : The role of FGFR3 in post-natal developmental MSC biology....152
5.1 Introduction....152
5.2 Aims....157
5.3 Methods and Materials....158
5.3.1 Generating FGFR3 cell line with CRISPR/Cas9....158
5.3.2 CRISPR/Cas9 On-target and Off-target Sequencing....158
5.3.3 Western Blot Analysis of FGFR3....159
5.3.3.1 Total Protein Isolation and Quantification....159
5.3.3.2 Gel electrophoresis and Western Blotting....159
5.3.4 qPCR Primers for FGFR3 Expression....160
5.3.5 In vitro differentiation....160
5.3.5.1 Osteogenic and adipogenic differentiation....160
5.3.5.2 Chondrogenic differentiation....160
5.3.6 *In vitro* scratch-wound assays....161
5.3.7 Transcriptome profiling by RNA-seq analysis....161
5.3.8 Ptychography and Cell Migration Analysis....161
5.3.9 Phalloidin staining of actin cytoskeleton....162
5.4 Results....163
5.4.1 FGFR3 sgRNA design and introduction of FGFR3 CRISPR/Cas9 into Y201 hTERT MSCs 163
5.4.2 FGFR3-KO hTERT MSCs are viable in long term culture and survive clonogenic assays 174
5.4.2.1 Vi-cell counter demonstrates viability of FGFR3-KO hTERT MSCs is comparable to wild type Y201 hTERT MSCs....174
5.4.3 FGFR3-KO hTERT MSCs produce comparable levels of colonies that cover a greater surface area than wild type counterparts....177
5.4.4 FGFR3-KO hTERT MSCs have increased proliferative capacity....179

5.4.5 FGFR3-KO hTERT MSCs have a significantly decreased differentiation capacity....182

5.4.6 Transcriptome analysis of FGFR3-KO hTERT MSCs by RNA sequencing 189

5.4.6.1 No FGFR3 transcripts detected by RNA-seq 189

5.4.6.2 Overview of transcripts in WT and FGFR3-KO hTERT MSCs shows most differentially regulated are protein-coding transcripts.....189

5.4.6.3 No significant alterations to FGF and FGFR expression caused by knocking out FGFR3 in hTERT MSCs 192

5.4.6.4 MAPK and PI3K pathways dysregulated in FGFR3-KO hTERT MSCs 209

5.4.6.5 Snail1, a transcriptional effector, of FGFR3 is downregulated in FGFR3-KO hTERT MSCs 212

5.4.6.6 Hedgehog signalling also appears to be differentially regulated as a result of knocking out FGFR3 212

5.4.6.7 Cell adhesion and extracellular matrix interactions downregulated consistently by pathway analysis.....214

5.4.6.8 Pathway analysis indicates regulation of actin cytoskeleton altered in FGFR3-KO hTERT MSCs 217

5.4.6.9 Genes relating to cancer and carcinogenesis upregulated in FGFR3-KO hTERT MSCs 222

5.4.7 Alterations in actin cytoskeleton morphologies as a result of FGFR3-KO 224

5.4.8 FGFR3-KO hTERT MSCs demonstrate increased scratch wound healing capacity in *in vitro* assays possibly due to alterations in population migration.....227

5.4.8.1 FGFR3-KO hTERT MSCs have an increased scratch wound healing capacity in in vitro scratch assays.....227

5.4.8.2 Ptychographic analysis indicates FGFR3-KO hTERT MSCs possess increased migratory capacity due to changes in collective migration but not changes at a single cell level 229

5.5 Discussion.....234

5.5.1 Confirmation of FGFR3 knock out status as a result of CRISPR/Cas9 genome editing 234

5.5.2 Mixed population of FGFR3 CRISPR/Cas9 hTERT MSCs display similar phenotype to FGFR3-KO hTERT MSCs 234
5.5.3 Removal of FGFR3 results in an increased proliferative capacity 235
5.5.4 FGFR3-KO hTERT MSCs demonstrate reduced capacity for differentiation 235
5.5.5 RNA-seq analysis determines removal of FGFR3 does not result in compensation in either FGFRs or FGFs 236
5.5.6 Removal of FGFR3 signalling appears to impact FGFR3 signalling networks determined by RNA-seq analysis 236
5.5.7 Removal of FGFR3 results in downregulation of transcripts related to cell-cell adhesion and ECM interactions 238
5.5.8 FGFR3-KO hTERT MSCs demonstrate increased *in vitro* scratch wound healing and disruption of collective cell migration 238
5.5.9 Cytoskeletal morphology impacted as a result of knocking out FGFR3 in hTERT MSCs 239
5.5.10 Concluding Remarks 239
Chapter 6 : Analysis of three dimensional *in vitro* spheroid models using hTERT MSCs and CRISPR/Cas9 knock out hTERT MSCs 242
6.1 Introduction 242
6.2 Aims 244
6.3 Methods 245
6.3.1 Cell Culture Methods 245
6.3.1.1 Pre-differentiation prior to spheroid formation 245
6.3.1.2 Pre-differentiation method development 245
6.3.1.3 Osteochondral differentiation media 245
6.3.2 Formation of 3D osteochondral interface spheroid models 246
6.3.2.1 Basal spheroid formation and culture 246
6.3.2.2 Osteochondral spheroid formation and culture 246
6.3.2.3 Osteogenic + chondrogenic spheroid formation and culture 246

6.3.2.4 Osteogenic spheroid + chondrogenic suspension 3D model formation and culture 246

6.3.2.5 CellTracker Labelling 247

6.3.2.6 Cryosectioning.....247

6.3.3 Spheroid Imaging and Analysis Methods.....247

6.3.3.1 Imaging spheroids with a multiphoton confocal microscope.....247

6.3.3.2 Imaging spheroids with a lightsheet microscope 247

6.3.3.3 Determination of size parameters using ImageJ 248

6.3.3.4 Quantification of Cell tracker labelling in osteogenic and chondrogenic regions of osteochondral sections.....248

6.4 Results.....249

6.4.1 Generation of 3D osteochondral spheroids from pre-differentiated hTERT MSCs 249

6.4.1.1 hTERT MSCs cannot reproducibly form osteogenic/chondrogenic spheroids using previously developed protocols 249

6.4.1.2 Reducing pre-differentiation allows single spheroid formation.....253

6.4.1.3 Confirming specific differentiation in 2D.....255

6.4.1.4 Y101 hTERT MSCs predifferentiated for 4 days reliably form osteochondral spheroids and demonstrate self-organisation 259

6.4.2 Osteogenic and chondrogenic spheroids combine in culture to form osteochondral interface 264

6.4.3 Combining an osteogenic spheroid and chondrogenic suspension formed from pre-differentiated Y201 hTERT MSCs results in lateral self-organisation 271

6.4.4 Combining CRISPR/Cas9 with 3D spheroid models – analysis of FGFR3-KO hTERT MSC spheroids 275

6.4.4.1 FGFR3-KO hTERT MSCs form basal spheroids with similar behaviours to WT hTERT MSCs but are also able to form both osteogenic and chondrogenic spheroids.....275

6.4.4.2 Osteogenic spheroid + chondrogenic suspension 3D model with FGFR3-KO hTERT MSCs results in apparent self-organisation but formation appears different to WT hTERT MSCs 279

6.5 Discussion....284
6.5.1 Length of pre-differentiation of hTERT MSCs impacts spheroid formation....284
6.5.2 hTERT MSC spheroids can be used for analysis of osteochondral interface without a scaffold or matrix....284
6.5.3 Applying the differential adhesion hypothesis to hTERT MSC spheroids....285
6.5.4 Time lapse imaging of spheroid formation can provide key insights into cellular phenotypes....285
6.5.5 Concluding Remarks....286
Chapter 7 : Discussion....287
7.1.1 The use of genome edited MSCS for skeletal disease modelling....287
7.1.2 Proof of concept – using CRISPR/Cas9 to knock out master transcription regulators in hTERT MSCs....288
7.1.3 Creating an *in vitro* skeletal disease model with hTERT MSCs and CRISPR/Cas9....288
7.1.4 FGFR3 has a potential role in MSC migration....289
7.1.5 The impact of removing FGFR3 on FGF signalling....290
7.1.6 FGFR3-KO hTERT MSC phenotype resembles a cancerous cell....290
7.1.7 Skeletal disease modelling in 3D *in vitro* spheroid models....291
7.1.8 Limitations of *in vitro* modelling with regards to serum....291
7.2 Future Directions....292
7.3 Concluding Remarks....293
Appendix: Analysis of a mixed population of FGFR3 targeted GM-hTERT MSCs....294
Mixed population of FGFR3 CRISPR/Cas9 hTERT MSCs display behaviours similar to FGFR3-KO hTERT MSCs....294
List of Abbreviations....287
References....302

List of Figures

Figure 1.4.1: Repair of DSBs to introduce mutations via engineered nucleases 25
Figure 1.4.2: Overview of zinc finger genome editing technology 27
Figure 1.4.3: Summary of TALEN technology.....29
Figure 1.4.4: Summary of CRISPR/Cas9 genome editing technology. 32
Figure 1.5.1: Overview of MSC differentiation capacity 39
Figure 3.4.1: Analysis of cell shape and diameter of low serum hTERT MSCs.....59
Figure 3.4.2: Viability and growth analysis of low serum hTERT MSCs and WT hTERT MSCs 60
Figure 3.4.3: Low serum hTERT MSCs have decreased adipogenic potential 62
Figure 3.4.4: Black/white pixel analysis gives further evidence for reduced adipogenisis in weaned hTERT MSCs.....63
Figure 3.4.5: Alizarin Red staining of hTERT MSCs show low serum hTERT MSCs have increased osteogenic potential 65
Figure 3.4.6: CPC elution of Alizarin Red staining for osteogenic induced hTERT MSCs over a timecourse 67
Figure 3.4.7: Alkaline phosphatase and von Kossa histological staining of weaned hTERT MSCs compared to WT hTERT MSCs. 68
Figure 3.4.8: Reduction of serum alone is not suffcient to increase ALP activty comparative to activity in weaned hTERT MSCs 70
Figure 3.4.9: Summary of transcripts differentially regulated in Y101.5 hTERT MSCs compared to Y101 hTERT MSCs.....73
Figure 3.4.10: Gene ontology analysis of downregulated Y101.5 hTERT MSCs by biological process 74
Figure 3.4.11: Gene ontology analysis of upregulated Y101.5 hTERT MSCs by biological process ..75
Figure 3.4.12: Top 10 upregulated reactome pathways as determined by Enrichr in the Y101.5 hTERT MSCs.....76
Figure 3.4.13: Analysis of fatty acid uptake in Y101 and Y101.5 hTERT MSCs after serum starvation 76

Figure 3.4.14: Cellular component analysis of all significantly differentially regulated transcripts identified by RNA-seq 77
Figure 3.4.15: Sytox blue staining of Y201 and Y201.5 hTERT MSCs in standard culture conditions and serum-free culture conditions 79
Figure 3.4.16: Significantly upregulated or downregulated proteins in Y201.5 hTERT MSCs compared to Y201 hTERT MSCs identified by antibody array.....80
Figure 3.4.17: Significantly upregulated or downregulated secreted proteins in Y201.5 hTERT MSCs compared to Y201 hTERT MSCs identified by antibody array 81
Figure 3.4.18: Significantly upregulated or downregulated secreted proteins in Y201.5 hTERT MSCs compared to Y201 hTERT MSCs identified by antibody array organised by cellular component 82
Figure 3.4.19: Y101.5 conditioned media stimulates increased early osteogenesis in Y101 hTERT MSCs.....89
Figure 4.1.1: Overview of fluorescent strategy to maximise possibility of generating GM hTERT MSCs.....96
Figure 4.3.1: Overview of CRISPR cloning methodology. 101
Figure 4.4.1: Confirming the insertion of the sgRNA into the pSpCas9(BB)-2A-GFP plasmid. 107
Figure 4.4.2: Lipid transfection of HEK293FT cells.....109
Figure 4.4.3: Lipid-based Transfection of MSCs.....111
Figure 4.4.4: Lipid-based transfection of hTERT MSCs with CRISPR/Cas9 results in very few isolatable cells by FACS.....113
Figure 4.4.5: FACs analysis of Y201 hTERT MSCs electroporated with Sox9 CRISPR/Cas9. 117
Figure 4.4.6: SURVEYOR mutation detection assay of heterogeneous Y201 hTERT Sox9 CRISPR/Cas9 MSCs.....120
Figure 4.4.7: Sequence traces of mixed population of CRISPR/Cas9 electroporated Y201 hTERT MSCs show mixed trace after PAM. 121
Figure 4.4.8: Confirmation of successful sgRNA sequence cloning into CRISPR/Cas9 vectors by Sanger sequencing. 122
Figure 4.4.9: On-target Sanger sequencing of PCR amplified Sox9-MP 1 hTERT MSC 127
Figure 4.4.10: On-target Sanger sequencing of PCR amplified Sox9-MP 2 hTERT MSC 128
Figure 4.4.11: Sequence trace of clonal Runx2 GM hTERT MSC line Runx2 A6F4.....131
Figure 4.4.12: Sequence trace of clonal Runx2 GM hTERT MSC line Runx2 A6H2 132
Figure 4.4.13: Qualitative morphological analysis of Runx2-GM Y201 hTERT MSCs by microscopy 134

Figure 4.4.14: Analysis of clonogenic and proliferation capabilities of Runx2-GM hTERT MSCs ...136
Figure 4.4.15: Osteogenic differentiation comparison of Runx2-GM hTERT MSCs and WT hTERT MSCs.....139
Figure 4.4.16: Adipogenic differentiation comparison of Runx2-GM hTERT MSCs and WT hTERT MSCs.....140
Figure 4.4.17: Vi-Cell analysis of Sox9-MP hTERT MSCs for viability and diameter 143
Figure 4.4.18: Clonogenic assay of Sox9-MP hTERT MSCs comparing colony forming ability to WT Y201 hTERT MSCs.....144
Figure 4.4.19: MTT assay assessing viable numbers of Sox9-MP hTERT MSCs 145
Figure 4.4.20: Adipogenic timecourse comparing differentiation capacity of Sox9-MP hTERT MSCs to WT hTERT MSCs.....147
Figure 5.1.1: Overview schematic of FGF signalling.....153
Figure 5.1.2: Schematic of transcriptional regulator, Snail1, in FGFR3 signalling 156
Figure 5.4.1: Confirming the insertion of the FGFR3 sgRNA sequence into the pSpCas9(BB)-2A-GFP plasmid.....164
Figure 5.4.2: FACS analysis of Y201 hTERT MSCs electroporated with FGFR3 sgRNA and ssODN .169
Figure 5.4.3: FGFR3 CRISPR/Cas9 resulted in FGFR3-KO hTERT MSC line with single A insertion .170
Figure 5.4.4: The predicted protein sequence for the FGFR3-KO hTERT MSC line indicates a truncated protein with no transmembrane domain 171
Figure 5.4.5: Analysis of FGFR3 protein expression in FGFR3-KO hTERT MSCs and development of FGFR3 transcript expression in HeLa cells. 172
Figure 5.4.6: FGF9 supplementation appears to result in varied pERK response from WT and FGFR3-KO hTERT MSCs.....173
Figure 5.4.7: Analysis of effect of removing FGFR3 using CRISPR/Cas9 on hTERT MSC viability ...175
Figure 5.4.8: Analysis of hTERT MSC morphology by phase imaging and crystal violet staining with diameter calculated by Vi-CELL.....177
Figure 5.4.9: Analysis of the clonogenic ability of FGFR3-KO hTERT MSCs and the resultant colonies formed.....178
Figure 5.4.10: EdU incorporated by WT hTERT MSCs and FGFR3-KO hTERT MSCs over 72 hours.180
Figure 5.4.11: Colorimetric MTT assay to assess numbers of viable hTERT MSCs after 48 and 96 hours in culture.....181
Figure 5.4.12: A timecourse of adipogenic stimulation of WT hTERT MSCs and FGFR3-KO hTERT MSCs.....183

Figure 5.4.13: A timecourse of osteogenic stimulation of WT hTERT MSCs and FGFR3-KO hTERT MSCs.....185
Figure 5.4.14: Alkaline phosphatase activity normalised to DNA content of WT hTERT MSCs and FGFR3-KO hTERT MSCs during early osteogenesis 186
Figure 5.4.15: qPCR analysis of chondrogenic markers at various intervals during chondrogenic differentation of WT and FGFR3-KO hTERT MSCs. 188
Figure 5.4.16: Summary of transcripts differentially regulated in FGFR3-KO hTERT MSCs compared to WT hTERT MSCs.....191
Figure 5.4.17: Overview of significantly differentially regulated transcripts in PI3K-Akt signalling pathway 210
Figure 5.4.18: Overview of significantly differentially regulated transcripts in MAPK signalling pathway 211
Figure 5.4.19: Significantly upregulated or downregulated transcripts in FGFR3-KO hTERT MSCs compared to WT hTERT MSCs identified by RNA-seq 213
Figure 5.4.20: Top 10 downregulated molecular functions in FGFR3-KO hTERT MSCs.....215
Figure 5.4.21: Top 10 cellular components where downregulated transcripts are found in FGFR3-KO hTERT MSCs.....216
Figure 5.4.22: Top 10 KEGG pathways downregulated in FGFR3-KO hTERT MSCs 218
Figure 5.4.23: Overview of significantly differentially regulated transcripts in focal adhesion linked pathways.....219
Figure 5.4.24: GSEA enrichment plots of focal adhesion and the regulation of the actin cytoskeleton 220
Figure 5.4.25: Overview of significantly differentially regulated transcripts in fthe regulation of the actin cytoskeleton.....221
Figure 5.4.26: Staining of hTERT MSCs for the filamentous actin cytoskeleton.....225
Figure 5.4.27: Morphological analysis of WT and FGFR3-KO hTERT MSCs.....226
Figure 5.4.28: Analysis of wound healing capacity of WT and FGFR3-KO hTERT MSCs by scratch assay 228
Figure 5.4.29: First and final frames of a hTERT MSC migration timelapse imaged using ptychography 230
Figure 5.4.30: Quantification of single cell migratory metrics from ptychographic timelapses 232
Figure 5.4.31: Evidence of collective migration in WT hTERT MSCs.....233
Figure 6.4.1: Overview of methodology used to create osteochondral spheroids 250

Figure 6.4.2: Z-stack images of osteochondral and basal spheroids formed after 7 days pre-differentiaton 252
Figure 6.4.3: Brightfield images of spheroids formed from hTERT MSCs differentiated for either 4 or 5 days prior to spheroid formation 254
Figure 6.4.4: Schematic summary of 2D differentiation timecourse. 256
Figure 6.4.5: Histological staining of partially differentiated Y101 hTERT-MSCs. 258
Figure 6.4.6: Fluorescent microscopy of osteochondral spheroids. 260
Figure 6.4.7: Shape analysis of Y101 osteochondral spheroids 261
Figure 6.4.8: Fluorescent microscopy of sectioned Y101 hTERT MSC osteochondral spheroids. 263
Figure 6.4.9: Section analysis of osteochondral spheroids of osteogenic and chondrogenic regions 263
Figure 6.4.10: Overview of methodology used to create osteogenic + chondrogenic spheroids 265
Figure 6.4.11: Fluorescent microscopy of osteogenic + chondrogenic spheroids. 266
Figure 6.4.12: Shape analysis of Y101 osteogenic + chondrogenic spheroids 268
Figure 6.4.13: Fluorescent microscopy of sectioned Y101 hTERT MSC osteogenic + chondrogenic spheroids. 269
Figure 6.4.14: Fluorescent microscopy using both a multiphoton and a lightsheet microscpe to image Y101 hTERT MSC osteogenic + chondrogenic spheroids. 270
Figure 6.4.15: Schematic overview of osteogenic spheroid + chondrogenic suspension model 272
Figure 6.4.16: Fluorescent microscopy of osteogenic spheroids + chondrogenic suspension 273
Figure 6.4.17: Fluorescent microscopy of sectioned Y201 hTERT MSC osteogenic spheroid + chondrogenic suspension model. 274
Figure 6.4.18: Comparison of basal spheroids formed from FGFR3-KO hTERT MSCs or WT hTERT MSCs 276
Figure 6.4.19: Size analysis of FGFR3-KO basal spheroids compared to WT hTERT MSC basal spheroids 277
Figure 6.4.20: Brightfield images of osteogenic and chondrogenic spheroids formed from FGFR3-KO hTERT MSCs 278
Figure 6.4.21: Timecourse of FGFR3-KO hTERT MSC osteogenic spheroid + chondrogenic suspension 280
Figure 6.4.22: Shape analysis of WT and FGFR3-KO hTERT MSC osteogenic spheroid + chondrogenic suspension models 281
Figure 6.4.23: Still frames from timelapse imaging of WT and FGFR3-KO hTERT MSC osteogenic spheroid + chondrogenic suspension models 283

List of Tables

Table 3.4.1: Significantly upregulated secreted proteins in Y201.5 hTERT MSCs compared to Y201 hTERT MSCs organised by KEGG 2016 pathways.....84
Table 3.4.2: Significantly downregulated secreted proteins in Y201.5 hTERT MSCs compared to Y201 hTERT MSCs organised by KEGG 2016 pathways.....86
Table 4.4.1: List of potential off-target effects identified for Sox9 sgRNA.....105
Table 4.4.2: List of potential off-target effects identified for Runx2 sgRNA.....106
Table 4.4.3: Electroporation efficiencies of hTERT MSCs using various electroporation parameters 115
Table 4.4.4: Off-target effects for Sox9-MP 1 sgRNA 123
Table 4.4.5: List of potential off-target effects for the Sox9 2 sgRNA 125
Table 5.3.1: Primers used in on-target and off-target sequencing.....159
Table 5.3.2: qPCR primers to analyse FGFR3 expression.....160
Table 5.3.3: qPCR primers to analyse chondrogenic marker expression.....161
Table 5.4.1: Overview of FGFR3 splice variant expression in WT and FGFR3-KO hTERT MSCs.....190
Table 5.4.2: FGFR transcript expression does not appear to be significiantly affected by knocking out FGFR3.....193
Table 5.4.3: Fibroblast growth factor ligands detected by RNA-seq, no significant difference in transcript levels between FGFR3-KO hTERT 201
Table 5.4.4: List of matrix metalloproteinases significantly differentially regulated in FGFR3-KO hTERT MSCs.....223
Table 5.5.1: Summary of phenotypic differences between WT and FGFR3-KO hTERT MSCS. 240

List of Accompanying Material

Supplementary Video 1: Timecourse of WT hTERT MSC migration

Supplementary Video 2: Timecourse of FGFR3-KO hTERT MSC migration

Supplementary Video 3: Overview of hTERT MSC migration analysed by ptychography

Supplementary Video 4: Analysis of WT hTERT MSC chondrogenic suspension interacting with osteogenic spheroid #1

Supplementary Video 5: Analysis of WT hTERT MSC chondrogenic suspension interacting with osteogenic spheroid #2

Supplementary Video 6: Analysis of WT hTERT MSC chondrogenic suspension interacting with osteogenic spheroid #3

Supplementary Video 7: Analysis of FGFR3-KO hTERT MSC chondrogenic suspension interacting with osteogenic spheroid #1

Supplementary Video 8: Analysis of FGFR3-KO hTERT MSC chondrogenic suspension interacting with osteogenic spheroid #2

Supplementary Video 9: Analysis of FGFR3-KO hTERT MSC chondrogenic suspension interacting with osteogenic spheroid #3

Acknowledgements

My PhD was funded by the National Centre for the Replacement, Refinement and Reduction of Animals in Research (NC/K001671/1), for which I am extremely grateful. First and foremost, I would like to thank my supervisor Paul Genever, for his guidance, supervision and assistance with this project. Throughout this PhD, Paul continued to believe in me and my ability to be the "CRISPR queen" even when I had doubts and for that I am extremely grateful. I would also like to thank my TAP panel, Harv Isaacs and Gonz Blanco, for their support and suggestions throughout their project. Thank you also to Ian Hitchcock, for his advice and expertise with the Neon electroporation. I am indebted to the imaging team for their continual assistance throughout my PhD, and whom I must have driven crazy with my constant queries as to what could be achieved with their equipment! Karen Hogg, Karen Hodgkinson and Graeme Park demonstrated extreme patience and I am so thankful for their assistance in establishing the fluorescent cell sorting strategy. I am also extremely grateful to Jo Marrison and her constant enthusiasm for my latest idea with the multi-photon microscope! I would also like to thank all the members of the Genever group and the J0 CBL corridor who provided not only a collaborative environment for a PhD student but an incredibly friendly and supportive environment as well. I doubt there is one person in the group who has not aided me in this PhD and so I am thankful to you all. I would particularly like to thank Becky Pennock and James Fox, both of whom kept me grounded and calm throughout my PhD, which I imagine was not always an easy task! To Amanda, Charlotte, Hayley, Katie, Julia, David, Kim, Paul S and Sam, your friendship has meant the world to me – thank you to all of you for your companionship over the last few years. I must also extend special thanks to Sally James, who has acted as my mentor since the final year of my undergraduate degree, my graduation to minion status never fails to make me laugh! Thank you Sally, for the advice, support and just general chitchat, it was always worth the walk up the stairs to come and visit you. Thank you also to my Mum and Dad for their continual love and support throughout my PhD, and thank you to my sister, Emily, who always kept me laughing throughout everything. Even whilst thesis writing, which is no mean feat! Thank you to Sara, for more than I could ever express in words, I hope you never doubt how much your friendship means to me. Finally, I must thank my partner through it all, Paul Jennings, without whom I'm not sure whether this thesis could have been completed. Paul, your love and support always astounds me, thank you for putting up with throughout it all!

Declaration

I declare that this thesis is a presentation of original work and I am the sole author. The work presented in this thesis was performed by the author between October 2013 and September 2016 in the laboratory of Professor Paul Genever, in the Biology Department of the University of York. All experiments were performed by the author with the exception of the FGFR3 CRISPR cloning and subsequent expression which was performed by Sophie Quick under the supervision of the author. Additionally, the EdU staining of the FGFR3-MP hTERT MSCs and subsequent analysis was also performed by Sophie Quick. All FACS sorts were performed by the staff of the Imaging and Cytometry team within the Technology Facility at the University of York. Library construction for RNA sequencing was performed by Dr. Sally James and the RNA sequencing run was performed by staff from the Genomics team at the University of Leeds. Subsequent analysis of the RNA sequencing was performed by Dr. Sandy MacDonald, Dr. Katherine Newling and the author. This work has not previously been presented for an award at this, or any other, University. All sources are acknowledged as References.

Chapter 1 : Introduction

1.1 The study of human disease

A comprehensive overview of genetics is crucial to understanding the biological processes behind human disease and how the disease in question might be prevented and/or treated. Genetically modified (GM) animal models provide us with the ability to understand gene function, and ultimately identify mutations that alter gene function resulting in human disease. For this reason, the number of animals used in scientific research is ever increasing, primarily due to the rising requirement for GM animals, which require extensive breeding programmes to introduce desired mutations (Hall et al., 2009; Home Office, 2016). Furthermore, for the first time in 2012, the number of procedures involving genetically modified (GM) animals was greater than the number performed on genetically normal (wild type) animals indicating the need for animals of this status (Home Office, 2013). However, there are a number of issues with the use of animal models in this way. The development of alternative models is critical to understand how findings in animals correlate to mechanisms in humans, to minimise the use of animals wherever possible, and to ultimately conduct biomedical research in a human setting.

1.2 Classical gene targeting technology – animal models for human disease

The ability to generate mutated genes within a mouse model was first demonstrated in the 1980s through homologous recombination, a major cellular pathway that uses an undamaged homologous sequence as a template to repair a double stranded break (DSB) in DNA (Renkawitz et al., 2014). Identifying a gene function, and its importance, is often the subject of experiments performed in this way as simply recognising amino acid motifs or comparing the gene to family members is not typically enough to characterise gene function (Iredale, 1999). By introducing a drug resistance gene into a critical region of the gene of interest, it is possible to disrupt expression creating a knockout mouse. The importance of understanding gene function has led to a drive in the scientific community to produce a knockout mouse for each of the ~25,000 genes within the animal (Austin et al., 2004).

There are a number of genes however, where the severity of the phenotype caused by the loss of function of the gene results in an embryonic lethal mutation. To compensate for this, techniques have been put in place that allow for a tissue-specific or inducible knockout, using the Cre/Lox system (Sauer, 1998). This system rapidly became a major technology routinely used for the specific modification of gene expression. It relies on the use of a Cre recombinase, originally derived from a P1 bacteriophage, which interacts with a 34 base pair Lox sequence (Abremski and Hoess, 1984). Upon recognition of a pair of directly repeating Lox sites, Cre is able to excise the sequence in between, which *in vivo* is combined with various promoters to control Cre expression in a temporal and spatial manner (Sauer, 1998). Before the development of this technology, it was approximated that 15% of knockout mice develop a phenotype which resulted in lethality but creating mouse models of disease using the Cre/Lox system overcame these difficulties allowing for meaningful analysis of these mutations (Hall et al., 2009).

1.3 Limitations of current approaches in modelling diseases

An enormous wealth of information regarding human disease and gene function has been gleamed using the laboratory mouse; however animal models are not without fault. Arguably the most notable issue is mice do not always faithfully replicate human physiology and disease. In fact in an EU meeting regarding the usage of mice as models it was commented several times that "'the best model for human disease research is the human" (European Commission Workshop, 2010). Mammalian genotypes are highly conserved throughout evolution, allowing for the modelling of human diseases in animal models. Yet, phenotypically there are a number of differences between humans and animal models used in this fashion.

Perhaps the most notable difference between mice and humans is size. As the two species diverged it is likely that environmental pressures selected for the size of organisms. A number of traits are therefore dependent on the size of an organism, one of which is the metabolic rate of an organism (Perlman, 2016). Metabolic rate is directly correlated to size and so the mouse has a specific metabolic rate roughly 7 times higher than that of a human (Jungers, 1986). This means that on a cellular level, the processes occurring in a mouse are different than a human's due to this increased metabolic rate. The mitochondrial density is higher in a mouse as is the production of reactive oxygen species and in addition, the fatty acid composition of the cell membrane differs to that seen in a human (Hulbert, 2008). This demonstrates just one of the phenotypic differences between mice and humans, which leads to differing cell, tissue and organ behaviours between the two species.

Further to the differences in phenotype, the use of the Cre/Lox system requires an extensive number of mice for breeding purposes in order to achieve the desired genotype, and the possibility

of making point mutations is also not possible using the previously described technologies. Some of these described limitations could be overcome with the use of a rapidly developing technology: engineered nucleases.

1.4 Genome editing using engineered nucleases

Genome editing has become a widely used technique over the past decade with the development of engineered nucleases. The ability to manipulate a genome to possess a desired mutation presents enormous opportunities to determine both gene function and the effects of mutations on said gene in health and disease, including point mutations that were previously not able to be easily studied with *in vivo* methods. The development of cell lines with given mutations to mimic those seen in disease allows for the development of therapeutics in a human background and removes the need for animal studies in this instance. There are three main engineered nucleases which have become prevalent in genome editing studies, and these will be reviewed and the advantages and disadvantages of each technique discussed. Other technologies, such as meganucleases and chemical DNA cutters, will not be covered here.

1.4.1 Mechanisms shared by engineered nucleases

The broad concept of genome editing with engineered nucleases relies on the creation of a DSB, as this was noticed to induce homologous recombination at an increased rate in mouse stem cells (Rouet et al., 1994). The endogenous repair machinery present in the cell recognises a DSB and repairs it through one of two pathways either induce homologous recombination, or on non-homologous end joining (NHEJ) (Figure 1.4.1). Homologous recombination uses a template to repair the DSB ensuring the repair is exactly correct and no errors will be introduced to the sequence. However, a template can be provided in the form of a single stranded oligonucleotide (ssODN) with the sequence required to induce a mutation, whether this is incorporated into the genome or just used as a template is unknown (Kim and Kim, 2014). Repair in this way can be used to generate point mutations and provide the exact genotype of a disease of interest. NHEJ is an error-prone process as no template is used to repair the DNA. This generates a high chance of introducing small insertions or deletions (indels) into the gene, which in turn introduce a frameshift in the sequence (Bibikova et al., 2002). Frameshifts are likely to disrupt the gene resulting in a knockout. The ability to harness these repair mechanisms allows for the manipulation of a gene in a multitude of ways enabling the generation of required mutations.

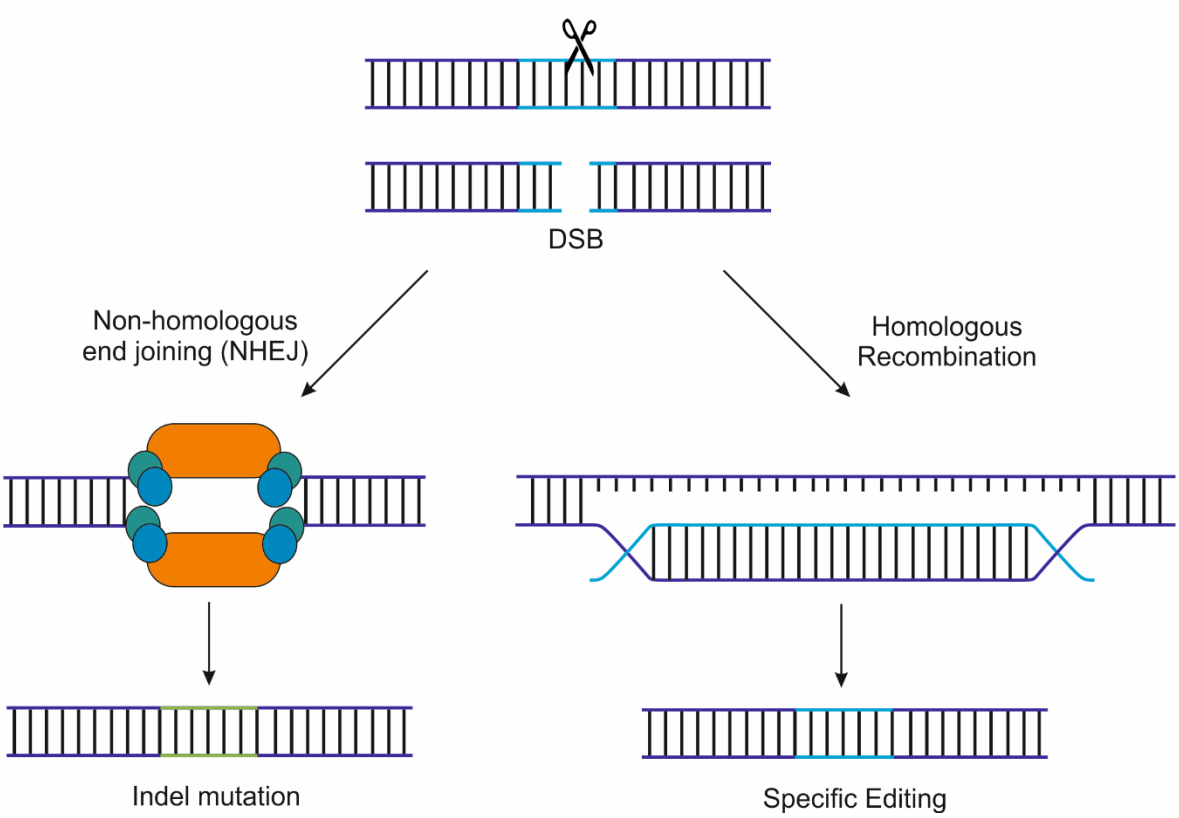

Figure 1.4.1: Repair of DSBs to introduce mutations via engineered nucleases

Schematic demonstrating how non-homologous end joining (NHEJ) (left) and homologous recombination (right) can be used to generate mutations in a gene of interest.

1.4.2 Zinc finger nucleases

The first engineered nucleases to be described were zinc finger nucleases (ZFNs) which have been used to modify genes in a number of organisms including viruses, bacteria, nematodes, frogs, fish, mammals and cultured cells (reviewed in Carroll, 2011). ZFNs have a modular structure consisting of two domains, a DNA binding zinc finger protein and a nuclease domain derived from the Fok1 enzyme. Fok1 has to dimerise to successfully cut DNA, creating the sought after DSB, therefore a pair of ZFNs are required for genome editing (Bitinaite et al., 1998). This increases the specificity of ZFNs thus reducing the likelihood of off-target effects. However, it was initially found that Fok1 could create homodimers, with just one of the ZFNs binding, which had to be rectified through mutagenesis of the protein (Miller et al., 2007; Szczepek et al., 2007). Further improvements have also been made to the Fok1 enzyme to improve activity (Guo et al., 2010; Doyon et al., 2011).

The creation of ZFNs to target specific recognition sites relies on the Cys_2-His_2 zinc-finger domain, one of the most common DNA-binding motifs in eukaryotes. Each domain is 30 amino acids in length and several of these bind 3bp within the major groove of the DNA strand (Miller et al., 1985). For a specific delivery to a single site in the human genome requires a 16bp recognition sequence, therefore a linker sequence was used to construct synthetic zinc finger domains that could recognise DNA sequences of 9-18bp in length (Liu et al., 1997). However, there are issues with this modular construction in that there is not a combination of zinc fingers that can recognise every DNA sequence, and the successful assembly of a ZFN does not guarantee it is able to create a DSB. It has been approximated that there exists a single functional ZFN per 100bp of DNA sequence on average (Kim et al., 2009).

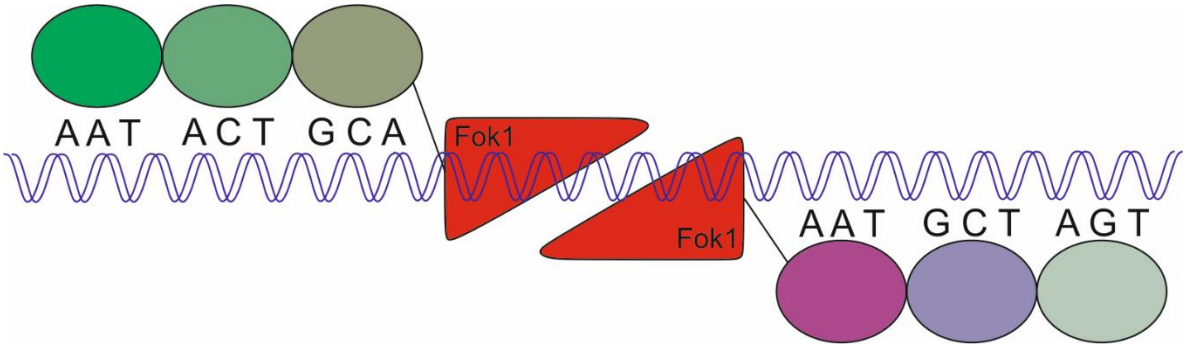

Figure 1.4.2: Overview of zinc finger genome editing technology

Zinc finger nucleases are modular structures consisting of a number of zinc finger domains linked to a Fok1 endonuclease. Each zinc finger repeat can recognise 3 bases in the major groove of DNA and a number of zinc finger repeats are linked to increase the specificity of the engineered nuclease.

1.4.3 Transcription activator-like effector nucleases (TALENs)

Transcription activator-like effector nucleases (TALENs) are another engineered nuclease that also uses the Fok1 nuclease to create DSBs in DNA. However, these rely on transcription activator-like effectors (TALEs) to direct the enzyme to the required sequence.

TALE repeat domains are highly conserved repeat domains possessing 1:1 binding properties with the four bases present within DNA and are found in the plant pathogenic bacteria genus *Xanthomonas,* where they are secreted to aid bacterial replication during plant infection (Kay et al., 2007). The binding of the TALEs to the targeted genes allows the *Xanthomonas* bacteria to activate genes beneficial to the bacterial infection. TALE binding was found to be solely specified by two hypervariable residues present within each domain (Boch et al., 2009; Moscou and Bogdanove, 2009). The combination of several TALEs together thus forms a protein able to recognise a specific DNA sequence, and further manipulation was then performed to combine the catalytic domains of Fok1 to the TALE repeat domains (Christian et al., 2010; Miller et al., 2011). These combined proteins are termed transcription activator-like effector nucleases or TALENs, providing a new platform for genetic engineering.

However, it is difficult to design novel TALEs using techniques such as PCR-based gene assembly due to TALE domains containing a large number of repeating units. This rendered the wide scale use of TALENs near impossible due to the costs of performing a large scale testing of TALEs design. A number of cloning strategies were developed to overcome this difficulty including the “Golden Gate” cloning method and the fast ligation-based automatable solid-phase high-throughput (FLASH) system (Cermak et al., 2011; Reyon et al., 2012).

The presence of the hypervariable residues means that TALENs are far easier to design than ZFNs, but as each TALE is approximately the same size as a zinc finger and each TALE recognises 1 bp, rather than the 3bp in ZFNs, TALENs are much larger constructs. This adds complexity in introducing TALENs into cells via viral methods, particularly in combination with the large amounts of repeating units present in TALENs. Yet, TALENs were also shown to cut DNA at a similar efficiency to ZFNs in a number of publications with lower cytotoxicity levels. It is likely that TALENS would have become the preferred method of genome editing despite these setbacks, but before this occurred, a new genome editing technique had been discovered.

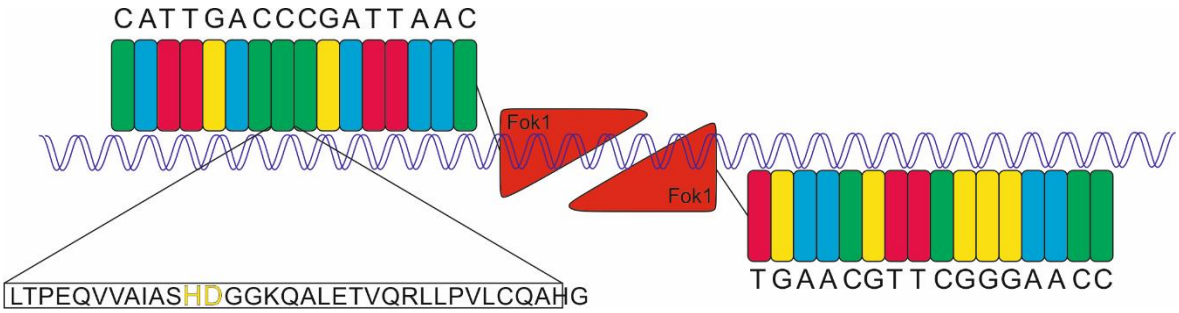

Figure 1.4.3: Summary of TALEN technology.

TALENs consist of a non-specific nuclease domain attached to modular repeat domains which specify the base of the DNA the domain can target. Two hypervariable residues (highlighted in yellow) provide this specificity. TALENs typically bind in pairs to the DNA as the Fok1 nuclease is a dimeric enzyme. Figure from Carstairs et al., 2014.

1.4.4 Clustered regularly interspaced short palindromic repeats (CRISPR)

Clustered regularly interspaced short palindromic repeats (CRISPR) were first identified in bacteria and archaea, as these organisms routinely capture small DNA fragments from invading viruses (Ishino et al., 1987; Jansen et al., 2002). These short repeats of viral DNA incorporated into the genome of bacteria provide a primitive immune-like system against further viral infections in combination with the Cas enzymes (Barrangou et al., 2007). The short repeats of viral DNA are transcribed into RNA, which acts as a target sequence for the Cas enzyme, an endonuclease. This CRISPR/Cas complex is then able to cut any DNA that matches the target sequence thus preventing viral infection.

There are three types of CRISPR system identified so far within prokaryotes, that differ based on the loci and proteins involved in targeting, the type II system is the basis for the newest genome editing technique (Figure 1.4.4). In the type II CRISPR system, the CRISPR loci are transcribed into a long pre-crRNA (precursor-CRISPR RNA) which is then matured into the CRISPR RNAs (crRNAs) that are able to target sequences. Processing is initiated by base pairing of each pre-crRNA repeat with a non-coding RNA named the trans-activating RNA (tracrRNA), these are then matured in the presence of Cas9 by RNA polymerase III (Deltcheva et al., 2011). The crRNA and tracrRNA remain duplexed and are able to direct the Cas9 endonuclease to DNA sequences specific to the crRNA. Added specificity is given to the system by a protospacer adjacent motif (PAM) recognised by the Cas9 enzyme, this sequence is specific to the Cas9 enzyme, and differing systems possess differing PAM sequences (Mojica et al., 2009).

The power of this CRISPR/Cas9 system, and its potential for use in genome editing, was first explored by using a single guide RNA (sgRNA) which comprised both of the crRNA and tracrRNA (Jinek et al., 2012). This created a system whereby the sgRNA could be designed to target a sequence as long as the Cas9 PAM sequence was adjacent to the target (Jinek et al., 2012). The sgRNA could then simply be redesigned and the two component system would be targeted against a different sequence. Both previously discussed genome editing techniques, ZFNs and TALENS, require the more difficult task of redesigning a protein. Conversely, the CRISPR/Cas9 system is an RNA based system which means only a new RNA transcript requires developing, a much easier experimental requirement than the development of a new protein.

Concerns over the specificity of CRISPR have been raised due to specificity being dictated by one strand of RNA in addition to the PAM of Cas9 (Marx, 2014). Initial reports using the CRISRP/Cas9 technology demonstrated a likelihood of secondary effects at alternative target sites (Fu et al., 2013; Pattanayak et al., 2013). A number of methods were developed to minimise these effects

including truncating the guide RNA and the recommendation of using a pair of CRISPR/Cas9 nickases, so that two recognised sequences are required to introduce mutations (Mali et al., 2013a; Ran et al., 2013; Fu et al., 2014). However, off target effects are typically rare if more than 3 mismatches are present between the locus and the RNA therefore intelligent designing of guide RNA sequences can minimise these effects (Cho et al., 2013). The position of the mismatches also impacts highly on the likelihood of mutations being introduced (Cho et al., 2013). The use of nickases is also affected by the requirement of two highly effects sgRNA sequences, which can be difficult to predict.

CRISPR has been further developed by manipulating the Cas9 enzyme. Cas9 possess two active sites, giving it the ability to cleave both strands of the DNA at once, but by inactivating one active site the Cas9 can act as a nickase. Combining two Cas9 nickases increases the specificity of genome editing using CRISPR by doubling the DNA required for binding (Ran et al., 2013; Cho et al., 2013; Shen et al., 2014). Additionally, both active sites can be inactivated to create what has been termed interference CRISPR or CRISPRi, this allows for genome regulation rather than genome editing (Qi et al., 2013). Further to these developments it has frequently been shown that CRISPR/Cas9 can use multiple guide sequences to enable simultaneous targeting of several loci within the genome (Cong et al., 2013; Mali et al., 2013b). This is not a possibility with either ZFNs or TALENs and presents a large advantage for the use of CRISPR/Cas9.

Since the first publication identifying the potential for CRISPR/Cas9 genome editing and its proof of principle *in vitro* (Gasiunas et al., 2012; Jinek et al., 2012), studies demonstrated the system as a viable genome editing method in human cells (Cong et al., 2013; Mali et al., 2013b). Since these discoveries, the CRISPR/Cas9 genome editing system has been used to edit DNA in a variety organisms such as mice, frogs, zebrafish and in human embryos (reviewed in Doudna and Charpentier, 2014).

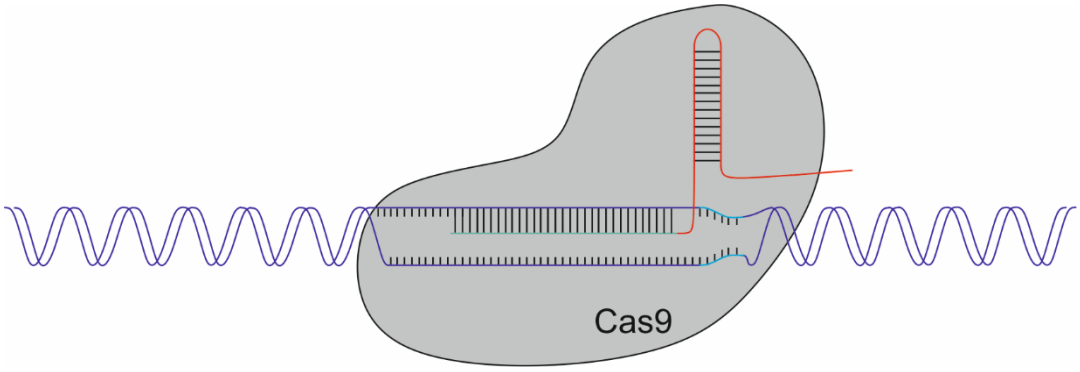

Figure 1.4.4: Summary of CRISPR/Cas9 genome editing technology.

CRISPR relies on RNA to direct the Cas9 nuclease to the target sequence within the DNA. The guide RNA consists of the CRISPR RNA (green) and a structural RNA (red). The protospacer adjacent motif (PAM) (blue) adds additional specificity to the enzyme. Cas9 possess two active sites and can cleave both DNA strands resulting in a double stranded break. Figure from Carstairs et al., 2014.

1.5 Stem cells

The creation of stem cell lines and development of *in vitro* differentiation protocols helps to overcome limitations of studying human disease in differentiated cell cultures and animal models. Stem cells are a class of primitive cells that have the potential to both self-renew and differentiate into a specialised cell type. These inherent properties of stem cells allow the study of genetic mutations and the resultant phenotypes in a range of cell types revolutionising the study of various types of diseases and subsequent drug development (Avior et al., 2016).

Broadly, there are two categories of stem cells, characterised by their location within an organism. Embryonic stem cells (ESCs), which arise from the blastocyst present in an embryo, and tissue-specific adult stem cells which exist outside the developmental continuum as reserve precursor cells (Young and Black, 2004). Stem cells are classified based on their ability to differentiate that is the number of lineages accessible via differentiation. Totipotent stem cells possess the capacity to differentiate into all cell types, there are two sources of totipotent stem cells, the fertilised egg and the blastomeres, which gradually lose totipotency during preimplantation development (De Paepe et al., 2014). Pluripotent stem cells are able to differentiate into all lineages derived from the three germ layers (ectoderm, endoderm and mesoderm) but not extra embryonic tissues such as the placenta. Multipotent stem cells have a restricted differentiation limited to number of lineages, typical of adult stem cells, and unipotent stem cells can differentiate into one lineage only.

The unique properties of stem cells to derive new tissues and repair old ones gives them a high therapeutic value and an overview of the two natural sources of stem cells is provided below.

1.5.1 Embryonic Stem Cells

A zygote proliferates and differentiates to form every cell and tissue of all developmental stages of the organism. The first inclination for the existence of pluripotent stem cells first came from work studying mouse teratocarcinomas, tumours which originated from mouse testes and were both malignant and upon transfer, induced tumours in other mice (Stevens and Little, 1954). Tumours of this nature also included an array of benign tissue types which were non-malignant leading to a hypothesis that a specific cell type within the tumour was giving rise to both the benign tissues and the malignancy of the tumour. Experiments demonstrated unequivocally that the transplantation of a single cell was able to give rise to a heterogeneous malignant teratocarcinoma and were termed “Embryonal Carcinoma Cells” (ECCs) (Kleinsmith and Pierce, 1964). Further experiments demonstrated the similarity of ECCs to cells within the inner mass of a mouse blastocyst which eventually led to the ability to isolate and grow ESCs in culture (Evans and Kaufman, 1981; Martin, 1981). When these ESCs were introduced back into the blastocyst, they were able to contribute to

the differentiation of all lineages win the mouse, that is tissues within the ectoderm, endoderm and mesoderm (Evans and Kaufman, 1981; Martin, 1981; Thomson et al., 1998). Mouse ESCs were also able to demonstrate the ability to differentiate into these cell types *in vitro*, and have also been shown to differentiate into germ cells (Bradley et al., 1984). Research then progressed to human ESCs and the ability to isolate them from fertilised embryos, which demonstrated similar features to the mouse cells with the pluripotent differentiation capacity (Thomson et al., 1998).

The ability to differentiate into all somatic cell types gives ESCs a unique therapeutic potential for the treatment and repair of damaged tissues in the body. However, the origination of ESCs from fertilised embryos creates an ethical concern surrounding their use both in therapies and in research. There are also a number of issues surrounding the nature of the ESCs that limits their potential for wide use in therapies. It is well established that undifferentiated ESCs when transplanted are able to generate teratoma tissues, with cells visible from each of the three germ layers. This concern may be alleviated by homogenously differentiating the ESCs into the somatic cell required *in vitro* before transplanting the cells.

Until recently, ESCs were the only known pluripotent stem cell, however in 2006, it was demonstrated that somatic cells could be reprogrammed into pluripotent cells, and so were termed induced pluripotent stem cells (iPSCs) (Takahashi and Yamanaka, 2006). This involved introducing four factors which resulted in fibroblasts producing colonies that appeared and behaved like embryonic stem cells. It was demonstrated that the four factors, Sox2, Oct4, c-Myc and Klf4, were sufficient for fibroblasts to be reprogrammed and these then display the morphology, growth properties and differentiation capacities of embryonic stem cells (Takahashi and Yamanaka, 2006). It has since been demonstrated that this reprogramming is possible both in mouse and human cells (Takahashi and Yamanaka, 2006; Takahashi et al., 2007).

1.5.2 Adult Stem Cells

Adult stem cells are classified as undifferentiated cells, situated amongst differentiated cells within a tissue or organ (Chanda et al., 2010). These cells, like other stem cells, possess the capacity to self-renew and differentiate into somatic cell types thus contributing to the repair and regeneration of the tissue type they exist in. Adult stem cells are unable to produce a viable offspring when injected into a blastocyst, and so are termed multipotent indicating their ability to differentiate into multiple cell types (Eggan and Jaenisch, 2003). For many years, it was thought that adult stem cells only existed for tissues which showed high turnover and extensive regeneration, for example the gut and the liver, but it has since been shown that organs such as the brain and heart also possess stem cells which give rise to these tissue types in specific circumstances (Altman and Das, 1965;

Rumyantsev and Borisov, 1987; Kuhn et al., 1996; Kajstura et al., 1998). Observations such as these led to an influx of research analysing the generation capacity of these types of adult stem cells and the potential for use in therapeutics, however the mechanisms of differentiation and the role of these cells in the homeostasis and regeneration of the tissue are largely unclear for a number of cell types (Wagers and Weissman, 2004).

The therapeutic potential of adult stem cells is arguably lower than ESCs due to the inability to differentiate into all tissue types, however the ethical concerns surrounding ESCs do not apply to adult stem cells. Often these can be harvested from a consenting adult, and fail to form teratomas when injected *in vivo*. The most well characterised adult stem cell is the haematopoietic stem cell, which gives rise to all other blood cells through haematopoiesis (Spangrude et al., 1988). The use of these cells in therapy is extensive and they have been used in transplants to treat sickle cell anaemia, leukaemia and other diseases of the blood in the form of bone marrow transplants (Copelan, 2006). Additionally, the use of skin transplants expanded via the use of autologous stem cells have been a focus of research in an attempt to provide an alternative to the more traditional use of skin grafts (reviewed in Chen et al., 2009). Another adult stem cell thought to have great therapeutic potential is the mesenchymal stem cell which is discussed in further detail below.

1.5.3 Mesenchymal Stem Cells

The term “MSC” has been traditionally used to represent this class of cell, but in reality the number of studies solely studying a homogenous population of “true stem cells” that is a cell that can differentiate and self-renew indefinitely are few. The vast majority of studies instead use a heterogeneous population of cells, some of which fulfil the definition of stem cell, whereas others are more committed progenitors. For this reason, it has been suggested that MSC be redefined to mesenchymal stromal cell in an attempt to provide a more accurate description of the cells being studied (Horwitz et al., 2005). Nevertheless, the term “mesenchymal stem cell” and its abbreviation “MSC” have become widely adopted and will be used as such throughout this thesis, with these caveats in mind.

The idea of a precursor stem cell for bone cells was first proposed in 1966 by Friedenstein *et al*, who demonstrated that subcutaneous transplant of bone marrow fragments and bone marrow cell suspensions did not result in the formation of blood cells, but instead reticular tissues and occasionally osteogenesis was seen to occur (Friedenstein et al., 1966). Further work also showed that when bone marrow suspensions were plated in monolayers, adherent fibroblast cells were able to form individual colonies, cells able to form colonies in this way are termed as fibroblast colony forming units (CFU-f). When implanted *in vivo*, a single colony forming unit was able to

differentiate into osteoblasts, chondrocytes, adipocytes and haematopoietic supporting stroma. These two qualities, self-renewal and differentiation, are hallmarks of stem cell behaviour giving an indication that the bone marrow contained another multipotent stem cell distinct from the previously isolated haematopoietic stem cell.

1.5.3.1 MSC sources and isolation

MSCs were first isolated from the bone marrow, and this is the most widely recognised source of MSCs, but various alternative tissues have been found to contain MSC-like cells (Pittenger et al., 1999). These include adipose tissue, dental pulp, placenta, umbilical cord blood, synovial membrane, and the periodontal ligament to name but a few (Gronthos et al., 2000; De Bari et al., 2001; Zuk et al., 2001; Fukuchi et al., 2004; Seo et al., 2004; Sarugaser et al., 2005). There is also evidence to suggest MSCs are present in almost all vascularised tissues due to a source of MSC-like cells existing within the wall of a blood vessel (Crisan et al., 2008).

One of the main issues surround MSC research is the lack of consensus on a single surface marker that identifies the MSC population. A minimum set of criteria have been defined to identify human MSCs. First, cells must retain plastic adherence when maintained in standard culture conditions. Second, cells must express the CD105, CD73 and CD90 surface markers, and lack expression of CD34, of CD45, CD34, CD14 or CD11b, CD79α or CD19 and HLA-DR surface molecules. Third, MSCs must be able to differentiate into osteoblasts, adipocytes and chondrocytes *in vitro* (Dominici et al., 2006). Other surface antigens have also been identified that are typically expressed by MSCs including CD13, CD29, CD44 and CD10 (Jones et al., 2002; Hermida-Gómez et al., 2011). The majority of these markers have been identified for MSCs isolated from the bone marrow, and evidence suggests that these markers may not be applicable for MSCs from other sources (reviewed in Lv et al., 2014). Additionally, MSCs have been shown to be a heterogeneous population of cells, particularly noticeable when cells isolated by plastic adherence are tested for multipotency. In experiments such as these, a number of cells are “true MSCs” demonstrating equal propensity for each of lineages MSCs are able to differentiate into. However, some cells appeared more committed to one of the lineages, with cells able to differentiate into osteoblasts more easily than adipocytes depending on the source of MSCs (Muraglia et al., 2000). Work from our laboratory also suggests a subset of MSCs exist that do not differentiate, yet satisfy all other criteria to be defined as an MSC (James et al., 2015).

1.5.3.2 MSC differentiation

As previously stated, one of the criterion to define an MSC is the ability to differentiate into osteoblasts, chondrocytes, and adipocytes; termed the tri-lineage differentiation potential of an MSC (Figure 1.5.1). Although some evidence also exists for the potential of MSCs to differentiate into lineages other than these, this remains controversial.

The study of MSC differentiation *in vitro* has been well characterised, with chemical stimuli and differentiation protocols established for each of the lineages of MSC differentiation. However, *in vitro* studies of MSC differentiation do face limitations in that the analysis of differentiation *in vitro* may not correlate to *in vivo* observations. Additionally, the pathways activated by chemical inductive stimuli *in vitro* may in fact be different to the pathways activated during *in vivo* differentiation. This has previously been noted in the impact of bone morphogenic proteins (BMPs) on osteogenesis and adipogenesis (Gimble et al., 2006). Regardless of these difficulties, the analysis of MSCs *in vitro* has revolutionised MSC biology by allowing the in-depth study of human MSC function in a controlled environment. As previously discussed, the results gleamed from using rodent models, and rodent cells, may not always correlate to results seen in a human background.

Osteogenesis is typically induced *in vitro* using dexamethasone, ascorbic acid and β-glycerophosphate (Jaiswal et al., 1997). It is a stepwise differentiation process where cells undergo an initial period of proliferation, followed by a progressive maturation to terminally differentiated osteoblasts. During this process, an increase in extracellular matrix (ECM) production and mineral deposition can also be determined. Expression markers specific to osteoblasts can also be detected at various stages of differentiation, with a rise of alkaline phosphatase (ALP) activity indicative of early osteogenesis followed by increased expression of osteopontin, osteonectin, osteocalcin, and bone sialoprotein. It has been shown that dexamethasone induces Runx2, the master transcription regulator of osteogenesis, and also enhances Runx2 activity during differentiation. Ascorbic acid leads to increased collagen I expression and β-glycerophosphate provides the phosphate required for mineral deposition during this process (Langenbach and Handschel, 2013).

MSCs can also be stimulated to undergo adipogenesis, which results in an alteration from the fibroblastic-like stem cells to lipid containing fat cells. This is typically achieved by a chemical stimulative cocktail. The most common approaches involve raising intracellular levels of cyclic adenosine monophosphate (cAMP) by stimulating cells with isobutylmethylxanthine (IBMX), a phosphodiesterase inhibitor (Klemm et al., 2001). This activates the transcription factor CREB, which is constitutively activated in pre-adipocytes and directly involved in the differentiation of adipocytes. Further compounds such as dexamethasone are also included which is a ligand for the

gluticorticoid receptor, which accelerates differentiation *in vitro* (Park and Ge, 2016). Most adipogenic cocktails also contain insulin, a potent adipogenic hormone that triggers a number of transcription factors in the differentiation of pre-adipocytes to adipocytes (Klemm et al., 2001). Often, fatty acids are also included in *in vitro* differentiation protocols (Diascro et al., 1998). Differentiation in this way commits the MSC to the adipogenic lineage by becoming a pre-adipocyte, which is technically indistinguishable from an MSC but is no longer able to differentiate into other lineages. Finally, terminal differentiation results in an insulin-sensitive cell capable of lipid transport, storage and synthesis. These cells also express adipocyte specific markers such as lipoprotein lipase, leptin, glucose transporter-4, and C/EBPα.

In contrast to the previously discussed differentiation lineages, chondrogenesis occurs most effectively when MSCs are cultured in three dimensional (3D) cultures. This mimics the *in vivo* process of condensation, but is not sufficient to generate chondrogenic differentiation alone. Typically, chondrogenic supplementation consists of dexamethasone and a transforming growth factor β (both 1 and 3 have been used in various studies) (Johnstone et al., 1998; Mackay et al., 1998). Chondrogenesis, similar to the other differentiation processes described above, occurs through a step-wise progression towards a terminally differentiated cell type. After the initial condensation step, MSCs differentiate into a proliferative pre-chondrocyte before further differentiation characterised by an alteration in collagen expression, from type I collagen to type II and type X collagen. At this point, cells differentiate into hypertrophic chondrocytes, indicated by the increased levels of type X collagen and associated rise in ALP (Johnstone et al., 1998).

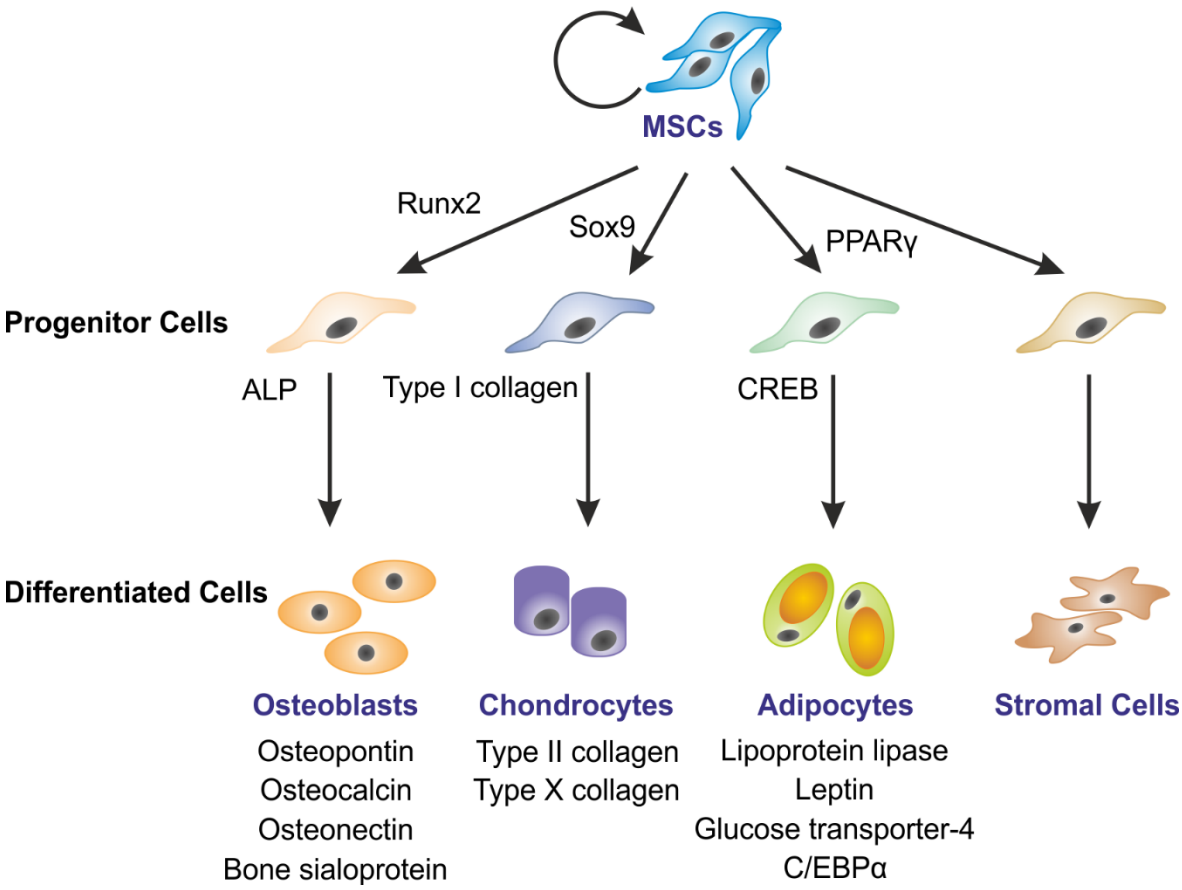

Figure 1.5.1: Overview of MSC differentiation capacity

MSCs are a multipotent stem cell able to self-renew and differentiate, via a stepwise maturation process, into multiple lineages from the mesenchyme. Typically MSCs are defined by their ability to differentiate into osteoblasts (bone), chondrocytes (cartilage), and adipocytes (fat). Markers described in section 1.5.3.2 are included for the tri-lineage typical of MSCs. Image adapted by David Cook from Caplan and Bruder, 2001.

1.5.3.3 MSCs as a cellular therapy

MSCs provide an attractive option for cell therapies, particularly for musculoskeletal diseases due to their tri-lineage differentiation potential. Shortly after the discovery of MSCs, therapeutic options for the use of MSCs were explored by an infusion of expanded cells intravenously, with no adverse reactions. A number of clinical trials exploring the use of MSCs in musculoskeletal repair have also been embarked upon (Carstairs and Genever, 2014). Bone grafting is a common transplant surgery performed but can lead to complications, cell infusion with MSCs is a potential alternative and has been trialled in patients with non-union fractures (Carstairs and Genever, 2014; Gómez-Barrena et al., 2015). Treatment with autologous MSCs attached to biphasic calcium phosphate resulted in 77% of the treated fractures being consolidated 6 months after treatment, providing evidence for the efficacy of bone regeneration by MSCs (Rosset et al., 2016). Articular cartilage has a limited capacity for repair due to the slow metabolism of the tissue and low vascularisation. Defects in cartilage caused by osteoarthritis, trauma or other degenerative conditions are often painful and difficult to treat successfully. Effective management treatments of these detrimental conditions are limited and many efficacy studies have been performed examining the potential for an MSC cell therapy. Early intervention for focal traumatic chondral and osteochondral defects with MSC therapies indicated improvement in the clinical outcomes of a number of trials, however, treatment of advanced degenerative conditions show less efficacy (Bornes et al., 2014). Many of these trials use MSCs seeded onto a biocompatible scaffold or gel matrix for implantation. MSCs also possess the ability to exert paracrine effects on host cells, another property which makes them highly attractive for tissue engineering and regenerative therapies.

Additionally, MSCs are also being extensively trialled for their effectiveness in treating various immunological conditions since the demonstration of their immunomodulatory functions. The exact mechanisms by which MSCs exert immunomodulation are not currently well understood, but most evidences support the theory that the cells posit effects either through cell-cell contact and/or the release of soluble cytokines. In this manner, MSCs are able to exert effects on the behaviour of a broad range of immune cells including T cells, natural killer T cells, dendritic cells, B cells, neutrophils, monocytes, and macrophages (Zhao et al., 2016). These effects are also independent of the major histocompatibility complex, as allogenic MSCs were able to impact on the behaviour of T cells at a similar capacity to autologous cells (Le Blanc et al., 2003). Furthermore, MSCs possess low levels of human leukocyte antigen I and no expression levels of human leukocyte antigen II so are also deemed to be hypoimmunogenic. This has led to a number of clinical trials for

immunological conditions such as graft versus host disease and multiple sclerosis (Chanda et al., 2010; Carstairs and Genever, 2014).

Despite the initial promising outlook, there are a number of issues surrounding MSC therapies meaning while many MSC therapies are in approved clinical trials, no MSC products are yet to receive Food and Drug Administration (FDA) approval for the wider market. Primarily this is due to the heterogeneous nature of MSCs and the lack of a cell surface marker to define the cell population. Cell products submitted for FDA approval typically have significant diversity in the criteria used to define the MSC population. Criteria identified in this manner include cell source, expression markers, and product manufacturing. A consensus on the definition of an MSC may well aid the development of cellular therapies allowing comparison between studies and potentially facilitating clinical use (Mendicino et al., 2014).

1.6 Isogenic human model systems – combining engineered nucleases and stem cells

The development of *in vitro* genome editing techniques allows for the development of isogenic human disease cell models without the requirement for patient contact. Combining the recently developed engineered nucleases with stem cells and established differentiation protocols creates an unprecedented capacity for applications in medical research allowing for greater understanding into the causatives for human disease. As previously discussed, stem cells are able to self-renew and also differentiate into more specialised cells. This provides the opportunity to create a mutation within a stem cell prior to differentiation into a specific relevant cell type and removes the requirement of mice. Without engineered nucleases it would take approximately 6 months or more to generate multiple iPSC lines both from a wild type setting and from a patient with the disease of interest. However, combining engineered nucleases with stem cells allows for the creation of a mutant iPSC line in a much shorter timeframe. Combination of stem cells and engineered nucleases also gives the novel ability to study a mutation's effects in various cell types, if the *in vitro* differentiation protocols are in place (Ding et al., 2013). This methodology has been used in various stem cells including ESCs and iPSCs (Hockemeyer et al., 2009, 2011b, 2011a). However, whilst the ability to edit tumorigenic cell lines with engineered nucleases reaches almost 100% efficiency, the efficiency of genome editing in iPSCs in particular is much lower. Additionally, at the time of writing, no attempt has been made to combine engineered nucleases with MSCs to the author's knowledge. Using engineered nucleases to create mutations in MSCs could give insight into the development of genetic skeletal diseases.

Typically, humans MSCs extracted from primary tissues, such as the bone marrow, undergo replicative senescence in culture similar to any somatic cell. After a number of passages, cells demonstrate morphological abnormalities, changes in surface marker expression and ultimately growth arrest (Hayflick, 1965; Wagner et al., 2008). MSCs therefore cannot be grown for prolonged periods *in vitro* creating a limit on work that can be performed on isolated cells. Additionally, MSCs exist as a heterogeneous population *in vivo*; meaning MSCs isolated from human tissue, for example bone marrow, are actually a heterogeneous stromal cell culture (Wagner and Ho, 2007). The cell isolate likely consists of many different stromal populations; some that fulfil the definition of a true MSC and some that perhaps do not. One method of resolving these issues is to introduce human telomerase reverse transcriptase (hTERT) into MSCs as it has been determined that *in vitro* expansion of MSCs results in a shortening of telomeres (Baxter et al., 2004). The insertion of the telomerase gene ensures that telomeres are not shortened during DNA replication thus removing one of the causative stresses of replicative senescence. In previous work, our laboratory has used lentiviral transduction to generate immortalised clonal human MSC cell lines, all isolated from a single donor. The activity of the telomerase gene was confirmed and the cells sustained exponential growth in culture over 400 days verifying immortalisation. These lines have been termed the hTERT-MSCs and four of these lines (Y101, Y201, Y102 and Y202) have been extensively characterised (James et al., 2015). The immortalisation of MSCs allows these cells to be edited with engineered nucleases for the first time, as senescence is no longer a limitation, which would prevent the generation and characterisation of genetically modified lines. By studying the effects of mutations in these cells, and differentiating them into either bone, cartilage or fat may provide insight into the treatment of human skeletal diseases in addition to further details into how these cells may be used in regeneration therapeutics.

1.7 Modelling skeletal disease

Bone is a dynamic organ, and plays an essential role in the structure, protection and movement of the body. Osteoclasts and osteoblasts constantly remodel the skeleton through the resorption of old tissue and the subsequent formation of new bone but bone is not a uniform structure, with cells existing at various developmental stages throughout the tissue (Del Fattore et al., 2010). Additionally, the cavities of bones are filled with bone marrow and blood vessels. The vasculature between the bone marrow and bone are shared and these two tissues are highly associated both by anatomy and by function. These shared properties give an indication that to understand diseases of the skeleton one should not exclude the bone marrow in considerations of the pathophysiology (Riminucci et al., 2015). It would follow that diseases of the skeleton would impact on the MSCs residing in the bone marrow, the function of these cells and their ability to give rise to differentiated

skeletal cells. The development of stem cell models for skeletal disorders gives unique insight into the disease of interest. The development of genetically engineered MSCs could allow for further understanding for a number of skeletal disorders and an overview of some of these are given along with a discussion of the disease models used.

1.7.1 Skeletal dysplasias resultant from FGFR3 mutations

Skeletal dysplasias are a heterogeneous group of genetic disorders characterised by abnormal development of the skeleton, including altered growth, differentiation and maintenance of bone and cartilage tissues (Cho and Jin, 2015). The most common of which is achondroplasia, a nonlethal condition that results from a point mutation in fibroblast growth factor receptor 3 (FGFR3). The point mutation is an activating mutation resulting in increased FGFR3 signalling activity, which results in the short stature typically observed with achondroplasia. Other skeletal dysplasias resultant from mutations in FGFR3 include hypochondroplasia, thanatophoric dysplasia (types I and II) and SADDAN (**s**evere **a**chondroplasia with **d**evelopmental **d**elay and **a**canthosis **n**igricans) dysplasia. These dysplastic disorders exist on a spectrum of graded severity.

The first achondroplasia mouse model was developed in 1999, where homologous recombination was used to introduce the most common human achondroplasia mutation (G380R) into the murine FGFR3 gene (Wang et al., 1999). Heterozygotes were derived which displayed phenotypic characteristics typical of dwarfism, including shortened bones, narrow growth plates and alterations to the skull. This demonstrated unequivocally that achondroplasia was caused by the mutation in FGFR3. Models such as these prove beneficial for the study of novel treatment strategies.

Further exploration of the impact of FGFR3 on development has also been explored by the creation of immortalised chondrocyte cell lines (Benoist-Lasselin et al., 2007). These were developed from foetal growth plate cartilage of aborted foetuses with either achondroplasia or thanatophoric dysplasia. The development of cell lines such as these allows comparison of the various signalling pathways involved in cellular behaviours. These cells revealed differences between mouse and human chondrocytes in that human chondrocytes do not demonstrate constitutive activation of the MAPK signalling pathway. It was hypothesised that cell lines such as these would increase the ease of the assessment of FGFR3 mutations on signalling pathways such as the MAPK signalling pathway and reveal other signalling pathways downstream of FGFR3.

1.7.2 Osteogenesis Imperfecta

Osteogenesis Imperfecta (OI) is a group of genetic skeletal dysplasias characterised by fragile bones with low mass, short stature and skeletal deformities. OI is a heterogeneous group of dysplasias with varying severities, ranging from forms lethal at birth to mild forms. The vast majority of OI cases are caused by dominant mutations in either the *COL1A1* or *COL1A2* genes, which encode for the α1 and α2 chains of type I collagen. However, a number of subtypes of OI are caused by recessive mutations in genes linked to collagen biosynthesis, post-translational modifications and collagen processing.

Research into understanding OI appears to be conducted almost exclusively in animals, albeit early studies which relied on patient samples (reviewed in Enderli et al., 2016). Predominantly, OI models are created in mice, and have been created presenting with phenotypes similar to a number of the subtypes of OI. Mice generated in this way are susceptible to fractures, and possess bones with decreased bone mass and volume. Interestingly, the first mouse model for OI was not generated for research but occurred via a spontaneous mutation in type I collagen, termed the osteogenesis imperfecta murine (oim) model (Chipman et al., 1993). A number of other organisms have also presented with natural mutations that caused OI, including zebrafish, beagles, dachsunds and Golden retrievers (Campbell et al., 1997, 2000; Drögemüller et al., 2009; Fisher et al., 2003; Seeliger et al., 2003; Asharani et al., 2012). Again, all organisms shared a similar skeletal phenotype and were susceptible to fractures. Animal models have revealed a cellular mechanism for the elevated bone turnover in OI by studying cells from the long bones within these animals, whereas human cells are isolated from biopsies from the iliac crest. The iliac crest does not load-bear in the same manner as long bones and OI fractures are far more likely to occur in long bones, which creates a definite advantage to the study of OI in mice. However, mouse bones do not allow for the same sample preparation as used in human bones, due to their small size, creating differences in mechanical studies. Furthermore, the structure of the mouse cortical bone varies to that seen in humans, as the mouse bone does not contain the Haversian system which again may alter the mechanics of the tissue (Launey et al., 2010).

1.7.3 Fibrodysplasia ossificans progressive

The formation of ectopic skeletal tissue in soft tissues is typically associated with severe tissue damage, however the genetic conditions fibrodysplasia ossificans progressive (FOP) and progressive osseous heteroplasia (POH) also present with this phenotype. These conditions result in progressive ossification of the soft tissues in a predictable anatomical pattern. Patients with FOP are often wheelchair bound by the third decade and the condition is typically fatal due to the

inability of the thorax to support normal breathing (Kaplan et al., 2008). The genetic cause of FOP was not discovered until 2006 where a genome-wide linkage study identified a recurrent mutation in the activin A type I receptor gene, a receptor for BMP (Shore et al., 2006). With the identification of the genetic causative, a knock-in mouse model was developed mimicking the condition. This animal model confirmed the activin A type I receptor gene as causative for FOP and that BMP signalling was activated in the majority of mutant cells within the developing ossification lesions (Chakkalakal et al., 2012). This finding provided an initial drug target for the development of FOP treatments.

1.8 Project Aims

The emerging technologies of engineered nucleases combined with stem cell lines and established differentiation protocols creates a unique opportunity for the analysis of human disease. As discussed, animal models (particularly mice) are predominantly used for the study of skeletal diseases and yet whilst a wealth of information regarding human diseases has been gleamed through the use of animal models, these technologies are fraught with issues. To further our understanding of skeletal disease, and to understand how the cells of the bone marrow are affected by gene mutations, it would be prudent to genetically modify MSCs.

The aims of this project is to develop a methodology to manipulate the genome of an immortalised MSC line (hTERT MSCs) using the CRISPR/Cas9 system. Initial work will aim to establish this methodology and optimise each step within the process in order to create a complete CRISPR/Cas9 workthrough that in theory could be used to target any gene of interest. Work will then proceed to:

- Determine the effects of serum reduction in hTERT MSCs to further understanding of how growing cells in a nutrient-rich environment affects MSC behaviours
- Genetically modify Runx2 and Sox9, two critical transcription factors of MSC differentiation
- Create a disease relevant human mutation of FGFR3 will then be explored to create the first CRISPR/Cas9 genetically modified isogenic MSC disease model
- Investigate the development of *in vivo* like 3D MSC culture conditions for combination with the CRISPR/Cas9 edited hTERT MSCs

Chapter 2 : Methods and Materials

2.1.1 Cell Culture

2.1.1.1 hTERT MSCs

hTERT MSCs were cultured from passage 40-90 in Dulbecco's Modified Eagle Medium (DMEM) *(Invitrogen)* supplemented with 100U/ml penicillin, 100µg/ml streptomycin, and 10% foetal bovine serum (FBS) *(BioSera).*

2.1.1.2 Human Embryonic Kidney 293FT cells

Human Embryonic Kidney 293FT (HEK293FT) cells were cultured in DMEM supplemented with 100 U/ml penicillin, 100µg/ml streptomycin, 0.1mM MEM non-essential amino acids (NEAA) *(Invitrogen)* and 10% foetal bovine serum (FBS).

All cells and cell lines were cultured in a humidified atmosphere at 37°C in 5% CO_2/95% air.

2.1.1.3 Cell Passage

Once cells had reached 70-90% confluency, culture medium was aspirated and disposed of. Cells were then rinsed with phosphate buffered saline (PBS) to remove all trace of FBS. Typically, 2mL of 0.25% Trypsin-ethylenediaminetetraacetic acid (EDTA) was added per 175cm^2 culture flask and the flask incubated at 37°C for 5 minutes to remove the adherent cells. Once approximately 75% of cells had rounded and detached from the flask surface, any remaining cells were removed by gentle tapping. Cells were sub-cultured as appropriate and the FBS present in the culture media acted as the neutralising agent of the trypsin-EDTA (Böker et al., 2008).

2.1.1.4 Cryopreservation

Cells were cryopreserved in 90% FBS and 10% dimethyl sulfoxide (DMSO). Detached cells were centrifuged at 1200rpm for 5 minutes and resuspended in 1ml of cryopreservation media into 2mL cryovials and transferred to -80°C in a freezing container. Cells to be stored long term were then transferred into liquid nitrogen at -196°C after having been stored at -80°C for at least 12 hours.

Cells were recovered from cryopreservation by thawing the cryovial rapidly in a 37°C water bath until 75% of the cellular suspension had defrosted. 1mL of pre-warmed culture medium was then added to the cryovial and the entire suspension transferred to the desired culture flask. An appropriate amount of pre-warmed culture medium was then added and the cells then incubated at 37°C in 5% CO_2. The cells were left to settle for 12 hours and the culture media containing DMSO aspirated and replaced with pre-warmed culture media to ensure the presence of DMSO did not affect the cells.

2.1.1.5 Colony forming unit assay

Cells were plated at 10 cells/cm^2 in 6 well plates and allowed to culture until colonies were visible under a microscope, for hTERT MSCs this culture time was typically between 1 and 2 weeks. Medium was changed every 3-4 days. When colonies were visible, the cells were washed once with 1xPBS before fixing in 95% ethanol for 5 minutes. Colonies were then stained with 0.5% Crystal Violet (made up in 95% Ethanol) for 30 minutes after which excess stain was removed by washing with tap water. Plates were left to dry before imaging.

2.1.2 Quantitative Real-Time PCR

2.1.2.1 Trizol Extraction

Total RNA was isolated by lysing the cells using Trizol reagent *(Invitrogen)*, 500µL was used for one well of a 6 well plate and 1mL used for a T25 flask. RNA was then extracted from the lysate according to the manufacturer's instructions. Extracted RNA was resuspended in 12µL of nuclease free water and the purity and concentration of the RNA assessed spectroscopically using a Nanodrop.

2.1.2.2 DNAse Treatment of Samples

Any remaining contaminants of genomic DNA were removed from the extracted RNA before cDNA synthesis. Up to 5µg of RNA was added to an Eppendorf tube along with 1µL 10x Reaction mixture, 1µL of DNAse I and the reaction mixture made up to 20µL with nuclease-free water. This reaction was then incubated for 30 minutes at 37°C, 1µL of EDTA was then added and the reaction incubated at 65°C for 10 minutes to inactivate the DNAse I.

2.1.2.3 cDNA Synthesis

cDNA was synthesised from an appropriate amount of RNA using SuperScript™ II Reverse Transcriptase Kit with the provided Oligo DT primers (*Invitrogen).* The supplier's protocol was followed with an extended incubation period of one hour at 42°C after the enzyme was added.

10ng of cDNA was analysed by quantitative PCR using a Stepone plus RT-PCR system *(Invitrogen)*, each reaction mixture (20µL) consisted of 1x Fast SYBR Green buffer *(Invitrogen)*, 10µM of each primer and nuclease-free water. The amplification programme used consisted of one cycle of 95°C for 20 seconds, followed by 40 cycles of 95°C for 15 seconds and 60°C for 30 seconds. A melting curve analysis was performed to determine whether any non-specific PCR products had been formed during amplification. This consisted of one cycle of 95°C for 15 seconds, 60°C for 60 seconds following by a temperature increase to 95°C at a rate of $0.3°Cs^{-1}$.

2.1.3 Differentiation Assays

2.1.3.1 Adipogenic Differentiation

10,000 cells were seeded per well in 96-well plates and after 24 hours, the media was changed to adipogenic media (DMEM + 10%/0.5% FBS + 1% penicillin-streptomycin supplemented with 1µM dexamethasone, 500 µM IBMX, 1µg/ml insulin and 100µM indomethacin) with medium changed every 3 days.

2.1.3.2 Oil Red O Staining

Cells were washed with PBS before being fixed with 4% w/v paraformaldehyde (PFA) solution for 10 minutes. After fixing, cells were washed with dH_2O, incubated for 5 minutes in 60% isopropanol and stained for 10 minutes in 0.3% Oil Red O. Cells were washed with 60% isopropanol and then three times with dH_2O. Adipocytes were photographed, in PBS, using a brightfield microscope.

2.1.3.3 Osteogenic Differentiation

Cells were seeded at $2x10^4$ cells/cm^2 in 24 well plates. 24 hours post seeding cells were cultured in osteogenic medium (DMEM + 10%/0.5% FBS + 1% penicillin-streptomycin supplemented with 50 µg/ml L-ascorbic acid-2-phosphate, 5mM β-glycerophosphate and 10nM dexamethasone) with medium changed every 3 days.

2.1.3.4 Alizarin Red Staining

Cells were washed once with PBS before fixing in 4% w/v PFA solution for 20 minutes. Cells were then washed three times with PBS and stained with 40mM Alizarin red solution (pH4.2) for 20 minutes before a further three washes in PBS followed by three washes in tap water. Plates were allowed to dry fully before imaging with a stereomicroscope.

Alizarin red staining was quantified by elution with 10% (wt/vol) cetylpyridinium chloride (CPC) (dissolved in dH2O) for 1 hour with gentle shaking every 15 minutes. Absorbance was read at 570nm.

2.1.3.5 Alkaline Phosphatase and Von Kossa Staining

Cells were washed twice in PBS and ALP stained using 0.2 mg/ml naphtol AS-MX in 1% N,N-dimethylformamide diluted in 0.1 M Tris (base) pH 9.2 with 1 mg/ml Fast Red TR for 2 minutes. Cells were then fixed in 4% PFA and stained for phosphate ions (present in calcium depositions) using 1% silver nitrate solution. Photochemical degradation of silver phosphate to silver ions is then performed using a lightbox for 1 hour. Staining was imaged using a stereomicroscope.

2.1.3.6 p-Nitrophenyl Phosphate Phosphatase Assay

Cells were lysed with 150µl Triton-X in 0.2M carbonate buffer and the lysates frozen at -80oC. Lysates went through three freeze-thaw cycles to lyse the cells. 50µL of lysate was replated and mixed with 50µL of phosphatase substrate at a final concentration of 900nM. Plates were incubated for one hour at 37^{o}C and absorbance read at 405nm. A standard curve was formed from 4-nitrophenol (pNP) and used to determine the µmol/ml of pNP produced as a result of alkaline phosphatase digesting the phosphatase substrate. A further 50µL of lysate was taken and used to determine DNA concentration using the Quant-iT™ PicoGreen dsDNA Reagent as described by the manufacturer. Salmon sperm DNA was used as a standard curve for comparison.

2.1.4 RNA-seq analysis

2.1.4.1 RNA isolation, cDNA library preparation and sequencing

Total RNA for transcriptome analysis was isolated by centrifuging hTERT MSCs for 5 minutes at 400g, before resuspension in 350µL of RA1 lysis buffer (Nucleospin RNA II kit) and 3.5µL of β-mercaptoethanol. Following lysis, RNA was extracted using the Nucleospin RNA II columns (Macherey-Nagel, Germany) following manufacturer's instructions. Briefly, lysates were cleared first by passing through the column before conditions were adjusted for optimal RNA binding by

mixing with 350µL of 70% ethanol. RNA was then bound to the column and the column desalted using provided membrane desalting buffer. The column was then treated with DNAse I for 15 minutes and the column washed and dried to remove the presence of buffer. RNA was then eluted in 30µL of RNAse-free H_2O and quantified spectroscopically using a Nanodrop. RNA quality was assessed using an Agilent 2100 Bioanalyzer.

mRNA was then captured using Oligo-dT beads which bind to the poly-A tails found specifically on mRNA, thus removing other RNA species such as ribosomal RNA which would contaminate the sample. mRNA is then fragmented and these fragments used as templates for cDNA synthesis, which were then ligated to adapters. This library was then amplified and sequenced using a HiSeq 2500 sequencer.

2.1.4.2 Read mapping

The STAR splice-aware read mapper (https://github.com/alexdobin/STAR) was used to map reads, with following options: "--outSAMstrandField intronMotif", "--outFilterType BySJout", "--outFilterIntronMotifs RemoveNoncanonical" and "--outSAMtype BAM SortedByCoordinate". Reads were mapped against the pre-computed indexed GRCh38 Gencode 24 version of the human genome provided by the STAR authors.

2.1.4.3 Quantitation and differential expression analysis

Cufflinks (http://cole-trapnell-lab.github.io/cufflinks/) was used to quantify mapped reads and perform differential expression analysis. The associated GTF annotation file from Gencode version 24 was provided with the "-g" option and cDNA fasta sequences with the "-b" option. The resulting GTF files, from Cufflinks, were merged with Cuffmerge and used with Cuffdiff for differential expression analysis.

2.1.4.4 Pathway analysis

Pathway analysis of the resultant significantly differentially regulated transcripts (defined as transcripts with a log2 fold change > +/-1, an adjusted p value < 0.05, and reads per kilobase transcript per million mapped reads > 0 in both groups) was performed using Enrichr software (Chen et al., 2013a; Kuleshov et al., 2016).

Gene set enrichment analysis (GSEA) was also used to highlight enrichment of upregulated or downregulated transcripts in pathways (Subramanian et al., 2005). Particular attention was paid to

the false discovery rate (FDR) of the pathways described to ensure analysis was likely to be significant.

Chapter 3 : Reduction of serum in mesenchymal stem cell *in vitro* culture conditions for a controlled proliferation and differentiation environment

3.1 Introduction

The determination of the exact requirements for adherent cells in culture was first discussed and compared for 2 individual cell types in 1955 in an attempt to simplify the complex systems used to propagate cells. Eagle determined the nutritional requirements of both HeLa cells and a mouse fibroblast line to the point where the removal of one identified component resulted in cell death. Strikingly the requirements of the two cell lines were similar enough for the creation of a minimum essential media, which could be supplemented with horse sera and allow for the extended growth of the cells in culture (Eagle, 1955).

Since that discovery, the propagation of cultured cells has largely remained the same, typically relying on the supplementation of a base media with animal serum. Currently, the most common practise is the use of foetal bovine serum (FBS), also known as foetal calf serum (FCS), which contains a rich variety of proteins (including vast amounts of bovine serum albumin), growth factors, hormones and other nutrients that allows for the sustained growth of cells in culture (Gstraunthaler, 2003). However, the exact composition of animal sera is undefined and the proportion of components can vary between batches of FBS. This can lead to varying growth rates and differentiation potential in stem cells, feasibly causing unreproducible experimental results (Morris and Warburton, 1994; Gong et al., 2009; Tateishi et al., 2008). It is therefore common to test batches of FBS in order to establish a specific batch of serum that provides optimum growth and successful differentiation. Future testing of FBS would then establish an efficacy within an acceptable range of the original batch of serum used, typically an efficacy of 80% is required for a batch to be successful (Froud, 1999). However, this still leaves a margin of error for all

experimentation conducted using these methods and with the continual use of serum in scientific research, variability between laboratories becomes a concern.

As previously discussed, MSCs have a number of properties beneficial for a wide range of therapeutics, and have been tested in a number of clinical trials (Carstairs and Genever, 2014). Cells for these trials will have likely been propagated with serum supplementation according to FDA guidelines, however, a study has shown that a preparation of 100 million MSCs contains between 7ng and 30ng of bovine proteins as a result of culture conditions (Spees et al., 2004). This raises a risk of inducing an immunogenic response in a treated patient against the bovine proteins, particularly if multiple cellular treatments are likely to be needed. Indeed, at least one patient treated with a human MSC cellular therapy has been identified as possessing antibodies against bovine serum proteins after treatment (Horwitz et al., 2002). Although it is feasibly possible to reduce the amount of bovine proteins present in a preparation ideally a xenogenic-free culture method is required (Spees et al., 2004).

One potential way of achieving a xeno-free culture system is the use of human plasma as a cell culture supplement. Human serum would likely be the most comparable substitute however, human plasma is more readily available being a by-product of blood donation, thus limiting the financial impact on cellular therapies. Furthermore, it is routinely screened as part of the procedure. In one study, MSCs showed comparable proliferation and differentiation levels when treated with autologous plasma, although this again could complicate cellular therapies with the constant need for autologous plasma (Lin et al., 2005). Additionally, there are a number of differences between human plasma and serum as to the concentrations of soluble factors, including 11 chemokines, which may be essential for cell signalling and behaviour (Ayache et al., 2006). It appears although human plasma may be scientifically suitable for sustaining MSC behaviour, it is likely not the most viable option for cell propagation and will still suffer the same consistency issues as animal sera.

Serum free culture systems are becoming increasingly available to attempt to define the additions required to culture media to provide standardisation in cell culture (Gottipamula et al., 2013; Swamynathan et al., 2014). This would create a more *in vivo* like environment in which to provide differentiation cues creating a unified, consistent *in vitro* cell culture system. Supplemented soluble factors, such as cytokines and chemokines, may be required in some form as it is likely cells are unable to successfully thrive on minimal essential media alone (Chase et al., 2010). It is also possible that changes in cell culture media may have an impact on cell behaviour, which is critical to determine for both cellular therapies but also to allow comparison between data derived from *in vitro* studies to those derived from *in vivo* studies.

Furthermore, animal sera is nutrient-rich and may not represent an accurate physiological buffer, leading to altered cellular metabolism in the presence of serum-containing media. Whilst the maintenance of MSCs in serum-containing media results in both the proliferation and differentiation of these cells *in vitro*, there remains a possibility that the artificial conditions in which these cells are maintained impact on cellular behaviour. If *in vitro* studies are to produce meaningful data resembling data obtained in *in vivo* studies, then a more physiologically relevant culture system is required. To provide a more physiologically relevant system to develop CRISPR/Cas9 GM-hTERT MSCs, it was decided to reduce the necessity for serum supplementation. The use of immortalised hTERT MSCs, compared to primary human MSCs, would allow the gradual reduction of serum from culture media, and therefore the Y101 and Y201 hTERT MSC cell lines were deemed as suitable candidates for attempting to develop a serum-free culture system.

3.2 Aims

The aims of the work in this chapter are to remove the dependence of the Y101 and Y201 hTERT MSCs on serum supplementation and to determine the effects of serum removal/replacement on these cells.

The specific objectives of this chapter are to:

- Wean the Y101 and Y201 hTERT MSC cell lines from media containing 10% FBS to chemically defined media if possible
- Determine the effects (if any) of removing/replacing serum on Y101 and Y201 cells specifically looking at survival, proliferation and differentiation

3.3 Methods and Materials

3.3.1 Reduction of serum from MSC maintenance media

The reliance of Y101 and Y201 hTERT MSCs on serum-containing media was reduced during time in culture, with serum reduced every other sub-cultivation of cells. The final concentration of serum in media was reduced by 1% at each step, until the cells were maintained in media containing a final concentration of 1% serum. At the following reduction step, the concentration of serum was reduced to 0.5% and this media used for the maintenance of the serum-reduced hTERT MSCs. To distinguish between hTERT MSCs grown in media containing 10% serum, to those maintained in 0.5% serum, the serum-reduced hTERT MSCs were termed as the Y101.5 and Y201.5 hTERT MSCs, and will be referred to as such throughout

3.3.2 Population Doublings

During routine cell culture 10µL of cells were taken and applied to a haemocytometer to acquire a cell count. The date and cell number were then used across a given number of days to calculate the cumulative population doublings of the cell lines of interest, this was calculated as the log2 ratio of the ratio of the final count (N) to the cells seeded (X). At each timepoint these were summed and plotted to establish cumulative population doublings.

$$PD = log2(\frac{N}{X})$$

3.3.3 Analysis of hTERT MSC differentiation

The comparative ability of the Y101, Y201, Y101.5 and Y201.5 hTERT MSCs to undergo osteogenesis and adipogenesis was analysed using the induction media and histological staining techniques, in addition to enzymatic assays described in section 2.1.3.

3.3.4 Raybiotech Antibody Array

A Human L1000 antibody array (L series, RayBiotech) was used to compare the effect of serum reduction on the secretome of the hTERT MSCs. This array detected 1000 human proteins, a list of targets can be found online (https://www.raybiotech.com/human-l-1000-array-glass-slide-2/). The array selected required cells to be maintained temporarily in serum-free culture conditions to ensure no contamination of the array chip with bovine proteins from the serum. To ensure this would not impact greatly on the viability of the Y201 and Y201.5 hTERT MSCs, both were tested for viability in a survival assay, described below.

3.3.4.1 hTERT Survival Assay

Y201 and Y201.5 hTERT MSCs were seeded in T25s and 24 hours after seeding, media was changed to contain either the usual culture conditions (10% or 0.5% serum) or to DMEM media containing no serum at all. At the time points specified cells were removed from the flasks using trypsin, centrifuged at 1200g for 5 minutes to pellet the cells. Cells were then washed in 1x PBS and centrifuged again. The pellet was then resuspended in 500µL 1xPBS and Sytox Blue added at a final concentration of 1µM. Sytox stained cells were then analysed by flow cytometry until a total of 10,000 events had been collected and a percentage of dead cells obtained.

3.3.4.2 Supernatant collection and protein preparation

$1x10^6$ Y201 and Y201.5 hTERT MSCs were seeded in a T75 flask and the media collected after 48 hours. The supernatant was then centrifuged for 10 minutes at 1000g.

Supernatants were dialysed for 3 hours into 1xPBS at 4°C, the buffer was then exchanged and a further dialysis performed. Dialysed samples were then centrifuged at 10,000rpm for 5 mins and transferred to clean tubes and the protein content assessed using the Pierce BCA assay as previously described. Protein samples were then biotinylated following manufacturer's instructions.

3.3.4.3 Array hybridisation

Arrays were first blocked for 30 minutes before biotinylated samples were added and incubated at room temperature with shaking for 2 hours. Arrays were then washed 3 times with wash buffer I for 10 minutes with shaking before washing with wash buffer II twice for 5 minutes. The resulting arrays were then stained with Cy3-Conjugated Streptavidin for 2 hours and washed further before being scanned by the Genomics Laboratory in the Technology Facility of the University of York.

3.3.4.4 Interpretation of results

Signal intensities were measured using ImageJ and the data analysed by subtracting background levels and normalising to the Y201 array performed to generate a final intensity value. These were then compared between the cell lines of interest and any ≥1.5-fold increase or ≤0.65-fold decrease in signal intensity for a single analyte between samples was deemed significant, as suggested by manufacturers.

Analytes deemed as either upregulated or downregulated were then entered into the Enrichr tool to analyse gene enrichment within the two groups (Chen et al., 2013a; Kuleshov et al., 2016).

3.3.5 Free fatty acid uptake

In order to determine the rate of free fatty acid uptake, which correlates to the lipid metabolism of cells, 6,666 cells/cm^2 were seeded per well in 96 well plates and allowed to adhere overnight in a black plate with a clear flat bottom. Media was then changed to serum-free medium to serum deprive the cells for 2 hours before applying the fatty-acid dye solution (Abcam, UK), made up as per manufacturer's instructions. After an hour incubation, the fluorescence was analysed using a plate reader with a 3x3 matrix bottom read mode at 485/515nm excitation/emission.

3.3.6 RNA-seq analysis

The transcriptome profiles of the Y101 and Y101.5 hTERT MSCs was compared through the use of RNA-seq, and the methods and subsequent analysis of data were described in section 2.1.4.

3.4 Results

3.4.1 Reduction of serum in Y101 and Y201 hTERT MSCs results in altered morphology and reduced growth rates

Serum starvation is typically used as a "shock" mechanism to arrest the cell cycle in order to synchronise cells as once serum is replaced cells all re-enter the cell cycle at approximately the same time. To avoid this shock mechanism and to encourage adaptation to the serum reduced conditions Y101 and Y201 hTERT MSCs gradually had serum removed from the culture medium over a number of weeks. Typically, cells were grown in 1% less serum per 2 passages equating to approximately 1% reduction in serum concentration per week of culture. Over a period of 12 weeks, Y101 and Y201 cells had serum levels reduced to 0.5% serum which was able to sustain continued viable growth. Further reduction of serum to a final concentration of 0% resulted in total cell death after 48 hours in both cell lines (results not shown). The addition of 1% BSA and 1% ITS was able to sustain cell culture until passaging whereupon cell growth arrested (results not shown). It was decided to proceed with the 0.5% cell culture conditions to establish the effects of serum reduction on the Y101 and Y201 hTERT MSCs. These "weaned" hTERT MSCs were termed the Y101.5 and Y201.5 cells to identify both the original cell line and the reduced serum levels. Often the Y101 and Y201 hTERT MSCs are referred to as wild-type (WT) hTERT MSCs in this chapter to distinguish them from the reduced-serum hTERT MSC lines.

Initially, the serum reduced cells were assessed for any morphological changes by phase microscopy and crystal violet staining. Serum contains a number of proteins and growth factors, some of which may be required for cell adherence therefore it was important to determine whether the Y101.5 and Y201.5 demonstrated any outward changes as a result. Figure 3.4.1A shows a comparison of the Y101.5 and Y201.5 cells with their WT counterparts. Moderate changes in morphology were observed in the Y101.5 and Y201.5 cells with an apparent increase in cell processes and a generally more rounded cell body, compared to the typical fibroblastic profile of the Y101 and Y201 cells. Despite these changes, no overall change in cell diameter was seen when analysed by the Vi-CELL cell counter and cell viability analyser. (Figure 3.4.1B).

Furthermore, the reduction in serum did not impact on cell viability, with no significant changes apparent between serum culture conditions (Figure 3.4.2A). Finally, it was apparent during the adaptation of the Y101.5 and Y201.5 cells to the reduced serum content that the growth rates of the cells reduced as the serum content dropped. After the serum reduction was complete, the cells were counted every passage to determine the cumulative population doubling rate, summarised in Figure 3.4.2B. Typically, the Y101 cells have a faster proliferation than the Y201 cells and this was

evident in the population doubling counts. Additionally, both the Y101.5 and Y201.5 cells had a slowed growth rate leading to an increased population doubling times. The reduced growth rate meant the 0.5% hTERT MSC cell lines had a very similar growth rate dissimilar to their WT counterparts.

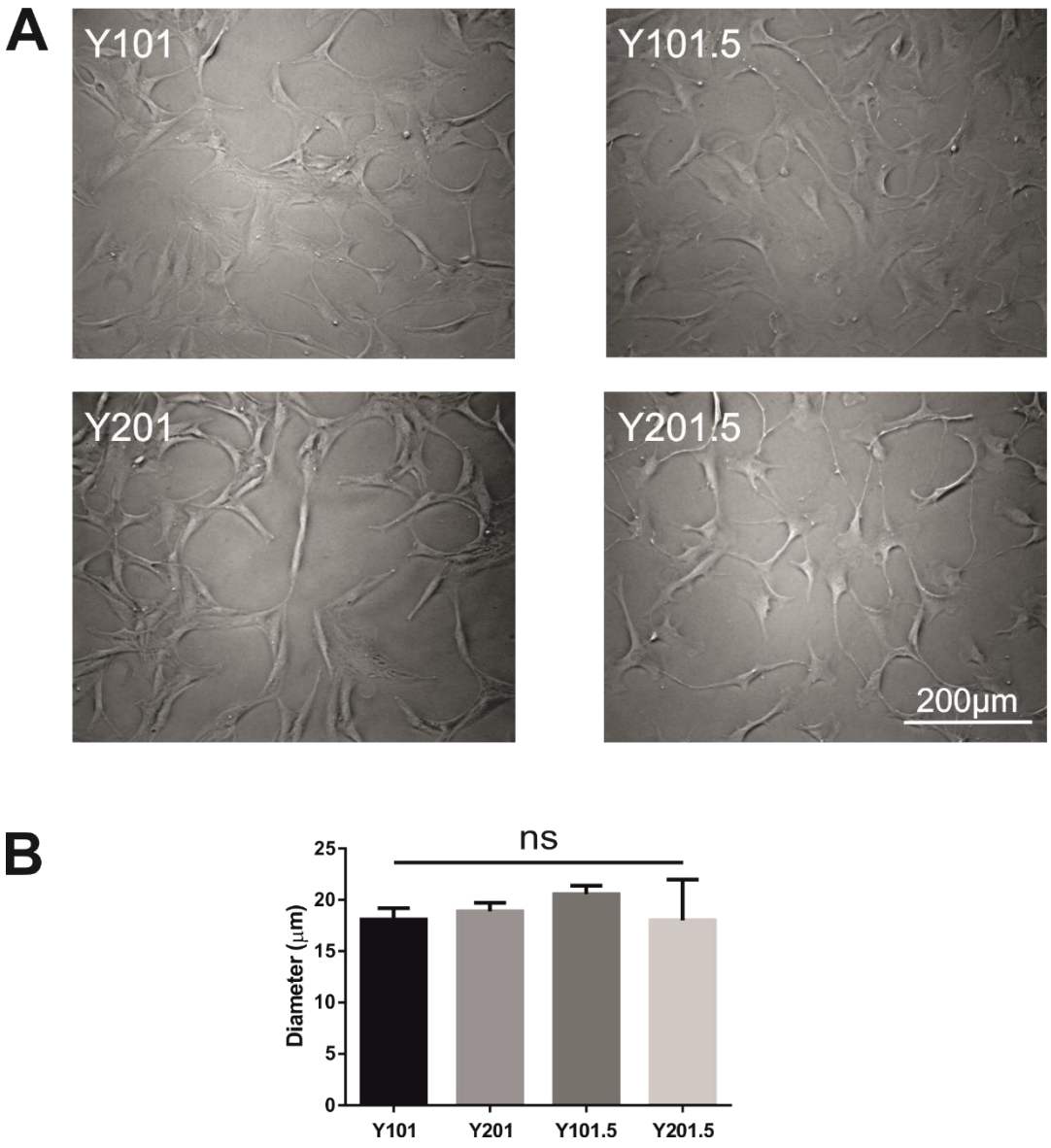

Figure 3.4.1: Analysis of cell shape and diameter of low serum hTERT MSCs

hTERT MSCs were weaned from 10% FBS supplemented DMEM to 0.5% FBS supplemented DMEM over 12 weeks. A) Both the newly weaned hTERT MSCs and the original hTERT MSCs were plated at 2x 10^4 cells/cm^2 and representative images of the cellular morphology taken by phase microscopy. B) Cell diameter of detached cells was also analysed by a Vi-CELL counter during culture and summarised in a bar chart. Values = mean ± SD, n=3.

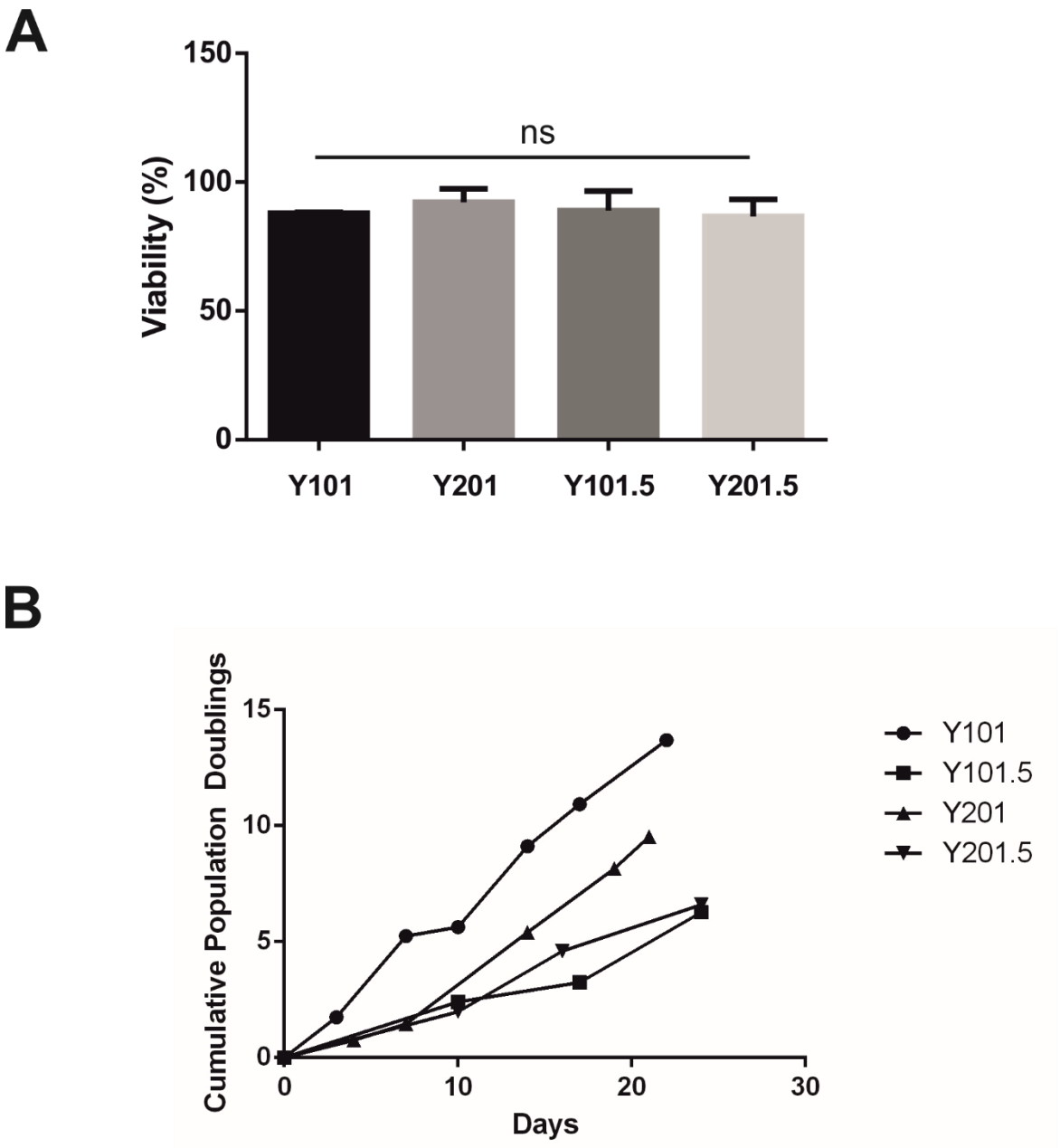

Figure 3.4.2: Viability and growth analysis of low serum hTERT MSCs and WT hTERT MSCs

During sustained culture, the cell number of both the low serum hTERT MSCs and WT hTERT MSCs were recorded every passage. A) The viability of the cells was also recorded and summarised in a bar chart. Values = mean ± SD, n=3 B) Recorded cell numbers were then used generate the cumulative population doublings over 3-4 weeks.

3.4.2 Y101.5 and Y201.5 cells have a reduced propensity for adipogenic differentiation

As previously discussed, the proliferation rate, differentiation potential and general behaviour of cells grown in culture can all be altered by changes in serum concentration or even serum batches. After establishing a difference in proliferation rates it was apparent the differentiation capacities of the Y101.5 and Y201.5 cells would need to be tested.

Initially, the Y101.5 and Y201.5 hTERT MSCs were seeded at confluency and stimulated to undergo adipogenesis using an adipogenic cocktail. These samples were stimulated for 21 days before fixing the cells with PFA and staining with Oil Red O to identify lipid droplet formation. The Y101, Y101.5, Y201 and Y201.5 hTERT MSCs were stimulated to undergo adipogenesis and demonstrated an ability to form lipid droplets in response to the stimulative cocktail (Figure 3.4.3). Y201 hTERT MSCs have an increased adipogenic potential in comparison to the Y101 hTERT MSCs and this is reflected in both the number and size of lipid droplets produced during the timecourse (James et al., 2015).

However, the adipogenic potential of both the Y101.5 and Y201.5 hTERT MSCs were markedly reduced in comparison to their WT counterparts. Both the Y101.5 and Y201.5 hTERT MSCs appeared to have fewer lipid droplets forming after supplementation. The Oil Red O staining was eluted using 100% isopropanol, however the small number of lipid droplets in all samples meant no significant difference could be determined between any of the conditions using these techniques (results not shown).

In order to determine whether there was any significance between the adipogenic potential of the weaned hTERT MSCs compared to the WT hTERT MSCs, ImageJ was used to analyse the black/white pixel ratio (Figure 3.4.4). In comparison to the low contrast of the cells, the lipid droplets have a much higher contrast and therefore can be made to be black against a white background through image manipulation. This was able to show that both the Y101.5 and Y201.5 hTERT MSCs have significantly fewer black pixels (assumed to be lipid droplets) than their WT counterparts. This analysis also showed no significance between the Y101 basal and Y101 adipogenic samples due to large amounts of background interference in the Y101 basal samples.

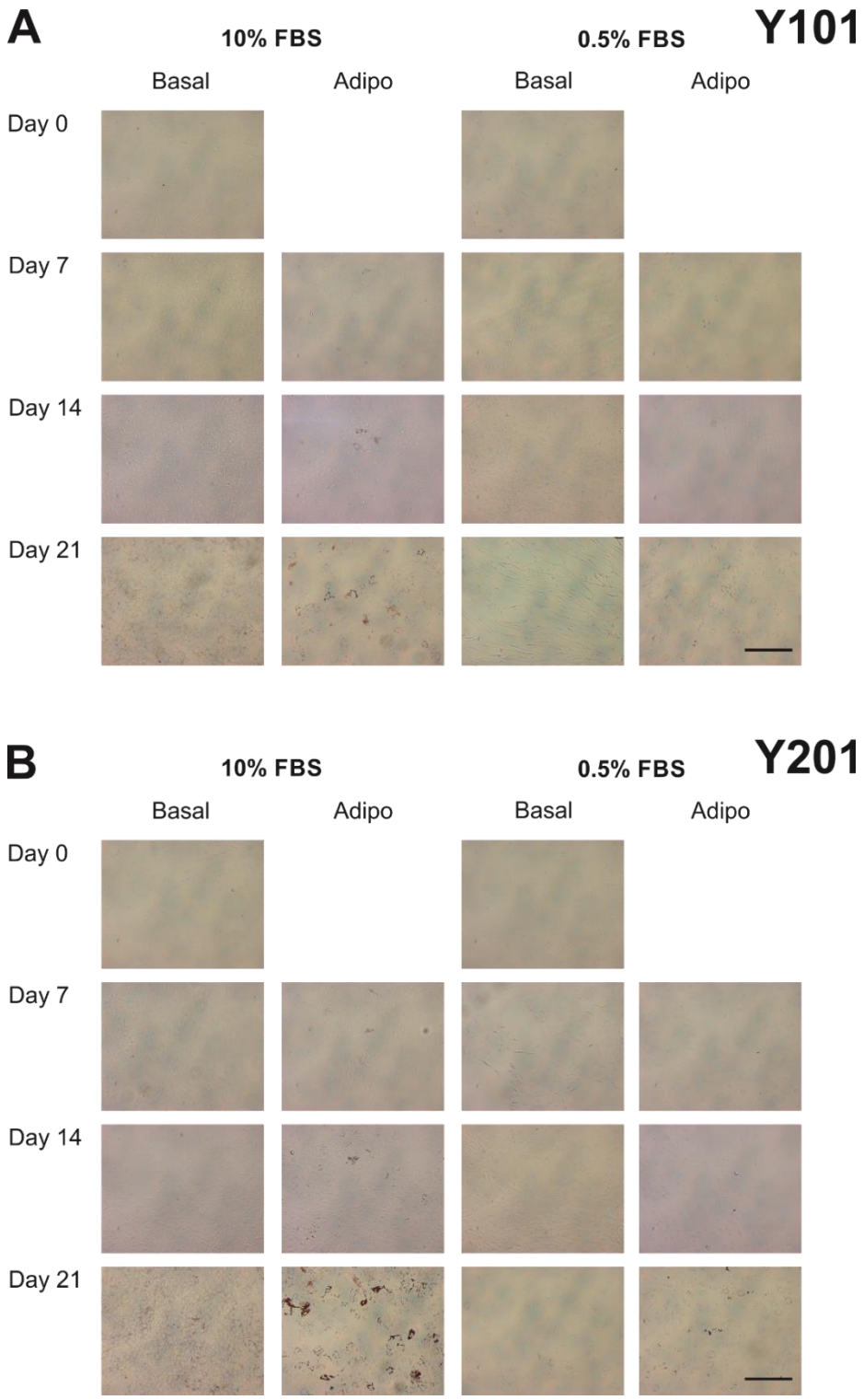

Figure 3.4.3: Low serum hTERT MSCs have decreased adipogenic potential

Oil Red O staining of hTERT MSCs after 21 days adipogenic treatment with either 10% serum supplementation or 0.5% serum supplementation throughout the timecourse. Both panels show representative brightfield microscopy images of lipid droplet accumulation. Scale bar = 250µm.

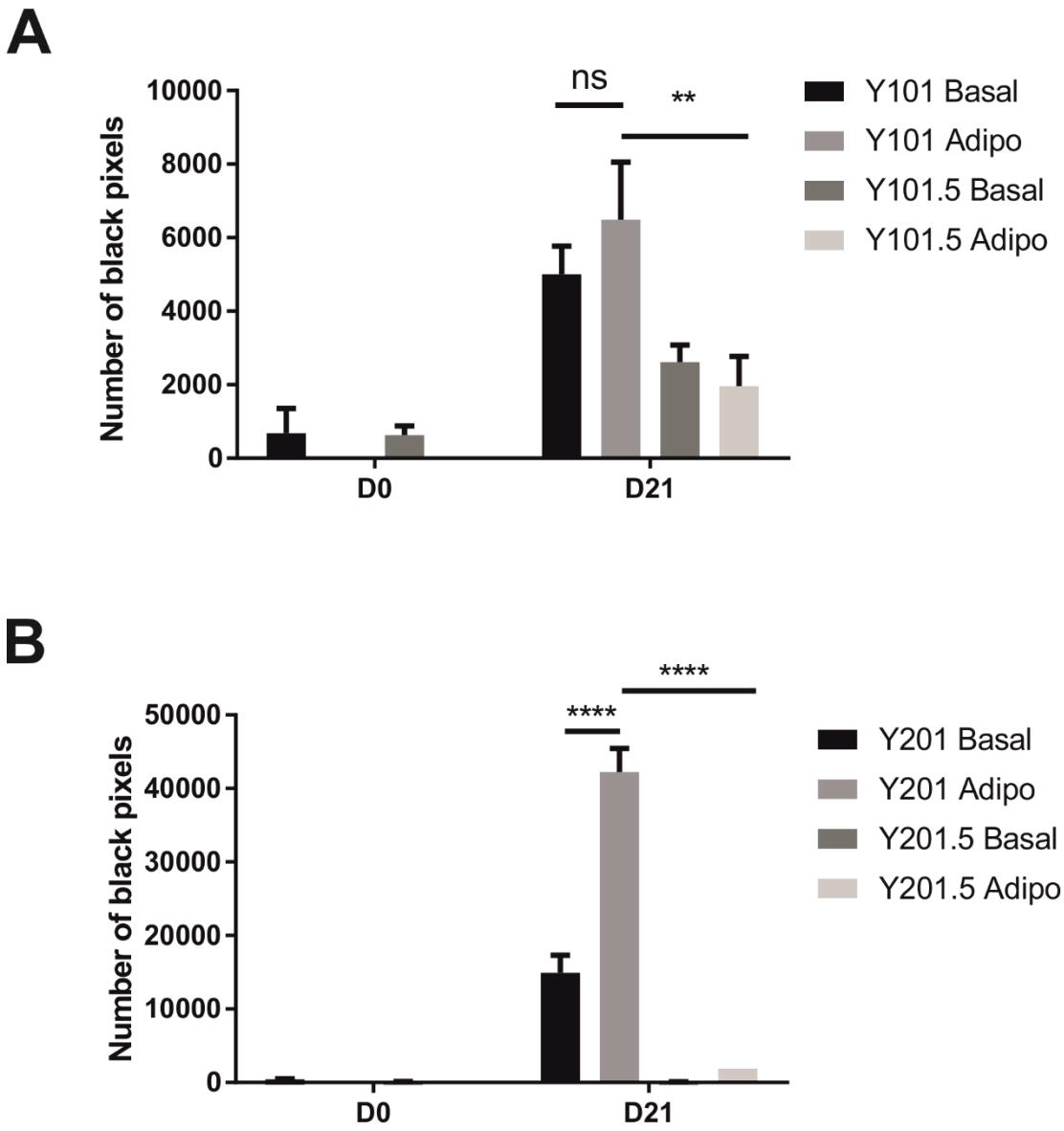

Figure 3.4.4: Black/white pixel analysis gives further evidence for reduced adipogenisis in weaned hTERT MSCs

ImageJ was used to set threshold values resulting in lipid droplets appearing black against a white cellular background. Black pixels were then counted and plotted in bar charts for both A) Y101 and Y101.5 hTERT MSCs and B) Y201 and Y201.5 hTERT MSCs. Values = mean ± SD, n=3 with statistical significance obtained using 2 way RM ANOVA with Tukey's multiple comparisons.

3.4.3 Y101.5 and Y201.5 hTERT MSCs have an increased osteogenic potential

In the previous section, it appeared the weaned hTERT MSCs had a reduced adipogenic capacity in comparison to the WT hTERT MSCs. It has previously been hypothesised that an inverse relationship exists between adipogenesis and osteogenesis, with one process occurring at the expense of the other (James, 2013). It was therefore decided to analyse the capacity of the Y101.5 and Y201.5 hTERT MSCs to undergo osteogenic differentiaton.

In a similar manner to adipogenic assays, the hTERT MSCs were seeded at confluency and differentiated towards osteoblasts using a classical osteogenic stimulative cocktail containing L-ascorbic acid, dexamethasone and β-glycerophosphate. After 21 days of differentiation, the calcium deposited during the timecourse was stained using Alizarin Red and imaged using a stereomicroscope to best observe the overall levels of calcium developed.

All of the four hTERT MSC lines (Y101, Y201, Y101.5 and Y201.5) analysed were able to differentiate down the osteogenic lineage as evidenced by increasing amounts of calcium deposited during the timecourse (Figure 3.4.5). Both the WT hTERT MSC lines showed some calcium deposition during the basal samples but this was far less in comparison to the osteogenic samples. The weaned hTERT MSCs showed far less basal calcium deposition but both contained increasing amounts of calcium during the osteogenesis. The Y201.5 hTERT MSCs showed similar levels of calcium deposition during the osteogenic timecourse compared to the Y201 hTERT MSCs. The Y101.5 hTERT MSCs however, demonstrated a notably increased level of calcium deposition compared to the Y101 hTERT MSCs, particularly in the earlier timepoints (day 7 and day 14).

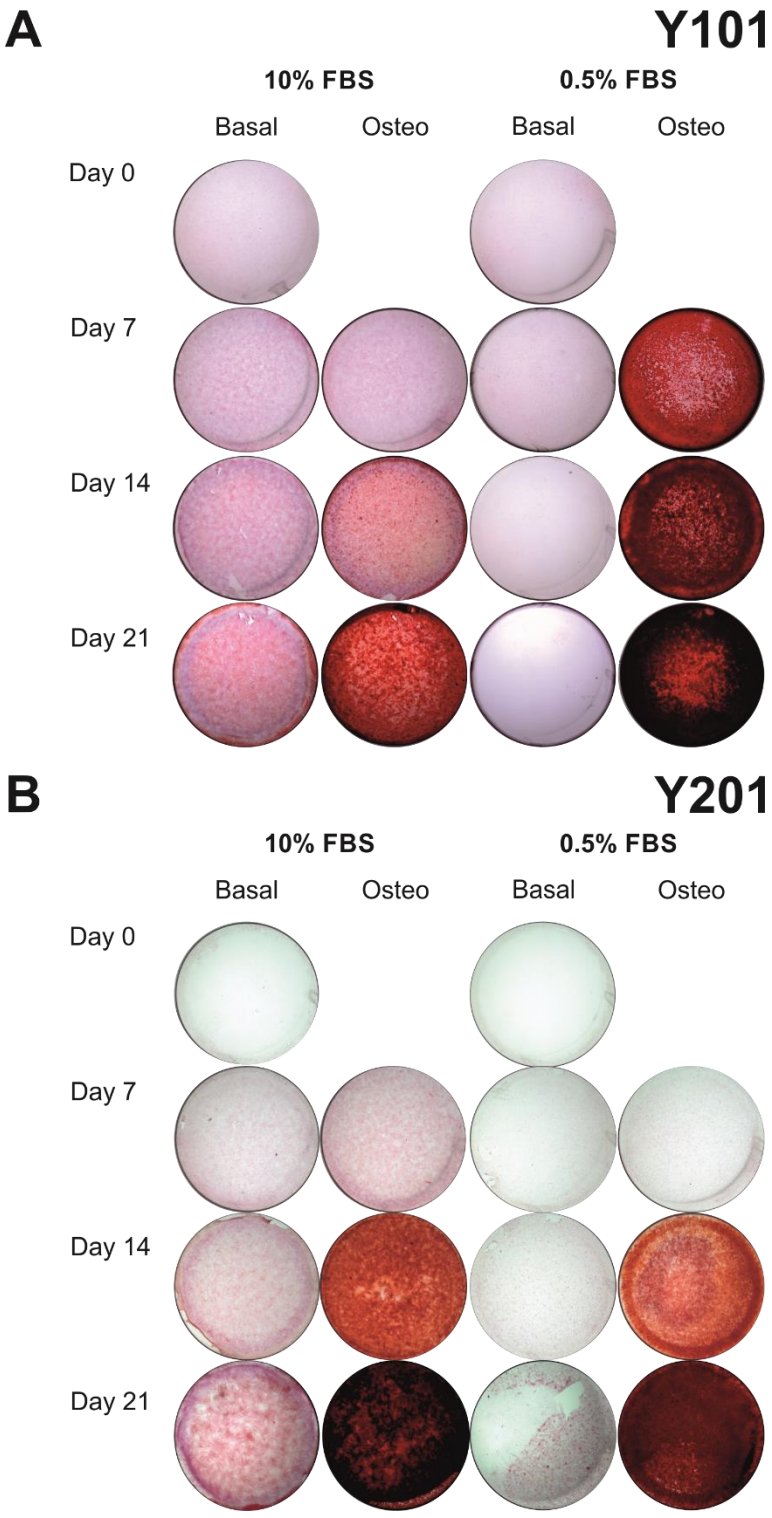

Figure 3.4.5: Alizarin Red staining of hTERT MSCs show low serum hTERT MSCs have increased osteogenic potential

Y101, Y101.5 (A), Y201 and Y201.5 (B) hTERT MSCs were cultured for 7, 14 and 21 days in osteogenic inductive media before staining with Alizarin red to stain for calcium deposition. Stereomicroscopy was used to image the well and representative images are shown.

To provide greater insight into alterations in calcium deposition during osteogenesis, the Alizarin Red stain was eluted with cetylpyridinium chloride (CPC) and the absorbance read using a plate reader. It became evident that the Y101.5 hTERT MSCs in particular were extremely capable of calcium deposition during osteogenesis (Figure 3.4.6). In fact, these cells deposited more calcium over 7 days than the Y101 hTERT MSCs were able to produce over the entire time course. The Y201.5 hTERT MSCs on the other hand demonstrated comparable calcium deposition to the Y201 hTERT MSCs until the last timepoint where the Y201.5 cells had deposited significantly more calcium.

This trend was also reflected when an alternative histological stain was used. ALP activity was analysed in addition to phosphate deposition using von Kossa staining with silver nitrate (Figure 3.4.7). Von Kossa staining reacts with the phosphate groups present in the depositions laid down by the differentiating hTERT MSCs, which is therefore taken as an indication that mineral deposition is occurring.

Basal ALP activity could be detected throughout the timecourse in both the Y101 and Y201 hTERT MSCs, but minimal basal ALP activity could be seen in the weaned hTERT MSCs (Figure 3.4.7). Similarly to the Alizarin Red staining (Figure 3.4.5), there was substantially more ALP activity present in the osteogenic samples of all the hTERT MSC lines tested. Increased mineralisation could also be seen in all samples during the osteogenic timecourse, with negligible von Kossa staining seen in the basal samples. The von Kossa phosphate staining in the weaned hTERT MSCs was considerably increased in comparison to their wild type counterparts, with a much more noticeable difference compared to the calcium stained by Alizarin Red staining.

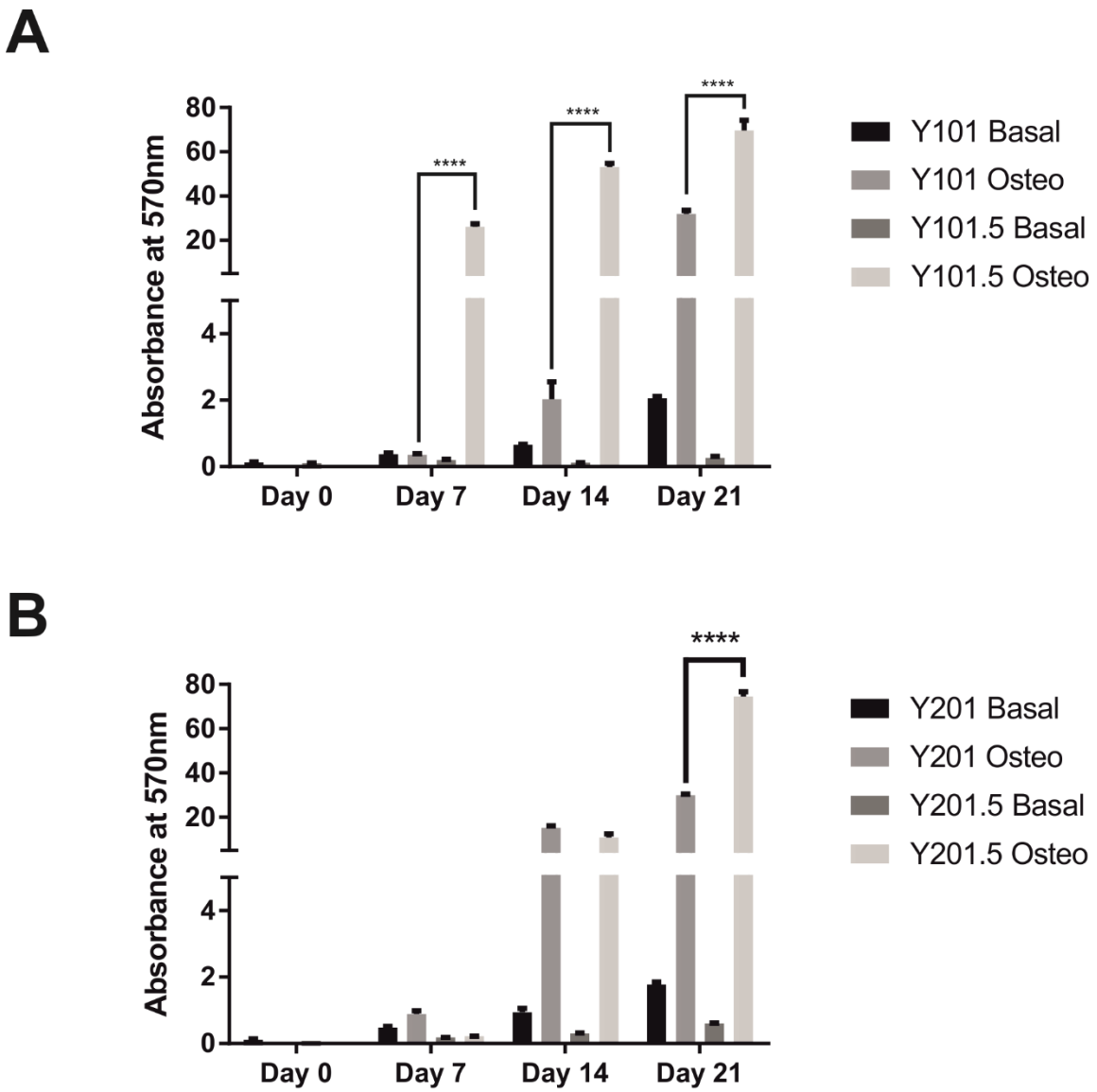

Figure 3.4.6: CPC elution of Alizarin Red staining for osteogenic induced hTERT MSCs over a timecourse

CPC elution was performed for 2 hours before the absorption of the Alizarin Red stain was read on a plate reader for Y101 and Y101.5 hTERT MSCs (A) and the Y201 and Y201.5 hTERT MSCs (B). Values = mean ± SD, n=3 with statistical significance obtained using 2 way RM ANOVA with Tukey's multiple comparisons.

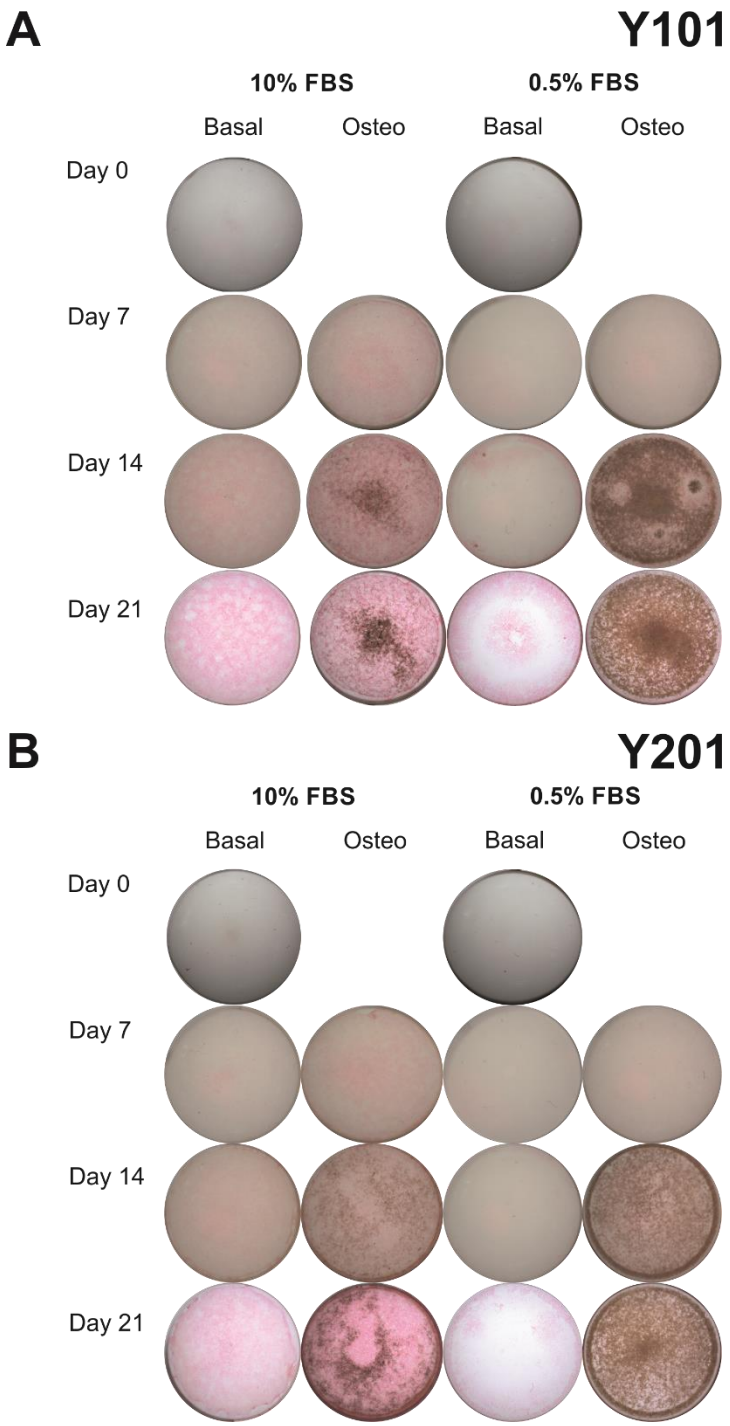

Figure 3.4.7: Alkaline phosphatase and von Kossa histological staining of weaned hTERT MSCs compared to WT hTERT MSCs.

Y101, Y101.5 (A), Y201 and Y201.5 (B) hTERT MSCs were cultured for 7, 14 and 21 days in osteogenic inductive media before staining for alkaline phosphatase activity and von Kossa histological stains to stain for calcium deposition. Stereomicroscopy was used to image the well and representative images are shown.

3.4.4 Mechanistic analyses of increased osteogenic potential in reduced serum hTERT MSCs

The reduction in serum appears to have shifted the differentiation potential of the hTERT MSCs towards osteogenesis at the expense of adipogenesis which may be due to a change in cellular behaviour as a response to the reduction in serum. However, it is also possible that FBS contains an inhibitor which is restricting the levels of osteogenesis, therefore removing the serum (and thus the inhibitor) increases the osteogenic ability of the hTERT MSCs.

To establish which of these hypotheses was more likely a p-Nitrophenyl Phosphate (PNPP) assay was performed analysing ALP activity. Y101/Y201 hTERT MSCs were differentiated with 0.5% serum containing media and Y101.5/Y201.5 hTERT MSCs differentiated in 10% serum containing media. This was then compared to the typical culture media used for each cell type. Figure 3.4.8 summarises the ALP activity during a 9 day timecourse and alterations caused by the changes in serum levels. Both the Y101.5 and Y201.5 cells display high ALP activity in osteogenic conditions throughout the time course which is decreased only slightly when the weaned cells were differentiated in medium containing 10% serum at the majority of the timepoints. However, this additional serum supplementation did not reduce ALP levels down to those observed in the Y101/Y201 hTERT MSCs. Conversely, reducing the serum content in the osteogenic media to 0.5% did not appear to significantly increase ALP activity in the Y201 hTERT MSCs. It would appear there is an increase in ALP activity in the Y101 hTERT MSCs when serum was reduced in both basal and osteogenic conditions, however this did not reach the activity levels of the Y101.5 hTERT MSCs when osteogenesis is stimulated. It would appear therefore that serum does not contain factors inhibitory to osteogenesis and that there is a change in cellular behaviour as a result of adaptation to reduced serum conditions.

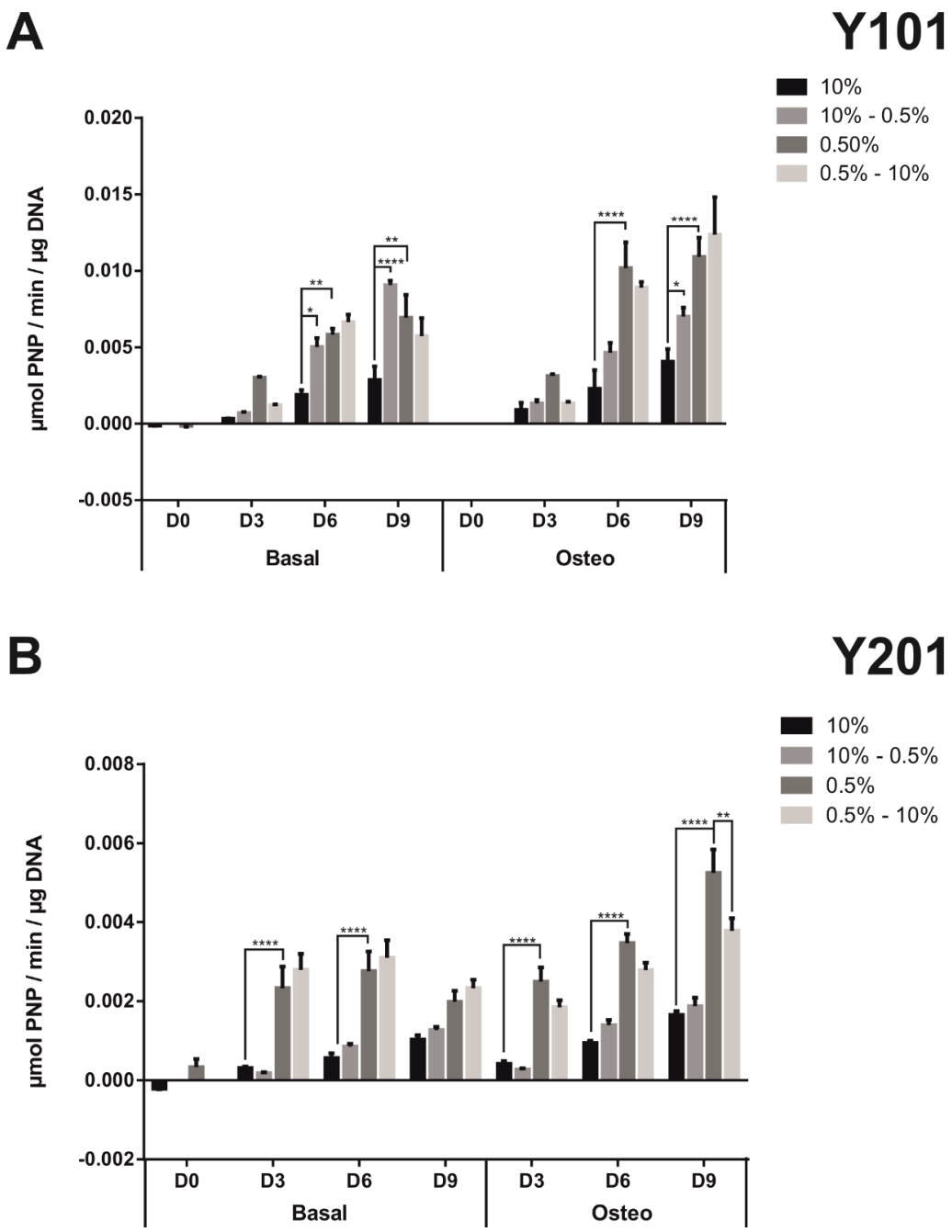

Figure 3.4.8: Reduction of serum alone is not suffcient to increase ALP activty comparative to activity in weaned hTERT MSCs

A) Y101 and Y101.5 hTERT MSCs and B) Y201 and Y201.5 hTERT MSCs were plated at confluency in 96 well plates and differentiated in osteogenic media for up to 9 days. ALP activity was normalised to cell number and is listed as (µmol PNP/min/µg DNA). Y101/Y201 hTERT MSCs were either differentiated in 0.5% serum containing media (10% - 0.5%) or in standard differentiation media (10%). Y101.5/Y201.5 hTERT MSCs were differentiated in media containing 10% serum (0.5% - 10% or in reduced serum differentiation media (0.5%). Values = mean ± SD, n=6 with statistical significance obtained using 2 way RM ANOVA with Tukey's multiple comparisons.

3.4.5 Transcriptome analysis shows Y101.5 hTERT MSCs to have increased lipogenic metabolism and alterations in secretome

The hTERT MSCs weaned to survive in 0.5% FBS appear to have adapted to the low serum conditions and altered their cellular behaviour due to the differences in supplement levels. In addition, the weaned cells display significantly enhanced osteogenic capacity, at the expense of adipogenesis, particularly noticeable in the Y101.5 MSCs. To help identify the molecular mechanisms involved, transcriptomic analyses were performed on the Y101.5 and Y101 hTERT MSCs and pathway analysis performed using Enrichr for comparative analysis.

Overall a total of 273 transcripts were found to be upregulated and 237 transcripts downregulated in the Y101.5 hTERT MSCs compared to the Y101 hTERT MSCs. These were deemed differentially regulated when both cell types analysed had reads per kilobase of transcript per million mapped reads (RPKM) > 0, an adjusted p value < 0.05 and a log2 fold change > +/-1. A number of transcripts were only found in either one of the cell types. The majority of transcripts altered were protein coding with a number of non-coding RNAs also present, summarised in Figure 3.4.9.

Gene ontology analysis of the transcripts by biological process showed downregulated transcripts in the Y101.5 hTERT MSCs were predominantly in processes involved in the regulation and progression of the cell cycle. Figure 3.4.10 shows the top 10 most downregulated biological processes within the Y101.5 hTERT MSCs, and the networks below demonstrate the association between the various affected pathways. The more links between the processes the more related the processes. The downregulated biological processes are all largely linked and involved in the progression of the mitosis and the cell cycle. It had already been previously determined that the growth rates of the Y101.5 and Y201.5 hTERT MSCs was markedly lower than the wild type hTERTs, likely due to this downregulation of mitosis related pathways. It was also notable by gene set enrichment analysis (GSEA) that transcripts in the G2M checkpoint and targets of E2F (both critical pathways involved in the cell cycle) were highly enriched in the Y101 hTERT MSCs but not in the Y101.5 hTERT MSCs.

Conversely, the most predominant biological processes upregulated in the Y101.5 hTERT MSCs were involved in metabolism, mainly involved in the synthesis and metabolism of fatty acids, steroids and alcohols. This switch in metabolism is likely due to the lack of FBS present in the growth media forcing the cells to adapt their metabolism to suit these conditions. This was also reflected in the pathways that were upregulated, where the primary pathways were involved in cholesterol biosynthesis, and the metabolism of lipids and lipoproteins (Figure 3.4.11). Further analysis of transcripts using the Reactome 2016 pathways also showed a majority of transcripts upregulated

were in pathways involved in metabolism (Figure 3.4.12). In fact, the most highly upregulated Reactome pathway was “Metabolism of lipids and lipoproteins”, other pathways identified were involved in cholesterol metabolism and synthesis in addition to the genes activated by sterol regulatory element binding proteins (SREBP) – the master transcription regulators of lipid homeostasis. Supportive of an increased lipogenic metabolism, a free fatty acid (FA) uptake assay demonstrated the Y101.5 hTERT MSCs have reduced their requirements for FA supplementation (Figure 3.4.13). Over 1 hour, the Y101.5 hTERT MSCs take up significantly less FA than their wild type counterparts after serum starvation.

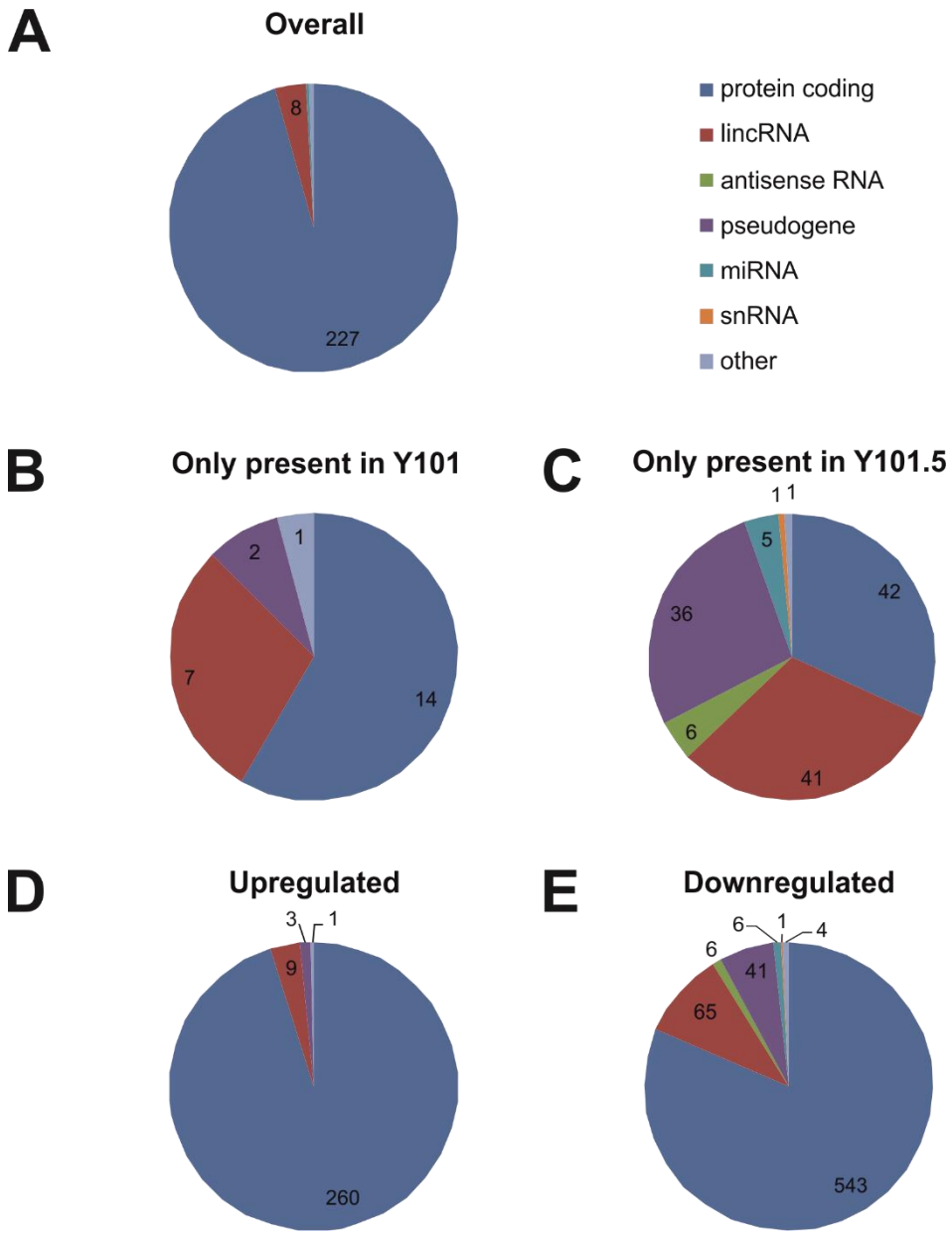

Figure 3.4.9: Summary of transcripts differentially regulated in Y101.5 hTERT MSCs compared to Y101 hTERT MSCs

Numbers of differentially regulated transcripts identified using RNA-seq summarising (A) the overall numbers of transcripts differentially regulated in the Y101.5 hTERT MSCs compared to the Y101 hTERT MSCs. Transcripts only present in (B) Y101 cells or (C) Y101.5 hTERT MSCs. A breakdown of transcripts (D) upregulated in Y101.5 hTERT MSCs or (E) downregulated in Y101.5 hTERT MSCs.

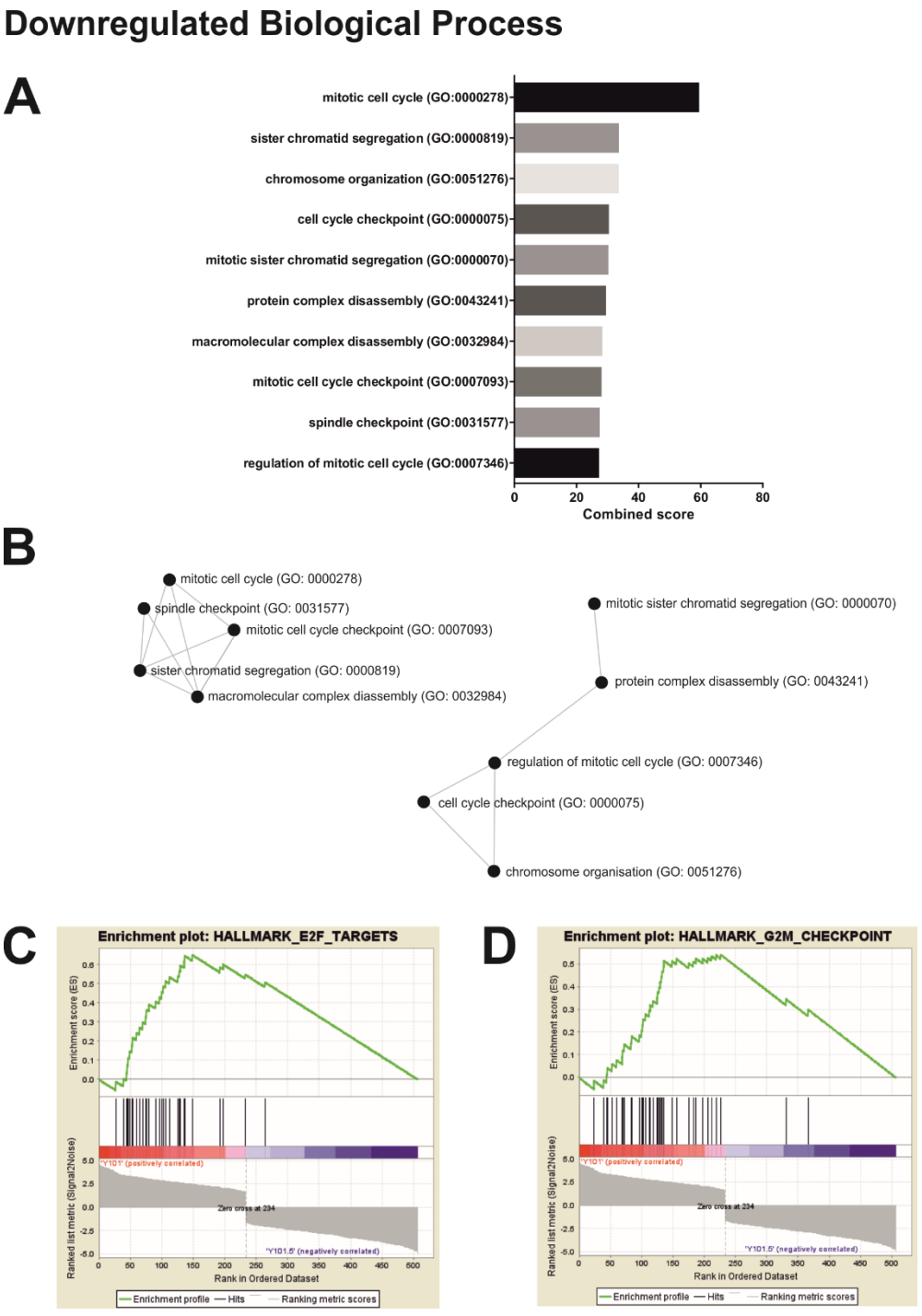

Figure 3.4.10: Gene ontology analysis of downregulated Y101.5 hTERT MSCs by biological process

Enrichr analysis showed downregulated biological processes were typically involved in cell cycle progression and mitosis. (A) Top 10 downregulated biological processes and (B) networks showing the links between the processes identified. These were identified using combined score as defined Enrichr. GSEA analysis also showed positive transcript enrichment in the (C) E2F targets and (D) G2M checkpoint targets of the Y101 hTERT MSCs.

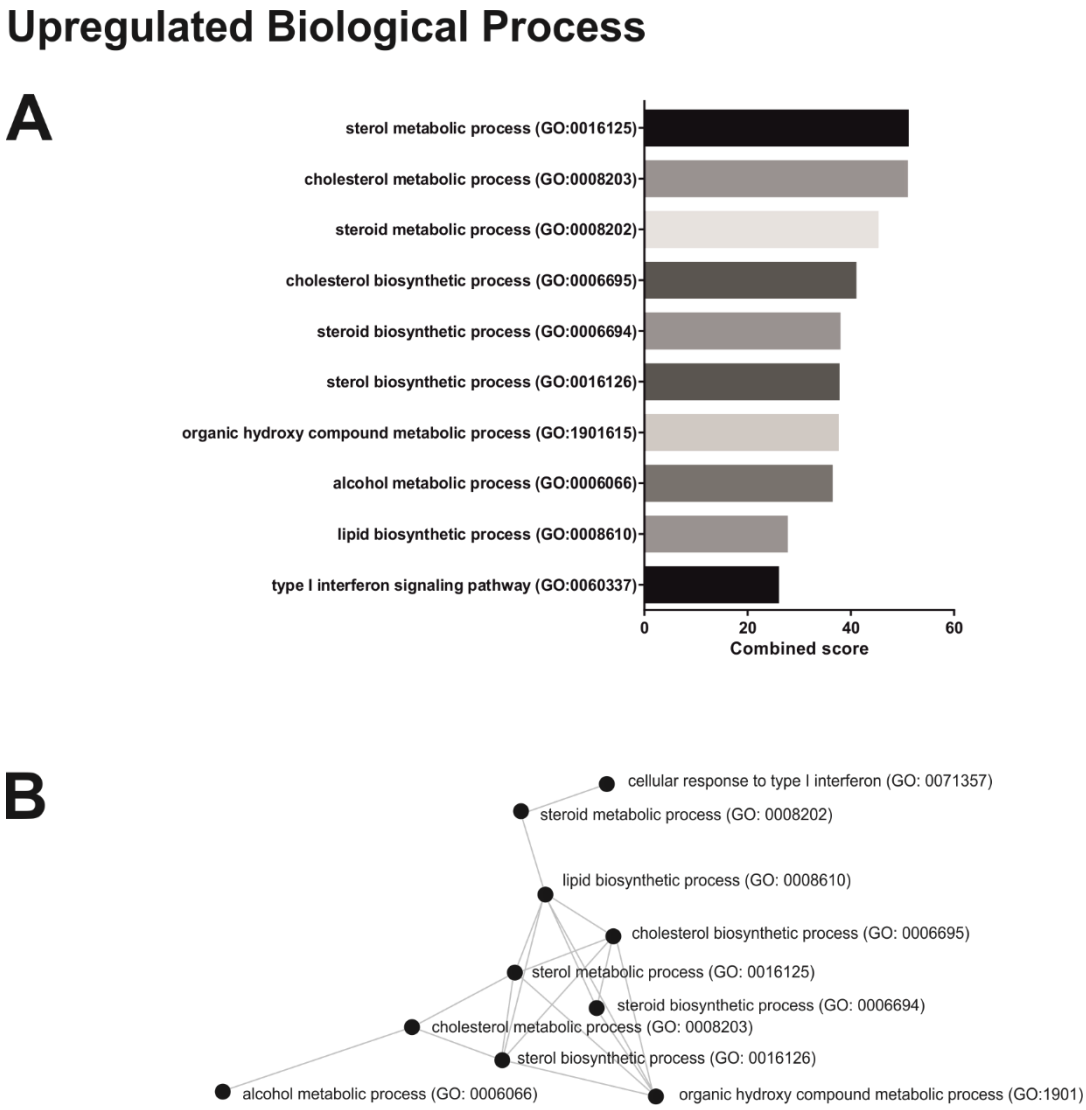

Figure 3.4.11: Gene ontology analysis of upregulated Y101.5 hTERT MSCs by biological process

Enrichr analysis showed the majority of upregulated biological processes were related to lipogenesis, cholesterol and alcohol synthesis. (A) Top 10 upregulated biological processes and (B) networks showing the links between the processes identified. These were identified using combined score as defined Enrichr.

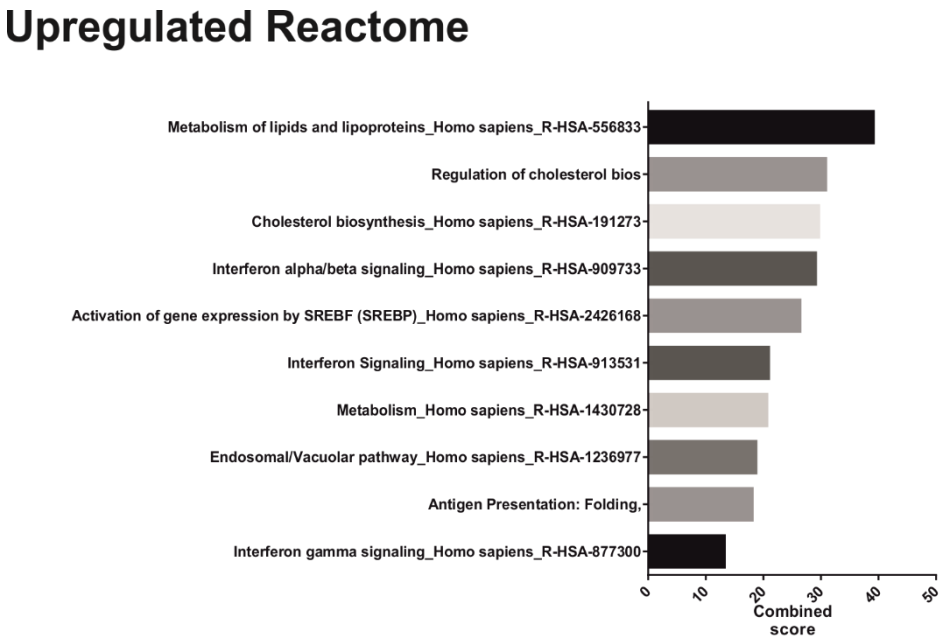

Figure 3.4.12: Top 10 upregulated reactome pathways as determined by Enrichr in the Y101.5 hTERT MSCs.

Enrichr analysis showed the majority of upregulated reactome processes were also related to metabolic processes in addition to a number of interferon and immune regulation processes.(A). These were identified using combined score as defined Enrichr.

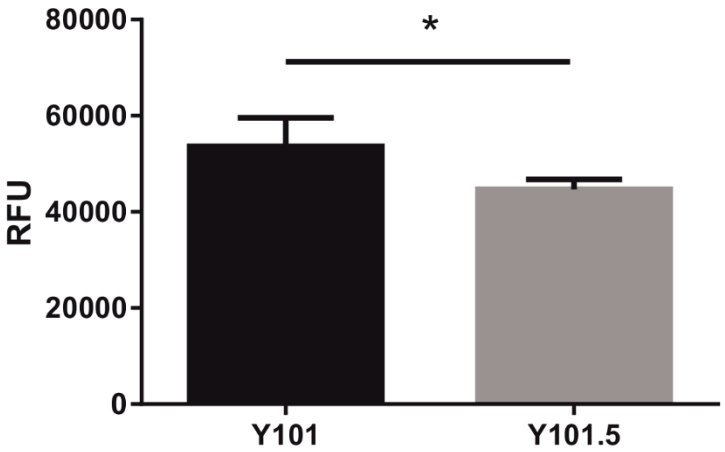

Figure 3.4.13: Analysis of fatty acid uptake in Y101 and Y101.5 hTERT MSCs after serum starvation

Cells were plated and allowed to adhere overnight before starving of serum for 2 hours. Analysis of fatty acid uptake was then performed by supplementing a fluorescent tagged fatty acid before washing the cells and reading the remaining fluorescence. Values = mean ± SD, n=6 with statistical significance obtained using 2 way RM ANOVA with Tukey's multiple comparisons.

3.4.6 Y101.5 hTERT MSCs secrete pro-osteogenic factors that aid osteogenesis

During transcript analysis it was noted that a number of upregulated transcripts encoded proteins secreted into the extracellular space, and these were predominantly found to be within extracellular vesicular exosomes (Figure 3.4.14). It was therefore hypothesised that the weaned hTERT MSCs were likely secreting proteins aimed at aiding both their survival and differentiation. In an attempt to determine which proteins were being secreted at biologically relevant levels, an antibody array was performed on media conditioned by either Y201 or Y201.5 hTERT MSCs. These cells were chosen as they are the most similar to a "true mesenchymal stem cell" and therefore any targets identified may be used in developing a serum-free media for use with both primary and immortalised MSCs.

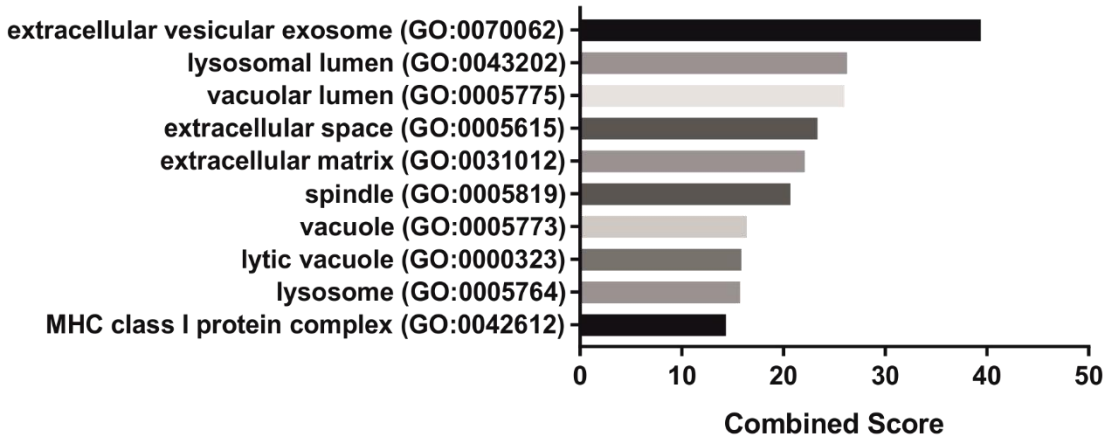

Figure 3.4.14: Cellular component analysis of all significantly differentially regulated transcripts identified by RNA-seq

All transcripts identified as significantly differentially regulated were analysed for the locations of gene products, the top 10 by combined score were listed in a bar chart.

The array required cells to be cultured without serum prior to analysis in order to avoid contaminating the array chip with serum related proteins. Y201 and Y201.5 hTERT MSCs were seeded into T25 flasks and cultured for 48 hours either in normal culture conditions or without serum, after which cells were trypsinised and stained with Sytox Blue. Sytox Blue is a live/dead exclusion dye therefore cells with perturbed membranes would stain positively, indicating the likelihood of a dead cell. Sytox blue staining was analysed by flow cytometry and is summarised in Figure 3.4.15. This demonstrated all cells retained high viability at the timepoints tested in serum free media, with a slight drop in viability seen in the Y201.5 hTERT MSCs at 48 hours. It was decided to proceed with the recommended time of 48 hours for the array analysis.

After the array was read and the data normalised as per manufacturer's instructions it became apparent there were large numbers of non-secreted targets registering as positively expressed. These were also registering as significantly different between the Y201 and Y201.5 hTERT MSCs, despite the fact no non-secreted targets should be present as the array chip was treated with conditioned media. The top 25 upregulated and downregulated targets are listed in Figure 3.4.16 with the non-secreted targets marked. The array data was thus adjusted to remove all targets that were not secreted into the extracellular space leaving behind only the targets relevant to this study and the new top 25 upregulated and downregulated targets were again listed (Figure 3.4.17). Figure 3.4.18 lists the top 10 cellular components where the gene products can be located, where the predominant location is now the extracellular space. This adjusted data was then analysed again using Enrichr to determine what biological processes and pathways the secreted proteins were involved in.

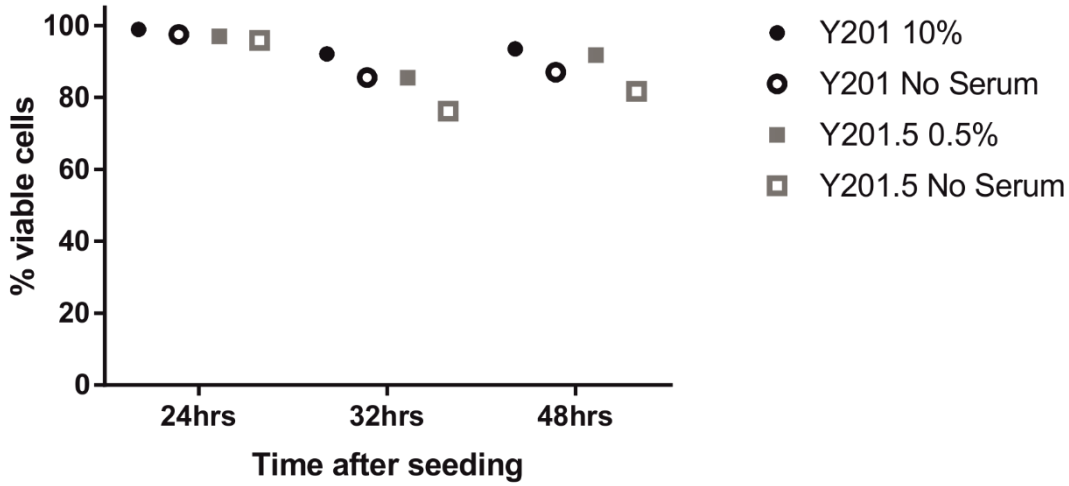

Figure 3.4.15: Sytox blue staining of Y201 and Y201.5 hTERT MSCs in standard culture conditions and serum-free culture conditions

Cells were seeded into T25 flasks and cultured either in standard conditions or in serum-free conditions before staining with Sytox Blue. Cells were analysed at varying timepoints to identify whether increased time in serum-free media would reduce viability.

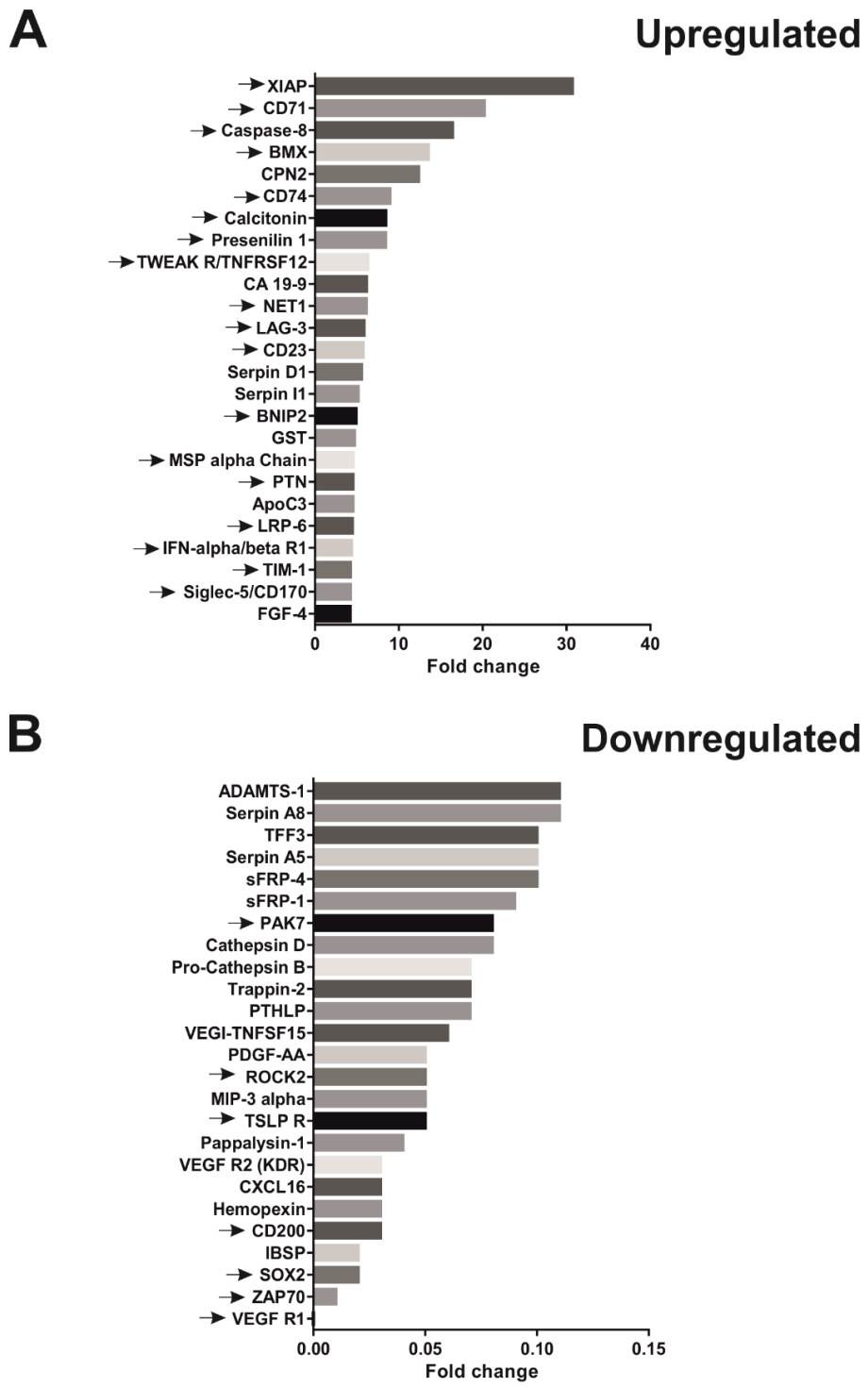

Figure 3.4.16: Significantly upregulated or downregulated proteins in Y201.5 hTERT MSCs compared to Y201 hTERT MSCs identified by antibody array

Proteins identified as significantly upregulated (A) or downregulated (B) according to manufacturer's instructions from the antibody array. All proteins deemed to not be secreted, as identified by Genecards, are marked with an arrow.

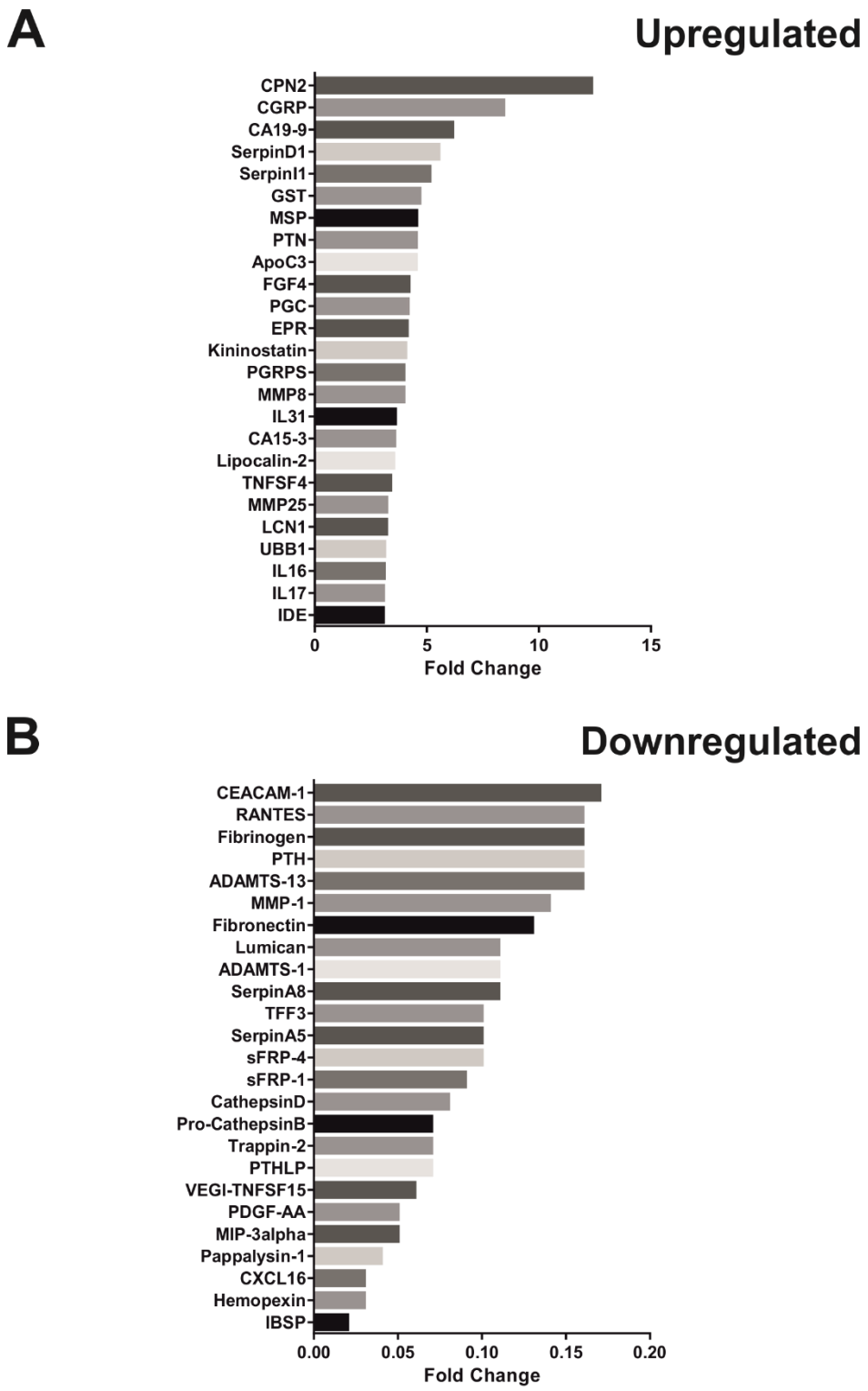

Figure 3.4.17: Significantly upregulated or downregulated secreted proteins in Y201.5 hTERT MSCs compared to Y201 hTERT MSCs identified by antibody array

Secreted proteins identified as significantly upregulated (A) or downregulated (B) according to manufacturer's instructions from the antibody array.

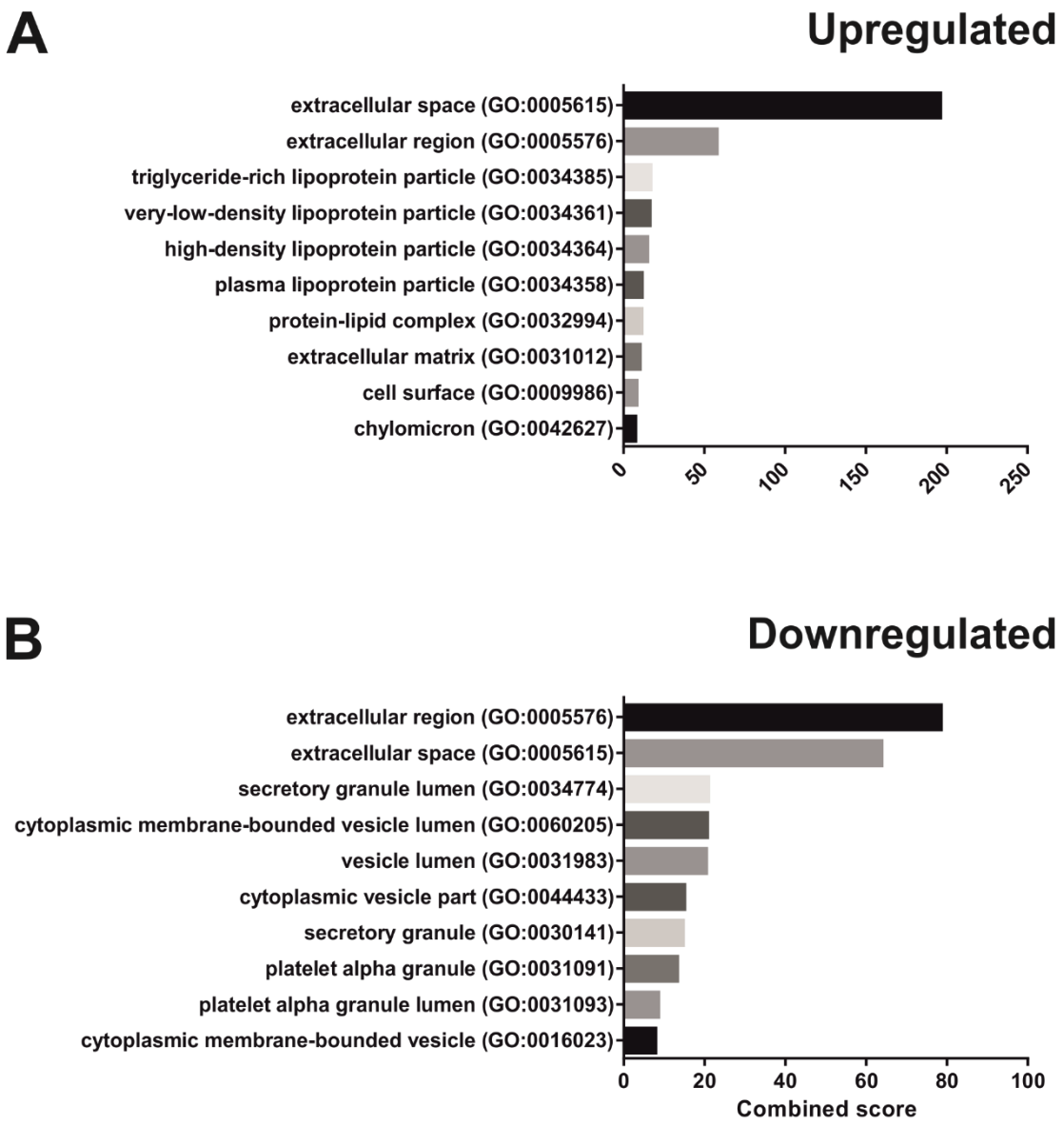

Figure 3.4.18: Significantly upregulated or downregulated secreted proteins in Y201.5 hTERT MSCs compared to Y201 hTERT MSCs identified by antibody array organised by cellular component

Secreted proteins identified as significantly upregulated (A) or downregulated (B) according to manufacturer's instructions from the antibody array. These were then summarised in a bar chart according to the cellular component of the gene product as classified by Enrichr.

The majority of proteins highlighted as differentially regulated were involved in cytokine-cytokine interactions, both upregulated and downregulated (Table 3.4.1 and 3.4.2 respectively). The upregulated proteins consistently appearing in searches were FGF ligands (FGF4, FGF5, FGF6 and FGF21), EGF and HGF which feature in a number of key signalling pathways in addition to pathways involved in cancer (Table 3.4.1). These proteins are also involved in differentiation pathways along with GDF5, which was also found to be significantly upregulated. The downregulated proteins appeared to have few linking pathways as many pathways identified in analysis only had 1 or 2 proteins listed as being differentially regulated (data not shown). It was also not possible to identify the upregulated proteins in the RNA-seq analysis previously shown, although these were analysed on different cell lines.

Nevertheless, both proliferative and differentiation inducing proteins were found to be upregulated in the Y201.5 hTERT MSCs. It was also evident that some transcripts previously identified in the Y101.5 hTERT MSCs were important in osteogenesis – the most notable example being BMP2, a known stimulative of osteogenesis. To confirm whether levels of secreted proteins were biologically relevant, Y101 hTERT MSCs were differentiated towards osteoblasts in the presence of Y101.5 conditioned media. These cells were chosen due to the more noticeable increase in osteogenesis in the Y101.5 hTERT MSCs. Conditioned media had been exposed to proliferating Y101.5 hTERT MSCs for 7 days, before being filtered using a 0.2µm filter and the usual osteogenic stimulative cocktail added as supplementation for a 21 day timecourse. Alizarin Red was then used to stain for calcium deposition, with both Y101 and Y101.5 hTERT MSCs included as controls.

Table 3.4.1: Significantly upregulated secreted proteins in Y201.5 hTERT MSCs compared to Y201 hTERT MSCs organised by KEGG 2016 pathways

Secreted proteins identified as significantly upregulated according to manufacturer's instructions from the antibody array. These were then analysed by which KEGG 2016 pathways the proteins participated in as classified by Enrichr. The name of the pathway, statistical analyses and genes included in each pathway are summarised in the table.

Term	Overlap	P-value	Adjusted P-value	Z-score	Combined Score
Cytokine-cytokine receptor interaction_Homo sapiens_hsa04060	17/265	4.13E-14	3.06E-12	-1.87718	49.77187085
Melanoma_Homo sapiens_hsa05218	6/71	3.98E-06	0.000147	-1.92368	16.97184922
PI3K-Akt signaling pathway_Homo sapiens_hsa04151	8/341	0.000635	0.012726	-2.01519	8.794488595
Chemokine signaling pathway_Homo sapiens_hsa04062	6/187	0.000688	0.012726	-1.85035	8.075135672
Pathways in cancer_Homo sapiens_hsa05200	8/397	0.001674	0.019316	-1.97631	7.800131701
Rap1 signaling pathway_Homo sapiens_hsa04015	6/211	0.001268	0.018774	-1.86085	7.39744122
Ras signaling pathway_Homo sapiens_hsa04014	6/227	0.001827	0.019316	-1.85338	7.314953672
Jak-STAT signaling pathway_Homo sapiens_hsa04630	5/158	0.002125	0.019658	-1.75279	6.887236751

MAPK signaling pathway_Homo sapiens_hsa04010	6/255	0.003235	0.026596	-1.79411	6.507243374
Regulation of actin cytoskeleton_Homo sapiens_hsa04810	5/214	0.007498	0.055482	-1.69832	4.911023787

Table 3.4.2: Significantly downregulated secreted proteins in Y201.5 hTERT MSCs compared to Y201 hTERT MSCs organised by KEGG 2016 pathways

Secreted proteins identified as significantly downregulated according to manufacturer's instructions from the antibody array. These were then analysed by which KEGG 2016 pathways the proteins participated in as classified by Enrichr. The name of the pathway, statistical analyses and genes included in each pathway are summarised in the table.

Term	Overlap	P-value	Adjusted P-value	Z-score	Combined Score	Genes
Cytokine-cytokine receptor interaction_Homo sapiens_hsa04060	5/265	1.74E-05	0.000262	-1.87718	15.48391	CCL13;CCL11;TNFSF15;LIF; CXCL16
Complement and coagulation cascades_Homo sapiens_hsa04610	03/79	0.000174	0.001303	-1.79153	11.9008	VWF;SERPING1;SERPINA5
Chemokine signaling pathway_Homo sapiens_hsa04062	3/187	0.002035	0.010175	-1.87629	8.607995	CCL13;CCL11;CXCL16
ECM-receptor interaction_Homo sapiens_hsa04512	02/82	0.005982	0.022434	-1.62138	6.156672	VWF;IBSP
Focal adhesion_Homo sapiens_hsa04510	2/202	0.032432	0.097295	-1.82143	4.243927	IBSP;VWF
PI3K-Akt signaling pathway_Homo sapiens_hsa04151	2/341	0.082641	0.172	-1.91148	3.364698	IBSP;VWF
Asthma_Homo sapiens_hsa05310	01/31	0.044688	0.111721	-1.323	2.899678	CCL11
Melanogenesis_Homo sapiens_hsa04916	1/100	0.134989	0.184076	-1.65494	2.800827	POMC

Adipocytokine signaling pathway_Homo sapiens_hsa04920	01/70	0.096718	0.172	-1.58947	2.797871	POMC
TNF signaling pathway_Homo sapiens_hsa04668	1/110	0.147418	0.184273	-1.61848	2.737398	LIF

All samples tested were able to differentiate down the osteogenic lineage as evidenced by the increasing levels of calcium deposited during the timecourse Figure 3.4.19A. There was also a notable difference between the basal conditions and the osteogenic conditions. As before, the Y101.5 hTERT MSCs appeared to have an increased level of osteogenic capacity in comparison to their wild type counterparts, which was particularly noticeable in the earlier (Day 7 and Day 14) timepoints of the experiment. Most notable however, was the increased osteogenic capacity of the Y101 hTERT MSCs stimulated in the presence of the conditioned media. Although these cells were not as osteogenic as the Y101.5 hTERT MSCs alone, there was an increased amount of deposited calcium at both Days 7 and 14 in comparison to the Y101 hTERT MSCs. By day 21 there was no longer any significance between the conditioned media and the standard conditions for the Y101 hTERT MSCs as shown in Figure 3.4.19B.

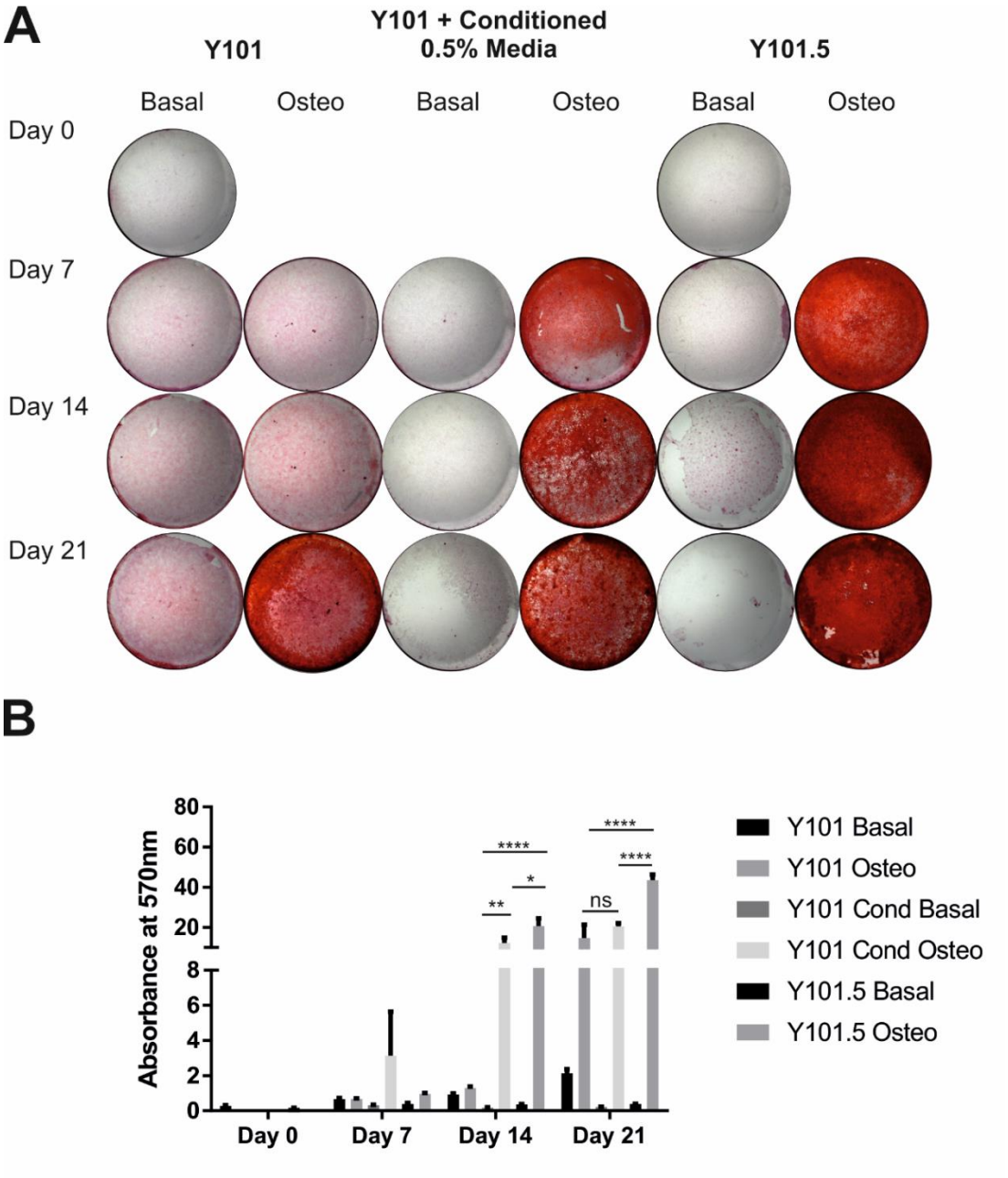

Figure 3.4.19: Y101.5 conditioned media stimulates increased early osteogenesis in Y101 hTERT MSCs

0.5% serum supplemented media exposed to proliferating Y101.5 hTERT MSCs was used to treat Y101 hTERT MSCs throughout a 21 day osteogenic timecourse. (A) Alizarin Red staining was used to stain deposited calcium which was then (B) eluted using CPC and the absorbance plotted in a bar chart where Y101 cond indicates the Y101 hTERT MSCs treated with conditioned media. Values = mean ± SD, n=6 with statistical significance obtained using 2 way RM ANOVA with Tukey's multiple comparisons.

3.5 Discussion

Cell culture typically relies on the supplementation of a minimal media with animal serum in order to sustain cell growth of adherent cells. However, this common practise suffers from reproducibility issues, both within the same laboratory and between laboratories. Standardisation of cell culture techniques would require an alteration in cell culture supplementation to a defined media. However, the alteration of any form of cell culture supplementation may result in a change in cellular behaviour, an avenue that would need to be explored before either standardisation or cellular therapies could be altered and developed. It was therefore decided to explore the alterations in cellular behaviour by reducing serum supplementation present in Y101 and Y201 hTERT MSCs propagation. Serum removal is typically used to synchronise cell cycles and sudden removal without resupplying was hypothesised to have drastic detrimental effects on the viability of the hTERT MSCs. It was therefore decided to gradually remove the serum over a number of weeks thus maximising the likelihood the cells would adapt to the altered culture conditions. This gradual reduction of the serum resulted in cells able to survive in media supplemented with 0.5% FBS in comparison to the usual supplementation of 10% FBS, which equates to 20-fold less serum present in the media.

3.5.1 Reduced serum hTERT MSCs increase osteogenic capacity at the expense of adipogenic differentiation potential

The most notable difference caused by the changes in reduction of serum was the very clear shift in differentiation propensity towards osteogenesis at the expense of adipogenesis. This was evident in multiple osteogenic assays looking at both calcium deposition and the upregulation of a major osteogenic marker, alkaline phosphatase. The Y101.5 hTERT MSCs in particular showed a large increase in calcium deposition as more calcium was deposited in 7 days compared to the 21 day timepoint of the Y101 hTERT MSCs. This result compliments results previously found in primary hMSCs whereby serum starvation and oxygen restriction resulted in an increase in calcium deposition (Binder et al., 2015). However, results shown in this chapter demonstrate reduced serum hTERT MSCs adapted to low serum conditions had further increased ALP activity compared to wild type hTERT MSCs treated with 0.5% FBS containing differentiation media. It appeared the alteration of differentiation propensity was shown to not be a reproducible simply by reducing serum in differentiation media, but arose out of a direct change in cellular behaviour of the low serum-adapted hTERT MSCs.

3.5.2 RNA-seq analysis indicates hTERT MSCs alter metabolism as a response to low serum culture

It was clear however from the RNA-seq analysis that an alteration in metabolism had occurred in the low serum hTERT MSCs. The majority of upregulated pathways involved the forming and breaking down of lipids, lipoproteins, alcohols and sterols. This is likely a direct response to the changes in culture conditions to ensure the cells are able to still proliferate and to replace the lost nutrients caused by serum deprivation. Interestingly, as osteoblasts are metabolically active cells *in vivo* they require a constant supply of metabolites in order to continue depositing the bone matrix (Shapiro and Haselgrove, 1991). Osteoblasts are able to oxidise fatty acids and this can make up between 40 and 80% of their energy requirements (Adamek et al., 1987). The Y101 hTERT MSCs have a bias towards osteogenic differentiation which was found to be increased in this chapter (James et al., 2015). Exposing these cells to more *in vivo* like conditions, by reducing serum content and increasing the dependency on lipogenesis and metabolism, seems to have increased this bias further.

3.5.3 Transcripts upregulated in reduced serum hTERT MSCs are predominantly expressed extracellularly

Additionally, RNA-seq analysis demonstrated upregulated transcripts were typically found to be secreted, most notably within exosomes. Exosomes are membrane-enclosed vesicles found to shuttle active cargoes to recipient cells, which typically includes proteins, lipids, and RNAs (both coding and non-coding) which can be taken up by target cells and functionally translated. The use of MSCs in therapeutics has been covered in section 1.5.3.3, however, the study of regeneration mediated by MSCs is undergoing a shift to include paracrine activity of the cells as it is widely accepted that MSCs secrete a number of factors able to influence immunomodulation, regeneration and angiogenesis (Caplan and Dennis, 2006). It has also been shown that conditioned media from MSCs was able to aid in the regeneration and support of injured organs such as the liver and kidney (van Poll et al., 2008; Zarjou et al., 2011). Research describing MSC exosomes has led to a surge in studies to understand how they could be harnessed for cell-free therapeutic strategies (Lai et al., 2010). Previous studies have demonstrated the ability of MSCs to form "osteogenic" exosomes, which promote calcium deposition (Narayanan et al., 2016) and it would appear the reduced serum hTERT MSCs also demonstrate this behaviour. However, the Y101.5 hTERT MSCs were able to increase calcium deposition in Y101 hTERT MSCs after one week of conditioning the media used in the experiment. This would suggest the potential for the reduction of serum, thus exposing cells to a more *in vivo* like physiology, as a simple way of increasing the potential of exosome therapy.

3.5.4 Concluding Remarks

Prior studies have examined the effects of serum-free culture on a number of MSC sources including a number of commercial options. Typically, these support the expansion of MSCs and yet the proliferation and differentiation of these cells can vary within commercial media (reviewed in Gottipamula et al., 2013). Additionally, it has been found that the expansion of MSCs in serum-free media can also lead to alterations in cell surface expression markers, as evidenced by the reduced expression of CD105, which is typically used in the panel of markers used to identify MSCs (Mark et al., 2013). Due to time constraints, it was not possible within the scope of this PhD to develop a serum-free media, but several conclusions can be drawn from this work that might aid the future development of serum-free media. Namely, that the metabolism of MSCs appears to link directly with their osteogenic capacity, which is typically desired in therapeutics rather than adipogenesis. If a media could be developed that could exploit these findings it may lead to an increased effectiveness of MSC treatment options.

In conclusion, it appears the culture conditions of the hTERT MSCs are crucial to the differentiation capacities of the cells and that serum levels may play a role in the regulation of osteogenesis. Reducing the reliance on serum as a supplementation appears to have favoured osteogenesis in the Y101 and Y201 hTERT MSCs at the expense of adipogenesis as shown in this chapter. This demonstrates the importance of the caveat of *in vitro* modelling and study of human biology in that artificial culture conditions may elicit cellular behaviours that do not represent those *in vivo*. This was further demonstrated by the changes to both the secretome and the metabolism of these cells and as these cells are a model for primary bone marrow MSCs, this may be a reflection on how these cells could also behave. The further development of CRISPR/Cas9 genetically modified hTERT MSCs, and the phenotypic behaviours established will have to be considered with this caveat in mind.

Chapter 4 : Establishing the CRISPR/Cas9 system in hTERT MSCs by targeting master differentiation transcription regulators

4.1 Introduction

As previously discussed, MSCs possess a tri-lineage differentiation potential with the capability of differentiating into osteoblasts, chondrocytes and adipocytes. Differentiation is a complex process governed by a number of proteins, signalling pathways and transcription factors and each lineage has a major transcription factor deemed to control lineage fate and commitment. Runx2, Sox9 and PPARγ are the master transcription regulators for osteogenesis, chondrogenesis and adipogenesis respectively. Previous *in vivo* studies have demonstrated that knocking out these genes results in restricted differentiation and perinatal lethality, or death shortly after birth (Komori et al., 1997; Barak et al., 1999; Akiyama et al., 2002). It was therefore hypothesised that knocking out a master transcription regulator in the hTERT MSCs would result in null differentiation of the appropriate lineage and provide a quantifiable endpoint for determining the consequence of genome editing with CRISPR/Cas9. Further, this would allow for direct comparison with results from other genome editing techniques already conducted to create KO animal models. Runx2 and Sox9 were chosen as candidate genes for CRISPR/Cas9 mediated depletion as a proof-of-principle study and a brief overview of these transcription factors is given below.

4.1.1 Runx2

Runx2 (Cbfa1) is a member of the Runx family of transcription factors and has been identified as the major transcription factor regulating osteogenesis, required for mesenchymal condensation, differentiation of MSCs into osteoblasts and the vascularisation of a developing skeleton, amongst other functions (Schroeder et al., 2005). Runx2 contains a highly conserved DNA binding Runt domain in addition to activation and repression domains allowing Runx2 to influence gene expression and similarly to other major developmental regulators, Runx2 is subject to multiple levels of control by multiple signalling pathways (Kania et al., 1990). These include the five major signalling pathways found extensively involved in embryonic development, namely BMP/transforming growth factor-β (TGFβ), FGF/EGF, Hedgehog, Notch, and Wnt signalling (reviewed in Schroeder et al., 2005).

In vivo studies confirmed the importance of Runx2 in skeletal development when mice deficient in Runx2 showed a complete lack of ossification and died shortly after birth (Komori et al., 1997). Mutations in Runx2 are also known to be a cause of Cleidocranial dysostosis, a rare autosomal dominant disease in humans which presents with abnormal skeletal phenotypes in the affected individuals (Otto et al., 1997). Conversely, overexpressing Runx2 in MSCs induces osteogenesis evidenced by increased osteogenic gene expression and increased mineralisation (Zhang et al., 2006b; Wojtowicz et al., 2010). The induction of osteogenesis in this manner also restricts the ability of MSCs to differentiate into other lineages, namely adipogenesis and chondrogenesis (Zhang et al., 2012).

4.1.2 Sox9

Similarly to osteogenesis there is also a master transcription regulator of chondrogenesis, Sox9. Sox9 is part of a family of 20 Sox transcription factors divided into subgroups based on homology of the shared DNA binding domain, high-mobility-group (HMG) box. Sox9 was first shown to be critical to chondrogenesis as mutations in the gene were found to be linked to the skeletal disease campomelic dysplasia (CD), a rare genetic disease presenting with bowing of the long bones and in some instances sexual reversal due to the involvement of Sox9 in male sexual development (Kwok et al., 1995). The conditional knockout of Sox9 from undifferentiated MSCs in limb buds *in vivo* resulted in very short deformed limbs with a complete lack of chondrogenic mesenchymal condensations, indicating that Sox9 is required for the onset of chondrogenesis (Akiyama et al., 2002). This study also showed that Sox9 was also needed for chondrogenesis after mesenchymal condensation as when Sox9 is knocked out after this process, there was still an almost complete absence of cartilage from the endochondral skeleton (Akiyama et al., 2002).

4.1.3 hTERT MSC CRISPR/Cas9 transfection and fluorescent sorting strategy

Transfecting hTERT MSCs with a liposome transfection agent typically results in poor efficiency with less than 5% of cells routinely displaying as GFP positive using a GFP expressing plasmid (Katherine Wilson, personal communication). This low ability to respond to a cationic lipid presents a problem for the generation of genetically modified hTERT MSCs. CRISPR/Cas9 targeting efficiency is favourable compared to other genome editing methods but is still not 100% efficient in cells. Additionally, different sgRNAs have differing efficiencies and at the time of writing, the efficiency of a particular sgRNA is not predictable. CRISPR/Cas9 is reported to have efficiencies ranging between 2 and 5% in iPSCs and if the hTERT MSCs have a similar efficiency this would make isolating GM-hTERT MSCs extremely difficult. Combined with a transfection efficiency of 5%, theoretically over 99% of transfected hTERT MSCs would either not be transfected or not be targeted successfully by the CRISPR/Cas9. In an attempt to improve the likelihood of generating GM hTERT MSCs a transfection strategy based on fluorescence was developed. This strategy involved inducing the expression of GFP when CRISPR/Cas9 is introduced into the hTERT MSCS to allow identification of successful and unsuccessful transfections. This follows a similar strategy to Ding et al. (2013) whereby cells are sorted by fluorescence to isolate only cells that have been successfully transfected, thus increasing the chances of isolating GM hTERT MSCs. The fluorescent strategy used a T2A viral peptide which induces ribosomal skipping to allow for co-expression of Cas9 and GFP this ensures that GFP is only expressed when Cas9 is present within the cell (Szymczak et al., 2004). The plasmid used contains an enhanced GFP (eGFP) cassette, which has a higher-intensity emission profile compared to WT GFP (Cinelli et al., 2000). The overview of using fluorescence to maximise the likelihood of generating GM-hTERT MSCs is summarised Figure 4.1.1. The work presented in this chapter will investigate the usage of this fluorescent sorting strategy to introduce CRISPR/Cas9 into the Y201 hTERT MSCs and examine the resultant effects on the genes targeted.

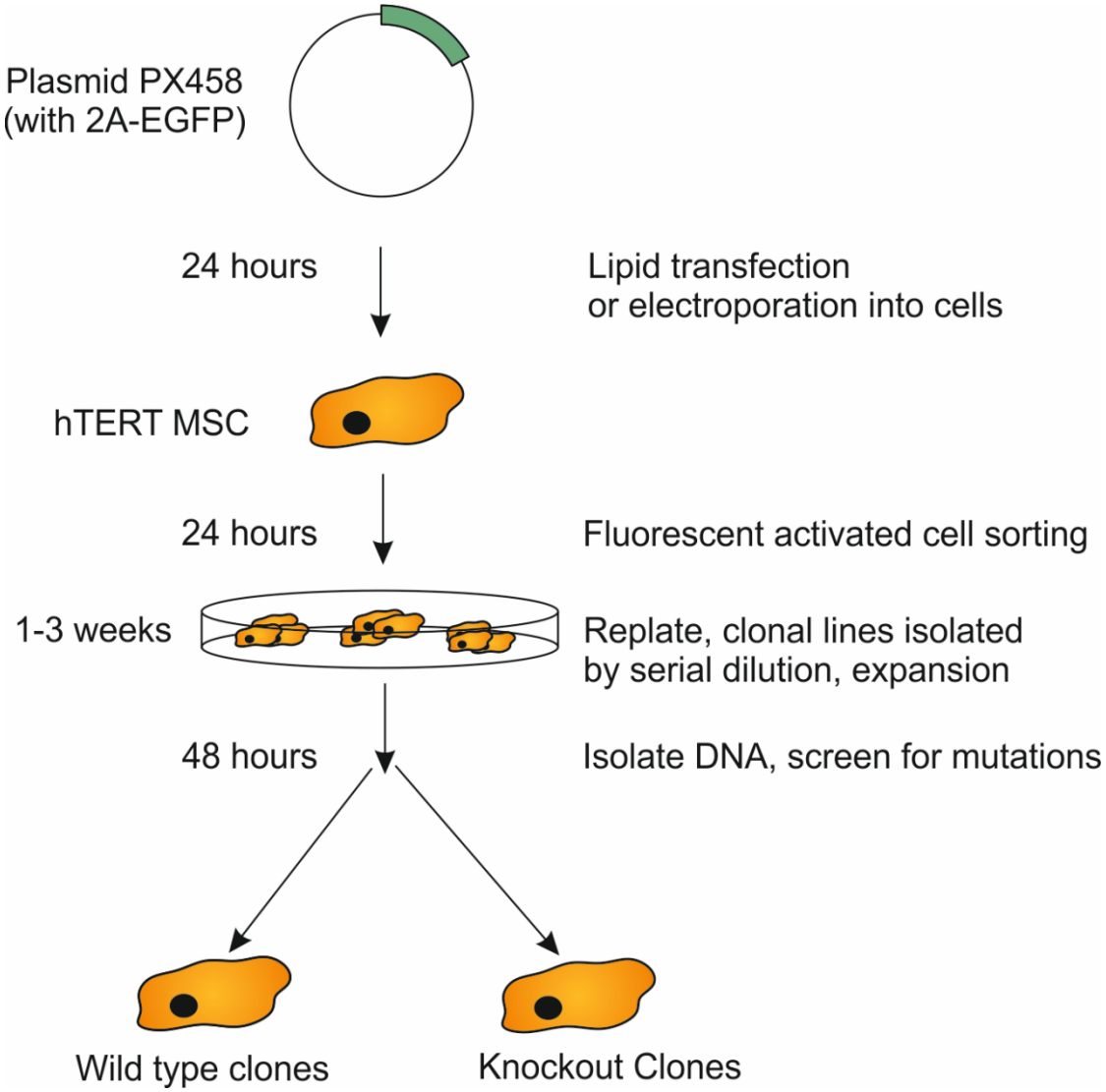

Figure 4.1.1: Overview of fluorescent strategy to maximise possibility of generating GM hTERT MSCs.

Schematic demonstrating the strategy planned to maximise the possibility of finding genetically modified hTERT MSCs, by using a CRISPR/Cas9 vector with GFP present so that where CRISPR/Cas9 is present cells should fluoresce. Sorting based on positive fluorescence and expansion of the sorted cells should reduce the number of cells without genetic modification therefore maximising success. Approximate times for each major step are included.

4.2 Aims

The aims of the work in this chapter are to establish the methods required to design, construct and introduce CRISPR/Cas9 into hTERT MSCs to develop genetically modified cell lines and study the effects of gene deletion on stem cell signalling and differentiation.

The specific objectives of this chapter are to:

- Design relevant sgRNA targets to target Runx2 and Sox9
- Construct CRISPR/Cas9 vectors able to be introduced into cells
- Establish methodology to increase likelihood of detecting genome editing by using a fluorescent marker to highlight cells with the potential for genome editing
- Isolate and validate clonal GM hTERT MSC cell lines
- Analyse both the genotype and phenotype of isolated clonal lines with targeted Runx2 and Sox9 deletions

4.3 Methods and Materials

4.3.1 Generating Knockout Cell Lines

4.3.1.1 Single Guide RNA and Single Stranded Oligonucleotide Design

Single guide RNA (sgRNA) structures were designed using the CRISPR design tool (crispr.mit.edu). Potential sequences were ranked by the programme based on specificity and off-target effects, sequences were chosen that possessed the fewest off target effects.

All primers were ordered from Sigma Aldrich or Integrated DNA Technologies and purified via desalting.

The sgRNA sequences selected are below (5' – 3'), initially one set of sgRNAs was tested for each gene, but after initial studies the Sox9 sgRNAs were redesigned. The redesigned sgRNAs are also listed:

Sox9 sgRNA Fwd CACCGTAAGTGCTCGCCGCGGTAGC

Sox9 sgRNA Rev AAACGCTACCGCGGCGAGCACTTAC

Runx2 sgRNA Fwd CACCGTCGGTGCGGACGAGTTCGGC

Runx2 sgRNA Rev AAACGCCGAACTCGTCCGCACCGAC

Sox9 1 sgRNA Fwd CACCGCATGAAGATGACCGACGAGC

Sox9 1 sgRNA Rev AAACGCTCGTCGGTCATC TTCATGC

Sox9 2 sgRNA Fwd CACCGTTCAGATCGGGCTCGCCCTT

Sox9 2 sgRNA Rev AAACAAGGGCGAGCCCGATCTGAAC

4.3.1.2 CRISPR Cloning

RNA guided nucleases were constructed by cloning the wanted sgRNA into the PX458 vector (Addgene plasmid 48138) which contains an enhanced green fluorescent protein (eGFP) marker, the cloning strategy is summarised for the Sox9 sgRNA in Figure 4.1.1. Primers were first phosphorylated and annealed using a thermocycler at 37°C for 30 min; 95°C for 5 min, this was then allowed to cool down to room temperature. The resulting construct was ligated into a BbsI digested PX458 vector in a one-step reaction for 6 cycles at 37°C for 5 min, 21°C for 5 min for a total of 1 hour.

4.3.1.3 Transformation of DH5α chemically competent E. coli

Constructs were transformed into DH5α chemically competent *E. coli*, these cells have been engineered to maximise transformation efficiency. 1µL of plasmid DNA was added to 20µL of cells and incubated on ice for 10 minutes. Heatshock was then performed at 42°C for 30 seconds before 50µL of LB Broth was added to the bacteria. After heatshock, cells were immediately plated onto LB Agar plates containing 100µg/mL ampicillin.

4.3.1.4 Construct Evaluation and DNA extraction

Constructs were analysed for the correct insertion of the sgRNA sequence via a colony PCR screen; screening primers are included on the plasmid map in Figure 4.3.1.

U6 Fwd Primer: GAGGGCCTATTTCCCATGATTCC

Single colonies were used to inoculate 5mL of LB Broth, grown for 6 hours at 37°C with shaking at 200rpm. DNA was extracted from this culture using the QIAGEN MiniPrep kit as per manufacturer's instructions. Alternatively, the culture was transferred to 100mL of LB Broth, with ampicllin at 100µg/mL, and incubated at 37°C overnight, 200rpm to replicate DNA suitable for extraction with the QIAGEN MaxiPrep kit. DNA was extracted following manufacturer's instructions.

Glycerol stocks were made by mixing 500µL of bacteria with 500µL of 50% glycerol and stored at -80°C.

MiniPrep DNA was analysed via in-house Sanger sequencing using the U6 Fwd primer as the sequencing primer. The sgRNA insert can then be found roughly 200-220 base pairs downstream from the binding site of this primer in sequencing. All CRISPR constructs were sequence confirmed before further use.

4.3.1.5 Lipid Transfection

Small scale transfections were carried out in 96 well plates, with 15,000 cells per well. 100ng per 15,000 cells was used for transfection at a ratio of 3:1 Fugene HD to DNA, DNA:lipid complexes were left to form for 15 minutes at room temperature prior to transfection. Medium without antibiotics was used throughout transfection so as not to impede the Fugene reagent. Transfections were left for 48 hours prior to analysis via either flow cytometry, fluorescent activated cell sorting or by confocal microscopy.

Larger scale transfections, i.e. for FACS, were carried out using identical quantities and ratios to the small scale transfections. 500,000 cells were used for controls and 1,000,000 cells used for the sorted sample.

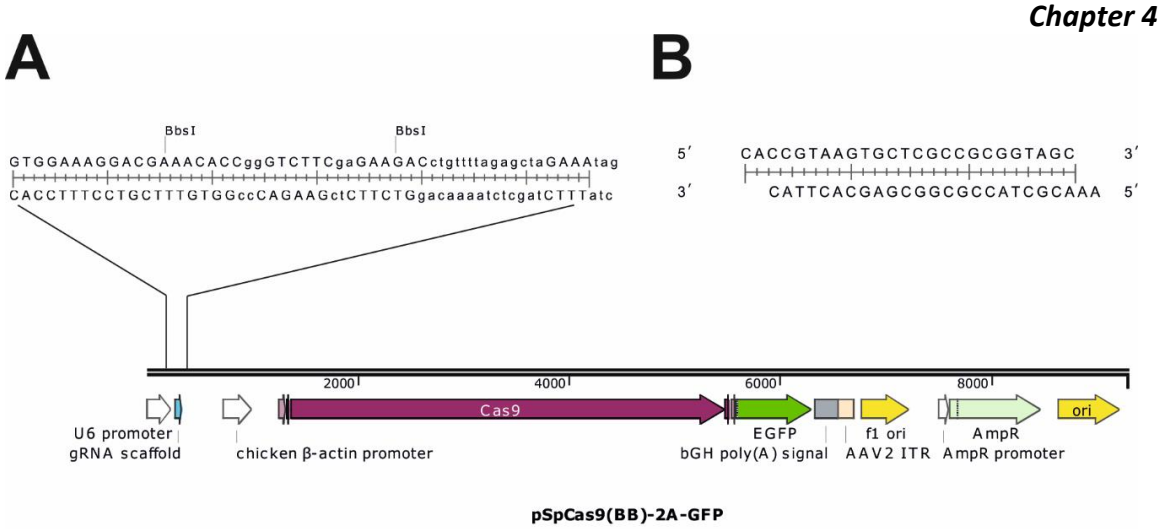
A
B
BbsI
BbsI
GTGGAAAGGACGAAACACCggGTCTTCgaGAAGACctgttttagagctaGAAAtag
CACCTTTCCTGCTTTGTGGccCAGAAGctCTTCTGgacaaaatctcgatCTTTatc
5′ CACCGTAAGTGCTCGCCGCGGTAGC 3′
3′ CATTCACGAGCGGCGCCATCGCAAA 5′
2000
4000
6000
8000
Cas9
ori
U6 promoter
gRNA scaffold
chicken β-actin promoter
EGFP
bGH poly(A) signal
f1 ori
AAV2 ITR
AmpR
AmpR promoter
pSpCas9(BB)-2A-GFP

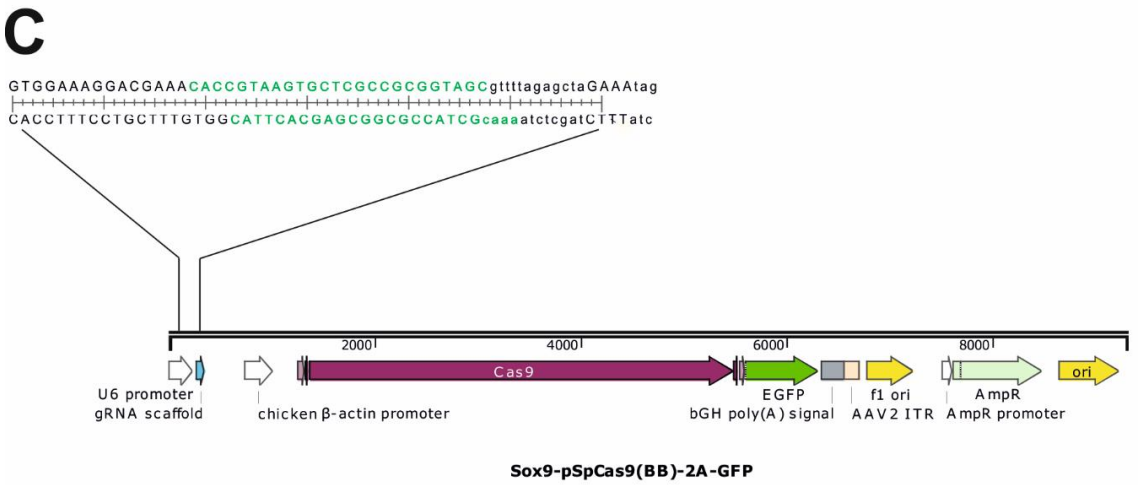
C
GTGGAAAGGACGAAACACCGTAAGTGCTCGCCGCGGTAGCgttttagagctaGAAAtag
CACCTTTCCTGCTTTGTGGCATTCACGAGCGGCGCCATCGcaaaatctcgatCTTTatc
2000
4000
6000
8000
Cas9
ori
U6 promoter
gRNA scaffold
chicken β-actin promoter
EGFP
bGH poly(A) signal
f1 ori
AAV2 ITR
AmpR
AmpR promoter
Sox9-pSpCas9(BB)-2A-GFP

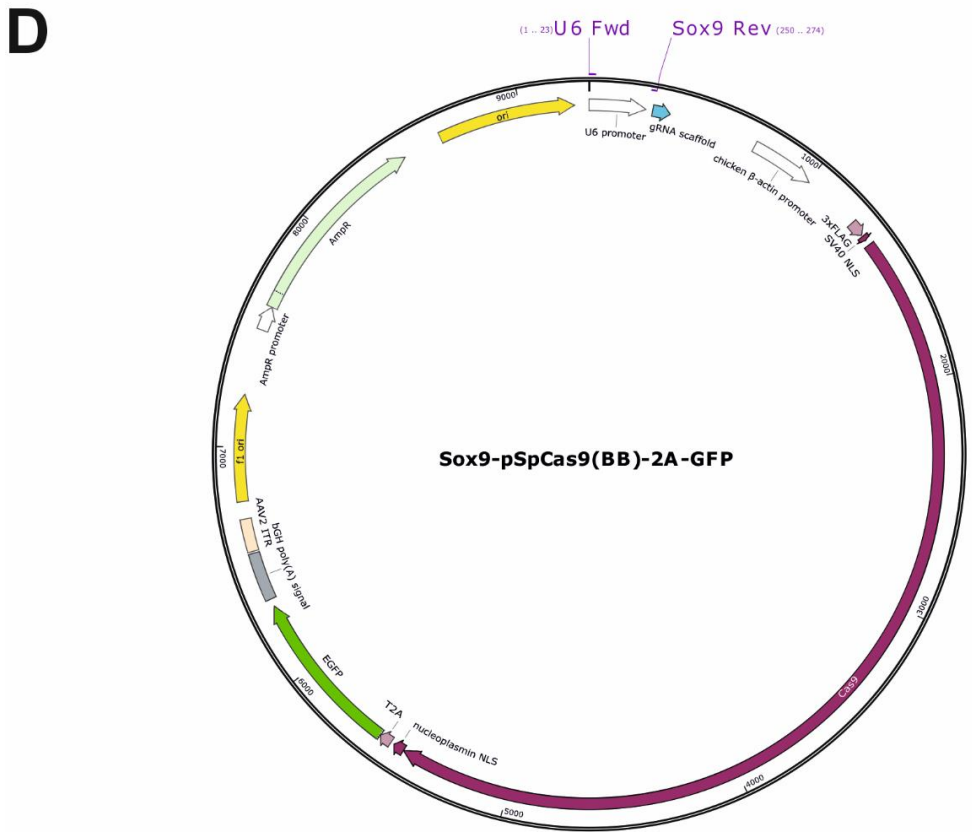
D
(1 .. 23)U6 Fwd
Sox9 Rev (250 .. 274)
9000
ori
U6 promoter
gRNA scaffold
chicken β-actin promoter
3xFLAG
SV40 NLS
AmpR
AmpR promoter
f1 ori
AAV2 ITR
bGH poly(A) signal
EGFP
T2A
nucleoplasmin NLS
Cas9
Sox9-pSpCas9(BB)-2A-GFP

Figure 4.3.1: Overview of CRISPR cloning methodology.

(A) Map of the pSpCas9(BB)-2A-GFP plasmid with BbsI sites highlighted. (B) Annealed sgRNA primers for Sox9. (C) Map of the Sox9 sgRNA cloned into the pSpCas9(BB)-2A-GFP plasmid. The cloned sequence has been highlighted in green. (D) Plasmid map with screening primers highlighted, U6 Fwd is also used for sequence confirmation of the cloned plasmid.

4.3.1.6 Neon Electroporation

Electroporation was performed using the Neon Transfection system in an attempt to increase initial transfection efficiencies. Y201 hTERT MSCs were washed with PBS before resuspending in Buffer R at a concentration of 100,000 cells per 10µL. Varying amounts of enhanced GFP (eGFP) plasmid was then added to the cell mixture, this uses the same GFP as found in the CRISPR/Cas9 plasmid detailed earlier. The electroporation parameters used were: 990 pulse voltage, 40ms pulse width, and a pulse number of 1. Cells were then replated into a 6 well plate and left for 24 hours before analysis via flow cytometry or sorting by FACS.

4.3.1.7 Fluorescent Activated Cell Sorting (FACS)

Transfected hTERT MSCs were incubated in 0.25% Trypsin-EDTA for 5 minutes and resuspended in normal culture medium prior to pelleting via centrifugation for 5 minutes at 1200rpm. Cells were then resuspended in 50% PBS : 50% serum free medium, supplemented with 5mM EDTA, 0.2% BSA and 1% FBS before sorting on the Beckman Coulter MoFlo Astrios using a 150µm nozzle. Live dead staining was performed by adding 1µL Sytox Blue per mL of cell suspension. Dead cells, debris and doublet cells were removed using forward scatter and side scatter gating in addition to the Sytox Blue staining. Cells positive for GFP, activated by a 488 laser, were collected in either 96 well plates (single cells) or into 50mL tubes and replated into 6 well plates. Data were analysed using Summit 6.2.

4.3.1.8 Clonal Selection

In order to isolate single colonies, serial dilutions were performed across a 96 well plate following the Corning protocol whereby 4000 cells are added to well A1 and serially diluted 1 in 2 down the wells in column A. The remaining wells were serially diluted across the rest of the plate so that each well contains a unique number of cells. Wells were then analysed by light microscopy for the presence of colonies and highlighted when one colony was present.

4.3.1.9 Genomic DNA Isolation

Genomic DNA was isolated from both mixed cell and clonal cell populations using the QIAGEN DNeasy Blood and Tissue Kit. Following manufacturer's instructions a minimum of 250,000 cells were pelleted by centrifugation, suspended in PBS and treated with Proteinase K. Cells were lysed and DNA captured using a DNeasy Mini spin column before being eluted in 100µL of the supplied buffer. DNA purity and concentration were assessed spectroscopically using a Nanodrop.

4.3.1.10 Transgenomic SURVEYOR Mutation Detection Assay

PCR amplification was performed using a high fidelity polymerase (PfuUltra II) with 100ng of genomic DNA, 10µM of each primer and 5% DMSO. The PCR protocol used an initial denaturation phase of 2 minutes at 95°C followed by 40 cycles at 95°C (30 seconds), 60°C (30 seconds) and a 30 second elongation phase at 72°C. A final extension (72°C) was then performed for 10 minutes. Resulting PCR products were purified with the QIAQuick PCR purification kit and eluted in 30µL of ddH_2O.

Equal amounts of test and reference DNA (wild type Y201) were mixed and annealed by heating the DNA to 95°C and cooling the mixture. These were then treated with the SURVEYOR nuclease and evaluated by agarose gel electrophoresis on a 1.5% agarose gel stained with SYBR Green I.

4.3.1.11 Sequencing

PCR amplification was performed using a high fidelity polymerase (PfuUltra II) with 100ng of genomic DNA, 10µM of each primer and 5% DMSO. The PCR protocol used an initial denaturation phase of 2 minutes at 95°C followed by 40 cycles at 95°C (30 seconds), 60°C (30 seconds) and a 30 second elongation phase at 72°C. A final extension (72°C) was then performed for 10 minutes. Resulting PCR products were purified with the QIAQuick PCR purification kit and eluted in 30µL of ddH2O.

PCR products synthesised were then sent for Sanger sequencing using a specifically designed forward primer unique to each gene at a 3.2µM concentration. Primers used for on target validation are listed below:

Sox9 Validation Fwd + Sequencing: TGC TTGCATCAAATCAACGGGA

Sox9 Validation Rev (used for all Sox9 PCR amplification): GTGCAAGTGCGGGTACTGGTC

Runx2 Validation Fwd + Sequencing: CCACTTCGCTAACTTGTGGCTGTTG

Runx2 Validation Rev: CCAAGGCAGGAGGTCTTGGAGGAC

Sox9 1 + 2 Validation Fwd + Sequencing: GTGGCGCGGAGACTCGCCAG

4.3.2 qPCR Primers

The primers used to quantify Runx2 expression using the protocol described in 2.1.2 were as follows:

Runx2 Fwd: GGTTAATCTCCGCAGGTCAC

Runx2 Rev: GTCACTGTGCTGAAGAGGCT

4.3.3 Analysis of GM-hTERT osteogenic and adipogenic differentiation

The capacity for the GM-hTERT MSCs to undergo osteogenesis and adipogeneisis was performed and analysed as described in section 2.1.3.

4.4 Results

4.4.1 sgRNA template construction

The major advantage of using the CRISPR/Cas9 system over other published genome editing techniques is the relative ease at retargeting the technology. The cloning techniques required for targeting CRISPR/Cas9 to a sequence need substantially less hands on time in comparison to the redesign and construction of new ZFNs or TALENS proteins. sgRNAs can be delivered in a number of formats to direct the Cas9 to the desired template, the method used here uses an sgRNA-expressing plasmid.

Initially, oligonucleotides were ordered after designing a sgRNA template on the crispr.mit.edu tool, these were picked based on the number of potential off-target effects each template was predicted to have, the potential off-targets for each sgRNA are listed in Table 4.4.1 and Table 4.4.2. No evidence of efficiency is provided by the tool or could be predicted from the template sequence at this time.

The relevant oligonucleotides required for sgRNA template construction were first annealed to form one product with sticky ends suitable for ligation. The overhangs should ensure the annealed oligonucleotides can only insert in one orientation within the digested PX458 vector. Ligation and digestion took place in a one-step reaction removing the requirement for plasmid purification. To determine whether ligation had been successful, colony PCR was performed amplifying the product directly from bacterial colonies using a primer targeting the promoter region (U6 primer) and the reverse sgRNA template oligonucleotide. The positions of these primers can be seen in Figure 4.3.1D. A specific product will be formed if ligation was successful, however if ligation was not successful only a faint non-specific product can be seen, caused by amplification by the U6 primer, which can target regardless of ligation success. Products were visualised by agarose gel electrophoresis and a negative control included, typically a colony from the negative ligation control plate, produced by a ligation without the annealed product, an example gel can be seen Figure 4.4.1A.

Table 4.4.1: List of potential off-target effects identified for Sox9 sgRNA

Off-targets are listed along with the number of mismatches present compared to the on-target sequence and the locus of where the off-target is found, an Ucsc gene number is given where the locus is exonic. An off-target score is computed as 100% minus a weighted sum of off-target scores in the target genome. 100 indicates an almost certain binding of CRISPR/Cas9 to the off-target and 0 indicates an extremely unlikely binding event.

Sequence	Score	Mismatches	Ucsc gene	Locus
GAAGTGCACTCCGCGGTACCCAG	0.5	4MMs [1:8:10:19]		chr3:-195857758
TGAGTGCTGGCCCCGGCAGCTGG	0.1	4MMs [2:9:13:17]		chr17:-77184361
TCTGTGCTGGCCGTGGTAGCCGG	0.1	4MMs [2:3:9:14]		chr19:+12291948
AAAGTGCTTGCCCCAGTAGCTGG	0.1	4MMs [1:9:13:15]		chr5:+162827321
GAAGTGCCCGCCGCCGTCGCAGG	0.1	4MMs [1:8:15:18]		chr14:+106067476
TAAGTACCCGCCGCGCGAGCTGG	0.1	4MMs [6:8:16:17]	NM_004831	chr19:-16738654
TAAGTGCTCTCCCCAGAAGCCAG	0.1	4MMs [10:13:15:17]		chr4:-155547736
TAAGTGCTTCCCGGGGCAGCAGG	0.0	4MMs [9:10:14:17]		chr3:+184226487
TAAGTGCTCACCCAGGTAACAGG	0.0	4MMs [10:13:14:19]		chr6:+170841622
TAAGTGCTACCCGAGGTTGCTGG	0.0	4MMs [9:10:14:18]		chr1:+5917494
TAAGTGCTTGCTGCTGTTGCTAG	0.0	4MMs [9:12:15:18]		chr5:+155652586

Table 4.4.2: List of potential off-target effects identified for Runx2 sgRNA

A score is given for each off-target defined as 100% minus a weighted sum of off-target scores in the target genome. 100 indicates an almost certain binding of CRISPR/Cas9 to the off-target and 0 indicates an extremely unlikely binding event.

Sequence	Score	Mismatches	UCSC gene	Locus
CCGCTGCGGCCGG GTTCGGCTAG	0.5	4MMs [1:4:10:13]		chr1:+36235060
TCGATGAGGATGA GTTTGGCAGG	0.2	4MMs [4:7:11:17]		chr16:-70452501
TCTGCGCGGAGGA GGTCGGCCAG	0.2	4MMs [3:5:11:15]	NM_001105577	chr13:+28552257
TGGGTGCTGAAGA ATTCGGCCAG	0.1	4MMs [2:8:11:14]		chr4:-39087720
TCAGTGGGGAGGA GTCCGGCAGG	0.1	4MMs [3:7:11:16]		chr20:-31564247
TGGGTGCGAAGGA GTCCGGCTGG	0.1	4MMs [2:9:11:16]	NM_058169	chr12:+12618825
TCGGTGAGGAGGG GTTGGGCAAG	0.1	4MMs [7:11:13:17]	NM_021903	chr6:-29591057
TTGGTGCGCACGG GTTCCGCCAG	0.1	4MMs [2:9:13:18]	NM_015517	chr11:+118992196
TCAGTGTGGACGA GTATGGCTGG	0.1	4MMs [3:7:16:17]	NM_001008704	chr6:+34214741
TGGGTGCGGACGG GGTAGGCAAG	0.1	4MMs [2:13:15:17]		chr3:-194054960
TCGGTGCGCACCAG CTCGCCCGG	0.0	4MMs [9:12:15:19]	NM_001122607	chr21:+36259211
TCGGTGAGCACGG ATTCGGCCGG	0.0	4MMs [7:9:13:14]	NR_104000	chr9:-37002717

Positive colonies were then taken forward for sequencing (Figure 4.4.1B), where the presence of the correct sgRNA sequence was confirmed by sequencing the plasmid using the U6 promoter primer. Each of the 6 colonies tested in B had the correct sequence and deemed suitable for further analysis.

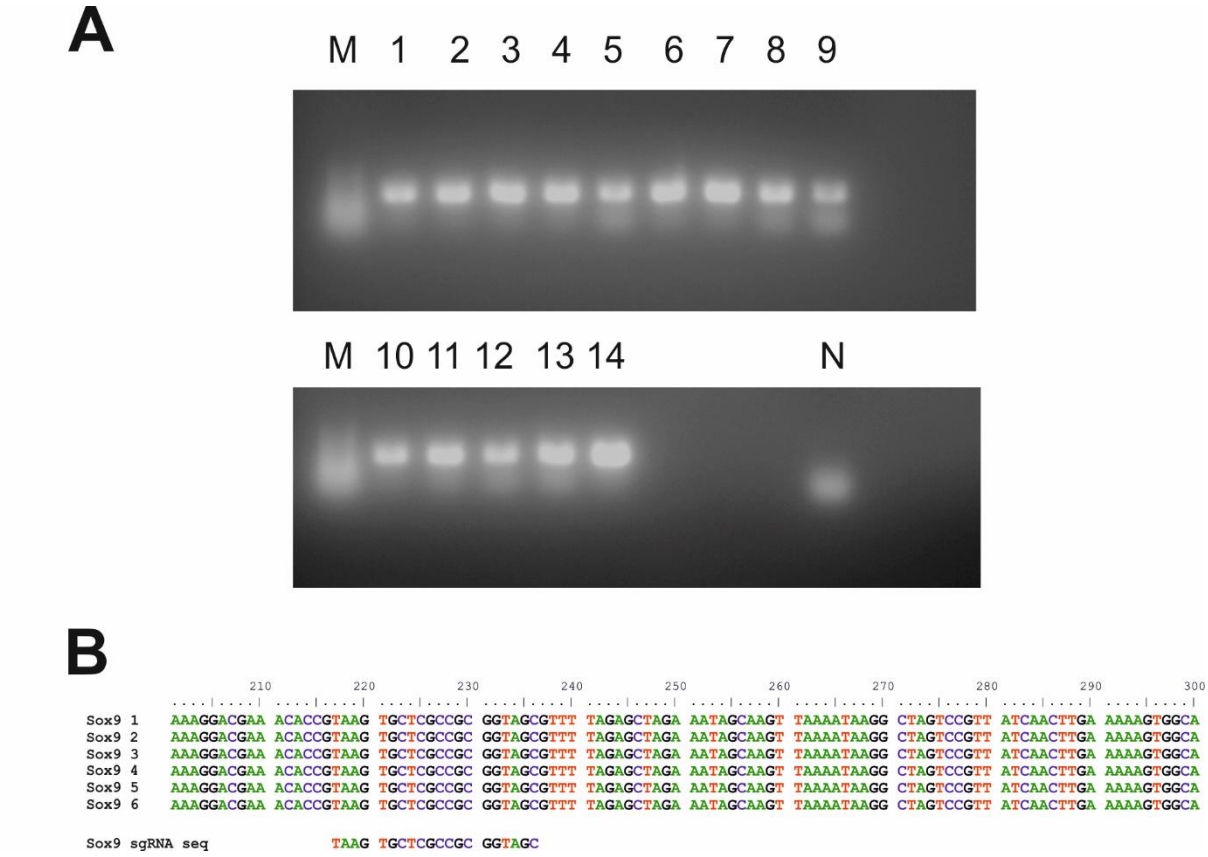

Figure 4.4.1: Confirming the insertion of the sgRNA into the pSpCas9(BB)-2A-GFP plasmid.

(A) PCR colony screen of single colonies picked from an agar plate. These were screened using the U6 Fwd primer and the Sox9 sgRNA Rev primer. A plasmid with the sgRNA successfully inserted will therefore amplify whereas plasmid without the insert will only have limited product produced by the U6 Fwd Primer. Each lane contains an individual colony picked from the agar plate, these are arbitrarily numbered. Molecular weight size marker marked M. A colony from the ligation control was also included and is marked N. (B) Clones highlighted as successful by the colony PCR were taken for Sanger sequencing. The template sequence for Sox9 has been listed below the consensus sequences. In this example all 6 clones tested had the Sox9 sgRNA present.

4.4.2 Detectable eGFP fluorescence is produced upon transfecting HEK293FT cells with CRISPR/Cas9

The PX458 vector contains an open reading frame consisting of the Cas9 enzyme in addition to eGFP which is separated from Cas9 by a 2A viral peptide. This peptide induces ribosomal skipping (reviewed in Felipe, 2004) meaning both Cas9 and eGFP are expressed simultaneously as two separate entities thus when Cas9 is present in cells, green fluorescence can be detected. This should give an indication as to the efficiency of transfection and allow for enrichment of a cell population which have the potential to possess an edited genome.

As previously mentioned, the hTERT MSCs typically have poor transfection efficiency so human endothelial kidney (HEK293FT) cells were transfected with a Sox9 CRISPR/Cas9 vector to confirm the effectiveness of the fluorescence strategy (Figure 4.4.2). HEK293FT cells are known to have a high propensity for transfection and so were used as a proof-of-concept of the fluorescent strategy to ensure fluorescence was observed after transfection with CRISPR/Cas9. 48 hours post transfection green fluorescence could be seen in HEK293FT cells transfected with the Sox9 CRISPR/Cas9 vector, indicating the potential for genome editing. A control vector containing eGFP under a cytomegalovirus (CMV) promoter, resulting in overexpression of eGFP, was included as a positive control. From this result it would appear screening by fluorescence is a viable system to enrich cell populations, for the presence of Cas9.

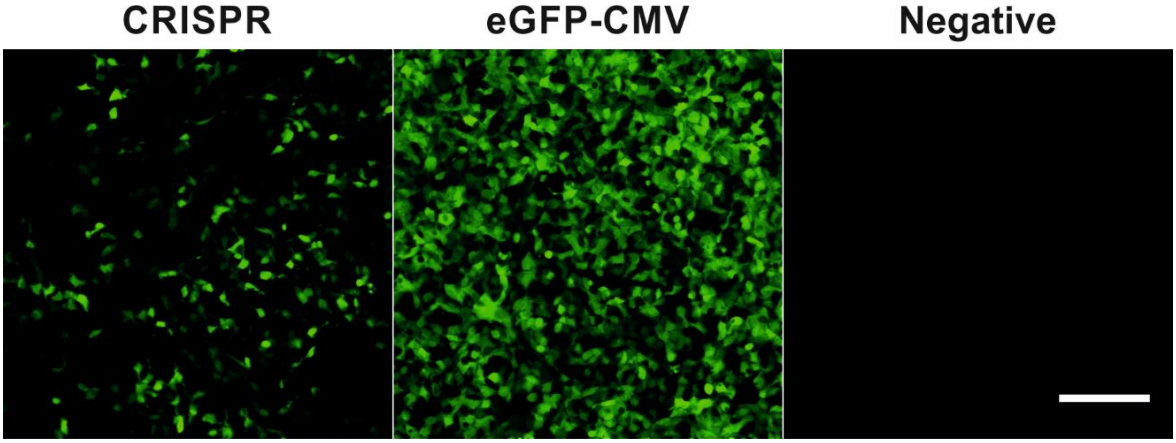

Figure 4.4.2: Lipid transfection of HEK293FT cells.

HEK293FT cells were chosen for their high transfection efficiency to test GFP expression upon transfection with the Sox9 targeting CRISPR/Cas9. A positive control plasmid (GFP-CMV) was also used alongside a cells only negative control. 48 hours post transfection fluorescence could be detected in both the positive control and CRISPR samples. The positive control has increased fluorescence due to the overexpression of eGFP caused by the CMV promoter. Scale bar represents 200μm.

4.4.3 Optimising CRISPR/Cas9 delivery into hTERT MSCs – comparison of lipid transfection and electroporation

4.4.3.1 Delivering CRISPR/Cas9 into hTERT MSCs by lipid transfection results in poor transfection efficiency

With evidence that the CRISPR/Cas9 system was able to be introduced and identified by fluorescence in the HEK293FT cells, lipid transfection was then used to determine whether fluorescence could be detected in the hTERT MSCs. The hTERT MSCs have a significantly reduced ability to be transfected in comparison to the HEK293FT cells with approximately 5% efficiency previously achieved using lipid transfection (Katherine Wilson, personal communication). The manufacturer's recommendations were followed initially to determine how viable lipid transfection was as a strategy.

Figure 4.4.3A shows the fluorescence detectable after transfection with either CRISPR or the eGFP-CMV vector in the Y201 hTERT MSCs. Weak fluorescence could be seen in the GFP positive controls, with approximately 2-3 fluorescent cells detectable per transfected well. However, no fluorescence could be detected when transfected with CRISPR/Cas9. This equates to an efficiency of approximately 0.05%, which is likely to be inadequate for finding successful genome editing. A mouse MSC line (CH310T1/2) is believed to have an increased transfection efficiency compared to the Y201 hTERT MSCs and therefore these were also transfected with CRISPR or the eGFP-CMV vector to determine whether an increased transfection efficiency would result in an increase in detectable fluorescence. Figure 4.4.4B shows that even with the increased lipid transfection efficiency of the CH310T1/2 MSCs, only one cell can be seen to be fluorescent in the CRISPR transfection. The drop in fluorescence between the eGFP-CMV vector and the CRISPR/Cas9 Sox9 vector, also seen in the HEK293FT cell line, may be responsible for the lack of fluorescence in the CRISPR panels.

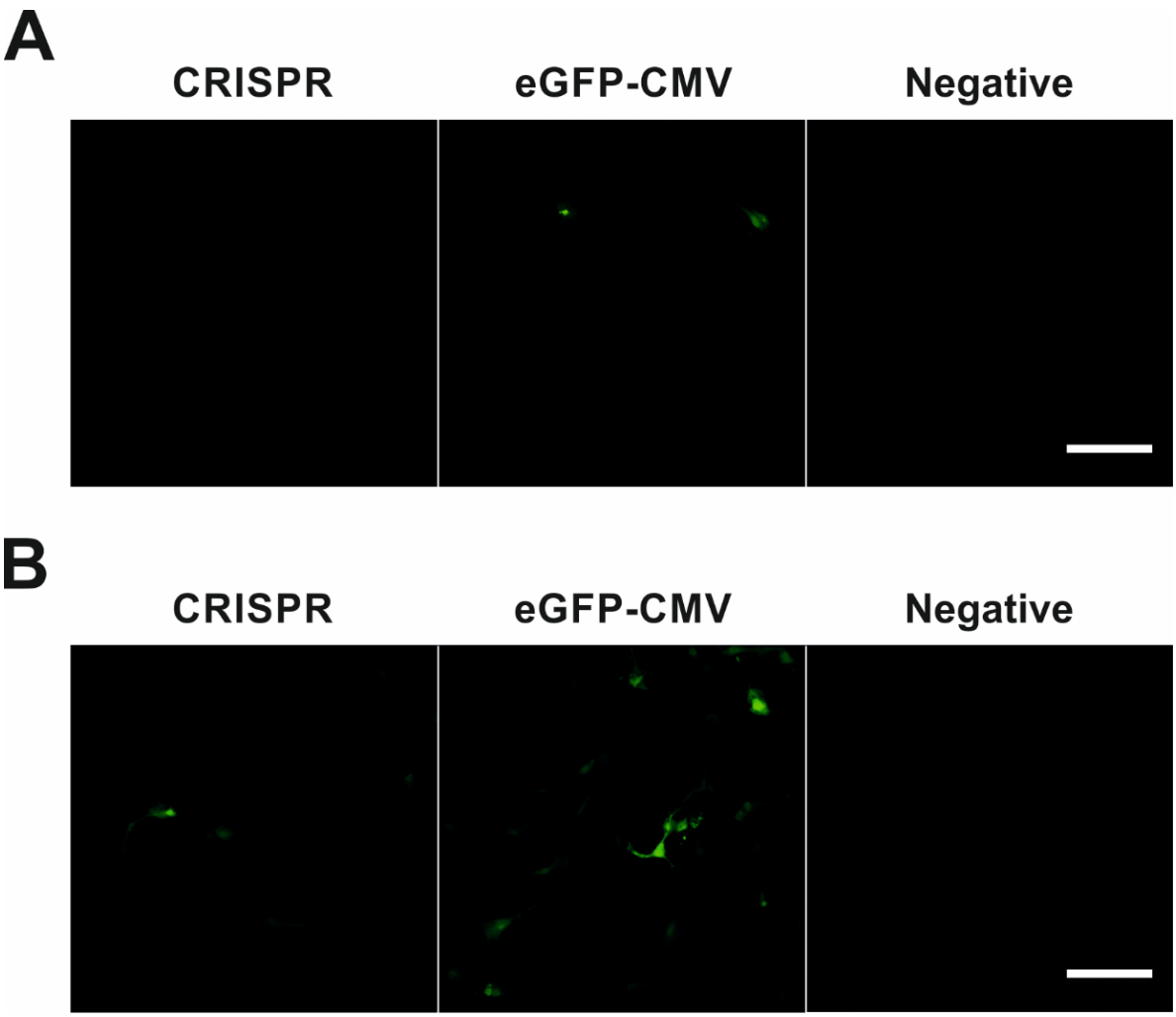

Figure 4.4.3: Lipid-based Transfection of MSCs

Two MSC (Y201 hTERT MSC (A) and C3H10T1/2 (B)) lines were transfected using lipid transfection following the standard protocol to test eGFP expression upon transfection with the Sox9 targeting CRISPR/Cas9. A positive control plasmid (eGFP-CMV) was also used alongside a cells only negative control. Very little fluorescence could be detected 48 hours post transfection in the positive control and no fluorescence could be detected in samples transfected with the CRISPR/Cas9 plasmid. Scale bar represents 200µm.

In an attempt to determine whether any successful transfections were occurring when hTERT MSCs were transfected CRISPR/Cas9, the cells were sorted via fluorescently activated cell sorting (FACS). FACS is more sensitive to low levels of fluorescence in comparison to confocal microscopy and will be the last stage in isolating genetically modified hTERT MSCs. It may be that if no fluorescence could be identified by confocal microscopy, differences in cellular fluorescence may be detected by FACS. Sorting was performed by gating to remove debris and doublet cells before normalising the autofluorescence of the Y201 hTERT MSCs to form a linear plot. eGFP-positive cells fluoresce in one channel (488-513/26) but not the other (488-576/21) created a shifted positive population. However, this sorting method isolated very few Y201 hTERT-MSCs at an efficiency of less than 1% (Figure 4.4.4).

Despite the increased sensitivity of FACS to low levels of fluorescence, less than 0.1% of hTERT MSCs sorted in this study presented with positive eGFP fluorescence. This equates to approximately 600 cells from a sort totalling 1,000,000 cells. Evidently this percentage is too low to reliably isolate genetically modified hTERT MSCs making this method unfeasible for further use.

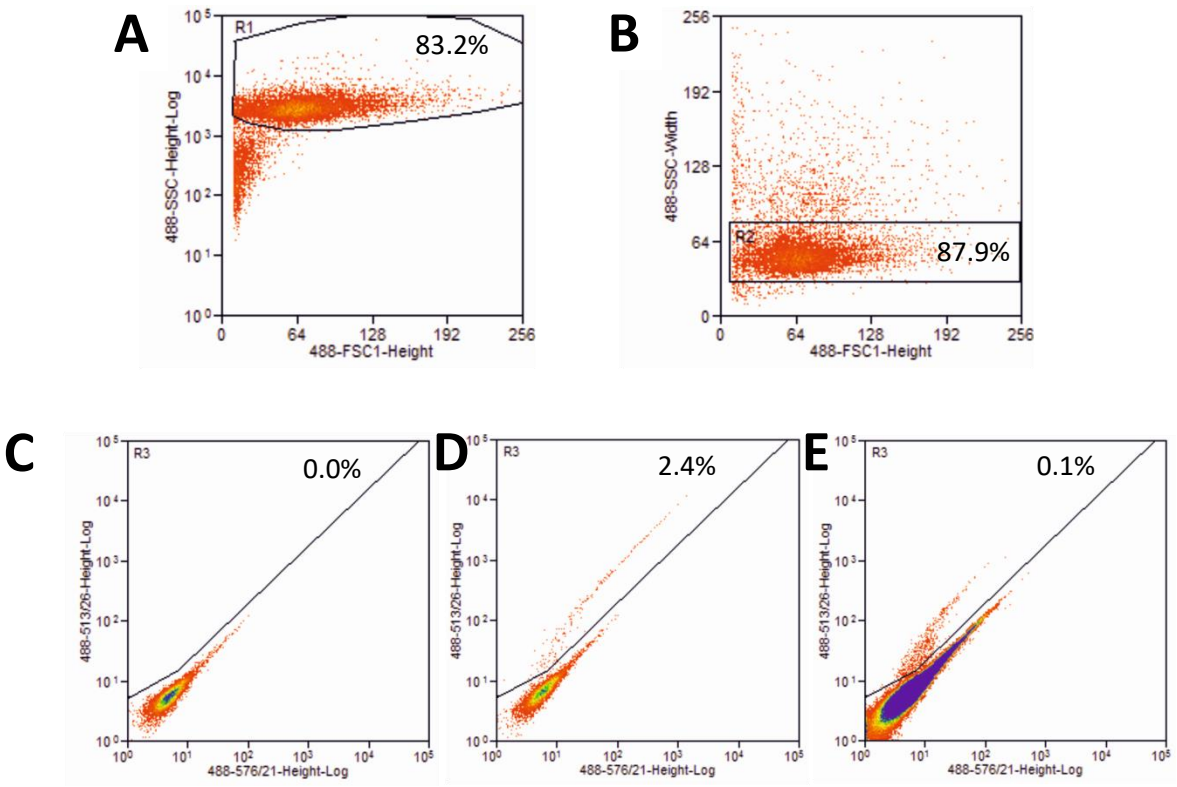

Figure 4.4.4: Lipid-based transfection of hTERT MSCs with CRISPR/Cas9 results in very few isolatable cells by FACS.

Dot plots demonstrating gating strategy removing dead cells/debris (A) and doublet cells (B) before plotting and normalising Y201 hTERT MSCs autofluorescence so that eGFP positive cells are shifted as a population. Each dot represents a single event as registered during the sort and gates have been drawn retrospectively to indicate the population segregation as performed during the sort. Percentages show the proportion of cells from the relevant histogram population present within the gate rounded to one decimal place. No events were recorded as positively expressing GFP in the cells only negative control (C) using this strategy whereas a shifted population can be seen in the positive control (D) and cells transfected with the Sox9 CRISPR/Cas9 (E).

4.4.3.2 Electroporation of hTERT MSCs with CRISPR/Cas9 results in viable fluorescent cells

An alternative method to lipid transfection was sought to improve efficiency and therefore the likelihood of successfully generating genetically modified hTERT MSCs. Mammalian cells respond well to electroporation with greater efficiencies compared to lipid transfection therefore electroporation using the Neon system was explored. Initially, Y201 hTERT MSCs were electroporated using various concentrations of the eGFP-CMV vector, with concentrations expanded above and below the manufacturer's recommended concentration for primary MSCs. Initial electroporations were performed using the recommended parameters for primary MSCs. The hTERT MSCs retained good viability (~80%) at all concentrations. The maximum efficiency obtained with these parameters was 12% with 8ug of DNA per million cells (results not shown), this concentration was therefore taken forward to determine optimal electroporation parameters.

Y201 hTERT MSCs were then tested with a range of electroporation parameters, varying pulse number, pulse width and pulse voltage, using the previously defined optimal DNA concentration. 100,000 cells were electroporated and replaced into a 6 well plate, one well per condition. After 24 hours viability and efficiency were analysed by flow cytometry, the results of which are summarised in Table 4.4.3. Several programmes resulted in few cells adhering after electroporation and these samples then had to be terminated before the required number of events was acquired during flow cytometery analysis. These samples (marked in red in Table 4.4.3) were excluded from further analysis. From this analysis the parameters used for sample 23, were deemed optimum resulting in a high viability (87.2%) and a high efficiency (51.6%). Roughly a one-hundred-fold increase in efficiency was achieved by electroporation compared to transfecting hTERT MSCs using a cationic lipid.

Table 4.4.3: Electroporation efficiencies of hTERT MSCs using various electroporation parameters

Sample	Pulse Voltage	Pulse Width	Pulse Number	Results	
				Efficiency (in live cells) (%)	Viability (%)
1	0	1	1	N/A	86.7
2	1400	20	1	33.7	86.0
3	1500	20	1	36.7	87.8
4	1600	20	1	N/A	19.3
5	1700	20	1	39.0	84.4
6	1100	30	1	18.7	87.7
7	1200	30	1	28.9	88.6
8	1300	30	1	23.3	90.9
9	1400	30	1	39.5	80.0
10	1000	40	1	25.0	86.2
11	1100	40	2	23.7	79.4
12	1200	40	2	12.7	61.8
13	1100	20	2	26.1	86.2
14	1200	20	2	78.5	40.3
15	1300	20	2	55.6	47.4
16	1400	20	2	39.4	89.2
17	850	30	2	18.9	87.4
18	950	30	2	20.5	62.6
19	1050	30	2	21.3	78.5
20	1150	30	2	30.1	86.0
21	1300	10	3	53.8	83.0
22	1400	10	3	48.5	88.8
23	**1500**	**10**	**3**	**51.6**	**87.2**
24	1600	10	3	49.7	71.3

Sox9 CRISPR/Cas9 was then delivered into Y201 hTERT MSCs using the optimised parameters and the cells sorted via FACS using the same gating strategy as before, 24 hours after electroporation (Figure 4.4.5). An efficiency of ~14% was achieved, a marked increase over that achieved using lipid transfection. No fluorescent cells were seen using this gating strategy when Y201 hTERT MSCs were electroporated with no plasmid present. Cells were replated at a maximum density of 100,000 cells per well of a 6 well plate and allowed to grow to confluency.

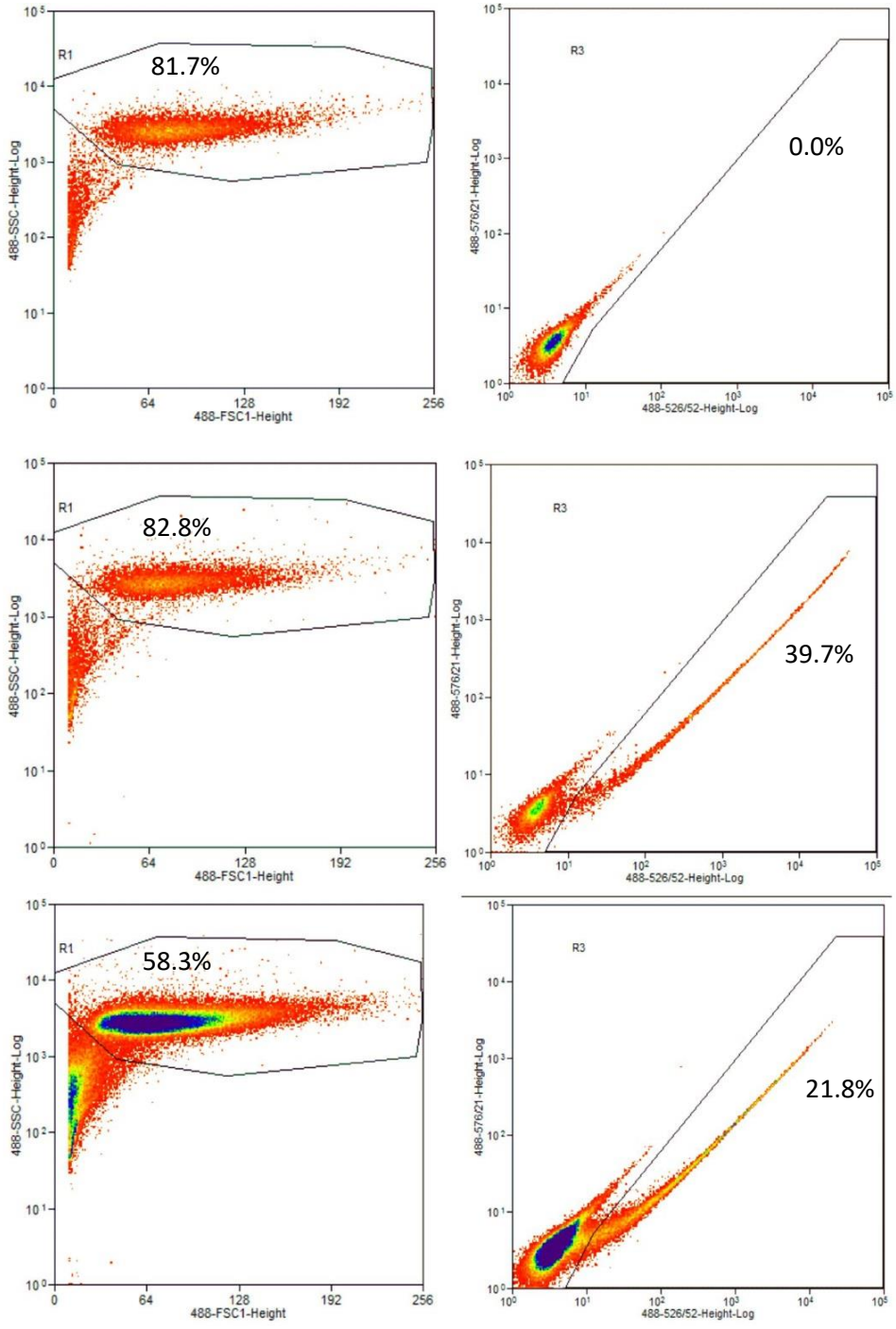

Figure 4.4.5: FACs analysis of Y201 hTERT MSCs electroporated with Sox9 CRISPR/Cas9.

Dot plot figures showing events recorded during the sorting of Y201 hTERT MSCs. These cells were gated first using forward scatter and side scatter to eliminate debris, dead cells and doublet cells. The remainder live single cells were sorted using the 488 laser where GFP positive cells show positive fluorescence on the X axis.

4.4.4 Mixed populations of CRISPR/Cas9 mutations can be identified by sequencing but not by SURVEYOR assay

CRISPR/Cas9 does not have 100% efficiency therefore Y201 hTERT MSCs isolated by FACS are not guaranteed to have mutations. The mixed population (MP) of cells isolated by FACS likely contains many wild type (WT) Y201 hTERT MSCs in addition to cells with heterogeneous and homogeneous mutations. It is also possible that the CRISPR/Cas9 sgRNA designed does not implement mutations effectively and that very few mutations will be observed in the MP. It would be beneficial to be able to determine whether any cells have been genetically modified before isolating clonal lines as derivation of a true clonal line can take a number of months to grow to a working capacity.

To determine whether any genome editing effects were seen in the Y201 hTERT MSCs, a mismatch nuclease assay was employed to examine differences between the WT Y201 hTERT MSCs and the CRISPR mixed population. Genomic DNA was isolated from both the WT and CRISPR mixed population cells and a relevant portion amplified by PCR as dictated by the manufacturers. These PCR products were then mixed and hybridised by heating and cooling to form duplexes *in vitro* and treated with the SURVEYOR mismatch nuclease. This nuclease recognises mismatches and polymorphisms in DNA and cleaves on the 3'-side of the mismatch site to form two (or more) products which can be compared to the profile seen in the wild type/control sample (Oleykowski et al., 1998). Hybridised duplexes were then analysed by agarose gel electrophoresis to discern any differences between the wild type and MP samples.

Figure 4.4.6 depicts the duplexes present when amplicons of WT Y201 hTERT MSC and MP Sox9 CRISPR DNA are hybridised and treated with the SURVEYOR mismatch nuclease. The WT control appears to have formed a homoduplex as evidenced by the single product still present after treating with the mismatch nuclease. The MP/WT control, however, is difficult to interpret. The dominant duplex within the sample appears to match that of the control, but an obvious reduction in signal is present and yet there are no additional bands present in the gel. Increasing exposure and retrospective image manipulation did not reveal any further bands. It may be possible that as the MP Sox9 CRISPR sample could possess many mutations that digestion results in a number of products not detectable by agarose gel electrophoresis.

In order to further determine whether any mutations were present in the MP CRISPR samples, both the Sox9 and Runx2 MP CRISPR samples were sent for sequencing. It was hypothesised that even though there may be a number of mutations, the sequencing trace would be perturbed upon reaching the PAM sequence targeted by the Cas9 enzyme. Primers were designed so that the PAM

site was at least 100bp downstream of the starting primer to ensure signal intensity was stable upon reaching the PAM sequence.

Figure 4.4.7 shows the sequence traces obtained for the Sox9 (A) and Runx2 (B) targeting CRISPRs. It was notable that the Sox9 sequencing trace appeared to show no alterations and a clean even trace was present until the end of the PCR product where the trace promptly ended. However, the Runx2 sequencing trace appeared clean until the PAM sequence of the CRISPR/Cas9, the trace after the PAM sequence appeared mixed with a number of smaller peaks appearing at each base point. This would indicate that the Runx2 CRISPR/Cas9 had successfully targeted and cut the DNA within these cells, this should result in a knockout of the Runx2 gene in some of these cells. The phenotype of these cells can therefore be observed to determine the effect of editing Runx2 in this fashion.

The Sox9 sgRNA will have to be redesigned in order to generate successful genome editing in the hTERT MSCs. Two new sgRNA sequences were therefore designed using crispr.mit.edu to attempt to create a successful Sox9-KO hTERT MSC cell line. The target was designed to be within the first exon, again to minimise the chances of a truncate protein having any activity. Figure 4.4.8 summarises the two sgRNAs chosen while Table 4.4.4 and Table 4.4.5 summarise the potential off-targets for each sgRNA.

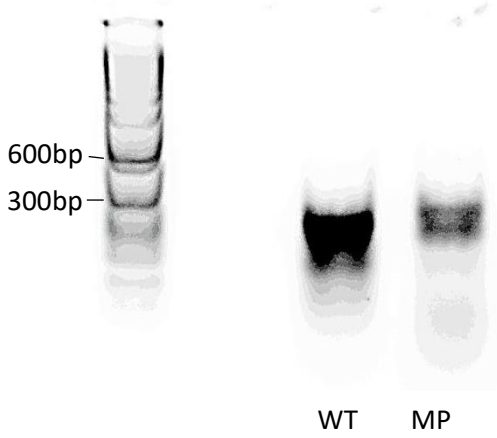

Figure 4.4.6: SURVEYOR mutation detection assay of heterogeneous Y201 hTERT Sox9 CRISPR/Cas9 MSCs.

PCR products roughly 500 base pairs in size were amplified from WT Y201 hTERT MSCs and a heterogeneous Y201 hTERT Sox9 CRISPR/Cas9 MSCs. These were annealed to form heteroduplexes and exposed to SURVEYOR mismatch nuclease. The control WT sample consists of 100% wild type DNA whereas the test sample consists of a 1:1 ratio of wild type and Sox9 CRISPR/Cas9 DNA. There appears to be a drop in full size product in the heterogenous CRISPR sample compared to the wild type reference sample. WT = wild type Y201 MP = Mixed population CRISPR

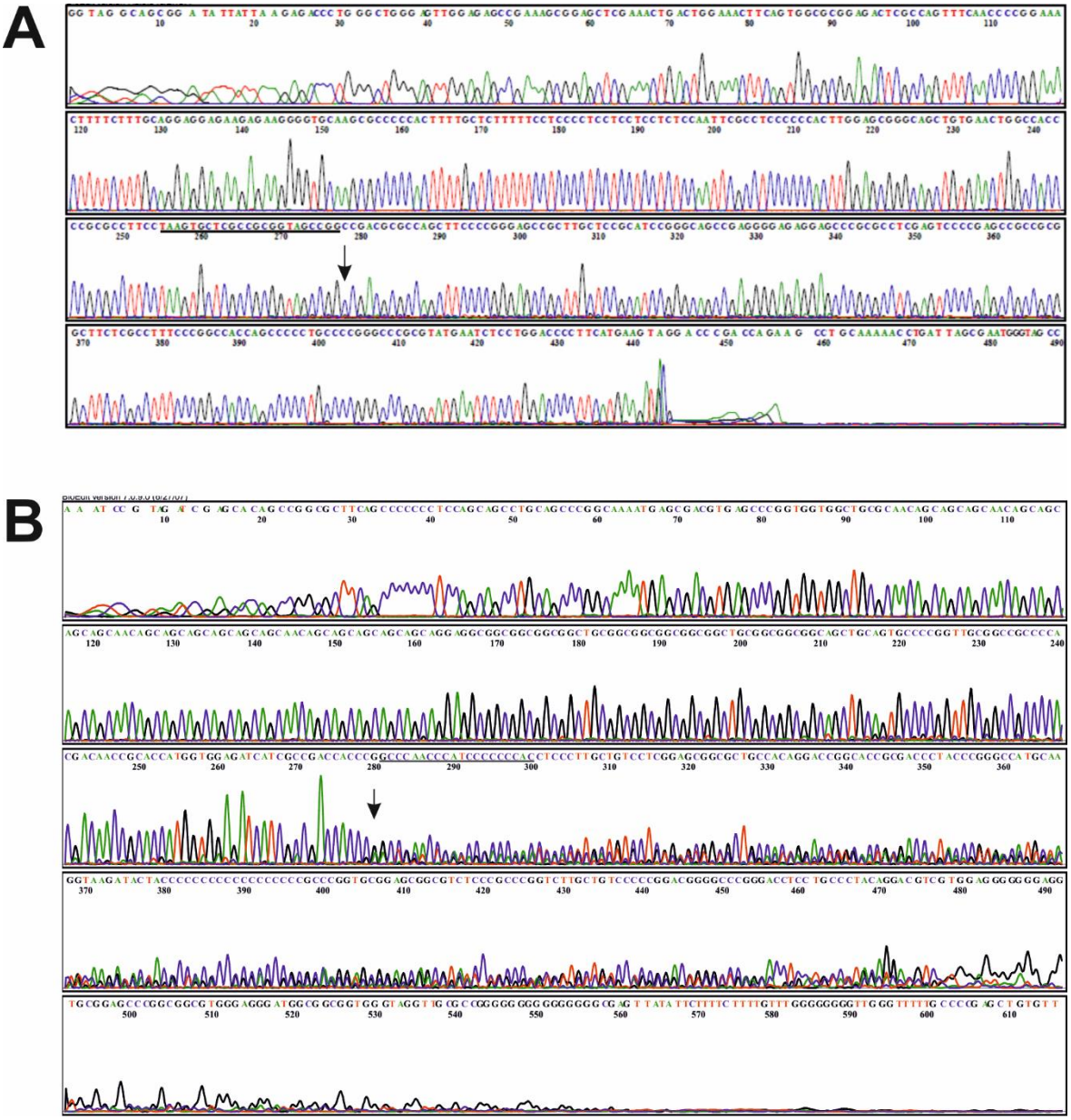

Figure 4.4.7: Sequence traces of mixed population of CRISPR/Cas9 electroporated Y201 hTERT MSCs show mixed trace after PAM.

PCR products were amplified from heterogeneous Y201 hTERT Sox9 (A) or Runx2 (B) CRISPR/Cas9 MSCs. These were submitted to Sanger sequencing to provide an overview of the traces present in the mixed population sample. The position of the sgRNA designed for each CRISPR is underlined in each instance. It is notable that after the PAM in the Runx2 CRISPR/Cas9 hTERT MSCs a mixed trace is suddenly apparent whereas this is not the case in the Sox9 CRISPR/Cas9 hTERT MSCs (the first base after the PAM is marked with an arrow).

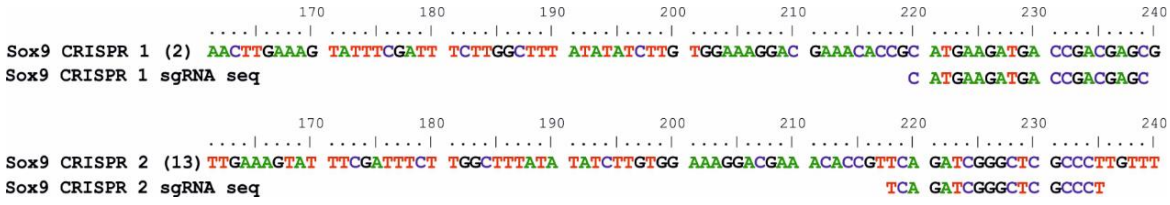

Figure 4.4.8: Confirmation of successful sgRNA sequence cloning into CRISPR/Cas9 vectors by Sanger sequencing.

Clones highlighted as successful by the colony PCR were taken for Sanger sequencing. The template sequence for each of the Sox9 sgRNAs has been listed below the consensus sequences.

Table 4.4.4: Off-target effects for Sox9-MP 1 sgRNA

Sequence	Score	Mismatches	Ucsc gene	Locus
CACGTCGCTGACC GACGAGCCGG	0.8	4MMs [3:5:6:8]	NM_001270366	chr19:+812787
AATGAAATTGACA GACGAGCAGG	0.4	4MMs [1:7:8:13]		chr20:+47066244
CATGAAGTGAACA GACGAGCCAG	0.3	4MMs [8:9:10:13]		chr16:+86856690
ATTGAAGATGACT GACAAGCTGG	0.2	4MMs [1:2:13:17]		chr7:-125085531
CCTGGAGATGACC GACGACAGAG	0.2	4MMs [2:5:19:20]		chr17:+79552292
CAAGAAGATGACC AACGAGGTAG	0.2	3MMs [3:14:20]	NM_001037329	chr11:+6262680
CATGATGAACACT GACGAGCCAG	0.2	4MMs [6:9:10:13]		chr8:+73786579
CATTAAGAAGAAG GACGAGCTGG	0.2	4MMs [4:9:12:13]	NM_001009	chr19:+58906067
CATGATGATCCCA GACGAGCTGG	0.2	4MMs [6:10:11:13]	NM_001193269	chr19:-46141822
CATCAAGATGCAC GACTAGCAAG	0.2	4MMs [4:11:12:17]		chr6:-2414224
CAGGAAGAGGACT GACGAGGAGG	0.2	4MMs [3:9:13:20]		chr15:-98721431
CATCCAGAGGACC GAGGAGCTGG	0.2	4MMs [4:5:9:16]	NM_020884	chr20:+33586684
CATGGGGATGACA GACCAGCCGG	0.1	4MMs [5:6:13:17]		chr8:+10072923
CGTGAAGGTGGCC TACGAGCAGG	0.1	4MMs [2:8:11:14]	NM_207360	chr6:-149777906
CAAGAAGATAACA GAAGAGCAAG	0.1	4MMs [3:10:13:16]		chr10:-8072635
CTTGGAGATGACT CACGAGCAGG	0.1	4MMs [2:5:13:14]		chr14:-76815313
CTTGAAGAGGAGC GAGGAGCTGG	0.1	4MMs [2:9:12:16]		chr14:-70495876
CATTAAGATGCCC GAAGAGGAAG	0.1	4MMs [4:11:16:20]	NM_015156	chr14:+103188724
CAGGAAGAAGAC GGAGGAGCCGG	0.1	4MMs [3:9:13:16]	NR_038257	chr21:+45845594
CCTGAAGATGATC GAGGAGGCAG	0.1	4MMs [2:12:16:20]	NM_181865	chr1:-6409845
CAGGAAGATGACT GACGGGTCAG	0.1	4MMs [3:13:18:20]		chr8:+72423756
CATGATGATAACC AACAAGCCAG	0.0	4MMs [6:10:14:17]		chr17:-67420119

Sequence	Score	Mismatches	Ucsc gene	Locus
CATTCAGATGACC CACGGGCTGG	0.0	4MMs [4:5:14:18]		chr2:-113900267
CATGAGGATGACC AATGAGCTAG	0.0	3MMs [6:14:16]		chr3:-127647583
CAGCAAGATGACC CATGAGCTGG	0.0	4MMs [3:4:14:16]		chr1:+208169533
CATGAAAATGAGC GATGAGAGAG	0.0	4MMs [7:12:16:20]		chr13:+92925194
CAGGAAGATGACA CACAAGCCAG	0.0	4MMs [3:13:14:17]		chrX:-120444871
CATGAAGATGAAG GACAATCCAG	0.0	4MMs [12:13:17:19]		chr4:-101437387
CATCAAGATGACA GTGGAGCCAG	0.0	4MMs [4:13:15:16]		chr7:+37397445
CAGGAAGATGACC TGCCAGCCGG	0.0	4MMs [3:14:15:17]		chr2:-20841293
CATGACGATGACA GAAAAGCAAG	0.0	4MMs [6:13:16:17]		chr18:-34490830
CATGAAGATGTCA GATCAGCAAG	0.0	4MMs [11:13:16:17]	NM_032445	chr15:-66188377
CAGGAAGATGAAC TAGGAGCTGG	0.0	4MMs [3:12:14:16]		chr20:+347399
CATGAAGATCCCC CAAGAGCCAG	0.0	4MMs [10:11:14:16]		chr11:+113240704
CATGAAGAGGACC GTCCTGCAAG	0.0	4MMs [9:15:17:18]		chr3:-45673422
CATGAAGAAGACC CACGAAGAGG	0.0	4MMs [9:14:19:20]		chr5:+79584876
CATGGAGATGACC AAGGAGAGAG	0.0	4MMs [5:14:16:20]		chr6:-21371690
CATGAAGATGAAA GCCGTGCTGG	0.0	4MMs [12:13:15:18]	NM_001127235	chr5:+56545369
CAAGAAGATGACC CAAGACCTGG	0.0	4MMs [3:14:16:19]		chr18:+9833084
CATGAAGATGAGA GTTGAGCCAG	0.0	4MMs [12:13:15:16]		chr15:+69903604
CATAAAGATGACC ACTGAGCTGG	0.0	4MMs [4:14:15:16]		chr2:-220847040
CATGATGATGACC AATGAGAAAG	0.0	4MMs [6:14:16:20]		chr16:+80607281
CATGAAGAGGACC CACCCGCCAG	0.0	4MMs [9:14:17:18]		chr15:+29645522
CATGAAGCTGACC ACTGAGCTAG	0.0	4MMs [8:14:15:16]		chr15:-64397993
CATGAAGCTGACC TGTGAGCCAG	0.0	4MMs [8:14:15:16]		chr5:-71541011

Sequence	Score	Mismatches	Ucsc gene	Locus
CATGAAGATGACC TCCTGGCTGG	0.0	4MMs [14:15:17:18]		chr1:-179793081

Table 4.4.5: List of potential off-target effects for the Sox9 2 sgRNA

Sequence	Score	Mismatches	Ucsc gene	Locus
ATCAGCTTGAGC TCGCCCTTGAG	0.8	4MMs [1:6:8:10]		chr18:+75883545
GTCTGATGGGGC TCCCCCTTTGG	0.4	4MMs [1:4:8:15]		chr2:+235697960
TTCGTCTCGGGC TCGCCCTGAGG	0.4	4MMs [4:5:6:20]	NM_003702	chr8:+54793674
TTAACATCAGGC ACGCCCTTTGG	0.3	4MMs [3:5:9:13]		chrX:+8192829
CTCAGGTCGAGC TCGCCCCTCGG	0.3	4MMs [1:6:10:19]	NM_001080209	chr18:+5890799
TACAGACCGGCC TCGCCCTGCAG	0.3	4MMs [2:7:11:20]	NM_032941	chr12:+21654288
TTCTCATGGGGC TTGCCCTTGAG	0.2	4MMs [4:5:8:14]		chr3:+127881544
CTCAGATCTGTC TCGCCCCTCAG	0.2	4MMs [1:9:11:19]		chr4:+60278549
TTCATTTCTGGCT CTCCCTTTAG	0.1	4MMs [5:6:9:15]		chr8:-94567932
CTGAGGTCGGGC TGGCCCTTTAG	0.1	4MMs [1:3:6:14]		chr9:-139079842
TTCCCATCAGGC TGGCCCTTTGG	0.1	4MMs [4:5:9:14]		chr8:-37691857
TTTAGCTGGGGC TGGCCCTTGGG	0.1	4MMs [3:6:8:14]		chr12:+4218862
TTGTGATCGGGG TCGGCCTTGAG	0.1	4MMs [3:4:12:16]	NM_001105574	chr10:-124896640
TTCAGGTCGGGC TTGCCCTGCGG	0.1	3MMs [6:14:20]	NM_001281454	chr19:+1584658
TCCAGCTCTGGC TCGCCGTTGAG	0.1	4MMs [2:6:9:18]	NM_004286	chr22:-39102112
ATCAGCTCGGGC TCACCCTGCAG	0.1	4MMs [1:6:15:20]		chr3:+34225289
TTCAGAAAGGGC CCCCCCTTTAG	0.1	4MMs [7:8:13:15]		chr10:-95795413
TACAGATGGGGC TGGCTCTTCGG	0.1	4MMs [2:8:14:17]		chr17:-73308292
TTCAGCATGGGC TGGCCCTTGGG	0.1	4MMs [6:7:8:14]	NM_002839	chr9:+8499670

Sequence	Score	Mismatches	Ucsc gene	Locus
TACAGATGGGGC TCTCCTTTAAG	0.1	4MMs [2:8:15:18]		chr11:-86599717
GTCAGCTCGGCC TGGCCCTTTGG	0.1	4MMs [1:6:11:14]	NM_001277378	chr19:+14192517
TTCAGATGAGGC TCACCCATGAG	0.1	4MMs [8:9:15:19]		chr8:-134979703
TTGAGTTCGGGC TCCACCTTGAG	0.0	4MMs [3:6:15:16]		chr13:-94825903
TTCAGATCTGTCT CTCCCATGAG	0.0	4MMs [9:11:15:19]		chr10:-92790425
TTCAGATGGAGC TAGCCTTTTAG	0.0	4MMs [8:10:14:18]	NM_022168	chr2:-163174326
TTCAGATCTGGC TCTCTCTGTGG	0.0	4MMs [9:15:17:20]		chr15:+60928147
TTCAGATCTGCC TCGGCCTCCAG	0.0	4MMs [9:11:16:20]		chr2:+38004482
TTCAGAACGGGC TCACTATTCAG	0.0	4MMs [7:15:17:18]		chr17:+59102487
TTCAGATGGGGC AAGTCCTTAAG	0.0	4MMs [8:13:14:16]		chr4:+186992404

The new Sox9 targeting sgRNA sequences were cloned into the CRISPR/Cas9 vector as before, and then the Y201 hTERT MSCs electroporated with the complete vectors. Electroporated hTERT MSCs were then sorted via FACS to isolate fluorescent cells as these had successfully electroporated and so had the possibility of possessing genome edits. The two mixed populations of Sox9 CRISPR/Cas9 hTERT MSCs were then assessed for their genotype and phenotype, these have been termed Sox9-MP 1 and Sox9-MP 2 to differentiate between the two sgRNAs used.

Figure 4.4.9 shows the on-target sequence obtained by Sanger sequencing of an amplified PCR product from the Sox9-MP 1, the sgRNA sequence has been underlined. Unlike the previous Sox9 targeting sgRNA, the sequence trace in this figure demonstrates obvious evidence of genome editing. After the PAM sequence, where the Cas9 is able to cut, the sequence trace no longer appears as one single clean trace, but rather multiple peaks are able to be seen at each base analysed. It would appear therefore that the first of the sgRNAs targeting Sox9 has been able to successfully direct Cas9 to the target sequence, resulting in genome editing. The effect is much less obvious in the Sox9-MP 2 cells (Figure 4.4.10), with a single clean trace appearing throughout the entirety of the sequence. However, there does appear to be a rise in the background after the PAM sequence, which may be evidence of genome editing.

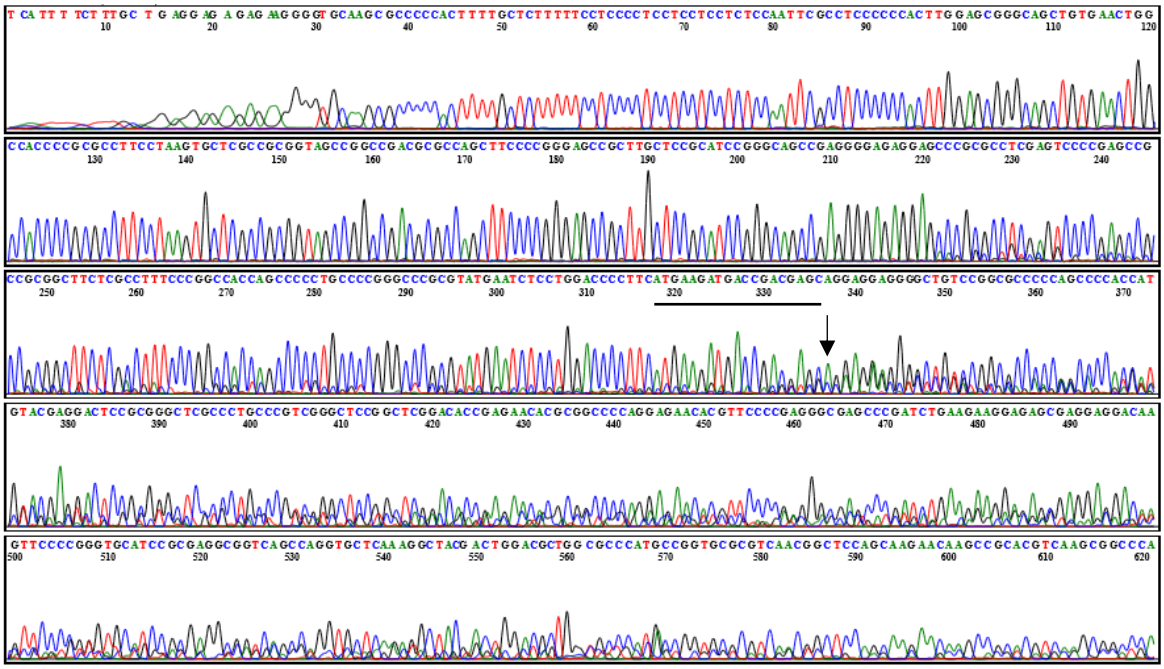

Figure 4.4.9: On-target Sanger sequencing of PCR amplified Sox9-MP 1 hTERT MSC

PCR products were amplified from heterogeneous Y201 hTERT Sox9-MP 1 CRISPR/Cas9 MSCs. These were submitted to Sanger sequencing to provide an overview of the traces present in the mixed population sample. The position of the sgRNA designed for the CRISPR is underlined. A mixed trace is evident after the predicted position of the DSB, the base after this break has been highlighted with an arrow.

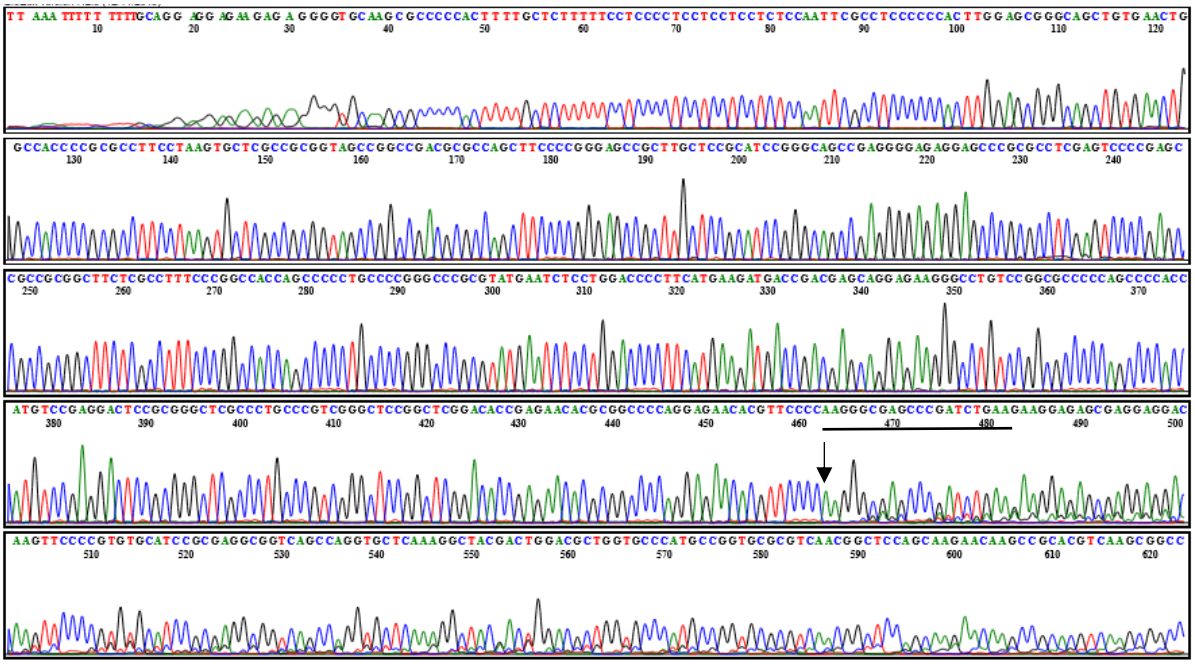

Figure 4.4.10: On-target Sanger sequencing of PCR amplified Sox9-MP 2 hTERT MSC

PCR products were amplified from heterogeneous Y201 hTERT Sox9-MP 2 CRISPR/Cas9 MSCs. These were submitted to Sanger sequencing to provide an overview of the traces present in the mixed population sample. The position of the sgRNA designed for this CRISPR is underlined, and the base after the DSB highlighted with an arrow. A drop in signal is seen after the DSB, but the mixed trace is not as evident in this sample as in previous samples.

4.4.5 Isolation of clonal lines by serial dilution results in individual mutations in relevant gene targeted by CRISPR/Cas9

Runx2 targeted Y201 hTERT MSCs successfully isolated using this method were expanded and serial dilution performed to isolate clonal lines. Approximately 10 days after seeding, when individual colonies were visible by light microscopy, wells were scored based on the number of colonies present. Wells were either marked as confluent, having multiple colonies present, single colonies present or no cells visible. A repeat scoring was made 4-5 days after the initial scoring to confirm single colony status and these individual colonies were expanded and coded. These cell lines were derived from an individual colony presumed to be initiated by a single cell and therefore all cells in this line should have the same mutation present as caused by the CRISPR/Cas9 genome editing system. Cell lines derived for the Runx2 targeted hTERT MSCs were coded as A6D5, A6F4, A6F6, A6H4, B6C8, B6F4 and B6F6, arbitrarily named based on well locations.

Finally, the PCR products from the clonal lines were sequenced and compared to the WT Y201 hTERT MSCs. The Runx2 clonal lines showed signs of genome editing in each of the lines (results discussed in 4.4.6). This would suggest that the CRISPR/Cas9 has been successful in these instances, but the exact effects on the gene would need to be investigated as the heterogeneous nature of the sequences made it impossible to determine the knockout status at this time. The clonal lines taken forward for further analysis were A6F4, A6H4, B6F4, B6F6 as these lines expanded to cell numbers suitable for phenotypic analysis most rapidly. These clonal lines were compared to WT hTERT MSCs and the initial mixed population the colonies were derived from (referred to as Runx2-MP hTERT MSCs).

The exact results of targeting Sox9 with CRISPR/Cas9 would need to be similarly confirmed by isolating clonal lines, and reanalysing the genotype of both the on-target and off-target sequences in these clonal lines. Due to the redesign of the Sox9 sgRNAs it was not possible to derive clonal lines for genotypic and phenotypic analysis within the timeframe of this thesis. However, some phenotypic behaviours may be observed in the mixed populations, if the sgRNA has a high efficiency, therefore the initial sorted mixed population of Sox9 targeted hTERT MSCs was taken forward for further experiments, these are continued to be referred to as Sox9-MP 1 and Sox9-MP 2 hTERT MSCs (results in 4.4.9).

4.4.6 Genotypic analysis of clonal GM Runx2 hTERT MSC lines

By serial diluting the cells and identifying colonies microscopically, it was possible to derive clonal lines from the Runx2 targeted hTERT MSCs (Runx2-GM hTERT MSCs). These could then be further

analysed and compared to the WT Y201 and Runx2-MP hTERT MSCs to give further insight of the genotype and phenotype of these cells as a result of the genome editing by CRISPR/Cas9.

Figure 4.4.11 and Figure 4.4.12 show on-target sequence traces of two of the clonal lines generated from the Runx2-MP hTERT MSCs, namely the A6F4 and A6H2 lines respectively. These are representative of the clonal lines taken forward for analysis and demonstrate the genome editing that has occurred as a result of the CRISPR/Cas9. After the PAM sequence in each instance the sequence trace signal drops and a mixed trace becomes present. This indicates that the sequences of the two alleles of the gene no longer match and a single sequence cannot be generated from the amplified PCR product. Although, this does not tell us the exact effect the genome editing has had, it gives an indication that the cell lines have perturbed Runx2 genes. This may result in a homogeneous or heterogeneous knockout, and the cell line will be analysed for any changes in cell behaviour as a result of this genome editing.

The potential of off-target effects for the Runx2 sgRNA (summarised in Table 4.4.2) were low but some were identified. This should be taken into account when analysing the phenotype of the clonal lines, in case any off-target effects were present in the cells. Due to the number of clonal lines derived, and the number of potential off-targets, off-target sequencing was not performed at this time.

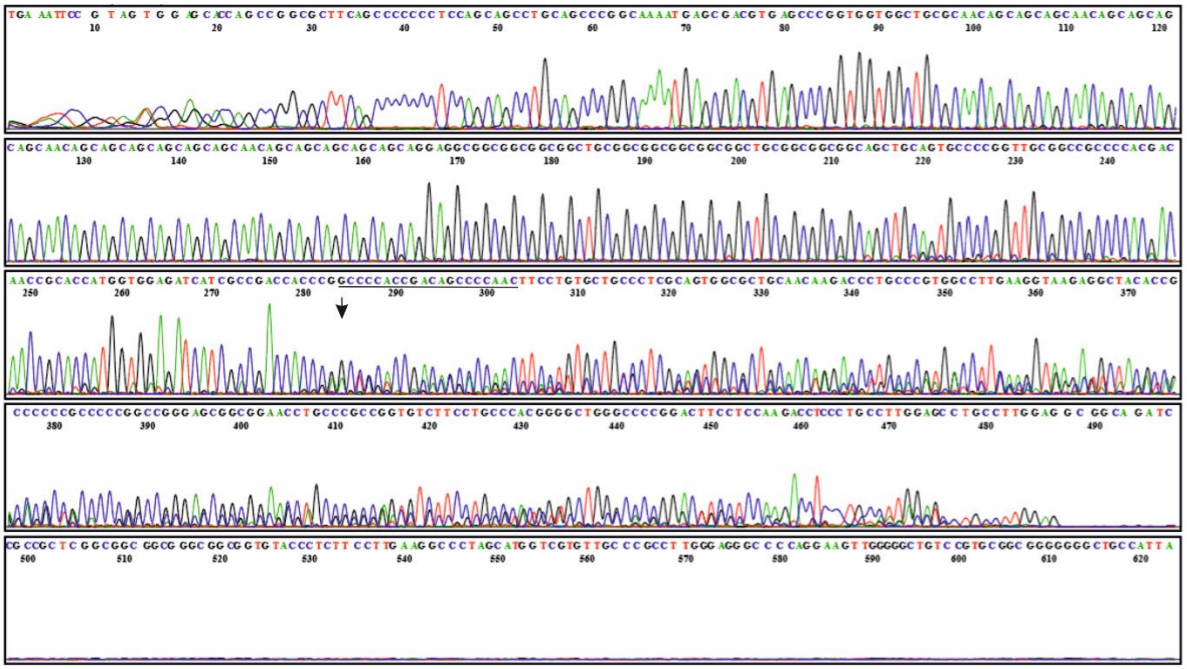

Figure 4.4.11: Sequence trace of clonal Runx2 GM hTERT MSC line Runx2 A6F4

Sequence trace generated of amplified PCR product examining on-target effects of Runx2 targeted CRISPR/Cas9. Genome editing effects can be seen after sequenced base 284, the predicted position of the DSB, where the signal drops and a mixed trace can be seen. The position of the sgRNA designed for the CRISPR is underlined and the base after the DSB has been highlighted with an arrow.

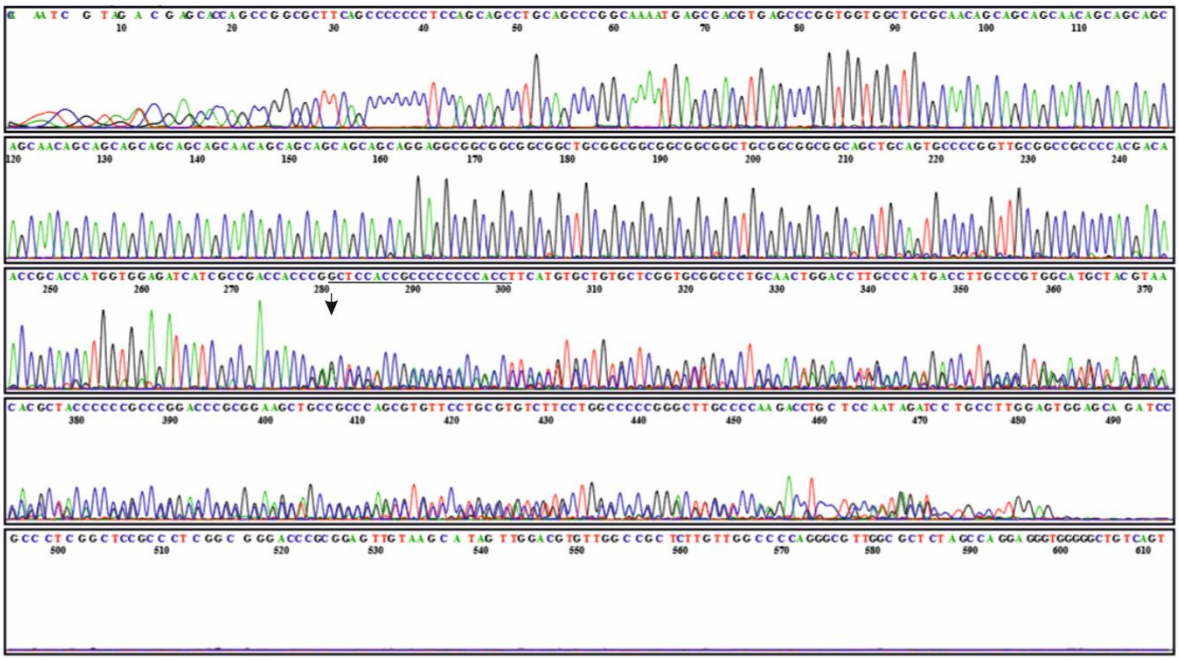

Figure 4.4.12: Sequence trace of clonal Runx2 GM hTERT MSC line Runx2 A6H2

Sequence trace generated of amplified PCR product examining on-target effects of Runx2 targeted CRISPR/Cas9. Genome editing effects can be seen after sequenced base 281, the predicted position of the DSB, where the signal drops and a mixed trace can be seen. The position of the sgRNA designed for the CRISPR is underlined and the base after the DSB has been highlighted with an arrow.

4.4.7 Genetic modification of Runx2 impacts colony forming capabilities of hTERT MSCs but does not appear to affect morphology or viability

Clonal lines were isolated and expanded for approximately 3 months to establish a bank of cells before phenotypic analysis was initiated. First the morphology of the clonal Runx2 cell lines was compared to the WT hTERT MSCs, either by crystal violet staining or by phase microscopy. Figure 4.4.13 summarises these results. The morphology of the Runx2 cell lines, and the Runx2-MP cells, were found to be very similar to the WT hTERT MSCs. All cells analysed possess a fibroblastic morphology typical of an MSC.

Next, the clonogenic ability of the clonal Runx2 cell lines (B6F4 and B6F6) were tested alongside the MP of Runx2-GM hTERT MSCs. These cells were plated at clonal density and allowed to grow until resultant colonies filled the field of view under a 10x microscope lens, approximately 12 days. These colonies were then fixed and stained with crystal violet solution, and the number of colonies scored and the efficiency of colony formation summarised in a bar chart (Figure 4.4.14A+B). It was notable that the colonies of the Runx2-GM hTERT MSCs, both MP and clonal lines, appeared to be more condensed than the WT hTERT MSCs. Cells appeared to be much more closer together and not spread evenly across the entirety of the colony. Additionally, the ability of the Runx2-GM hTERT MSCs to form colonies in this manner appeared greatly impaired compared to the WT hTERT MSCs. Whereas the WT hTERT MSCs routinely produced between 30 and 40 colonies in each instance, the Runx2-GM hTERT MSCs typically only produced approximately 10 colonies per plate analysed.

Finally, an MTT assay was performed over 72 hours analysing numbers of viable cells in the clonal lines, Runx2 A6F4 and A6H2. Over this timeframe it was found that the two clonal lines tested appeared to have increased cell numbers compared to the WT hTERT MSCs (Figure 4.4.14C). Comparing these results to the CFU-F assay, it would appear that there potentially may be an increased number of cells in the colonies analysed, however this would need to be further quantified to prove accurate. It would appear therefore that the alteration of Runx2 in this manner has impacted negatively on the colony forming ability of the Y201 hTERT MSCs but conversely also increased the proliferative rate of these cells.

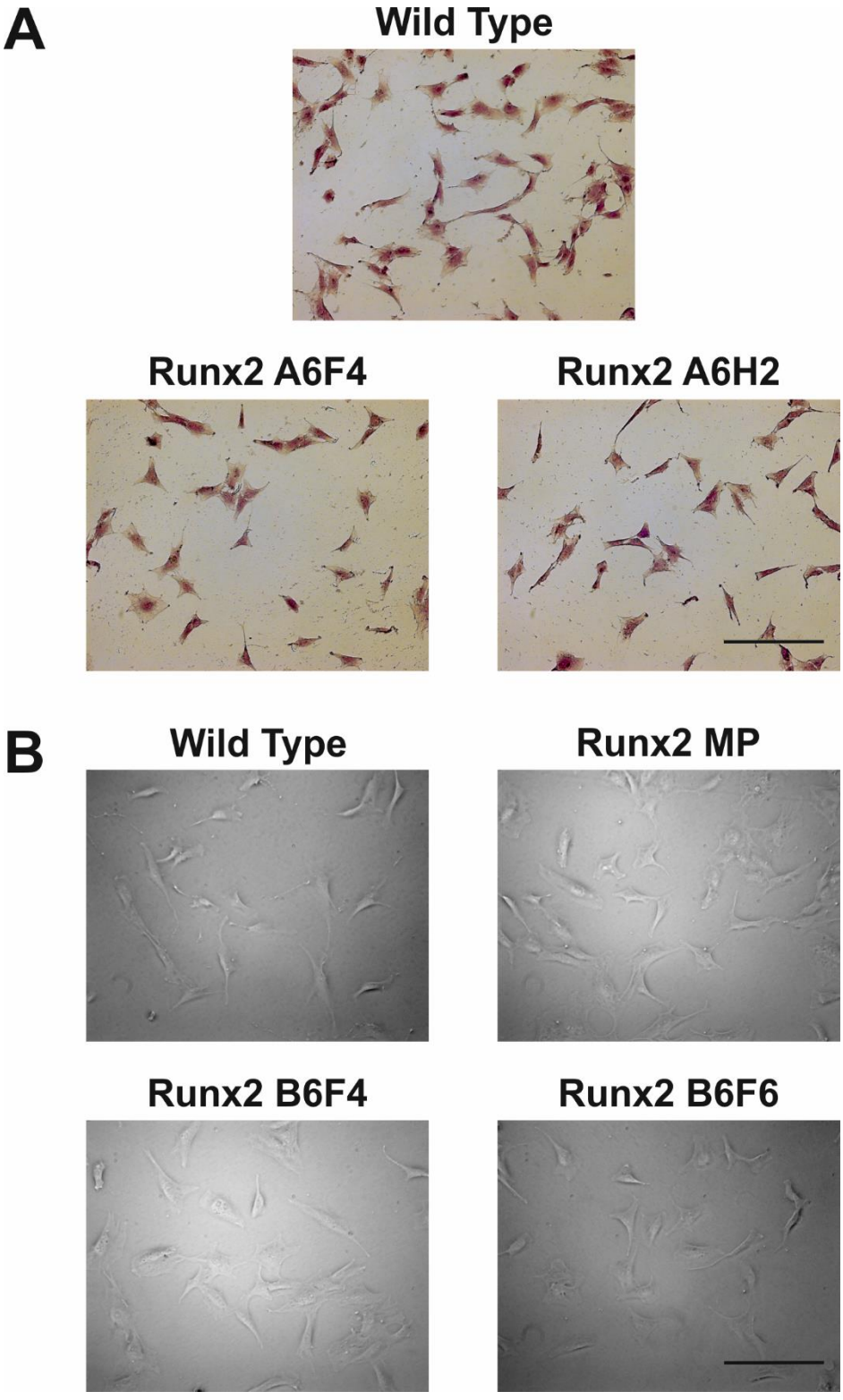

Figure 4.4.13: Qualitative morphological analysis of Runx2-GM Y201 hTERT MSCs by microscopy

Cells were plated subconfluence, cultured for 24 hours and either (A) fixed and stained with crystal violet stain before imaging or (B) imaged using phase microscope. Scale bar = 200µm.

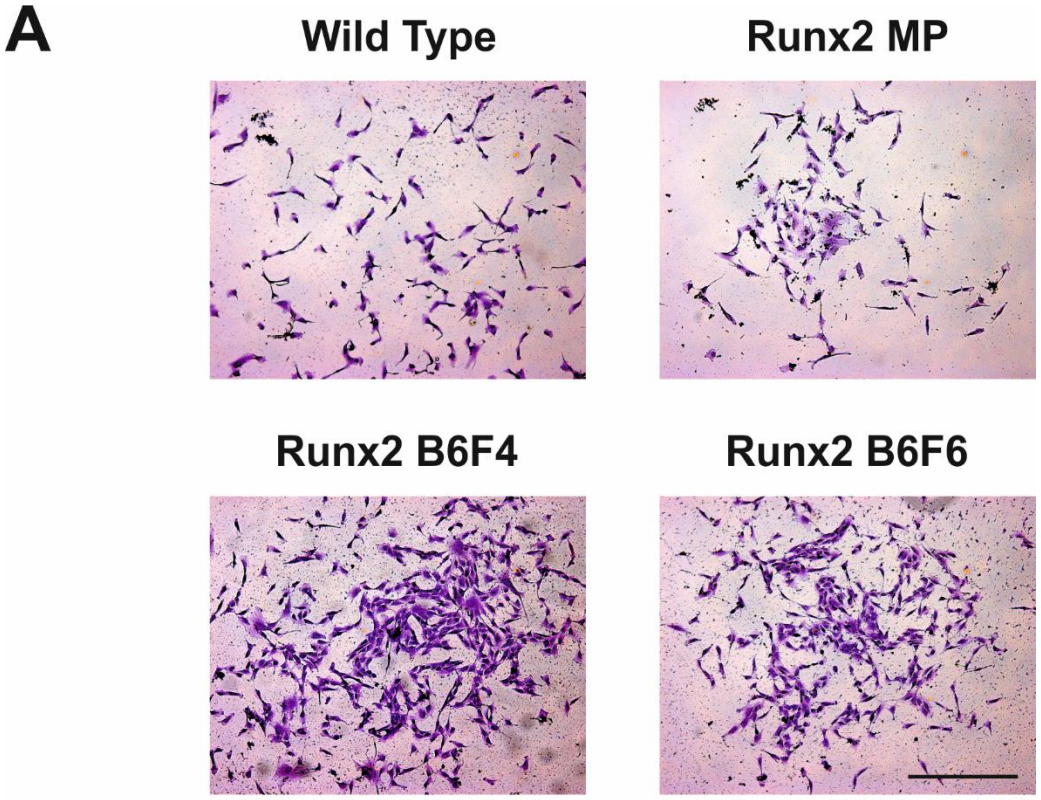
A
Wild Type
Runx2 MP
Runx2 B6F4
Runx2 B6F6

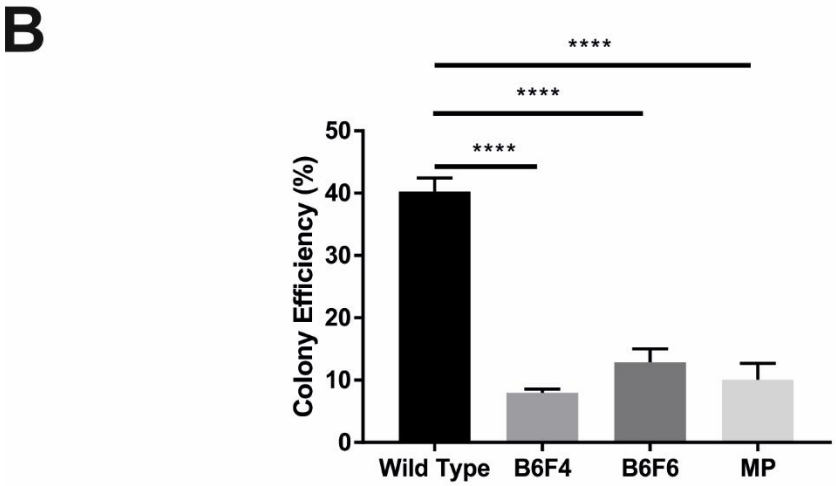
B
****
****
****
Colony Efficiency (%)
50
40
30
20
10
0
Wild Type
B6F4
B6F6
MP

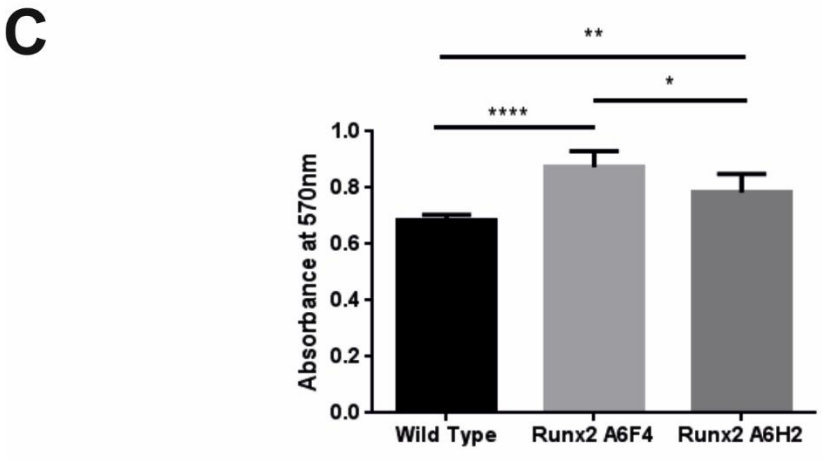
C
**
*
****
Absorbance at 570nm
1.0
0.8
0.6
0.4
0.2
0.0
Wild Type
Runx2 A6F4
Runx2 A6H2

Figure 4.4.14: Analysis of clonogenic and proliferation capabilities of Runx2-GM hTERT MSCs

Cells were plated subconfluence, cultured for 24 hours and either (A) fixed and stained with crystal violet stain before imaging or (B) imaged using phase microscope. Scale bar = 200µm. An MTT assay (C) was performed to analyse the number of viable cells after 72 hours culture period, $5x10^3$ cells/cm^2 plated. After 72 MTT was added for 3 hours, eluted with acidic isopropanol and the absorbance read.

4.4.8 Runx2-GM hTERT MSCs retain osteogenic differentiation and show increased capacity for adipogenic differentiation

With the initial results indicating the genome editing achieved in Runx2 was impacting on the proliferation of the cells, and the ability of the cells to form colonies, it was then decided to establish the impact on the differentiation of the hTERT MSCs. Initially, the ability of the cells to differentiate into osteoblasts was analysed by differentiating for 21 days with an osteogenic simulative cocktail and staining the resulting deposited calcium with Alizarin Red. This was first performed for the clonal lines A6F4 and A6H2 and representative images of the timecourse are shown in Figure 4.4.15A. Runx2, as previously discussed in 4.1.1, is the master transcription regulator of osteogenesis therefore it was hypothesised that the osteogenic capability of these cells should be impacted. However, Figure 4.4.15A would suggest that the clonal lines A6F4 and A6H2 retained their ability to differentiate into osteoblasts. The Alizarin Red stain was eluted and quantified to confirm the conclusions drawn from the microscopy, Figure 4.4.15B. This indicated that indeed the osteogenic ability of the Runx2 A6F4 and A6H2 clonal lines was retained and, in the case of the A6F4 cell line, was even significantly higher than the WT hTERT MSCs throughout the timecourse. To confirm that this instance was not unique to the A6F4 and A6H2 clonal lines, the remaining clonal lines (B6F4 and B6F6) in addition to the Runx2-MP hTERT MSCs were also differentiated down the osteogenic lineage, Figure 4.4.15C summarises the elution of the Alizarin Red stain of this timecourse. This indicated that all of the clonal lines and the Runx2-MP cells were able to differentiate into osteoblasts and deposit calcium, either at a comparable level to WT hTERT MSCs (A6H2, B6F4, B6F6, MP) or at a significantly higher level (A6F4).

The ability of the Runx2-GM hTERT MSCs to differentiate into adipocytes was then tested, to determine if the genome editing using CRISPR/Cas9 had impacted on another of the differentiation lineages of the cells. The clonal lines B6F4 and B6F6 alongside the Runx2-MP cells were differentiated into adipocytes using a stimulative cocktail and the resulting lipid droplets stained with Oil Red O (Figure 4.4.16A). All of the cells differentiated showed a stepwise increase in the number of lipid droplets formed at each timepoint, which were also higher than the basal control

in each instance. A large amount of background staining was seen in all wells in the day 21 basal control, but this was still much reduced in comparison to the staining seen in the adipogenic samples. It was also notable that the Runx2-GM cells analysed in this timecourse had an increased capacity for adipogenic differentiation, as by day 21 a larger number of lipid droplets were visible which were combining to form larger droplets, an indication of a later stage of adipogenesis. The Oil Red O stain was eluted and quantified to provide a quantitative analysis of these observations. Figure 4.4.16B shows this quantification in a bar chart, and indicates that at day 21 both the clonal line B6F4 and the Runx2-MP hTERT MSCs had a significantly increased level of staining compared to the WT hTERT MSCs at the later stages of the timecourse. The clonal line B6F6 showed comparative staining levels to the WT cells throughout the timecourse. Another clonal line, A6F4, was also tested in a separate experiment Figure 4.4.16C, and this clonal line again seemed to have a similar capacity for adipogenic differentiation to the WT hTERT MSCs.

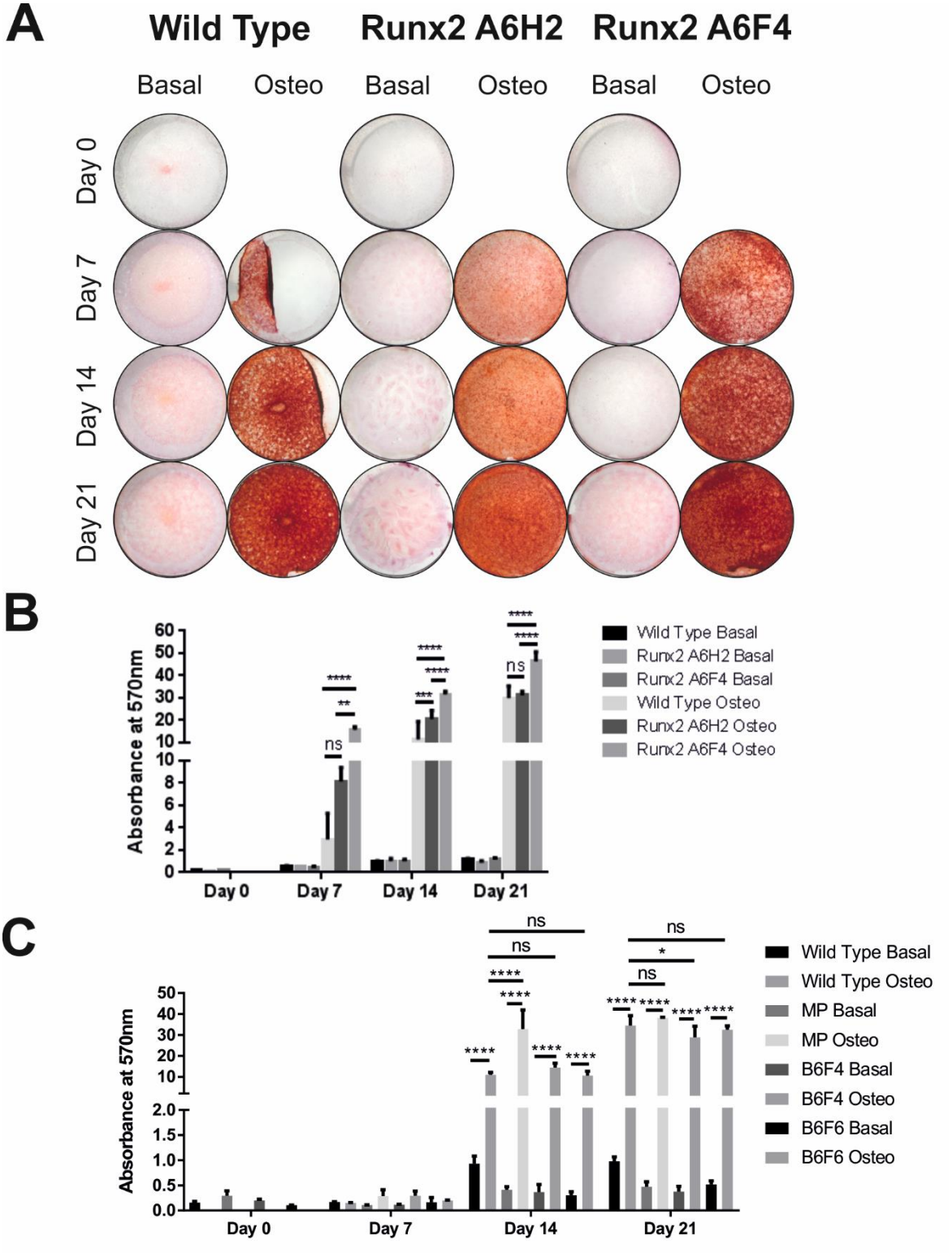
A
Wild Type
Runx2 A6H2
Runx2 A6F4
Basal
Osteo
Basal
Osteo
Basal
Osteo
Day 0
Day 7
Day 14
Day 21
B
Absorbance at 570nm
Day 0
Day 7
Day 14
Day 21
Wild Type Basal
Runx2 A6H2 Basal
Runx2 A6F4 Basal
Wild Type Osteo
Runx2 A6H2 Osteo
Runx2 A6F4 Osteo
C
Absorbance at 570nm
Day 0
Day 7
Day 14
Day 21
Wild Type Basal
Wild Type Osteo
MP Basal
MP Osteo
B6F4 Basal
B6F4 Osteo
B6F6 Basal
B6F6 Osteo

Figure 4.4.15: Osteogenic differentiation comparison of Runx2-GM hTERT MSCs and WT hTERT MSCs

Cells were plated at 2x104/cm^2 and induced to undergo osteogenesis for up to 21 days. At each timepoint, cells were fixed and mineralisation visualised by staining with Alizarin Red S. Representative images were taken with a stereo microscope (A) Alizarin Red S stain was then eluted and quantified by reading absorbance with a plate reader for two separate experiments comparing clonal and Runx2-MP cells with WT hTERT MSCs (B+C). Values = mean ± SD, n=3 with statistical significance obtained using 2 way RM ANOVA with Tukey's multiple comparisons.

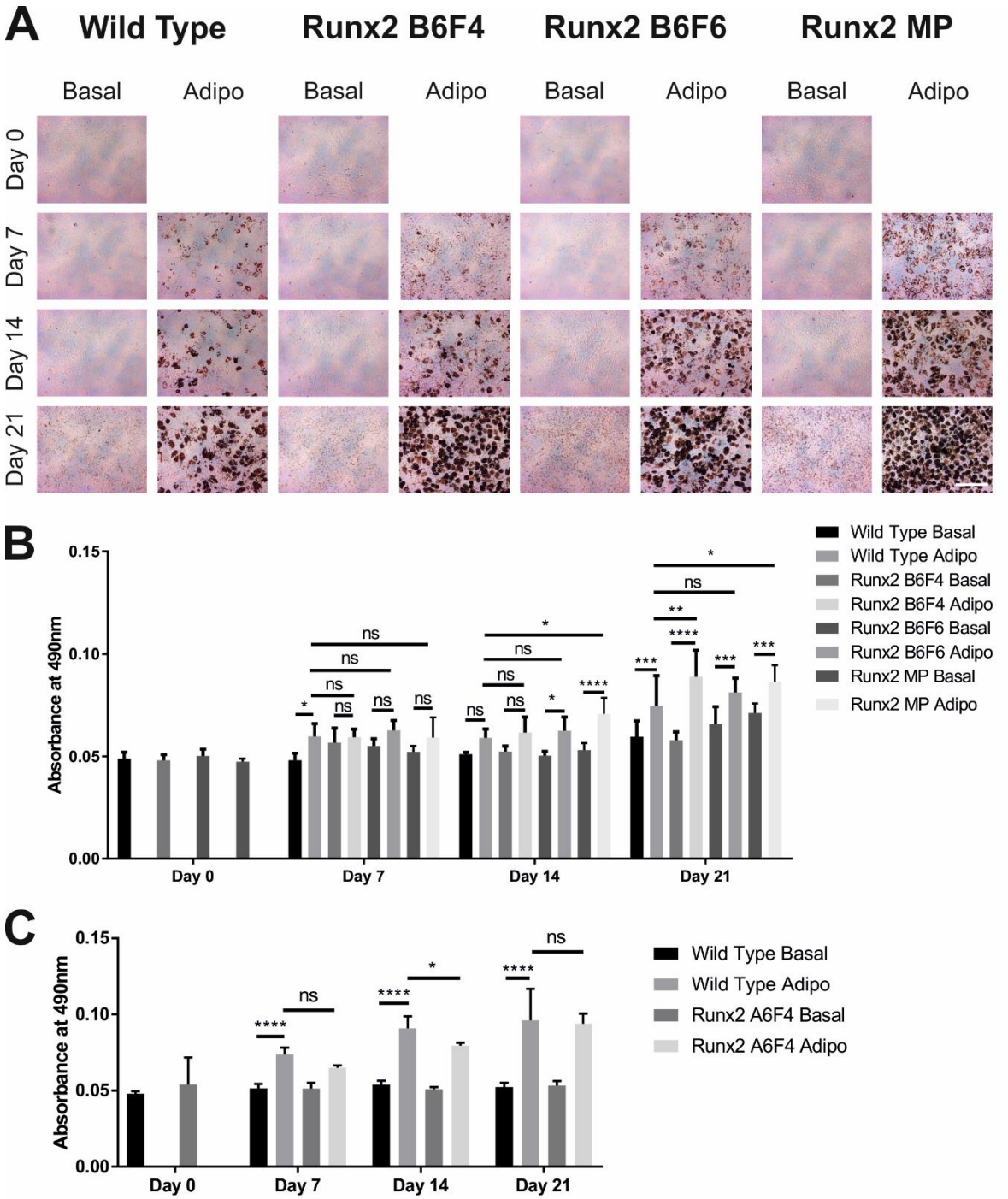

Figure 4.4.16: Adipogenic differentiation comparison of Runx2-GM hTERT MSCs and WT hTERT MSCs

10,000 cells were plated per well and induced to undergo adipogenesis for up to 21 days. At each timepoint, cells were fixed and lipid droplets visualised by staining with Oil Red O. Representative images were taken with a brightfield microscope, scale bar = 200µm (A) Oil Red O stain was then eluted and quantified by reading absorbance with a plate reader for two separate experiments comparing clonal and Runx2-MP cells with WT hTERT MSCs (B+C). Values = mean ± SD, n=6 with statistical significance obtained using 2 way RM ANOVA with Tukey's multiple comparisons.

4.4.9 Analysis of GM Sox9 hTERT MSCs indicated reduced adipogenic capacity

First, the viability and diameter of the Sox9-MP cells was analysed by the Vicell during routine cell culture. Figure 4.4.17A shows the editing of Sox9 does not appear to have affected the viability of the cells, with each line having greater than 90% viability. Additionally, the diameter of the cells was not significantly affected by the editing of Sox9 (Figure 4.4.17B).

Next the clonogenic ability of the Sox9-MP hTERT MSCs were tested in a colony forming assay, by seeding cells at low density and cultured for approximately 14 days to observe their ability to form colonies. Figure 4.4.18 summarises the ability of the cells to form colonies, it was found there was no significance in the efficiency of the Sox9-MP hTERT MSC to form colonies compared to the WT Y201 hTERT MSCs. The resulting colonies were fixed and stained in crystal violet stain in order to view the colonies and the cells that made up each colony, a representative colony is shown in Figure 4.4.18. It was immediately noticeable that the Sox9-MP 2 hTERT MSC line resembled the WT Y201 hTERT MSC line in both cellular morphology and colony formation. However, the Sox9-MP 1 hTERT MSCs form a much more condensed colony, with cells also appearing much more spread than the typical fibroblastic morphology displayed by the WT Y201 hTERT MSCs. Additionally, the viable numbers of the Sox9-MP hTERT MSCs was analysed by MTT assay. The metabolic rate of both the Sox9-MP hTERT MSCs was found to be significantly reduced compared to the WT hTERT MSCs. Additionally at later timepoints, the Sox9-MP 1 hTERT MSCs had reduced cell numbers than the Sox9-MP 2 hTERT MSCs (Figure 4.4.19).

Finally, the Sox9-MP hTERT MSCs were assayed for their ability to differentiate down the adipogenic lineage, this assay was selected due to the low cell numbers required for analysis. The cells were stimulated by an adipogenic cocktail for 21 days and assessed for lipid content with Oil Red O, representative images were taken with a brightfield microscope (Figure 4.4.20). It was evident each of the cell types tested was able to undergo adipogenesis, with lipid droplets forming in each cell type after 7 days differentiation. However, over the timecourse the WT Y201 hTERT MSCs demonstrate an increase in lipid droplets, which become more numerous over time before developing into larger droplets. This does not appear to occur in the Sox9-MP hTERT MSC lines to the same extent. To quantify these observations, ImageJ was used to set each image as black/white with the lipid droplets appearing black in each instance. The number of black pixels could then be quantified in each case, with the assumption that at the threshold chosen the more black pixels present, the increased number of lipid droplets are present in the field of view. Figure 4.4.20B+C summarises the number of black pixels calculated in this fashion for 3 brightfield images of differentiation at each timepoint, with Figure 4.4.20B comparing the WT Y201 hTERT MSCs to the Sox9-MP 1 hTERT MSCs and Figure 4.4.20C comparing the Sox9-MP 2 hTERT MSCs to the wild type

cells. It was evident from this analysis that the Sox9-MP hTERT MSCs, whilst both being able to differentiate, did not show much increase in differentiation after the first timepoint. The WT Y201 hTERT MSCs, however, have an increased number of black pixels stepwise throughout the timecourse, leading to significantly more black pixels within the images at both days 14 and 21. This would give evidence that the genome ed.iting of the Sox9-MP hTERT MSC cells has negatively impacted on the cells' ability to differentiate into adipocytes.

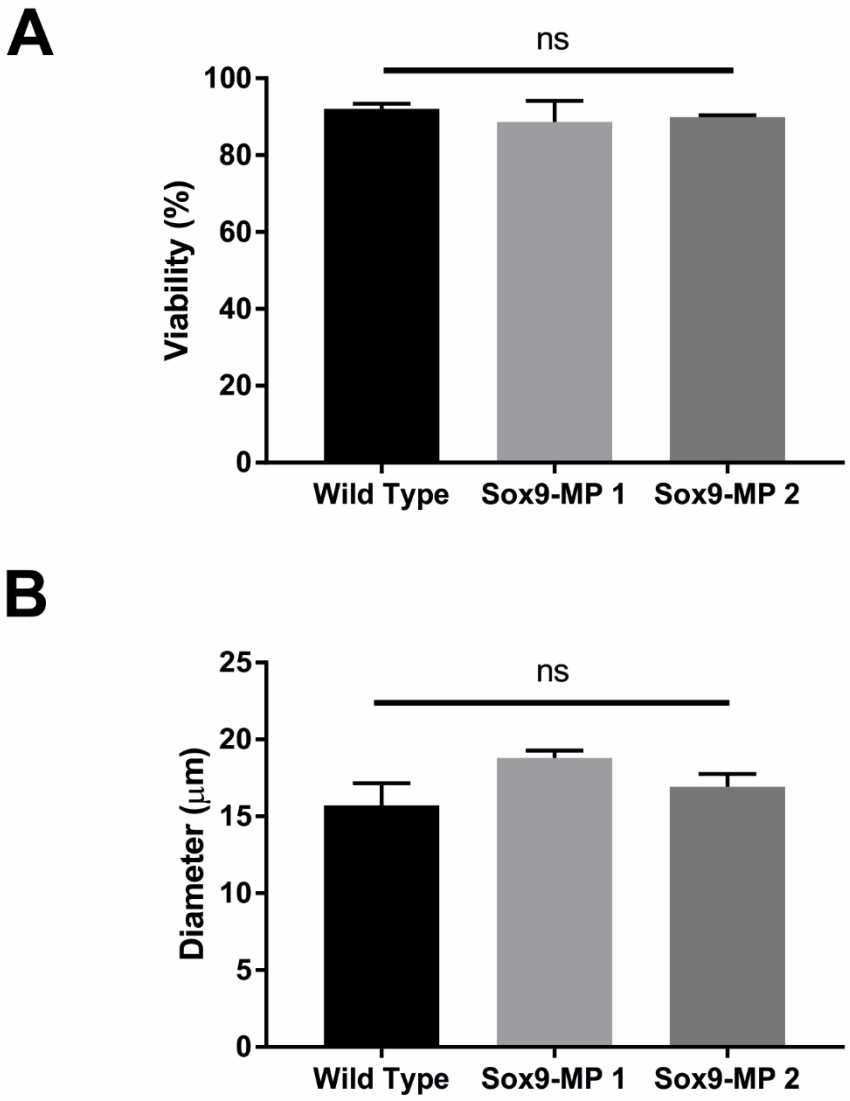

Figure 4.4.17: Vi-Cell analysis of Sox9-MP hTERT MSCs for viability and diameter

100,000 cells of each sample of interest were taken from culture and analysed using the Vi-CELL counter for viability using the trypan blue exclusion dye. All stained objects were counted and the average viability across three samples. Values = mean ± SD, n=3 (Sox9-MP 1 n = 2) with statistical significance obtained using 1 way RM ANOVA with Tukey's multiple comparisons.

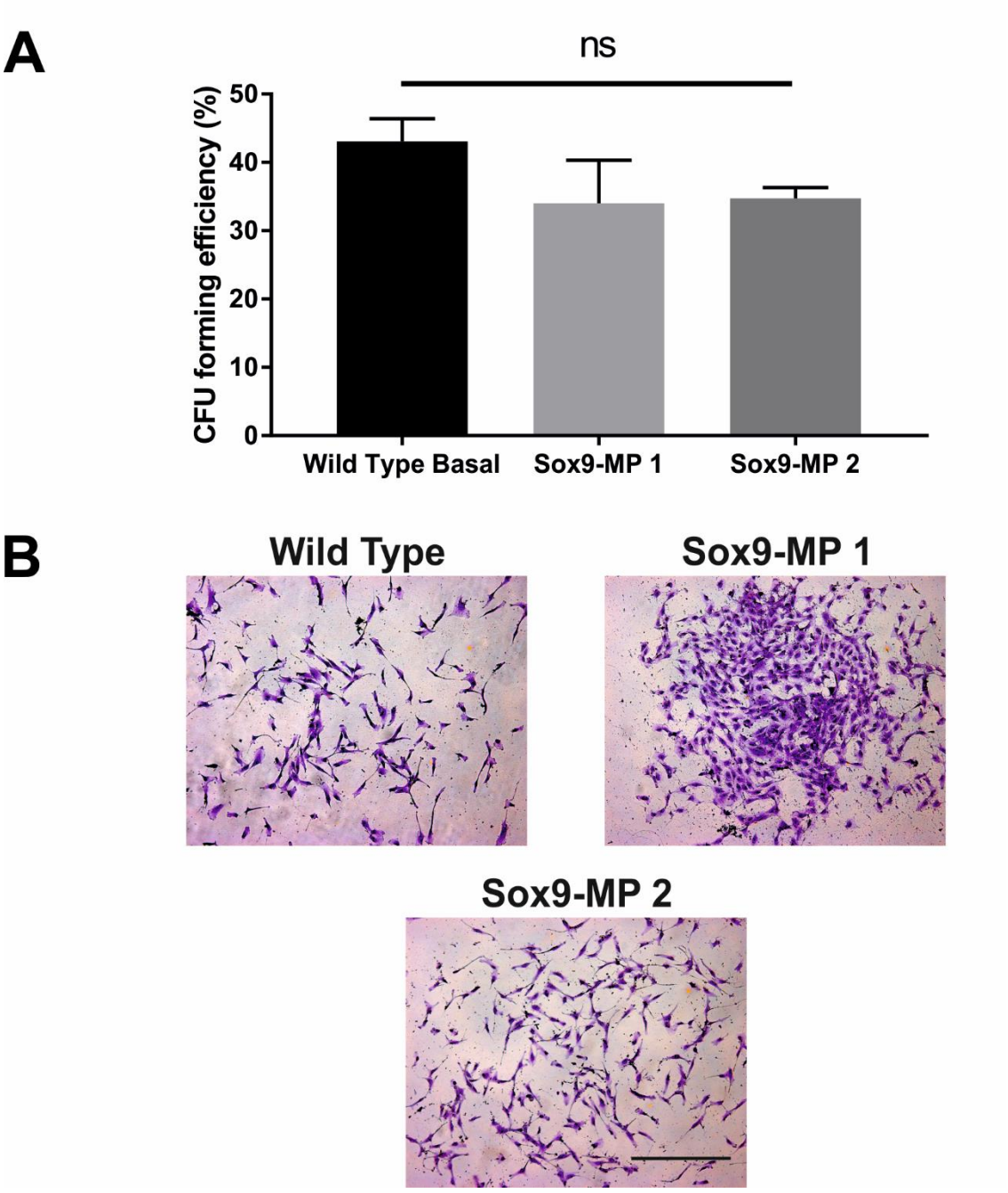

Figure 4.4.18: Clonogenic assay of Sox9-MP hTERT MSCs comparing colony forming ability to WT Y201 hTERT MSCs

Cells were seeded at clonal density (10 cells/cm^2) and resultant colonies fixed and stained with crystal violet. Distinct colonies were then counted and summarised in a bar chart (A). Representative brightfield images of a stained colony of each cell sample. Scale bar = 200µm (B). Values = mean ± SD, n=3 with statistical significance obtained using 1 way RM ANOVA with Tukey's multiple comparisons.

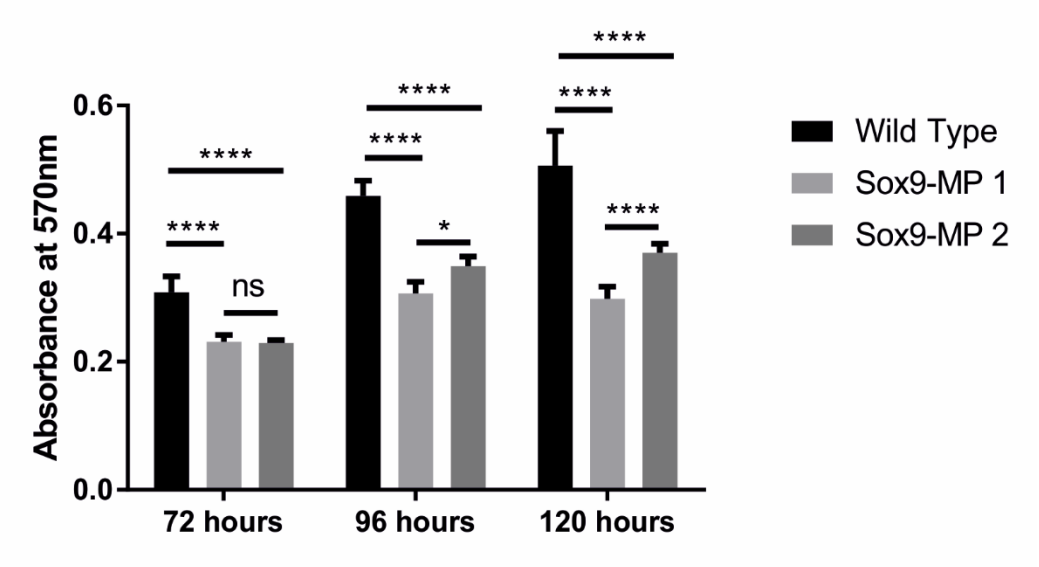

Figure 4.4.19: MTT assay assessing viable numbers of Sox9-MP hTERT MSCs

Cells were seeded at $5x10^3/cm^2$ and allowed to proliferate for up to 120 hours, at which point the metabolic rate was estimated using MTT. Values = mean ± SD, n=6 with statistical significance obtained using 2 way RM ANOVA with Tukey's multiple comparisons.

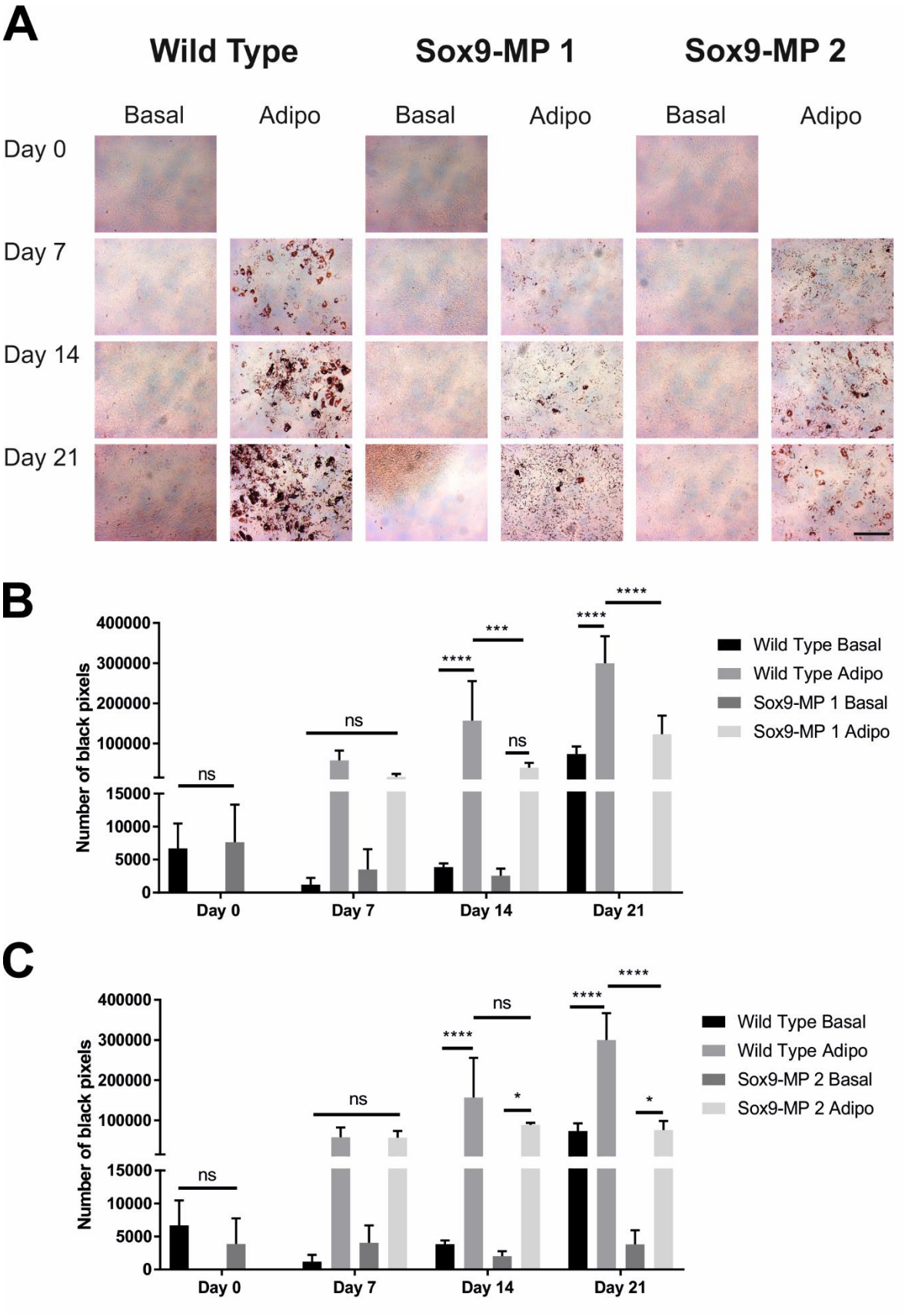
A
Wild Type
Sox9-MP 1
Sox9-MP 2
Basal
Adipo
Basal
Adipo
Basal
Adipo
Day 0
Day 7
Day 14
Day 21
B
Number of black pixels
400000
300000
200000
100000
15000
10000
5000
0
ns
ns
****
***
ns
****
****
Day 0
Day 7
Day 14
Day 21
Wild Type Basal
Wild Type Adipo
Sox9-MP 1 Basal
Sox9-MP 1 Adipo
C
Number of black pixels
400000
300000
200000
100000
15000
10000
5000
0
ns
ns
****
ns
*
****
****
*
Day 0
Day 7
Day 14
Day 21
Wild Type Basal
Wild Type Adipo
Sox9-MP 2 Basal
Sox9-MP 2 Adipo

Figure 4.4.20: Adipogenic timecourse comparing differentiation capacity of Sox9-MP hTERT MSCs to WT hTERT MSCs

10,000 cells were seeded per well and stimulated with an adipogenic cocktail for 21 days, negative controls with no treatment were included for every sample. At each timepoint, cells were fixed and stained with Oil Red O and brightfield images taken of each samples Scale bar = 200µm (A) ImageJ was used to convert all images to black/white and a threshold limit set that highlighted lipid droplets in black with backgrounds set as white. The number of black pixels was then counted and summarised in a bar chart. (B). Values = mean ± SD, n=3 with statistical significance obtained using 2 way RM ANOVA with Tukey's multiple comparisons.

4.5 Discussion

The discovery of CRISPR/Cas9 and its implementation in molecular and cell biology has revolutionised the field by offering the ability to create precise and efficient targeted genome changes. Many studies have demonstrated the ease of the CRISPR/Cas9 system, and in particular its power when combined with stem cells (reviewed in Musunuru, 2013). The aim of this chapter was to establish a methodology suitable for using CRISPR/Cas9 with the Y201 hTERT MSCs to create precise genome editing events in specific genes. The initial targets were Runx2 and Sox9 as it was hypothesised that knocking out these genes would render differentiation unable to occur thus giving a visual endpoint. However, the methodology developed should be suitable for successfully creating any gene knockouts.

4.5.1 Generation and identification of genetically modified hTERT MSCs

Electroporation of Y201 hTERT MSCs routinely resulted in between 10 – 20% of sorted cells being identified as positively fluorescent. Without removing the non-fluorescent cells the efficiency of electroporation may still have not been high enough to guarantee finding a knockout clone even with a highly efficient sgRNA. Electroporation, cell sorting and growth in low cell density are all procedures that cause high levels of cellular stress and may not be suitable for a number of cell lines. However, the immortalisation of the hTERT MSCs allowed the cells to survive these conditions and for the genome editing of an immortalised MSC for the first time. However, there is currently no way to determine whether designed sgRNAs will successfully direct Cas9 to the target sequence, or at what efficiency the process will be without performing studies *in vitro*. Without the ability to predict the efficiency of CRISPR/Cas9 it was apparent in this thesis that it is prudent to design multiple sgRNAs to maximise the chance of successfully generating a knockout cell line.

The identification of genome editing was first attempted using an enzymatic assay, however, this assay was not sensitive enough to provide an accurate insight into knockout status. This was remedied by using Sanger sequencing. Sanger sequencing of the CRISPR/Cas9 targeted region demonstrated clearly whether genome editing had taken place by the presence of multiple traces. Albeit if the two alleles of the gene have dissimilar edits, the mixed trace does not allow for the determination of the exact edit and this would need to be discerned by cloning the two alleles separately. Regardless, Sanger sequencing is a straight-forward method of detection that requires a small amount of genomic DNA and gives information both for homogeneous and heterogeneous genomic edits.

4.5.2 Osteogenesis does not appear to be disrupted in hTERT MSCs where Runx2 was targeted with CRISPR/Cas9

Using the developed methodology, preliminary evidence of genome editing was determined by Sanger sequencing for both the Runx2 and Sox9 genes. However, it was hypothesised that the genome editing events in Runx2 would lead to the disruption of osteogenic differentiation, or osteogenesis would be non-existent, and this was not the case for the cells tested in this chapter. Runx2 is the master transcription factor of osteogenesis, and many studies have demonstrated that differentiation into osteoblasts requires Runx2 (Ducy et al., 1997; Komori et al., 1997; Otto et al., 1997). In addition, studies have shown that a haploinsufficiency of Runx2 also results in a decreased formation of bone *in vivo* in both humans and mice (Otto et al., 1997; Tu et al., 2008). The results in this chapter show that any genetic modifications achieved to Runx2 did not appear to impact on their capability for osteogenesis, with all lines tested demonstrating an ability to deposit calcium when stimulated by a typical osteogenic cocktail. Previous studies have demonstrated that the impact of knocking out Runx2 was directly dependent on which stage of skeletogenesis was disrupted. Mice with Runx2 disrupted in already committed osteoblasts demonstrated similar levels of intramembranous and endochondral ossification, indicating Runx2 may only be required for the initiation of skeletogenesis (Takarada et al., 2013). MSCs typically demonstrate an increase in Runx2 during the early stages of osteogenesis, but to my knowledge no *in vitro* differentiation studies have been performed on Runx2-KO MSCs. The demonstration of the Runx2-GM hTERT MSCs to undergo osteogenesis may suggest Runx2 is not critical for *in vitro* MSC differentiation. Additionally, *in vitro* differentiation is typically stimulated using L-ascorbic acid, dexamethasone and β-glycerophosphate which are broad chemical supplements and may not necessarily be the best representation of *in vivo* osteogenic differentiation. Whether the induction of osteogenesis in this instance removes/reduces the need for Runx2, or impacts on the way the hTERT MSCs differentiate would be an interesting avenue of study. It is clear that to understand the phenotype of the Runx2-KO cells, both alleles need to be sequenced individually to confirm the exact sequence of Runx2 in each instance. It would be surprising that all of the cells generated in this chapter possess wild type sequence for both alleles when all demonstrated a mixed trace evident of genome editing.

4.5.3 Phenotypic analysis of Runx2-GM hTERT MSCs demonstrates increase in adipogenesis and increase in viable cell numbers

However, some of the other behaviours identified in the Runx2-GM hTERT MSCs have previously been linked with functions of Runx2. A number of skeletal diseases that present with defective osteoblast differentiation are also associated with an increase in adipogenesis (Meunier et al., 1973; Minaire et al., 1984; Justesen et al., 2001). Additionally, cells isolated from a Runx2 null background

spontaneously differentiate into adipocytes (Akune et al., 2004; Enomoto et al., 2004). Several of the Runx2-GM hTERT MSCs showed an increased propensity for adipogenesis compared to the WT hTERT MSCs, with increased numbers of lipid droplets which appear to collect together.

Further, the Runx2-GM hTERT MSCs showed an increase in viable cell numbers by MTT assay compared to the WT hTERT MSCs, indirectly providing potential evidence for an increased proliferative rate. It was demonstrated that cells from a Runx2-null background had an increased growth rate, in addition to increased DNA synthesis and increased cell cycle markers, such as cyclin E (Pratap et al., 2003; Galindo et al., 2005; Young et al., 2007). As might be expected of a growth suppressor it has also been demonstrated that a number of osteosarcomas show a downregulation of Runx2 for this reason (Kansara and Thomas, 2007). It has been proposed that Runx2 acts in this way through its interactions in the cell cycle, as Runx2 expression in osteoblasts fluctuates with the cell cycle (Pratap et al., 2003; Galindo et al., 2005, 2007). The clonogenicity of the Runx2-GM hTERT MSCs also appeared to be affected by the genome editing events in the Runx2-GM hTERT MSCs. This has not previously been reported in these studies of Runx2 in preosteoblastic cells but may be linked to the role of Runx2 in cell cycle progression. It would be interesting to determine whether the cell cycle proteins, such as cyclins A, D1 and E, have been influenced by the CRISPR/Cas9 editing of Runx2, and whether the expression of Runx2 detected altered with the cell cycle. Additionally, the activity of Runx2 and its ability to translocate to the nucleus could be determined to better understand whether the activity of Runx2 has been impacted by genome editing. Previously a study into Runx2 expression in a patient with CD showed Runx2 expression was not impacted by a mutation but instead the truncated protein presented with less activity and a lessened ability to translocate to the nucleus (Xu et al., 2017). However, the effect of off-targets cannot be overlooked, off-target effects were not analysed in this study, and although were controlled for, may still be having an impact on these cells.

4.5.4 Early analysis of Sox9-MP hTERT MSCs indicates genetic modification results in negative impacts to proliferation and adipogenesis

The redesign of the Sox9 sgRNAs resulted in evidence of successful genome editing in at least one instance in the Sox9-MP 1 cells, further analysis of clonal lines derived from both mixed populations will provide further insight as to whether knockout status has been achieved. Due to time constraints, it was not possible to derive clonal lines for this study, nor was it possible to expand the generated mixed populations of cells to provide the number of cells required for chondrogenic differentiation. The disruption of Sox9 should impact on the chondrogenic capability of the hTERT MSCs, and this would need to be investigated with histological stains and gene expression to

confirm knockout status. However, a phenotype was identified in these cells with both the proliferative and adipogenic capacities being negatively affected. The negative impact of Sox9 on MSC proliferation and adipogenic differentiation has already been observed in adult rat mesenchymal stem cells. This phenotype identified by Stöckl et al. (2013) appears to be similar to the phenotype of the Sox9 MP hTERT MSCs. It would be interesting to determine whether the apoptotic nature identified in the rat MSCs also correlates to the cells in this study.

4.5.5 Concluding Remarks

Taken together, the data from the Runx2 and Sox9-GM hTERT MSCs indicate the methodology developed in this chapter to create CRISPR/Cas9 edits in the hTERT MSCs has promise. More studies with the cells derived should develop a greater understanding about the knockout status of these cells and the phenotypes developed as a result. However, the methodology developed should be applicable to any gene where edits are wanted in the hTERT MSCs, and the fluorescent strategy implemented from Ding et al (2010) should allow many hard to transfect cells to be edited with CRISPR/Cas9.

Chapter 5 : The role of FGFR3 in post-natal developmental MSC biology

5.1 Introduction

Recent advancements in genome editing technology allow for the creation of cell lines with human disease relevant mutations, thus potentially replacing the need for animal models in this instance. The creation of genetically modified stem cell lines adds a further level of complexity to the study as stem cells can be differentiated into multiple lineages. This allows for the study of the effects of a mutation in multiple cell types with only one genome editing event required. With this in mind, we set out to create an hTERT MSC line with a human disease relevant mutation to demonstrate the power of combining stem cells with genome editing technologies.

Fibroblast growth factor (FGF) and fibroblast growth factor receptor (FGFR) signalling plays essential roles in development and disease (Turner and Grose, 2010). The mammalian FGFR signalling family is composed of 18 different secreted FGF proteins which bind to and activate four receptor tyrosine kinases. Furthermore, FGFRs 1-3 possess alternative splicing giving rise to variant receptors which possess distinct ligand binding properties and varying tissue expression. Signalling via the FGF pathway is activated by a ligand-receptor interaction resulting in an autophosphorylation of a tyrosine residue (Ornitz and Itoh, 2015). FGF signalling activation is associated with a number of downstream signalling pathways, the most common (and most understood) being the Janus kinase/signal transducer and activator of transcription (Jak/Stat), phosphoinositide phospholipase C (PLCγ), phosphatidylinositol 3-kinase (PI3K) and mitogen-activated protein kinase/extracellular signal-regulated kinase (MAPK/ERK) (Teven et al., 2014). Figure 5.1.1 shows a schematic overview of the FGF signalling pathway.

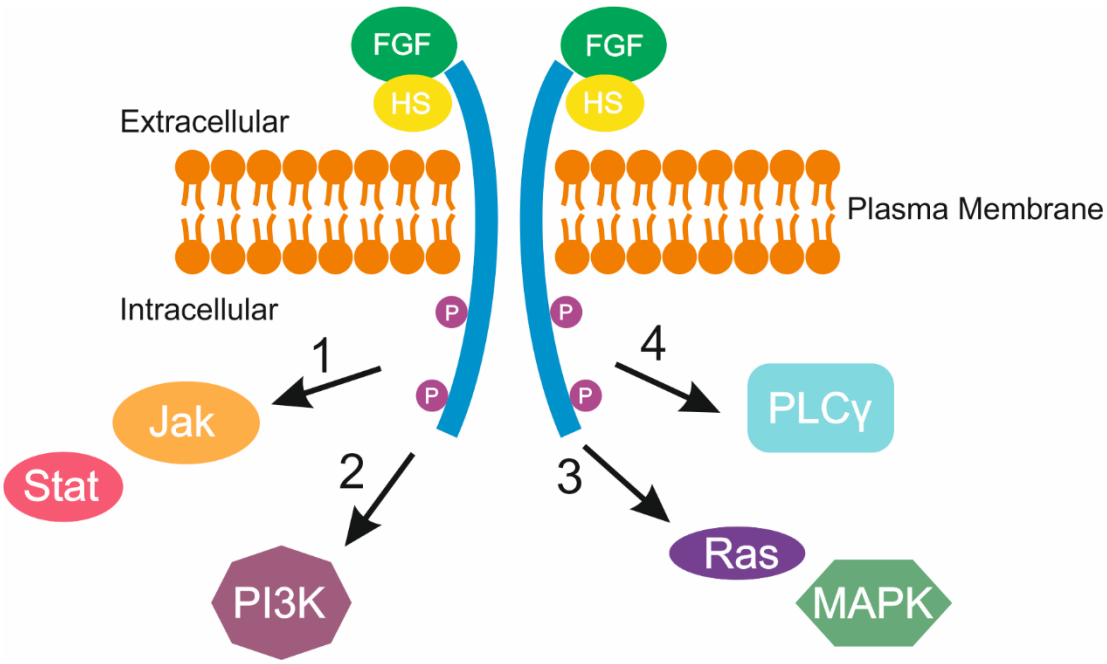

Figure 5.1.1: Overview schematic of FGF signalling

FGF ligands bind pairwise with heparin sulfate (HS) and FGF receptors to form an activated phosphorylated complex (P) which can activate one of four (1-4) main downstream signalling pathways. These downstream pathways are the Jak/Stat, PI3K, MAPK/ERK and PLCγ pathways which result in alterations to various cellular behaviours.

It is well documented that FGF signalling is critical for skeletal development with FGF ligands and receptors being expressed throughout skeletal development, from the developing limb bud to terminally differentiated tissues (Su et al., 2014). One of the critical FGF receptors for bone and cartilage growth and maintenance is FGFR3, evidenced by the number of diseases caused by point mutations in the FGFR3 gene. A number of skeletal dysplasias are caused by gain-of-function mutations in FGFR3, including achondroplasia, hypochondroplasia, thanatophoric dysplasia and SADDAN, which have been discussed in section 1.7.1 (Shiang et al., 1994; Su et al., 2014). All of these conditions cause a common symptom of shortened bones due to poor bone development, albeit with different severities (Krakow and Rimoin, 2010). Achondroplasia is the most common and most well understood of the dysplasias, with 99% of cases being caused by one of two mutations in FGFR3 (Pauli, 1993).

Loss-of-function mutations in FGFR3 are far less common than gain-of-function mutations and as a result are less well understood. Three families worldwide have presented with camptodactyly, tall stature, and hearing loss (CATSHL) syndrome and each has been reported to have a mutation variant of FGFR3 present in affected individuals (Toydemir et al., 2006; Makrythanasis et al., 2014; Escobar et al., 2016). The syndrome presents similar symptoms to phenotypes previously identified in FGFR3 -/- mouse studies whereby long bones formed by endochondral ossification overgrow extensively (Colvin et al., 1996; Deng et al., 1996). It has been demonstrated that patients with CATSHL have loss-of-function mutations in FGFR3 of varying degrees of severity.

Due to the number of skeletal diseases caused by mutations in FGFR3 it is evident that FGFR3 is integral to the normal development of bones formed by endochondral ossification. FGFR3 is first expressed in chondrocytes during mesenchyme condensation and later in development is expressed in proliferating chondrocytes, mature osteoblasts and osteocytes (Delezoide et al., 1998; Peters et al., 1993). However, the exact role FGFR3 plays in chondrogenesis and osteogenesis is somewhat obscured by evidence for both agonistic and antagonistic roles of FGFR3 in these developmental pathways.

FGFR3 has been shown to impact negatively on chondrocyte differentiation by promoting their proliferation and expansion. Several reports link this effect to occurring through the Stat pathway, namely through the activation and translocation of Stat1, which then results in the upregulation of cell cycle inhibitors and the ultimate arrest of cell growth (Su et al., 1997; Li et al., 1999; Sahni et al., 1999). This would therefore explain why in skeletal dysplasias, chondrocyte expansion plates were considerably smaller than in wild type cases. Additionally, FGFR3 is thought to impact on chondrocyte differentiation through the MAPK/ERK pathway demonstrated by the rescue of an

FGFR3 deficient background by the constitutive activation of MEK1 in chondrocytes (Murakami et al., 2004). This would suggest a model whereby FGFR3 impacts negatively on chondrocyte proliferation via Stat1 and chondrocyte differentiation via MEK1 (Murakami et al., 2004; Zhang et al., 2006a). However, reports have also shown FGFR3 to positively regulate chondrocyte differentiation, particularly in response to treatment with FGF18 (Ellsworth et al., 2002; Davidson et al., 2005). Discrepancies between studies may be due to the varying stages of chondrogenesis analysed suggesting FGFR3 may have differing roles in different developmental stages of cartilage formation.

Further evidence has also shown a role for Snail1 as a transcriptional regulator of this signalling mechanism, a summary of the interactions of these pathways is shown in Figure 5.1.2. The induction of aberrant Snail1 expression in transgenic mice also resulted in achondroplasia, similar to effects generated by activating mutations in FGFR3 (de Frutos et al., 2007). Studies have shown that Snail1 is able to act through both the Stat and MAPK pathways, impacting on chondrocyte proliferation and differentiation through these signalling events (de Frutos et al., 2007). In this way, FGFR3 directly affects skeletal development through Snail1 specifically, and not through other Snail family members such as Slug (alternative name Snail2) (de Frutos et al., 2007; Chen and Gridley, 2013).

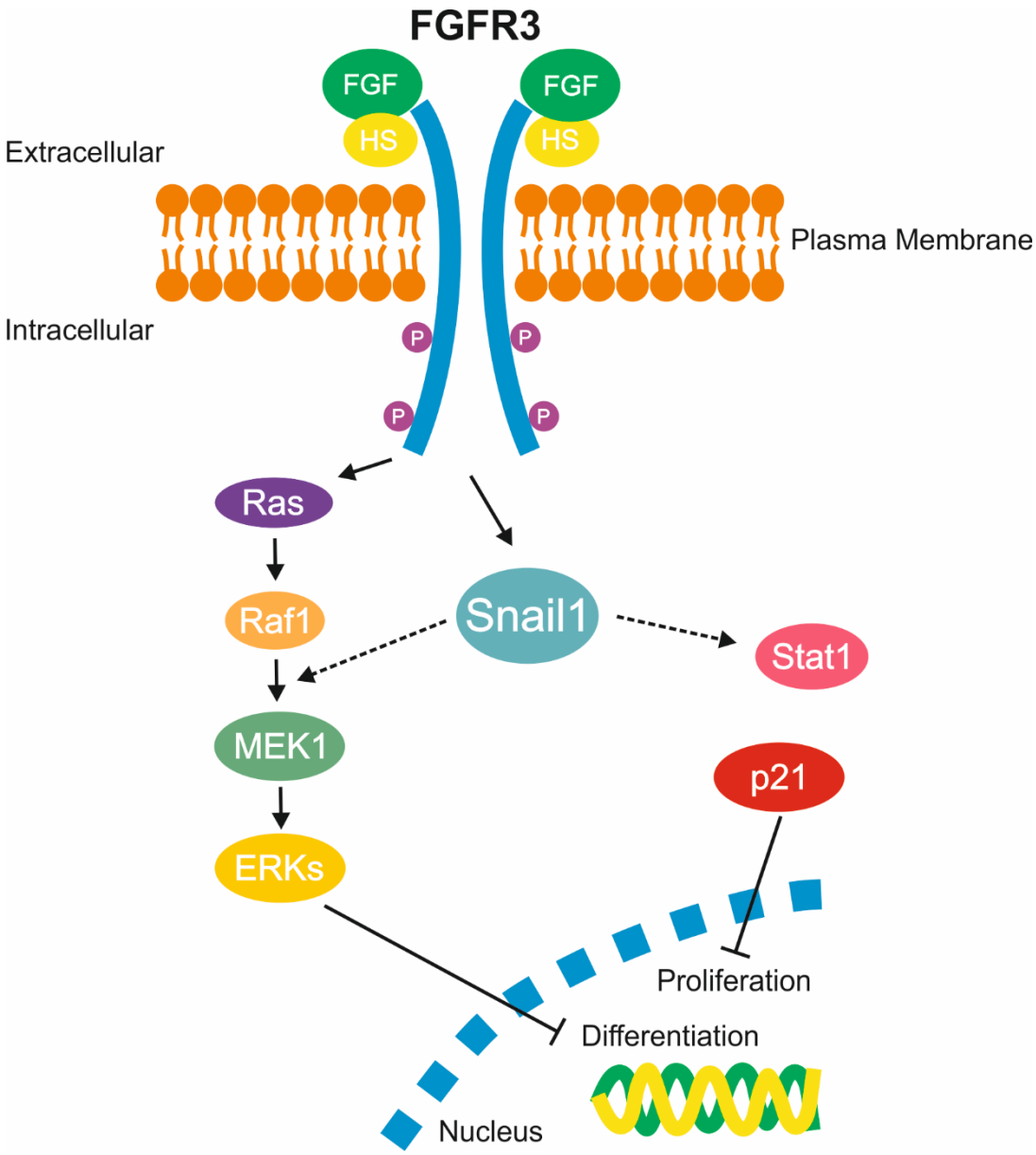

Figure 5.1.2: Schematic of transcriptional regulator, Snail1, in FGFR3 signalling

Snail1 lies downstream of FGFR3 and acts a transcriptional regulator that can impact on both the MAPK and Jak/Stat pathways, which can influence both MSC proliferation and differentiation. Figure based on Martínez-Frías et al., 2010.

The involvement of FGFR3 in osteogenesis has been noted but, currently, it is not clear whether FGFR3 plays an agonistic or antagonistic role. As previously discussed, inhibition of FGFR3 activity results in individuals developing severe, progressive overgrowth of the long bones (Colvin et al., 1996; Deng et al., 1996; Toydemir et al., 2006; Escobar et al., 2016). However, studies also show that activating mutations of FGFR3 result in increased osteoblast and osteoclast activities, typically with increased levels of osteogenic markers such as osteonectin, osteopontin and osteocalcin (Chen et al., 1999; Su et al., 2010). These studies also showed that overall the density of bone was reduced and mineralisation levels were decreased. It would therefore appear that the alteration of FGFR3 activity in either a positive or negative fashion results in disordered osteogenesis.

Fewer studies have been made on the effects of FGFR3 on MSCs, the cells that all the previously described skeletal elements derive from. A heterozygous activating mutation made in mice led to reduced MSC proliferation and an increase in *in vitro* osteogenic differentiation with increases in ALP activity and osteogenic genes (Su et al., 2010). These effects were shown in part to be due to signalling alterations of the ERK/MAPK pathways. MSCs isolated from FGFR3 knockout mice were shown to have a higher proliferative capacity than cells isolated from a WT mouse and a reduction of mineralisation despite osteogenic markers being expressed (Valverde-Franco et al., 2004).

One of the issues of studying primary MSCs from GM mice, as previously discussed, is their relatively limited culture time as they undergo cellular senescence. Using recent advances in genome editing techniques combined with the immortalised hTERT MSCs we are able to create a FGFR3 mutation relevant to human disease. This should provide a setting in which to analyse the effect of FGFR3 activity on MSCs without the complications of cellular senescence or the heterogeneous nature of primary MSCs.

5.2 Aims

The aims of this chapter are to develop a human disease relevant FGFR3 mutation using the CRISPR/Cas9 genome editing system and study the effects of FGFR3 on mesenchymal stem cell signalling and differentiation.

The specific objectives of this chapter are to:

- Design a relevant sgRNA to target FGFR3
- Isolate and validate a clonal genetically modified FGFR3 hTERT MSC cell line
- Analyse both the genotype and phenotype of the isolated clonal line

5.3 Methods and Materials

5.3.1 Generating FGFR3 cell line with CRISPR/Cas9

sgRNA structures were designed using the CRISPR design tool (crispr.mit.edu). Potential sequences were ranked by the programme based on specificity and off-target effects, sequences were chosen that possessed the fewest off target effects. The sgRNA sequences selected are below: (5' – 3')

sgRNA Fwd: CACCGCATCCGGCAGACGTACACGC

sgRNA Rev: AAACGCGTGTACGTCTGCCGGATGC

A single stranded oligonucleotide (ssODN) was designed to introduce a specific base mutation in the FGFR3 sequence by homologous recombination. The ssODN was designed so the double stranded break introduced by Cas9 was within 100 base pairs of the mutation and to avoid the Cas9 enzyme targeting the ssODN, the antisense of the wanted sequence was used. The ssODN sequence is below: (5' – 3')

ssODN:
CAGCACCGCCGTCTGGTTGGCCGGCAGCCCCGCCTGCAGGATGGGCCGGTGCGGGGAGCACTCCAGCAC
GTCCAGCGTGTACGTCTGCCGGATGCTGCCAAACTTGTTCTCCACGACGCA

All primers were ordered from Integrated DNA Technologies and purified via desalting.

Y201 hTERT MSCs were electroporated, using previously optimised parameters, and serial dilution used to isolate individual colonies as described in 4.3.1. Y201 hTERT MSCs were used as a WT control throughout results to compare to the CRISPR/Cas9 treated cells, these are referred to as WT hTERT MSCs throughout.

5.3.2 CRISPR/Cas9 On-target and Off-target Sequencing

PCR amplification was performed as described in Chapter 4 and products sent for Sanger sequencing using the unique forward primer at a 3.2μM concentration. The primers used for amplification and sequencing are in Table 5.3.1.

Table 5.3.1: Primers used in on-target and off-target sequencing

Primer Target	Forward Primer (5' – 3')	Reverse Primer (5' – 3')
FGFR3 CRISPR/Cas9 Validation	CAC GGC CCA GCT CTG AGA AAG	ACC CAA ATC CTC ACG CAA CC
FGFR3 Offtarget 1	CAT CAA GCC ATC CAC TAT ACA G AGG CGT CTG GGA GAC ATA CA	CTA CAC TGT CCA CCA TAC TTA TGC TGG ATG TAT GGG GCT
FGFR3 Offtarget 2	CCT GTC CTC CAT TCA CCC ACA C	GAG TTC AGT GAA GGG GAG CC
FGFR3 Offtarget 3	CTG AGA AAG AGG TCA GGA G	CTG CTA GAG CAG GAG TGA GG
FGFR3 Offtarget 4	CGG GTC CCA CTC CTA GAC AC	CGG CCC TTA CCG ATA CTT CAT
FGFR3 Offtarget 5	CAA TAA ACG TTG GGT GCC GC	CTC AGT AAG TGC TGG CCT CTG

5.3.3 Western Blot Analysis of FGFR3

5.3.3.1 Total Protein Isolation and Quantification

hTERT MSCs were grown in a monolayer as required and then lysed and the protein harvested, at the indicated time points using 200µL of RIPA Buffer (Sigma Aldrich, UK), supplemented with 0.5% protease inhibitor cocktail set III (Calbiochem) and 100µM Na_3VO_4 (Sigma Aldrich, UK) to prevent degradation.

The concentration of protein was determined using the Pierce BCA Protein assay kit (Pierce, #23227); this was performed as per manufacturer's instructions. Absorbance was read at 570nm using a plate reader and concentrations calculated using a standard curve created by known concentrations of BSA.

5.3.3.2 Gel electrophoresis and Western Blotting

20µg of sample protein was mixed with 4x Laemmeli buffer and heated for 5 minutes at 95°C. Samples were then loaded onto a 10% SDS acrylamide gel with a 5% SDS acrylamide stacking gel and electrophoresed at 130V during the stacking gel and 160V during the resolving gel. Resolved proteins were transferred to a nitrocellulose membrane (GE Healthcare) for 1 hour at 200mA. Membranes were blocked with 4% non-fat dry milk in Tris-buffered saline with Tween-20 for 1 hour at room temperature before being incubated overnight at 4°C with a 1:500 dilution of α-FGFR3 mouse polyclonal IgG1 primary antibody (Abcam, #ab89660). The membrane was washed for 5

minutes three times in TBS-T before incubation with a 1:2000 diluted α-mouse horseradish peroxidase (HRP) labelled secondary antibody (Santa Cruz, #SC-2005) for 1 hour at room temperature. After incubation, blots were washed and proteins detected using the Amersham ECL Western Blotting Detection Reagents (GE Healthcare, #RPN2109). Westerns were run in duplicate and the second membrane used to probe for GADPH using α-GADPH mouse monoclonal IgG1 (Genetex, #GTX28245). The same secondary antibody was used and the blot imaged as before.

5.3.4 qPCR Primers for FGFR3 Expression

Total RNA isolation, cDNA synthesis and qPCR was performed as described in 2.1.2 with the following primer sets for FGFR3:

Table 5.3.2: qPCR primers to analyse FGFR3 expression

Primer Target	Forward Primer (5' – 3')	Reverse Primer (5' – 3')
FGFR3 Primer Set 1	GAG GCC ATC GGC ATT GAC	TGG CAT CGT CTT TCA GCA TCT
FGFR3 Primer Set 2	ACC AAT GTG TCT TTC GAG GAT GCG	AGA GCA CGC AGC TTG TCA CAT AGA

5.3.5 In vitro differentiation

5.3.5.1 Osteogenic and adipogenic differentiation

Osteogenic and adipogenic differentiation of WT and FGFR3-KO hTERT MSCs was performed and analysed via histological staining as described in section 2.1.3.

5.3.5.2 Chondrogenic differentiation

Chondrogenic differentiation was performed in pellet culture, whereby 40,000 hTERT MSCs, either WT or FGFR3-KO hTERT MSCs, were added to a well of a non-adherent U bottomed 96 well plate and the plate centrifuged for 5 minutes at 300g. Pellets were left to condense overnight before the medium was aspirated. Chondrogenic medium consisted of DMEM +1% penicillin-streptomycin supplemented with 50 µg/ml L-ascorbic acid-2-phosphate, 100nM dexamethasone, 40 µg/ml L-Proline, 1% ITS and 10ng/mL TGF-β3 with medium changed every 3 days.

For assessment of chondrogenic genes, 3 pellets were combined in a 1.5 mL Eppendorf tube and frozen in 1ml of Trizol. These were freeze-thawed three times to attempt to disaggregate the pellet before Trizol extraction and subsequent isolation of RNA was performed as described in 2.1.2.

The primer sets used for chondrogenic marker expression analysis were as follows:

Table 5.3.3: qPCR primers to analyse chondrogenic marker expression

Primer Target	Forward Primer (5' – 3')	Reverse Primer (5' – 3')
Sox9	TTC CGC GAC GTG GAC AT	TCA AAC TCG TTG ACA TCG AAG GT
Aggrecan	TGG AGG ACA GCG AGG CC	TCG AGG GTG TAG CGT GTA GAG A

5.3.6 *In vitro* scratch-wound assays

WT and FGFR3-KO hTERT MSCs were seeded at confluency ($2x10^4/cm^2$) in 6 well plates and allowed to adhere for 24 hours. Upon confirmation of confluency in the centre of the well, by brightfield microscopy, the medium was aspirated and a scratch wound created across the middle of the well using a 200µL pipette tip. Care was taken to ensure even pressure was applied across the well. 1xPBS was then used to gently remove debris from the wound, and media reapplied to the well. The wound was then imaged using a brightfield microscope and marks made to ensure the same field of view was consistently imaged. Cells were incubated at 37°C and at repeating intervals an image taken of the healing wound.

Corel Draw was used to overlap the resulting microscope images so that the fields of view in every image were identical. The edges of the wound were then marked and Image J used to calculate the percentage of the area healed by the proliferating and migrating cells.

5.3.7 Transcriptome profiling by RNA-seq analysis

The transcriptomes of the FGFR3-KO hTERT MSCs were compared to the WT hTERT MSCs as described in 2.1.4. Additionally, analysis was performed by KeggArray by uploading upregulated and downregulated transcripts to provide pathway maps of significantly differentially regulated pathways as identified by Enrichr analysis.

5.3.8 Ptychography and Cell Migration Analysis

WT and FGFR3-KO hTERT MSCs were seeded into an Ibidi Culture-Insert plate, according to manufacturer's recommendations and allowed to attach to the surface overnight. Inserts were then removed and plates inserted into a stage top incubator, kept at 37°C with CO_2 supplementation for the imaging using an Olympus microscope customised for pytchographic imaging by PhaseFocus (Sheffield, UK). Regions of interest were selected to given an overview of the gap and all images were acquired with a 10x objective. Data was then collected for up to 18 hours at 5 minute intervals for the duration of the timecourse. Images were analysed using Cell Analysis Toolbox (CAT)

Software, developed by PhaseFocus, briefly the contrast of images was set so cells were visible against the background and an advanced fuzzy threshold algorithm used to segment cells allowing morphological information to be gathered. Videos were generated and exported from the software and metrics of gap closure calculated.

Migration directness was calculated by dividing the shortest distance from the start point to the endpoint (Euclidean distance) by the total distance travelled (accumulated distance), both calculated on an individual cell basis. This is summarised in the equation below:

$$D_i = \frac{d_{i,euclid}}{d_{i,accum}}$$

5.3.9 Phalloidin staining of actin cytoskeleton

WT or FGFR3-KO hTERT MSCs were plated on an 8mm glass coverslip in 1 well of a 24 well plate, at 10,000 cells/cm^2. These were then allowed to adhere overnight at 37^{o}C before the cells were washed with 1xPBS and fixed using 4% PFA for 10 minutes at room temperature. The cells were then washed a further three times with 1xPBS and the membranes permeabilised with 0.25% Triton-X for 30 minutes. Alexa Fluor® 647 conjugated Phalloidin (Thermofisher, UK) was then applied at a dilution of 1 in 10,000 in 1xPBS for 2 hours before the cells were washed a further two times with 1xPBS. Cells were then counterstained with 4',6-diamidino-2-phenylindole (DAPI) for 5 minutes. Resulting cover slips were mounted on glass microscopy slides using Vectashield mounting medium (Vector Labs, Peterborough, UK) and the cover slips fixed in place. Slides were imaged using an LSM710 confocal imaging system (Zeiss).

5.4 Results

5.4.1 FGFR3 sgRNA design and introduction of FGFR3 CRISPR/Cas9 into Y201 hTERT MSCs

Initially, an sgRNA was designed which targeted the correct part of the FGFR3 gene, along with a singular stranded oligonucleotide (ssODN) to introduce a mutation that would mimic the most commonly found mutation in type I thanatophoric dysplasia. Using the crispr.mit.edu function alongside The Human Gene Mutation Database both a sgRNA and an ssODN were designed to introduce a missense R to C mutation at position 248 in FGFR3. As described in section 4.4.1 oligonucleotides were designed, annealed and a one-step digestion/ligation performed to complete the FGFR3 targeting CRISPR/Cas9 plasmid. Colony PCR was then performed using the ubiquitous U6 promoter targeting primer and the reverse sgRNA oligonucleotide to amplify specifically plasmids containing the correct sgRNA sequence. Amplified products were then visualised by agarose gel electrophoresis (results not shown). Plasmids that had successfully amplified were then sequenced to confirm the presence of the sgRNA sequence (Figure 5.1.1).

Figure 5.4.1: Confirming the insertion of the FGFR3 sgRNA sequence into the pSpCas9(BB)-2A-GFP plasmid.

Clones highlighted as successful by colony PCR were taken for Sanger sequencing. The template sequence for FGFR3 has been listed below the consensus sequences. In this example all 4 clones tested had the FGFR3 sgRNA present.

Y201 hTERT MSCs were then electroporated using the previously determined parameters (discussed in 4.4.3) with both the designed sgRNA and ssODN. Y201 hTERT MSCs were also electroporated with an eGFP-CMV plasmid and a no plasmid control generated to provide positive and negative controls respectively for FACS sorting. After cells had been incubated at 37^{o}C for 24 hours to recover from electroporation they were sorted for GFP fluorescence, cells were also gated to exclude dead cells, debris and doublet cells using forward scatter and side scatter. Events collected during the sort are summarised in Figure 5.4.2**.**

Y201 hTERT MSCs were then serially diluted across a 96 well plate to isolate clonal lines and two clonal lines were successfully expanded and submitted to Sanger sequencing, upon which it was revealed that one of these clonal lines was an FGFR3-KO hTERT MSC line (Figure 5.4.3)**.** This recapitulates mutations found in humans that results in Camptodactyly, Tall Stature, and Hearing Loss (CATSHL) syndrome whereby bones formed by endochondral ossification are dramatically elongated. Little is known about this disease and how it affects MSCs therefore it was decided to proceed with the FGFR3-KO hTERT MSC line and determine what effects FGFR3 deletion has on these cells.

The FGFR3-KO hTERT MSC line was found to have a single base insertion in position 8417 within exon 6 of the FGFR3 gene. Figure 5.4.4 shows the predicted protein sequence as a result of the insertion whereby an early stop codon was introduced in the extracellular domain of the protein. This results in a truncation before the transmembrane domain making it likely that any truncated protein will have little to no activity as the receptor will not be able to insert into the cell membrane. Analysis of the alternative splice variants of FGFR3 indicates this mutation should be effective in all splice variants rendering these cells depleted of any form of FGFR3.

The off targets of the FGFR3 targeted sgRNA were highlighted upon design by the design tool and are summarised in Table 5.4.1. Each of the predicted off-targets have a predicted change of less than 0.5% of occurring using the design tool's algorithm, where 100% is considered almost certain and 0% is considered almost impossible, therefore off-targets are unlikely to be an issue with this design. Nevertheless, primers were designed and used to expand regions encompassing the top 5 predicted off target effects and the resulting PCR products sent for Sanger sequencing for sequence determination. The 4 highlighted predicted off-targets all gave wild type sequences in the FGFR3-KO hTERT MSCs, however the top predicted off target PCR product failed to sequence with two separately designed primer pairs. The likelihood of the off-target occurring is extremely low, and the sequence is present within an intron region and therefore also unlikely to affect the cells if a mutation was present.

Table 5.4.1: Predicted off-target effects of selected FGFR3 sgRNA

Sequence	Score	Mismatches	UCSC gene	Locus
CGTCTGGGAGACATACA CGCTGG	0.6	4MMs [2:5:8:13]		chrX:+39552795
CCTTCAGCAGACATACAC GCTGG	0.3	4MMs [2:4:6:13]		chr16:-34467058
GATCAGGGAGACGTACA GGCCAG	0.3	4MMs [1:5:8:18]		chr3:+167088929
CGTCCGCCAGACGGACA CGCTGG	0.3	3MMs [2:7:14]	NM_001199862	chr1:+6111669
TATCCTGGAGACGTGCA CGCTGG	0.3	4MMs [1:6:8:15]		chr20:-3827025
CATACAGCATACGTACAT GCAGG	0.2	4MMs [4:6:10:18]		chr10:-73583353
CATACAACAGACGTACA AGCTAG	0.1	4MMs [4:6:7:18]		chr3:+35221249
CATGGGGCAGACTTACA AGCCAG	0.1	4MMs [4:5:13:18]		chr6:-21031923
TATCCTGCAGACGTACAT GGTAG	0.1	4MMs [1:6:18:20]		chr12:+109597219
CATCCAGCATACGTACA GGAAAG	0.1	4MMs [6:10:18:20]	NM_001185077	chr17:-79827053
CATCGGGCAGACGTTCG CGATGG	0.1	4MMs [5:15:17:20]	NM_001082	chr19:-15989713
CATCTGGCAGAGGTACA AGTCAG	0.1	4MMs [5:12:18:20]		chr2:+238209894
CATCCAGCAAACTTACAT GCTGG	0.1	4MMs [6:10:13:18]		chr1:+247283345
CCTCCGGCACACGCGCA CGCAGG	0.1	4MMs [2:10:14:15]	NM_152326	chr14:-102975791
CATCCTGCAGATATACAC ACTGG	0.1	4MMs [6:12:13:19]		chr11:-95490355

GATCCGGCGGACACACACGCAGG	0.1	4MMs [1:9:13:14]		chr7:-150734813
CATCCGGCAGACATGCAGGCAGG	0.1	3MMs [13:15:18]		chr7:-73949287
CATCCGAGAGACGGACACACGGG	0.0	4MMs [7:8:14:19]		chr21:+43391561
AATCCTGCAGACGCACACCCCAG	0.0	4MMs [1:6:14:19]		chr1:-227916754
CACCCGGGAGACGCAGACGCCAG	0.0	4MMs [3:8:14:16]		chr5:+115297523
CATCCCGCAGCCGTACAAACTGG	0.0	4MMs [6:11:18:19]	NM_014080	chr15:+45400277
CATCCGGCAGAAATGCACGAAGG	0.0	4MMs [12:13:15:20]		chrX:-65294888
CATCCGGCAGAAATGCACGAGGG	0.0	4MMs [12:13:15:20]		chr16:-47599501
CATCCTGCAGACATACATGGTAG	0.0	4MMs [6:13:18:20]		chr8:-2351144
CATCCTGCAGAGGGACACTCCGG	0.0	4MMs [6:12:14:19]		chr3:+62203204
CATCCCGCAGGCGGCCACGCTGG	0.0	4MMs [6:11:14:15]	NM_001003800	chr9:+95485046
CATCCGGCTGATGAATACGCCGG	0.0	4MMs [9:12:14:16]	NM_001204218	chr12:+117657881
CATCCAGCAGACCAACAGGCAGG	0.0	4MMs [6:13:14:18]		chr4:+184178679

The FGFR3-KO hTERT MSC line was expanded and total cellular protein harvested by lysis. This was then used to probe for the presence of FGFR3 by Western Blot and the results from this summarised in Figure 5.4.5. HeLa and HEK293FT cells were used as positive controls as according to the Human Protein Atlas (www.proteinatlas.org) these cells should both be positive for FGFR3, additionally WT Y201 hTERT MSCs were included to provide a comparison for FGFR3 levels in the FGFR3-KO hTERT MSCs. The antibody used in this study did not give a unique band pattern for FGFR3 as predicted, but instead 4 bands were present. Using the reported molecular weight of FGFR3, one band was deemed as being representative of FGFR3 present in the cells and this band was the most dominant is the positive controls (Figure 5.4.5A). Initially it is apparent that there is a far higher expression of FGFR3 detected in the HeLa and HEK293FT cells than in the WT hTERT MSCs, 2 times and approximately 6 times higher respectively (Figure 5.4.5B). There appears to be a very faint band present in the FGFR3-KO hTERT MSCs, which contradicts the predicted expression pattern by the sequencing data. Multiple antibodies were used to further analyse the expression of FGFR3 in these cells, yet none gave signals in any of the cell lines tested (results not shown). Flow cytometry was also used to attempt to determine FGFR3 levels by using antibodies targeted to the extracellular domain, which should not be displayed in FGFR3-KO hTERT MSCs, however the antibodies appeared to stick to the cell surface giving a positive signal for all cell lines tested (results not shown).

Finally, the FGFR3-KO hTERT MSCs were treated with FGF9, a growth factor which is not specific to FGFR3 but has a high affinity for the receptor, and the resulting increase in the phosophorylation of ERK was measured by Western Blotting. Figure 5.4.6 shows the comparison of pERK levels in the FGFR3-KO hTERT MSCs and WT hTERT MSCs at 20 minutes post FGF9 treatment and 6 hours post FGF9 treatment. The WT hTERT MSCs demonstrated a low basal level of pERK which rapidly increased upon treatment with FGF9, this reduced after 6 hours but still levels of pERK were higher than basal levels. The FGFR3-KO hTERT MSCs also were able to respond to the FGF9 treatment, which is possible as FGF9 is not solely able to bind to FGFR3 alone, and the pERK levels increased at 20 minutes. However, the sustained levels of pERK seen in the WT hTERT MSCs were not seen in the FGFR3-KO hTERT MSCs and the signal dropped at 6 hours back to basal levels. It would appear from this experiment that the MAPK/ERK pathway has been somewhat altered by the removal of FGFR3 and the signalling events within the cell may have changed as a result.

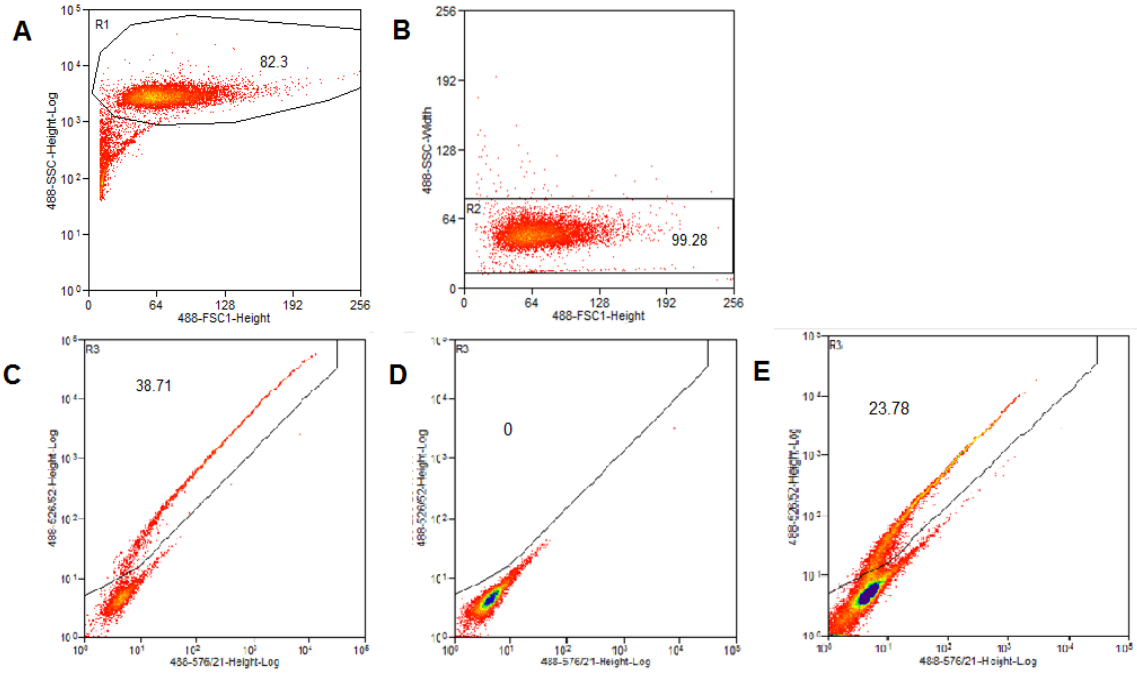

Figure 5.4.2: FACS analysis of Y201 hTERT MSCs electroporated with FGFR3 sgRNA and ssODN

Events collected during sorting of Y201 hTERT MSCs to isolate potential genetically modified cells. Gating strategy removed debris/dead cells (A) and doublet cells (B) using forward scatter and side scatter. Y201 hTERT MSCs electroporated with an overexpressing eGFP vector (C) and with no plasmic (D) were included as controls. (E) shows Y201 hTERT MSCs electroporated with the FGFR3 sgRNA and ssODN and 23.78% were isolated and replated for clonal isolation.

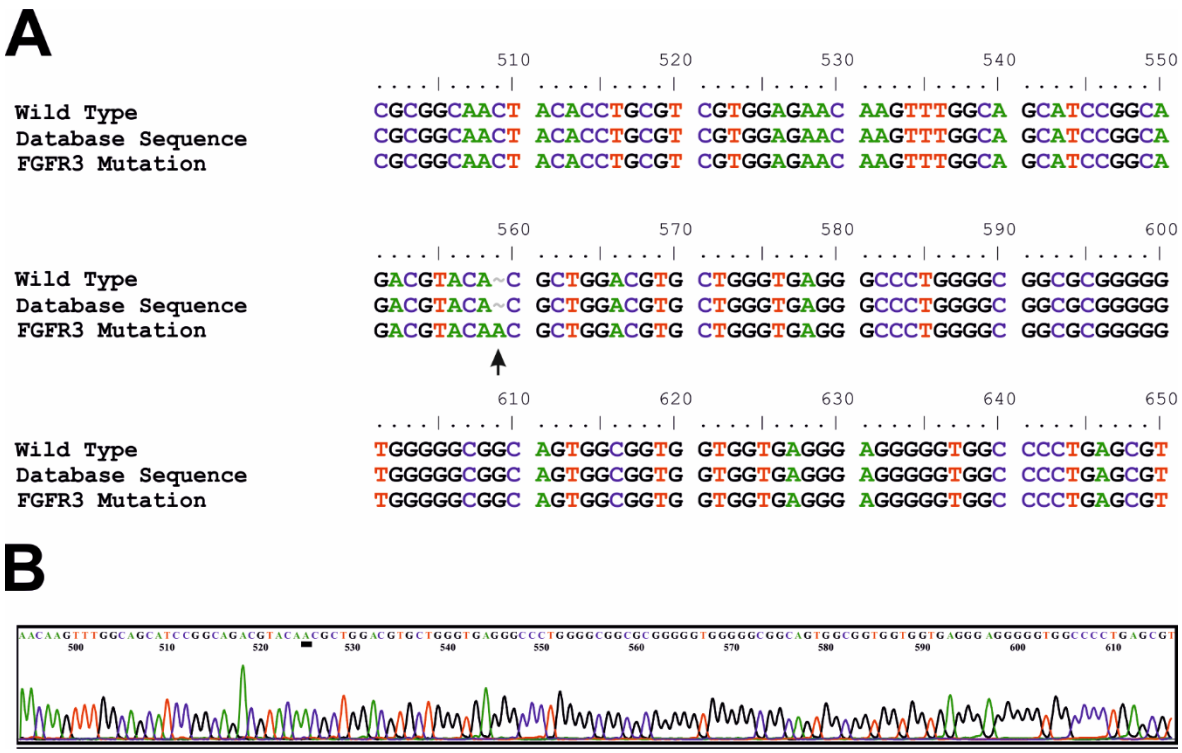

Figure 5.4.3: FGFR3 CRISPR/Cas9 resulted in FGFR3-KO hTERT MSC line with single A insertion

One of the clonal lines isolated from the MP of GM FGFR3-KO hTERT MSC lines was found to have a single base insertion when examined by Sanger sequencing (A). The sequencing trace for the cell line is also shown (B) where a clean trace can be seen for the insertion suggesting a homogeneous FGFR3-KO hTERT MSC line.

A

Wild Type FGFR3 Protein Sequence

```
MGAPACALAL CVAVAIVAGA SSESLGTEQR VVGRAAEVPG PEPGQQEQLV FGSGDAVELS PPPGGGPMG
PTVWVKDGTG LVPSERVLVG PQRLQVLNAS HEDSGAYSCR QRLTQRVLCH FSVRVTDAPS GDDEDGEDE
AEDTGVDTGA PYWTRPERMD KKLLAVPAAN TVRFRCPAAG NPTPSISWLK NGREFRGEHR GGIKLRHQQ
WSLVMESVVP SDRGNYTCVV ENKFGSIRQT YTLDVLERSP HRPILQAGLP ANQTAVLGSD EFHCKVYSD
AQPHIQWLKH VEVNGSKVGP DGTPYVTVLK TAGANTTDKE LEVLSLHNVT FEDAGEYTCL GNSIGFSHH
SAWLVVLPAE EELVEADEAG SVYAGILSYG VGFFLFILVV AAVTLCRLRS PPKKGLGSPT HKISRFPLK
RQVSLESNAS MSSNTPLVRI ARLSSGEGPT LANVSELELP ADPKWELSRA RLTLGKPLGE CFGQVVMAE
AIGIDKDRAA KPVTVAVKML KDDATDKDLS DLVSEMEMMK MIGKHKNIIN LLGACTQGGP YVLVEYAAK
GNLREFLRAR RPPGLDYSFD TCKPPEEQLT FKDLVSCAYQ VARGMEYLAS QKCIHRDLAA NVLVTEDNV
MKIADFGLAR DVHNLDYYKK TTNGRLPVKW MAPEALFDRV YTHQSDVWSF GVLLWEIFTL GSPYPGIPV
EELFKLLKEG HRMDKPANCT HDLYMIMREC WHAAPSQRPT FKQLVEDLDR VLTVTSTDEY DLSAPFEQY
SPGGQDTPSS SSSGDDSVFA HDLLPPAPPS SGGSRT.
```

FGFR3 G4 Protein Sequence

```
MGAPACALAL CVAVAIVAGA SSESLGTEQR VVGRAAEVPG PEPGQQEQLV FGSGDAVELS PPPGGGPMG
PTVWVKDGTG LVPSERVLVG PQRLQVLNAS HEDSGAYSCR QRLTQRVLCH FSVRVTDAPS GDDEDGEDE
AEDTGVDTGA PYWTRPERMD KKLLAVPAAN TVRFRCPAAG NPTPSISWLK NGREFRGEHR GGIKLRHQQ
WSLVMESVVP SDRGNYTCVV ENKFGSIRQT YNAGRAGALP APAHPAGGAA GQPDGGAGQR GVPLQGVQ.
```

B

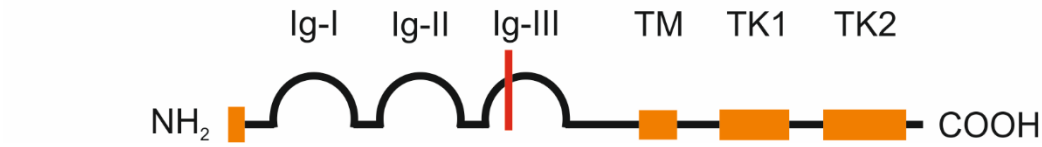

Figure 5.4.4: The predicted protein sequence for the FGFR3-KO hTERT MSC line indicates a truncated protein with no transmembrane domain

The FGFR3-KO hTERT MSC line has been shown to have a single base insertion in exon 6 of the gene, (A) shows the comparative difference between the wild type FGFR3 protein sequence and the predicted protein sequence for GM FGFR3 whereby a premature stop codon has been introduced effectively truncating the protein. (B) A schematic of the FGFR3 protein indicating where the premature stop codon truncates FGFR3 in the third immunoglobulin domain of the extracellular region of FGFR3.

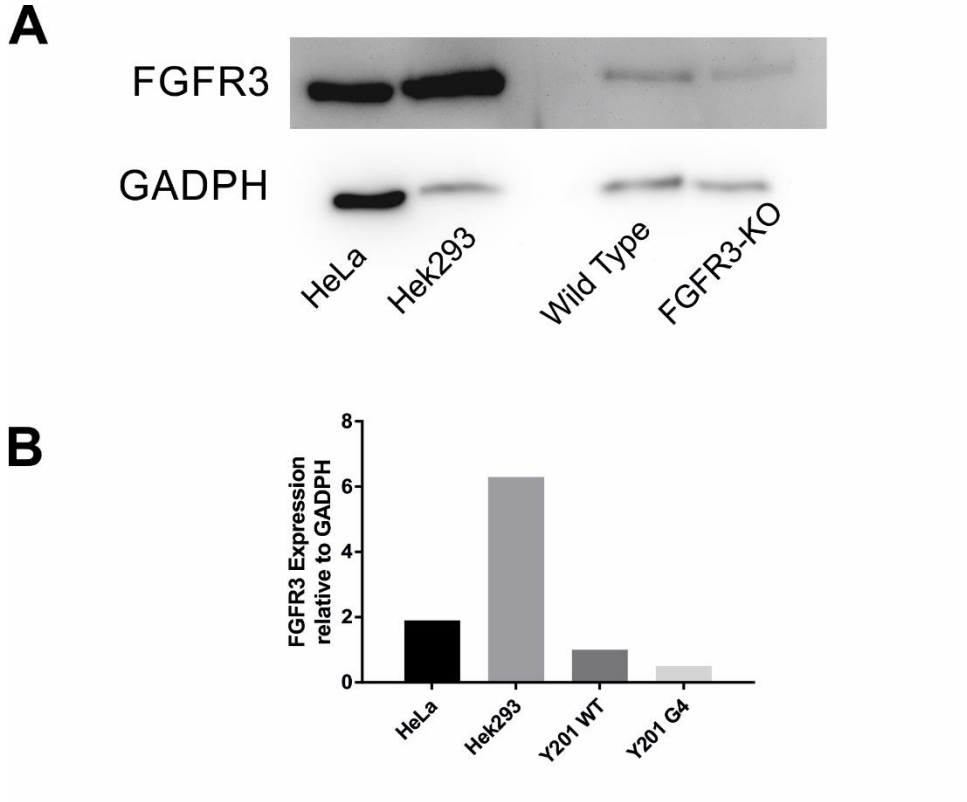

Figure 5.4.5: Analysis of FGFR3 protein expression in FGFR3-KO hTERT MSCs and development of FGFR3 transcript expression in HeLa cells.

FGFR3 expression was analysed by Western Blot to provide evidence of knockout status. A) Total protein samples were separated by gel electrophoresis and probed against FGFR3 and GADPH, used as a loading control. B) Densitometry was calculated using ImageJ and normalised against GADPH levels. This summarises one technical repeat from a single experiment.

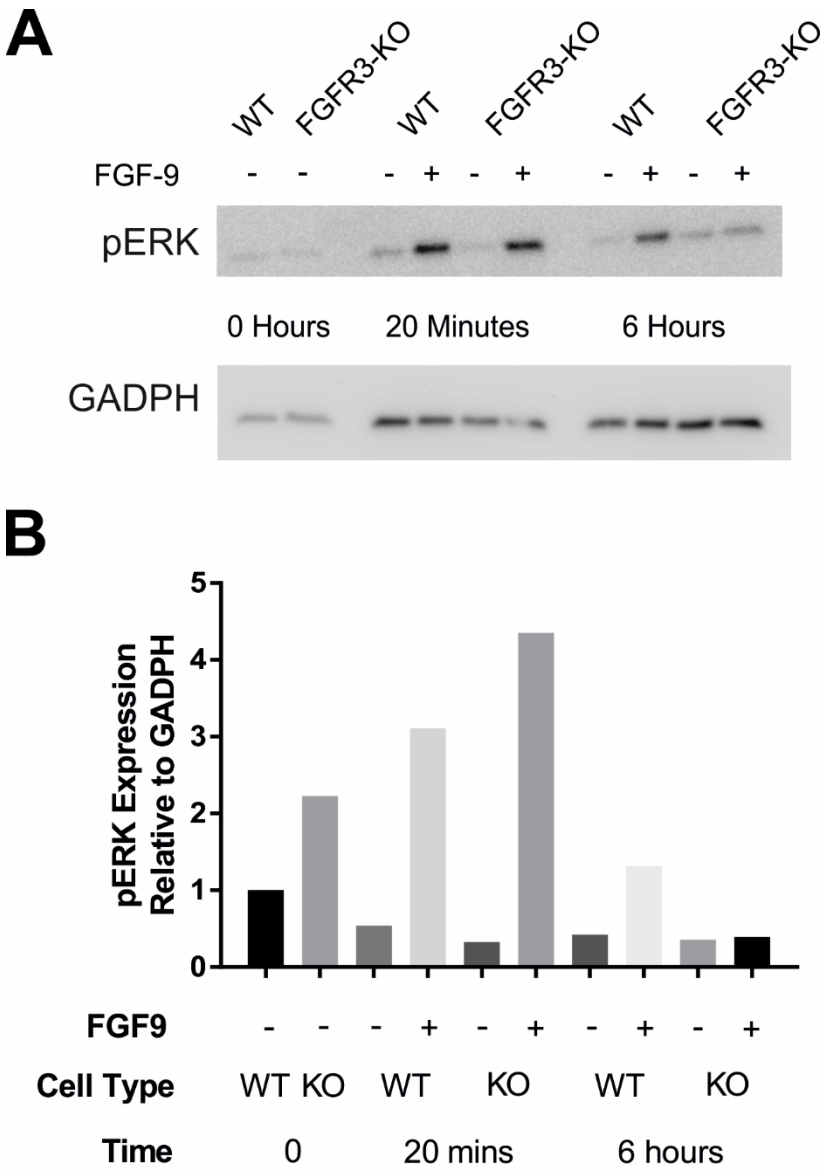

Figure 5.4.6: FGF9 supplementation appears to result in varied pERK response from WT and FGFR3-KO hTERT MSCs

WT and FGFR3-KO hTERT MSCs were treated with 20ng/mL FGF9 and the resultant alteration of ERK phosphorylation was analysed by Western blot (A). Densitometry was used to quantify the changes in expression with GADPH expression used as an internal control, n=1 (B).

5.4.2 FGFR3-KO hTERT MSCs are viable in long term culture and survive clonogenic assays

5.4.2.1 Vi-cell counter demonstrates viability of FGFR3-KO hTERT MSCs is comparable to wild type Y201 hTERT MSCs

During routine cell culture, samples of both the WT hTERT MSCs and the FGFR3-KO hTERT MSCs were taken and analysed using the Vi-CELL cell counter and viability analyser. This uses the trypan blue living cell exclusion dye to stain cells with a non-intact membrane therefore giving an indication to the number of dead cells in a sample. Figure 5.4.7 shows the results gained across three separate Vi-CELL readings giving an average viability of the samples tested. No significant difference between the wild type WT hTERT MSCs and the FGFR3-KO hTERT MSCs could be detected and both cell lines had an average viability of approximately 96%.

In order to compare any morphological differences between the WT hTERT MSCs and the FGFR3-KO hTERT MSCs, both were seeded into well plates, fixed and stained with crystal violet solution. The wild type cells had typical fibroblastic morphology whereas although the FGFR3-KO hTERT MSCs appeared fibroblastic-like in shape they are more elongated with extended processes with a tendency to have what appeared to be broad lamellipodia (indicated with arrows in Figure 5.4.8A). However, despite the apparent morphological changes, when the sizes of trypsinised cells were analysed for by the Vi-CELL, no significant differences in diameter could be detected (Figure 5.4.8B). This would indicate that there is no loss of cell volume but an alteration to the cell shape of adherent FGFR3-KO hTERT MSCs compared to WT controls.

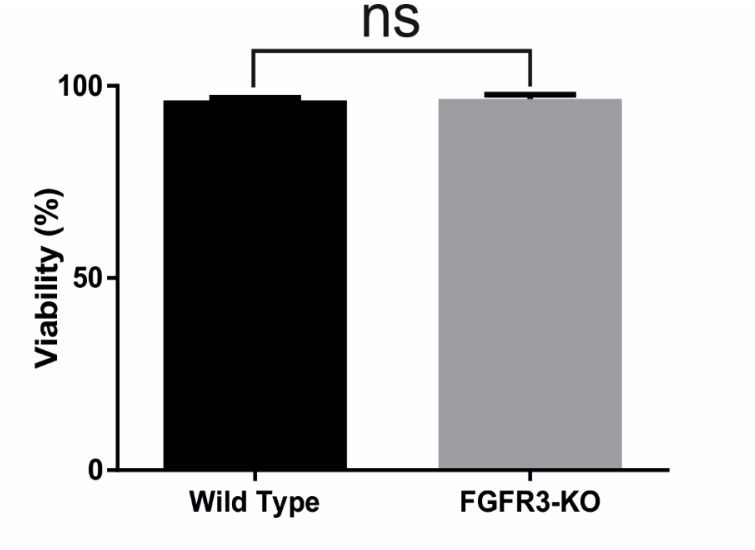

Figure 5.4.7: Analysis of effect of removing FGFR3 using CRISPR/Cas9 on hTERT MSC viability

100,000 WT hTERT MSCs and FGFR3-KO hTERT MSCs were sampled from cell cultures and analysed using the Vi-CELL counter for viability using the trypan blue exclusion dye. All stained objects were counted and the average viability across three samples. Values = mean ± SD, n=3 with statistical significance obtained using unpaired t-test with Welch's correction.

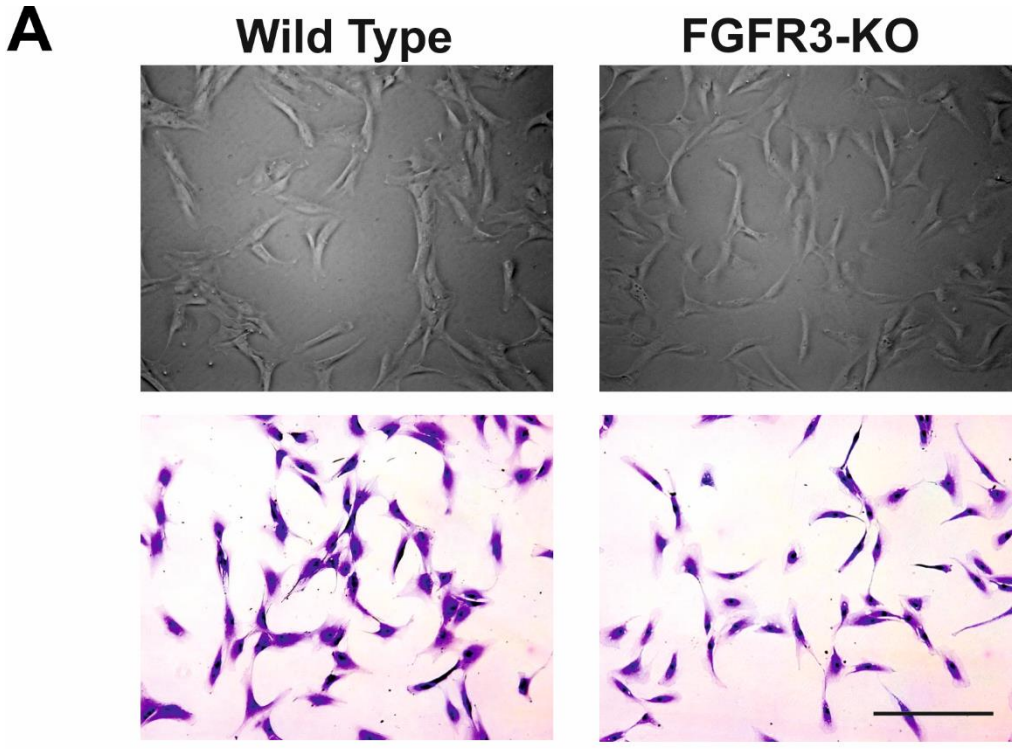
A
Wild Type
FGFR3-KO

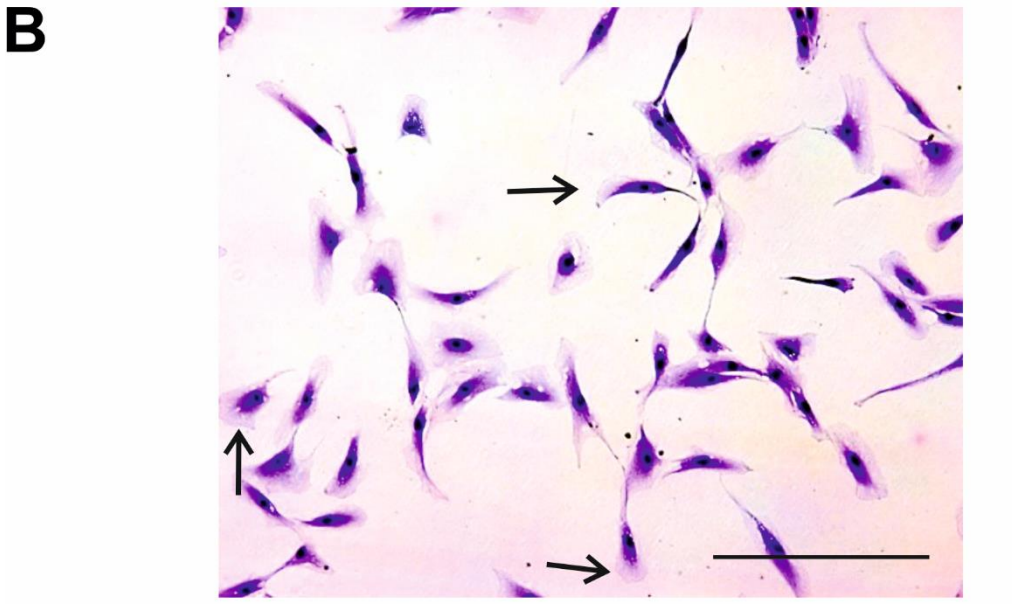
B

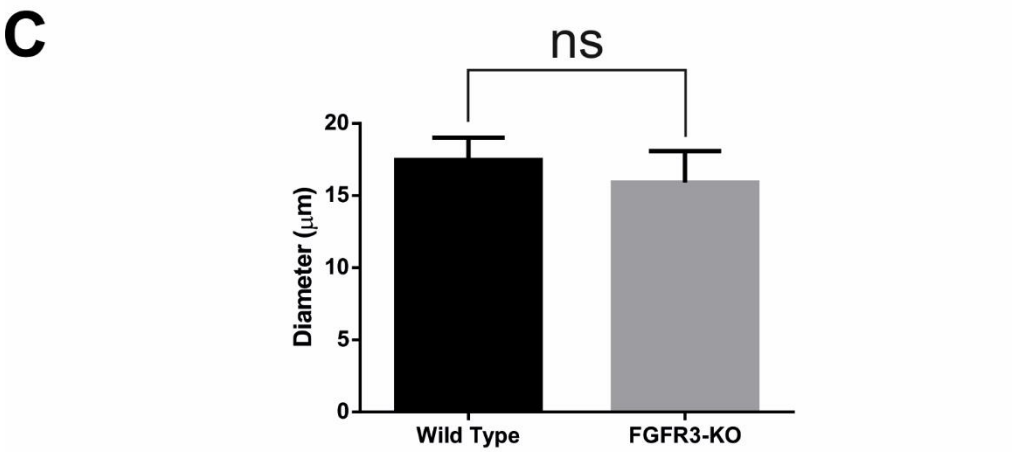
C
ns
Diameter (μm)
20
15
10
5
0
Wild Type
FGFR3-KO

Figure 5.4.8: Analysis of hTERT MSC morphology by phase imaging and crystal violet staining with diameter calculated by Vi-CELL

Samples of WT hTERT MSCs and FGFR3-KO hTERT MSCs plated at subconfluency and imaged using phase contrast (A top panels) or fixed and stained with crystal violet solution (A bottom panels). Scale bar = 200µm. (B) The stained FGFR3-KO hTERT MSCs were enlarged and some examples of broad lamellipodia highlighted with arrows. Scale bar = 200µm (C) Cells were also analysed for diameter during viability analysis and no significance difference found by Vi-CELL. Values = mean ± SD, n=3 significance calculated by unpaired t-test with Welch's correction.

5.4.3 FGFR3-KO hTERT MSCs produce comparable levels of colonies that cover a greater surface area than wild type counterparts

The WT hTERT MSC line demonstrates typical MSC behaviour, with the propensity to differentiate into the tri-lineage potential typical of MSCs (osteoblasts, adipocytes and chondrocytes) in addition to the ability to form colonies when plated at low density. We therefore wished to determine to what extent the FGFR3-KO hTERT MSCs were able to recapitulate these abilities. First, both the WT hTERT MSCs and the FGFR3-KO hTERT MSCs were plated at low density (10 cells/cm^2) and incubated until discrete colonies could be identified. These colonies were then fixed and stained with crystal violet solution (Figure 5.4.8A). The ability of the FGFR3-KO cells to form colonies did not appear impaired, with both colony efficiency and number of colonies formed showing as non-significant between the two cell types (Figure 5.4.8B). However, the size of the individual colonies, in addition to the surface area of plate covered by colonies, was significantly increased in the FGFR3-KO hTERT MSCs demonstrating a potentially increased proliferative and migratory status (Figure 5.4.8C+D). It was also notable there were morphological differences between the two cell types as the FGFR3-KO hTERT MSCs, similarly to before, were elongated with broad lamellipodia.

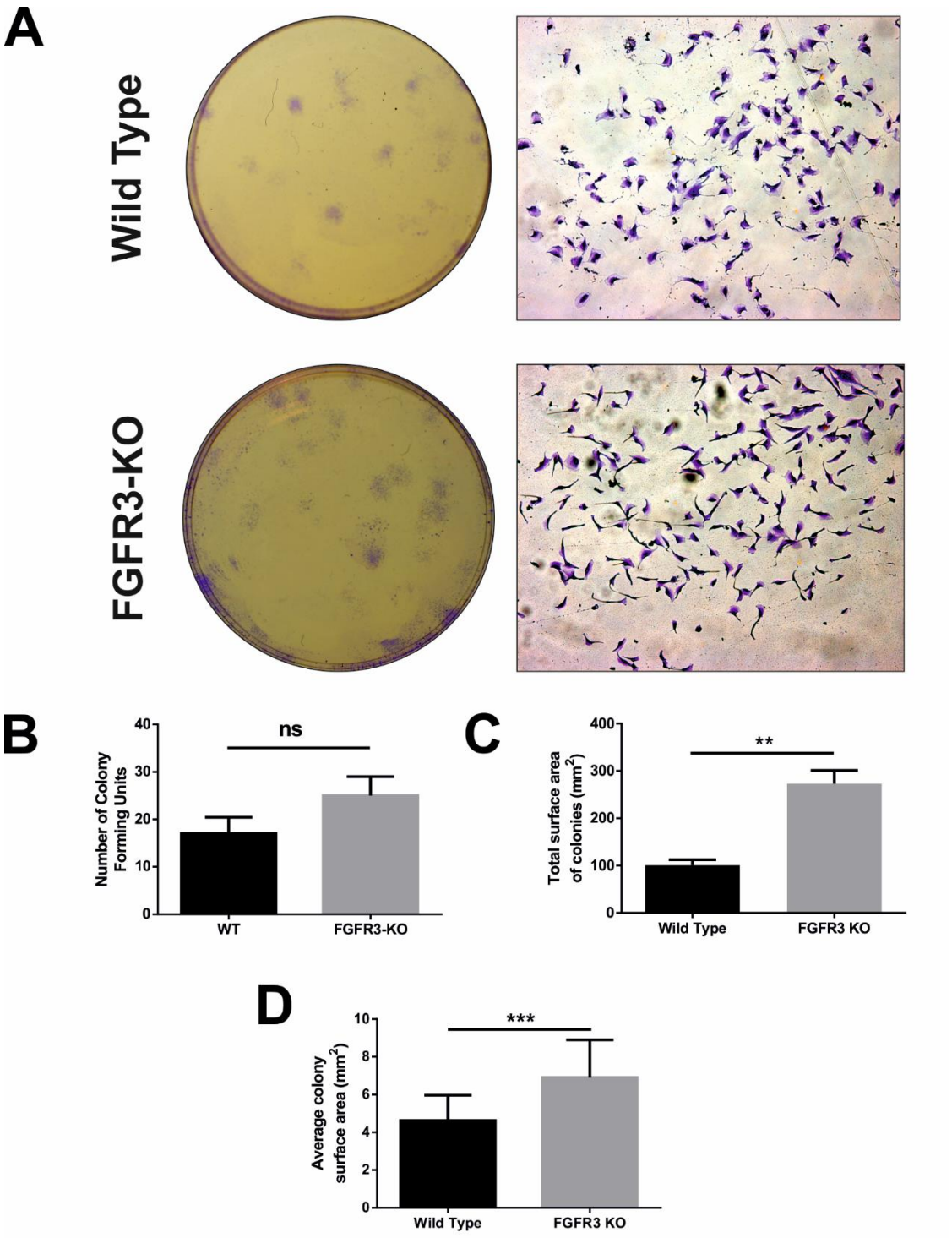

Figure 5.4.9: Analysis of the clonogenic ability of FGFR3-KO hTERT MSCs and the resultant colonies formed

Samples of WT hTERT MSCs and FGFR3-KO hTERT MSCs plated at 10 cells/cm^2 in well plates, fixed and stained with crystal violet solution (well overview, left and colony overview, right). Colonies were counted and averaged across three plates (B) and the total surface area of the plate covered by colonies (C) also calculated. The average surface area of each colony was also calculated. Values = mean ± SD, n=3 significance obtained by unpaired t-test with Welch's correction.

5.4.4 FGFR3-KO hTERT MSCs have increased proliferative capacity

Colonies formed by FGFR3-KO hTERT MSCs covered a larger surface than their wild type counterparts, giving evidence for an increased number of cells in these colonies. This would indicate the FGFR3-KO hTERT MSCs are proliferating at an increased rate. To test this hypothesis, both WT hTERT MSCs and FGFR3-KO hTERT MSCs were analysed for EdU incorporation during synthesis phase of the cell cycle. Cells were first seeded and starved of serum for 24 hours to synchronise the cell cycle, EdU was then supplemented in typical hTERT MSC growth media and the cells left to proliferate for 72 hours. Proliferating cells were then analysed by flow cytometry to provide a quantitative measure to the percentage of cells that had undergone a cell cycle during the incubation period. Figure 5.4.10A shows events recorded during the flow cytometry analysis of both WT hTERT MSCs and FGFR3-KO hTERT MSCs. Dead cells and debris were removed using forward scatter and side scatter to provide a better estimate of proliferating cells. The results were then summarised in a bar chart (Figure 5.4.10B). It was evident that during the 72 hour incubation period, significantly more FGFR3-KO hTERT MSCs had undergone a cell cycle and incorporated EdU compared to the wild type cells. In fact, only 5% of FGFR3-KO hTERT MSCs had not incorporated EdU during the 72 hour incubation period compared to 23% of WT hTERT MSCs.

To provide further evidence for the increased proliferative capacity of the FGFR3-KO hTERT MSCs, an MTT assay was performed. This colorimetric assay assesses metabolic activity using the reduction of the MTT salt into its insoluble form as a measure for the number of viable cells present. The FGFR3-KO hTERT MSCs were compared to WT hTERT MSCs after 48 hours and 96 hours, time points 24 hours either side of the previous EdU assay, and the results are summarised in Figure 5.4.11. After 48 hours, there was no significant difference between the WT and the FGFR3-KO hTERT MSCs however, after 96 hours there were significantly more viable FGFR3-KO hTERT MSCs present.

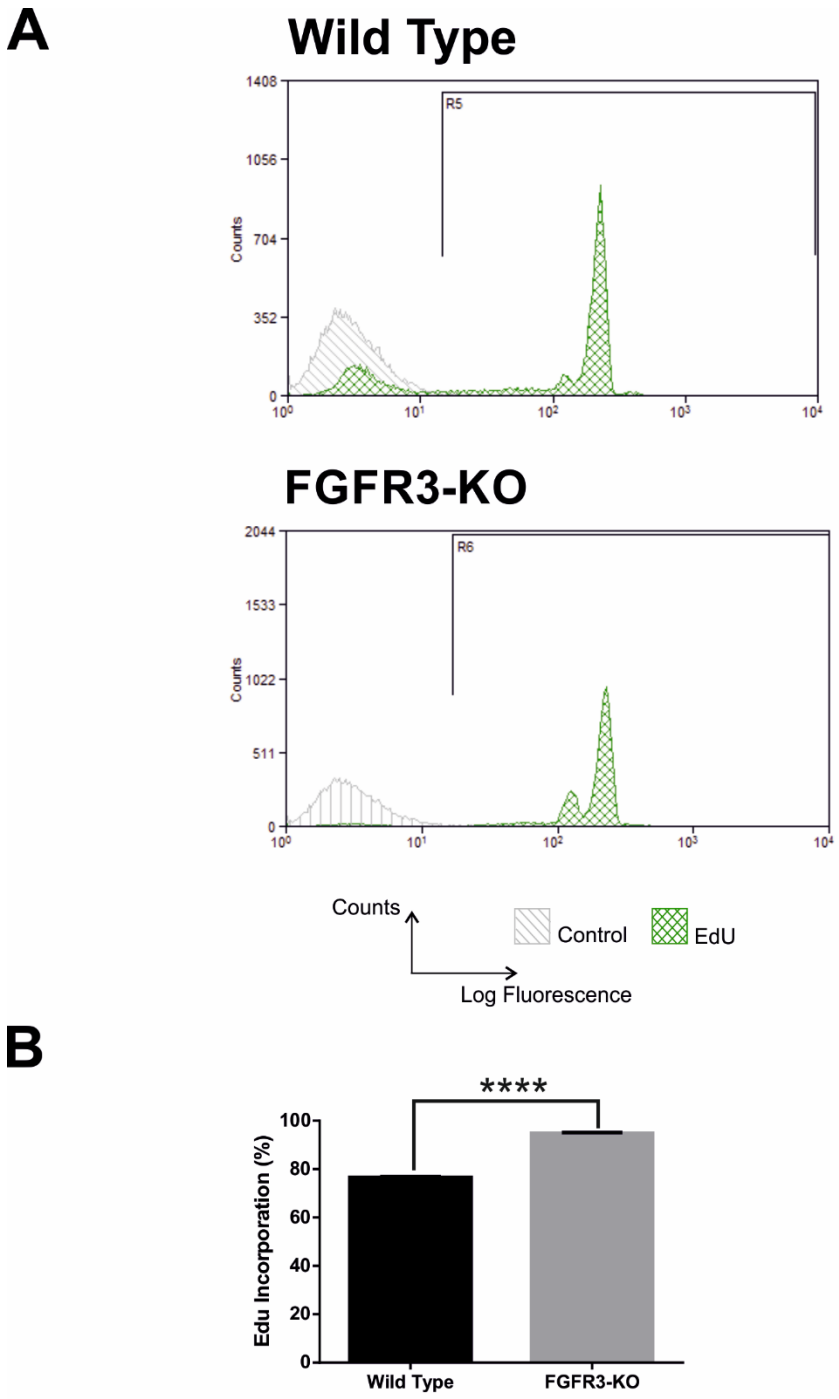

Figure 5.4.10: EdU incorporated by WT hTERT MSCs and FGFR3-KO hTERT MSCs over 72 hours

WT hTERT MSCs and FGFR3-KO hTERT MSCs were synchronised by serum starvation and supplemented with EdU over 72 hours. Cells were then analysed by flow cytometry to quantify fluorescent cells (A) and the events summarised in a bar chart (B). Values = mean ± SD, n=3 significance obtained by unpaired t-test with Welch's correction.

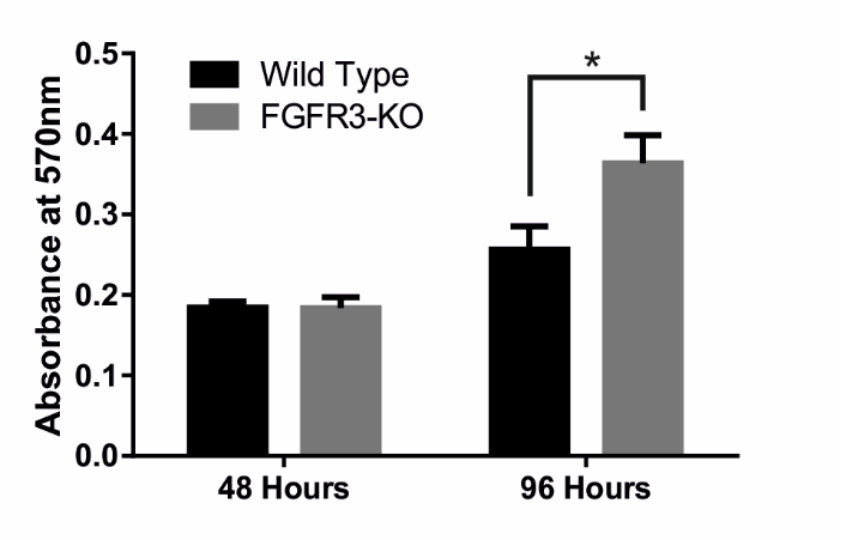

Figure 5.4.11: Colorimetric MTT assay to assess numbers of viable hTERT MSCs after 48 and 96 hours in culture

WT hTERT MSCs and FGFR3-KO hTERT MSCs were seeded at $5x10^3/cm^2$ and allowed to proliferate for either 48 hours or 96 hours. Cells were then supplemented with MTT for 3 hours before the cells and dye are solubilised and the absorbance quantified by a plate reader. Values = mean ± SD, n=3 significance obtained by unpaired t-test with Welch's correction.

5.4.5 FGFR3-KO hTERT MSCs have a significantly decreased differentiation capacity

With evidence that the FGFR3-KO hTERT MSCs had the capability to recapitulate the self-renewal behaviours of stem cells it was pertinent to determine whether they could also differentiate into the lineages typical of an MSC.

In order to study the effects of FGFR3 removal on MSC adipogenic differentiation, both FGFR3-KO hTERT MSCS and WT hTERT MSCs were seeded at confluency and induced to form adipocytes. These samples were allowed to differentiate for 21 days before the cells were fixed with paraformaldehyde and stained for the presence of lipid droplets using Oil Red O. The WT hTERT MSCs readily formed lipid droplets in the early stages of the differentiation timecourse, with the smaller lipid droplets combining to form large lipid droplets by the last timepoint (Figure 5.4.12A). However, in comparison the ability of the FGFR3-KO hTERT MSCs to form lipid droplets was severely impaired with apparent decreases in numbers of lipid droplets throughout the timecourse. The Oil Red O stain was eluted from each of the samples using isopropanol and quantified by absorbance at 450nm summarised in Figure 5.4.12B. This demonstrated that throughout the timecourse the absorbance of the adipogenic stimulated WT hTERT MSCs was significantly higher than that of the basal control. However, the FGFR3-KO hTERT MSCs consistently had an absorbance comparable to that of the basal control. Furthermore, the absorbance of the adipogenic stimulated WT hTERT MSCs was significantly more than the FGFR3-KO hTERT MCSs at every timepoint measured.

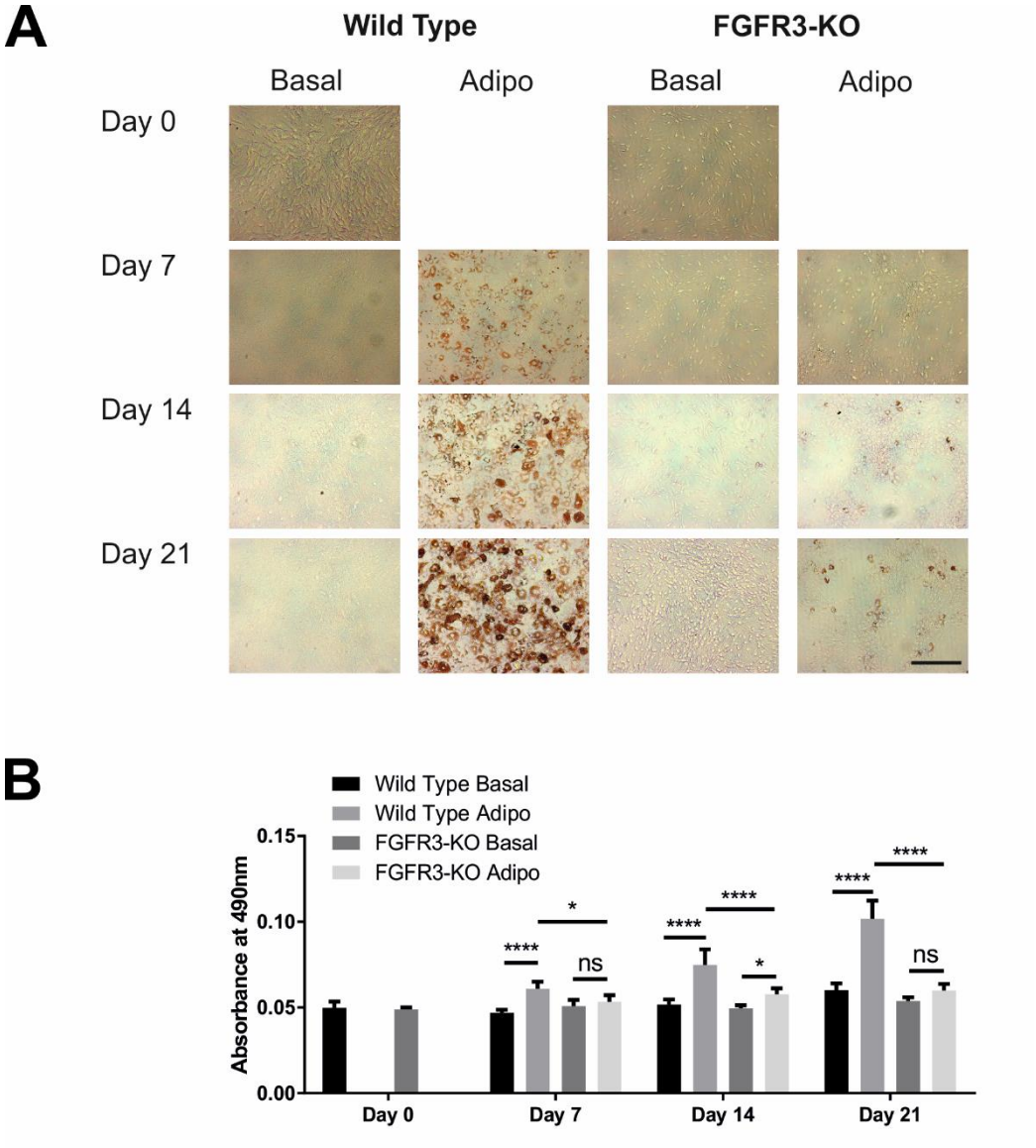

Figure 5.4.12: A timecourse of adipogenic stimulation of WT hTERT MSCs and FGFR3-KO hTERT MSCs

10,000 WT hTERT MSCs and FGFR3-KO hTERT MSCs were seeded in 96 well plates and treated with an adipogenic cocktail for up to 21 days A) Representative brightfield images of Oil Red O staining showing lipid droplet accumulation. Scale bar = 200µm B) Eluted Oil Red O stain quantified by absorbance at 450nm. Values = mean ± SD, n=3 significance 2 way RM ANOVA with Tukey's multiple comparisons.

A similar experiment to analyse the propensity of the FGFR3-KO hTERT MSCs to differentiate into osteoblasts was then set up. As before, WT hTERT MSCs and FGFR3-KO hTERT MSCs were seeded at confluency and stimulated with an osteogenic cocktail for 21 days. Upon completion of the timecourse, the samples were fixed in paraformaldehyde and stained with Alizarin Red S, which stains calcium deposition. Figure 5.4.13A shows representative wells of the samples analysed during the timecourse imaged using a brightfield microscope. The WT hTERT MSCs demonstrate increased amounts of calcium being deposited during the timecourse with considerably more calcium being stained and present at Day 21. The FGFR3-KO hTERT MSCs conversely demonstrate little difference between the basal controls and the osteogenic stimulated samples. This was further confirmed by eluting the Alizarin Red S stain using 10% CPC and quantifying the stain by reading the absorbance at 570nm (Figure 5.4.13B). The FGFR3-KO hTERT MSCs demonstrated a minimal increase in absorbance at this wavelength in the osteogenic samples compared to the basal controls, whereas a noticeable and significant difference could be detected at Day 21 in the WT hTERT MSCs. This increase in absorbance in the osteogenic WT hTERT MSCs was also significantly more than the absorbance of the osteogenic FGFR3-KO hTERT MSCs.

Osteogenesis, as previously discussed, occurs in multiple stages with calcium deposition occurring during the latter stages. To determine whether the FGFR3-KO hTERT MSCs demonstrated any evidence of early osteogenesis an enzymatic alkaline phosphatase (ALP) assay was set up and the enzyme activity normalised to DNA content. The distribution of the ALP activity was then normalised to a scale where 0 indicates no enzymatic activity and 1 is the maximum activity demonstrated during the assay. The assay was conducted over a shorter timepoint as ALP is one of the initial osteogenic markers to show an increase during differentiation. The WT hTERT MSCs when stimulated to undergo osteogenesis showed a continual increase in osteogenic activity during the timecourse and at each timepoint this activity was significantly more than that seen in the basal control. The FGFR3-KO hTERT MSCs, however, demonstrated no ALP activity significantly above that of basal levels during any of the timepoints.

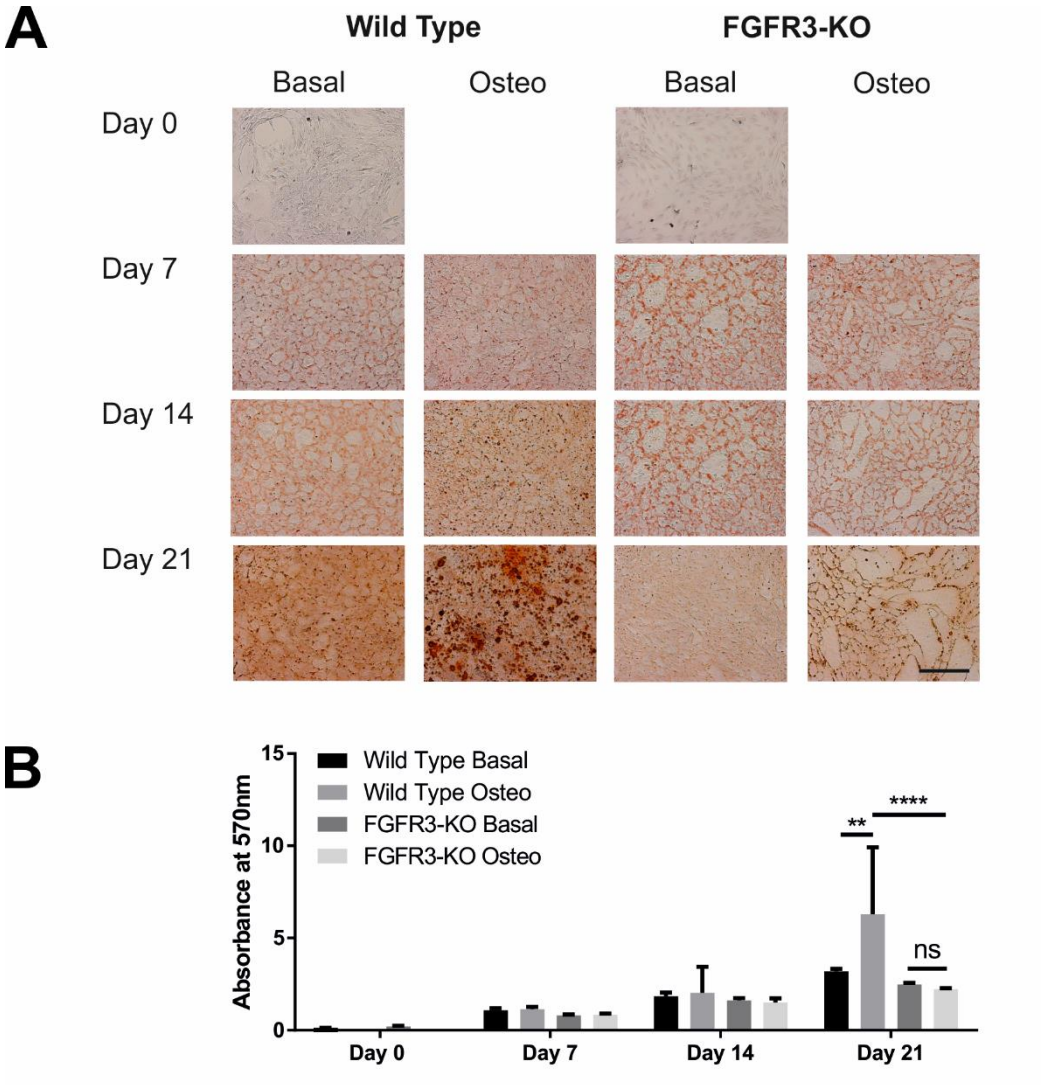

Figure 5.4.13: A timecourse of osteogenic stimulation of WT hTERT MSCs and FGFR3-KO hTERT MSCs

WT hTERT MSCs and FGFR3-KO hTERT MSCs were seeded at confluency in 24 well plates and treated with an osteogenic cocktail for up to 21 days A) Representative brightfield images of Alizarin Red S staining showing calcium deposition. Scale bar = 200µm B) Eluted Alizarin Red S stain quantified by absorbance at 570nm. Values = mean ± SD, n=3 significance 2 way RM ANOVA with Tukey's multiple comparisons.

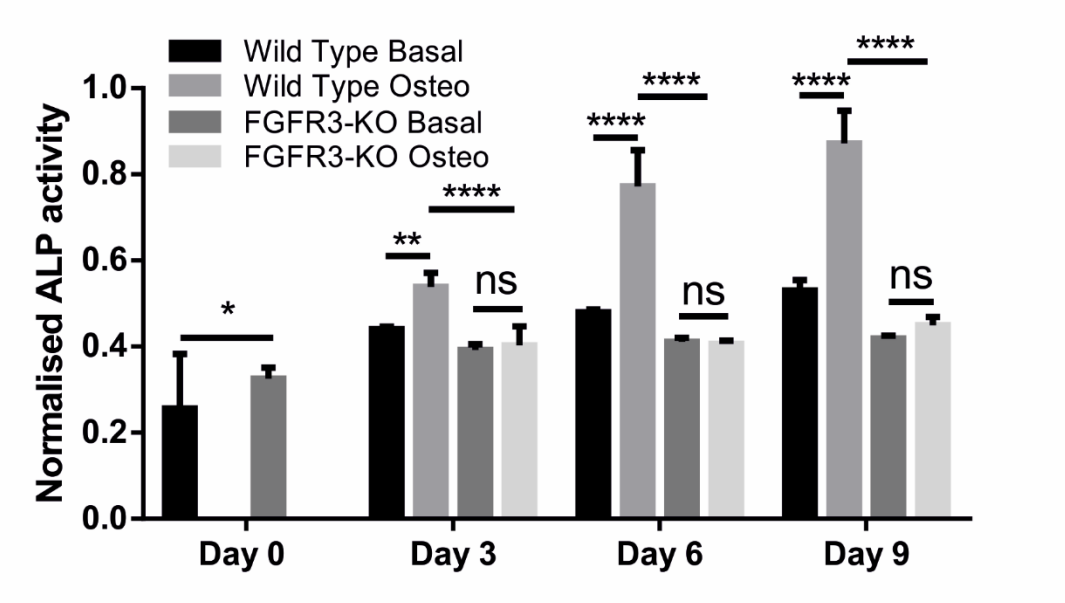

Figure 5.4.14: Alkaline phosphatase activity normalised to DNA content of WT hTERT MSCs and FGFR3-KO hTERT MSCs during early osteogenesis

WT hTERT MSCs and FGFR3-KO hTERT MSCs were seeded at confluency in 96 well plates and treated with an osteogenic cocktail for up to 9 days. At each timepoint ALP activity was measured and normalised to DNA content, calculated using picogreen fluorescence, after the assay was complete the data was normalised on a 0 – 1 distribution. Values = mean ± SD, n=6 significance 2 way RM ANOVA with Tukey's multiple comparisons.

Finally, both WT hTERT MSCs and FGFR3-KO hTERT MSCs were induced to undergo chondrogenesis. Both cell lines were centrifuged to induce the formation of pellets and differentiated for up to 21 days before 3 pellets were combined. RNA samples were then isolated and extracted using Trizol, reverse transcribed into cDNA and used to analyse the chondrogenic markers Sox9 and Aggrecan. Basal controls at each time point were compared to samples exposed to the chondrogenic inductive supplements.

Sox9, as previously discussed, is the master transcription regulator of chondrogenesis and expression levels are expected to rise and peak early during differentiation before falling again. In this timecourse (Figure 5.4.15A), it was evident that Sox9 expression was higher in WT hTERT MSC chondrogenic differentiated samples in comparison to the basal controls at days 7 and 14. At day 21, Sox9 expression had fallen to basal levels. There did not appear to be a correlation between the differentiation status of the FGFR3-KO hTERT MSCs and the levels of Sox9, as at days 7 and 14 basal samples exhibited higher levels of Sox9 expression.

Aggrecan is a major proteoglycan found in cartilage and can be found to accumulate in a time dependent fashion during chondrogenesis (Kiani et al., 2002). Figure 5.4.15B shows that the Aggrecan expression levels were found to be increased in chondrogenic WT hTERT MSCs compared to basal samples, at both days 7 and 14. However, there was a sharp drop in expression at day 21 albeit with expression still appearing increased in chondrogenic conditions comparatively to the basal control. Throughout the majority of the timecourse, there appeared to be decreased expression levels of Aggrecan during chondrogenesis in the FGFR3-KO hTERT MSCs. It is not immediately apparent if the WT hTERT MSCs in this instance are successfully differentiating into chondrocytes, but overall, the expression markers indicative of chondrogenesis appear dysregulated in the FGFR3-KO hTERT MSCs and in chondrogenic stimulated conditions are typically lower than WT hTERT MSC levels.

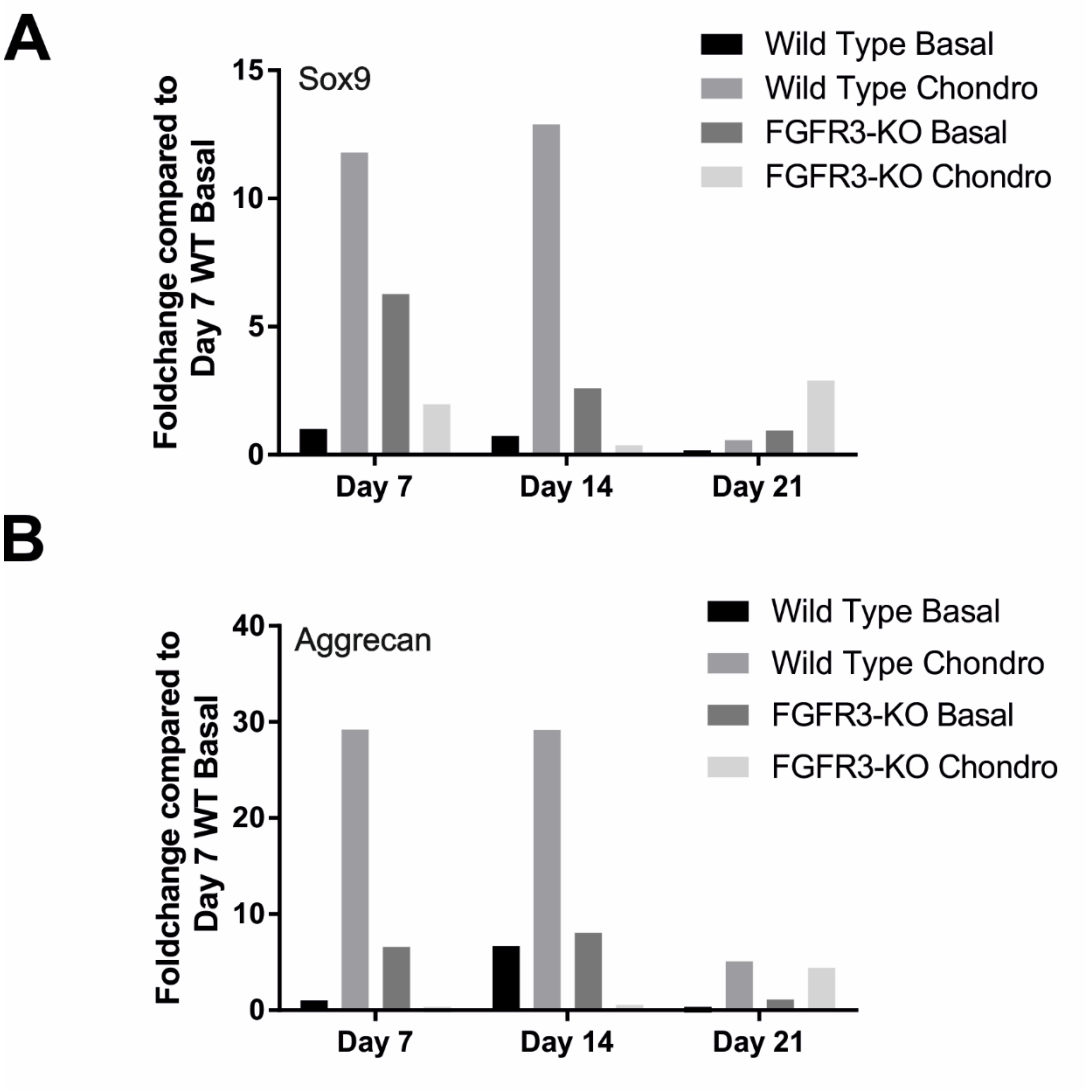

Figure 5.4.15: qPCR analysis of chondrogenic markers at various intervals during chondrogenic differentation of WT and FGFR3-KO hTERT MSCs.

200,000 WT hTERT MSCs or FGFR3-KO hTERT MSCs were pelleted by centrifugation in U-bottomed 96 well plates the media changed for either basal media or a chondrogenic inductive cocktail after 24 hours. Differentiation was then allowed to occur for up to 21 days. cDNA samples were then generated and analysed for A) Sox9 expression or B) Aggrecan expression. Expression of each gene was made relative to the housekeeping gene RPS27a and foldchanges calculated as $2^{-\Delta\Delta ct}$ these values were then made relative to the WT hTERT MSC Day 7 Basal sample. The data summarised in these graphs are the mean of 3 technical replicates from one experiment.

5.4.6 Transcriptome analysis of FGFR3-KO hTERT MSCs by RNA sequencing

Considering the earlier phenotypic observations, it was decided to analyse the transcriptome of the WT and FGFR3-KO hTERT MSCs to determine the effects of the KO on the transcriptome profile. This was performed in triplicate before the transcriptomes of the two cell lines were compared.

5.4.6.1 No FGFR3 transcripts detected by RNA-seq

Firstly, the RNA-seq data was analysed to examine readouts of FGFR3 RNA and determine whether any differences between the WT and the FGFR3-KO hTERT MSCs could be seen in order to provide further evidence to the knockout status of these cells. Table 5.4.1 shows a summary of the FGFR3 reads analysed by the RNA-seq for both cell types. None of the FGFR3 splice variants analysed were found in the FGFR3-KO hTERT MSCs, but were present in the WT hTERT MSCs. No significant differences were found between the reads, most likely due to the low fragments per kilobase of transcript per million mapped reads (FPKM) found in the WT hTERT MSCs. However, these data would again suggest that the CRISPR/Cas9 has resulted in the knockout of FGFR3 in the FGFR3-KO hTERT MSCs.

5.4.6.2 Overview of transcripts in WT and FGFR3-KO hTERT MSCs shows most differentially regulated are protein-coding transcripts

Overall, 397 transcripts found to be up-regulated and 506 transcripts down-regulated in the FGFR3-KO hTERT MSCs compared to the WT hTERT MSCs. These were deemed differentially regulated when both cell types analysed had reads per kilobase of transcript per million mapped reads (RPKM) > 0, an adjusted p value < 0.05 and a log2 fold change > +/-1. Predominantly, these differentially regulated transcripts were protein coding, an overview of the differentially regulated transcripts can be found in Figure 5.4.16.

.

Table 5.4.1: Overview of FGFR3 splice variant expression in WT and FGFR3-KO hTERT MSCs

Transcript ID	Gene Name	Status	Y201 WT FPKM	FGFR3-KO FPKM	Log2 Fold Change	P Value	Q Value	Significant?
TCONS_00217794	FGFR3	NOTEST	0	0	0	1	1	no
TCONS_00217795	FGFR3	NOTEST	0	0	0	1	1	no
TCONS_00217796	FGFR3	NOTEST	0	0	0	1	1	no
TCONS_00217797	FGFR3	NOTEST	0	0	0	1	1	no
TCONS_00217798	FGFR3	NOTEST	1.43E-05	0	N/A	1	1	no
TCONS_00217799	FGFR3	NOTEST	0	0	0	1	1	no
TCONS_00217801	FGFR3	NOTEST	6.19E-08	0	N/A	1	1	no
TCONS_00217802	FGFR3	NOTEST	0.01005	0	N/A	1	1	no
TCONS_00217803	FGFR3	NOTEST	0	0	0	1	1	no
TCONS_00217804	FGFR3	NOTEST	0	0	0	1	1	no
TCONS_00217805	FGFR3	NOTEST	0.0134938	0	N/A	1	1	no

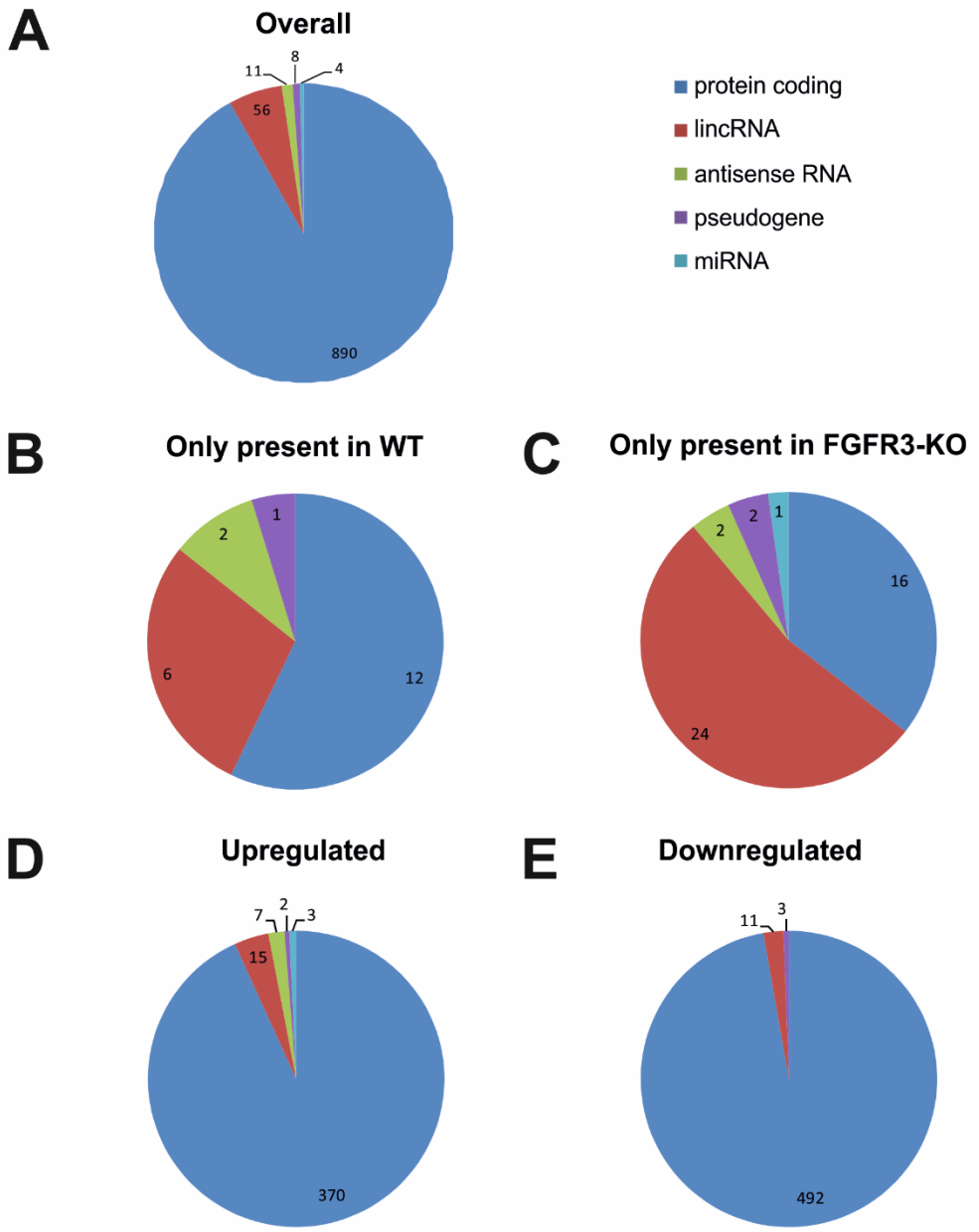

Figure 5.4.16: Summary of transcripts differentially regulated in FGFR3-KO hTERT MSCs compared to WT hTERT MSCs

Numbers of differentially regulated transcripts identified using RNA-seq summarising (A) the overall numbers of transcripts differentially regulated in the FGFR3-KO hTERT MSCs compared to the WT hTERT MSCs. Transcripts only present in (B) WT cells or (C) FGFR3-KO hTERT MSCs. A breakdown of transcripts (D) upregulated in FGFR3-KO hTERT MSCs or (E) downregulated in FGFR3-KO hTERT MSCs.

5.4.6.3 No significant alterations to FGF and FGFR expression caused by knocking out FGFR3 in hTERT MSCs

The FGF receptors exist as a gene family, and there is a possibility that the alteration of expression of one of the FGFRs would result in alterations of expression in the other receptors. Deng et al. showed no alterations in FGFR1 mRNA expression in the growth plates of two day old FGFR3-KO mice and no FGFR2 was detected, suggesting the removal of FGFR3 does not alter FGFR expression in chondrocytes. However, it is not possible to tell from these data whether the removal of FGFR3 impacts on the FGF signalling of the MSCs from which these skeletal elements arise. To examine whether knocking out FGFR3 from the hTERT MSCs impacted on the expression levels of the other FGFRs, the expression values of all transcripts from the RNA-seq analysis were tabulated, and compared between the WT and FGFR3-KO hTERT MSCs in Table 5.4.2.

No significance differences were found between the expression levels of any of the FGFR splice variants between the WT and the FGFR3-KO hTERT MSCS. However, some slight deviations between the transcripts of FGFR1 and FGFR4 were noticeable, with a number of transcripts present only in one of the cell types. No FGFR2 transcripts were detectable in either the WT or the FGFR3-KO hTERT MSCs (Table 5.4.2).

The FGF ligands have different specificities to the FGF receptors, with the differing subfamilies demonstrating increased binding to some of the FGFRs and their splice variants. With the removal of FGFR3, it was hypothesised that the expression of the FGF ligands with high specificities to FGFR3 may be altered. The FGF transcripts were tabulated, similarly to the receptors, and the expression values compared between the WT and FGFR3-KO hTERT MSCs (Table 5.4.3). Again, there were no significant differences between the expression levels of any of the FGF transcripts but there was variance between the transcripts and FGFs being expressed. Very little variance could be seen in the FGF1 subfamily (FGF1 and FGF2) which bind the majority of the FGFRs and a number of the FGFs were undetectable in both the WT and FGFR3-KO hTERT MSCs. The FGF8 (FGF8, FGF17 and FGF18) and FGF9 (FGF9, FGF16 and FGF20) subfamilies preferentially bind FGFR3c over other FGFRs and splice variants and are highlighted in Table 5.4.3. There appeared to be a tendency for these genes to be upregulated in the FGFR3-KO hTERT MSCs, other than FGF16 which was found only in the WT hTERT MSCs and FGF9 which was not expressed in either cell line. As previously mentioned, these tendencies are not significant, likely due to the very low levels of expression detected but may show the FGFR3-KO hTERT MSCs attempting to compensate for the lack of FGFR3 signalling by upregulating FGF ligands with preferential binding to the FGFR3 receptor.

Table 5.4.2: FGFR transcript expression does not appear to be significiantly affected by knocking out FGFR3

Transcript ID	Gene Name	Status	Y201 WT FPKM	FGFR3-KO FPKM	Log2 Fold Change	P Value	Q Value	Significant?
TCONS_00271878	FGFR1	OK	8.68E-01	1.18E-01	-2.87396	0.39115	0.994836	no
TCONS_00271853	FGFR1	OK	5.96E-01	1.41E-01	-2.07946	0.4811	0.994836	no
TCONS_00271881	FGFR1	NOTEST	1.88E-01	5.51E-02	-1.77046	1	1	no
TCONS_00271887	FGFR1	NOTEST	1.92E-01	6.83E-02	-1.49308	1	1	no
TCONS_00271872	FGFR1	NOTEST	1.88E-01	9.16E-02	-1.03789	1	1	no
TCONS_00271838	FGFR1	OK	1.76E+00	1.53E+00	-0.206966	0.8803	0.994836	no
TCONS_00271859	FGFR1	NOTEST	2.19E-01	1.91E-01	-0.201266	1	1	no
TCONS_00271836	FGFR1	NOTEST	0	0	0	1	1	no
TCONS_00271868	FGFR1	NOTEST	0	0	0	1	1	no
TCONS_00271874	FGFR1	NOTEST	0	0	0	1	1	no
TCONS_00271837	FGFR1	NOTEST	0	0	0	1	1	no
TCONS_00271861	FGFR1	NOTEST	0	0	0	1	1	no

TCONS_00271883	FGFR1	NOTEST	0	0	0	1	1	no
TCONS_00271842	FGFR1	NOTEST	0	0	0	1	1	no
TCONS_00271835	FGFR1	NOTEST	0	0	0	1	1	no
TCONS_00271882	FGFR1	NOTEST	0	0	0	1	1	no
TCONS_00271882	FGFR1	NOTEST	0	0	0	1	1	no
TCONS_00271866	FGFR1	NOTEST	0	0	0	1	1	no
TCONS_00271852	FGFR1	NOTEST	0	0	0	1	1	no
TCONS_00271848	FGFR1	NOTEST	0	0	0	1	1	no
TCONS_00271857	FGFR1	NOTEST	0	0	0	1	1	no
TCONS_00271860	FGFR1	NOTEST	0	0	0	1	1	no
TCONS_00271863	FGFR1	NOTEST	0	0	0	1	1	no
TCONS_00271873	FGFR1	NOTEST	0	0	0	1	1	no
TCONS_00271862	FGFR1	NOTEST	6.59E-02	7.10E-02	0.106696	1	1	no
TCONS_00271847	FGFR1	OK	1.81E+01	2.00E+01	0.146712	0.6959	0.994836	no

TCONS_00271849	FGFR1	OK	3.93E+01	4.51E+01	0.199516	0.44305	0.994836	no
TCONS_00271833	FGFR1	OK	7.72E+00	9.31E+00	0.270326	0.63685	0.994836	no
TCONS_00271841	FGFR1	NOTEST	5.39E-02	6.53E-02	0.27736	1	1	no
TCONS_00271843	FGFR1	OK	2.67E-01	3.26E-01	0.287929	0.8883	0.994836	no
TCONS_00271867	FGFR1	OK	7.01E-01	1.05E+00	0.577144	0.7457	0.994836	no
TCONS_00271846	FGFR1	NOTEST	1.41E-01	2.23E-01	0.65797	1	1	no
TCONS_00271869	FGFR1	OK	1.07E+00	1.70E+00	0.668921	0.64425	0.994836	no
TCONS_00271850	FGFR1	NOTEST	6.18E-02	1.00E-01	0.693447	1	1	no
TCONS_00271880	FGFR1	OK	2.15E-01	3.49E-01	0.699715	0.7979	0.994836	no
TCONS_00271858	FGFR1	OK	6.62E-01	1.26E+00	0.92378	0.68285	0.994836	no
TCONS_00271864	FGFR1	OK	6.66E-01	1.37E+00	1.03827	0.5057	0.994836	no
TCONS_00271876	FGFR1	OK	7.91E-01	1.65E+00	1.05984	0.513	0.994836	no
TCONS_00271854	FGFR1	OK	4.57E-01	9.87E-01	1.1113	0.5409	0.994836	no
TCONS_00271877	FGFR1	OK	1.09E+00	2.60E+00	1.25431	0.53505	0.994836	no

TCONS_00271870	FGFR1	OK	2.76E-01	7.32E-01	1.40876	0.4086	0.994836	no
TCONS_00271885	FGFR1	OK	1.61E-01	5.62E-01	1.80656	0.46985	0.994836	no
TCONS_00271845	FGFR1	OK	2.97E-01	1.05E+00	1.82707	0.36885	0.994836	no
TCONS_00271879	FGFR1	NOTEST	3.10E-02	2.29E-01	2.88849	1	1	no
TCONS_00271871	FGFR1	OK	2.49E-01	1.85E+00	2.89623	0.29245	0.994836	no
TCONS_00271834	FGFR1	NOTEST	1.52E-02	2.23E-01	3.87317	1	1	no
TCONS_00271875	FGFR1	NOTEST	0	5.98E-02	N/A	1	1	no
TCONS_00271840	FGFR1	NOTEST	0	4.70E-03	N/A	1	1	no
TCONS_00271886	FGFR1	NOTEST	0	5.67E-02	N/A	1	1	no
TCONS_00271865	FGFR1	NOTEST	0	7.23E-02	N/A	1	1	no
TCONS_00271839	FGFR1	NOTEST	6.35E-02	0	N/A	1	1	no
TCONS_00055876	FGFR2	NOTEST	0	0	0	1	1	no
TCONS_00055870	FGFR2	NOTEST	0	0	0	1	1	no
TCONS_00055877	FGFR2	NOTEST	0	0	0	1	1	no

TCONS_00055871	FGFR2	NOTEST	0	0	0	1	1	no
TCONS_00055874	FGFR2	NOTEST	0	0	0	1	1	no
TCONS_00055882	FGFR2	NOTEST	0	0	0	1	1	no
TCONS_00055885	FGFR2	NOTEST	0	0	0	1	1	no
TCONS_00055881	FGFR2	NOTEST	0	0	0	1	1	no
TCONS_00055857	FGFR2	NOTEST	0	0	0	1	1	no
TCONS_00055886	FGFR2	NOTEST	0	0	0	1	1	no
TCONS_00055880	FGFR2	NOTEST	0	0	0	1	1	no
TCONS_00055865	FGFR2	NOTEST	0	0	0	1	1	no
TCONS_00055879	FGFR2	NOTEST	0	0	0	1	1	no
TCONS_00055883	FGFR2	NOTEST	0	0	0	1	1	no
TCONS_00055863	FGFR2	NOTEST	0	0	0	1	1	no
TCONS_00055854	FGFR2	NOTEST	0	0	0	1	1	no
TCONS_00055873	FGFR2	NOTEST	0	0	0	1	1	no

TCONS_00055851	FGFR2	NOTEST	0	0	0	1	1	no
TCONS_00055884	FGFR2	NOTEST	0	0	0	1	1	no
TCONS_00055872	FGFR2	NOTEST	0	0	0	1	1	no
TCONS_00055859	FGFR2	NOTEST	0	0	0	1	1	no
TCONS_00055858	FGFR2	NOTEST	0	0	0	1	1	no
TCONS_00055856	FGFR2	NOTEST	0	0	0	1	1	no
TCONS_00055855	FGFR2	NOTEST	0	0	0	1	1	no
TCONS_00055852	FGFR2	NOTEST	0	0	0	1	1	no
TCONS_00055861	FGFR2	NOTEST	0	0	0	1	1	no
TCONS_00055860	FGFR2	NOTEST	0	0	0	1	1	no
TCONS_00055867	FGFR2	NOTEST	0	0	0	1	1	no
TCONS_00055862	FGFR2	NOTEST	0	0	0	1	1	no
TCONS_00055868	FGFR2	NOTEST	0	0	0	1	1	no
TCONS_00055878	FGFR2	NOTEST	0	0	0	1	1	no

TCONS_00055866	FGFR2	NOTEST	0	0	0	1	1	no
TCONS_00055864	FGFR2	NOTEST	0	0	0	1	1	no
TCONS_00055869	FGFR2	NOTEST	0	0	0	1	1	no
TCONS_00055853	FGFR2	NOTEST	0	0	0	1	1	no
TCONS_00234209	FGFR4	NOTEST	6.47E-02	4.38E-07	-17.1704	1	1	no
TCONS_00234223	FGFR4	NOTEST	2.42E-02	2.57E-06	-13.2023	1	1	no
TCONS_00234222	FGFR4	NOTEST	3.37E-02	1.32E-02	-1.34539	1	1	no
TCONS_00234203	FGFR4	NOTEST	0	0	0	1	1	no
TCONS_00234218	FGFR4	NOTEST	0	0	0	1	1	no
TCONS_00234214	FGFR4	NOTEST	0	0	0	1	1	no
TCONS_00234220	FGFR4	NOTEST	0	0	0	1	1	no
TCONS_00234227	FGFR4	NOTEST	0	0	0	1	1	no
TCONS_00234217	FGFR4	NOTEST	0	0	0	1	1	no
TCONS_00234211	FGFR4	NOTEST	0	0	0	1	1	no

TCONS_00234206	FGFR4	NOTEST	0	0	0	1	1	no
TCONS_00234205	FGFR4	NOTEST	0	0	0	1	1	no
TCONS_00234207	FGFR4	NOTEST	0	0	0	1	1	no
TCONS_00234208	FGFR4	NOTEST	0	0	0	1	1	no
TCONS_00234204	FGFR4	NOTEST	0	0	0	1	1	no
TCONS_00234219	FGFR4	NOTEST	1.35E-03	2.83E-02	4.38594	1	1	no
TCONS_00234221	FGFR4	NOTEST	0	6.48E-07	N/A	1	1	no
TCONS_00234224	FGFR4	NOTEST	0	2.79E-02	N/A	1	1	no
TCONS_00234225	FGFR4	NOTEST	0	3.68E-05	N/A	1	1	no
TCONS_00234216	FGFR4	NOTEST	0	7.06E-06	N/A	1	1	no
TCONS_00234210	FGFR4	NOTEST	0	1.19E-05	N/A	1	1	no
TCONS_00234212	FGFR4	NOTEST	0	2.01E-02	N/A	1	1	no

Table 5.4.3: Fibroblast growth factor ligands detected by RNA-seq, no significant difference in transcript levels between FGFR3-KO hTERT MSCs and WT hTERT MSCs could be detected but slight changes in regulation can be detected. Ligands with preferential binding to FGFR3 are highlighted.

Transcript ID	Gene Name	Status	Y201 WT FPKM	FGFR3-KO FPKM	Log2 Fold Change	P Value	Q Value	Significant?
TCONS_00238933	FGF1	NOTEST	1.08E-01	4.25E-02	-1.33938	1	1	no
TCONS_00238934	FGF1	OK	8.62E-01	3.53E-01	-1.28957	0.59735	0.994836	no
TCONS_00238923	FGF1	NOTEST	1.56E-01	7.52E-02	-1. 05671	1	1	no
TCONS_00238929	FGF1	NOTEST	3.03E-01	2.25E-01	-0.429093	1	1	no
TCONS_00238930	FGF1	NOTEST	6.43E-02	5.23E-02	-0.29656	1	1	no
TCONS_00238917	FGF1	OK	1.05E+00	9.46E-01	-0.152957	0.87835	0.994836	no
TCONS_00238922	FGF1	OK	5.67E+00	5.49E+00	-0.0457645	0.9147	0.994836	no
TCONS_00238918	FGF1	NOTEST	0	0	0	1	1	no
TCONS_00238919	FGF1	NOTEST	0	0	0	1	1	no
TCONS_00238920	FGF1	NOTEST	0	0	0	1	1	no

TCONS_00238921	FGF1	NOTEST	0	0	0	1	1	no
TCONS_00238924	FGF1	NOTEST	0	0	0	1	1	no
TCONS_00238925	FGF1	NOTEST	0	0	0	1	1	no
TCONS_00238925	FGF1	NOTEST	0	0	0	1	1	no
TCONS_00238928	FGF1	NOTEST	0	0	0	1	1	no
TCONS_00238935	FGF1	NOTEST	0	0	0	1	1	no
TCONS_00238936	FGF1	NOTEST	0	0	0	1	1	no
TCONS_00238937	FGF1	NOTEST	0	0	0	1	1	no
TCONS_00238927	FGF1	OK	6.71E-02	6.05E-01	3.17307	0.455	0.994836	no
TCONS_00238931	FGF1	NOTEST	6.66E-02	0.00E+00	N/A	1	1	no
TCONS_00238932	FGF1	NOTEST	2.09E-01	0.00E+00	N/A	1	1	no
TCONS_00221331	FGF2	OK	1.71E+01	1.24E+01	-0.469313	0.025	0.580488	no
TCONS_00221333	FGF2	OK	2.62E+00	4.15E+00	0.663185	0.52775	0.994836	no
TCONS_00069645	FGF3	NOTEST	0	0	0	1	1	no

TCONS_00069642	FGF4	NOTEST	0	0	0	1	1	no
TCONS_00069643	FGF4	NOTEST	0	0	0	1	1	no
TCONS_00069644	FGF4	NOTEST	0	0	0	1	1	no
TCONS_00220216	FGF5	OK	3.36E-01	1.24E-01	-1.44456	0.5085	0.994836	no
TCONS_00220222	FGF5	OK	3.10E+00	1.50E+00	-1.04537	0.58735	0.994836	no
TCONS_00220221	FGF5	NOTEST	0	0	0	1	1	no
TCONS_00220215	FGF5	OK	5.23E+01	6.02E+01	0.201964	0.41665	0.994836	no
TCONS_00220220	FGF5	OK	2.18E+01	2.64E+01	0.277643	0.8922	0.994836	no
TCONS_00220219	FGF5	OK	1.37E+01	1.77E+01	0.373162	0.38565	0.994836	no
TCONS_00220213	FGF5	OK	1.30E+00	1.96E+00	0.588947	0.5131	0.994836	no
TCONS_00080899	FGF6	NOTEST	0	0	0	1	1	no
TCONS_00080900	FGF6	NOTEST	0	0	0	1	1	no
TCONS_00080901	FGF6	NOTEST	0	0	0	1	1	no
TCONS_00080902	FGF6	NOTEST	0	0	0	1	1	no

TCONS_00105038	FGF7	OK	3.53E+00	4.84E-02	-6.18814	0.1412	0.994836	no
TCONS_00105036	FGF7	OK	1.46E+00	5.26E-02	-4.80086	0.0737	0.994836	no
TCONS_00105040	FGF7	NOTEST	0	0	0	1	1	no
TCONS_00105037	FGF7	NOTEST	1.52E-02	0	N/A	1	1	no
TCONS_00105039	FGF7	OK	4.58E-01	0	N/A	0.17955	0.994836	no
TCONS_00105041	FGF7	NOTEST	2.05E-02	0	N/A	1	1	no
TCONS_00105035	FGF7	NOTEST	2.73E-01	0	N/A	1	1	no
TCONS_00055206	**FGF8**	**NOTEST**	**0**	**0**	**0**	**1**	**1**	**no**
TCONS_00055207	**FGF8**	**NOTEST**	**0**	**0**	**0**	**1**	**1**	**no**
TCONS_00055209	**FGF8**	**NOTEST**	**0**	**0**	**0**	**1**	**1**	**no**
TCONS_00055210	**FGF8**	**NOTEST**	**0**	**0**	**0**	**1**	**1**	**no**
TCONS_00055211	**FGF8**	**NOTEST**	**0**	**0**	**0**	**1**	**1**	**no**
TCONS_00055212	**FGF8**	**NOTEST**	**0**	**0**	**0**	**1**	**1**	**no**
TCONS_00055208	**FGF8**	**NOTEST**	**0**	**1.73E-02**	**N/A**	**1**	**1**	**no**

TCONS_00088886	**FGF9**	**NOTEST**	**0**	**0**	**0**	**1**	**1**	**no**
TCONS_00088887	**FGF9**	**NOTEST**	**0**	**0**	**0**	**1**	**1**	**no**
TCONS_00088888	**FGF9**	**NOTEST**	**0**	**0**	**0**	**1**	**1**	**no**
TCONS_00088889	**FGF9**	**NOTEST**	**0**	**0**	**0**	**1**	**1**	**no**
TCONS_00235840	FGF10	NOTEST	0	0	0	1	1	no
TCONS_00235838	FGF10	NOTEST	8.00E-03	0	N/A	1	1	no
TCONS_00235839	FGF10	NOTEST	3.03E-07	0	N/A	1	1	no
TCONS_00127453	FGF11	NOTEST	8.78E-02	1.55E-02	-2.50132	1	1	no
TCONS_00127452	FGF11	NOTEST	0	0	0	1	1	no
TCONS_00127451	FGF11	NOTEST	8.36E-03	1.02E-02	0.284508	1	1	no
TCONS_00127443	FGF11	NOTEST	2.99E-02	0	N/A	1	1	no
TCONS_00127445	FGF11	NOTEST	1.95E-02	0	N/A	1	1	no
TCONS_00216856	FGF12	NOTEST	0	0	0	1	1	no
TCONS_00216859	FGF12	NOTEST	0	0	0	1	1	no

TCONS_00216862	FGF12	NOTEST	0	0	0	1	1	no
TCONS_00216865	FGF12	NOTEST	0	0	0	1	1	no
TCONS_00216866	FGF12	NOTEST	0	0	0	1	1	no
TCONS_00216858	FGF12	OK	5.41E-02	3.79E-01	2.80834	0.32385	0.994836	no
TCONS_00216854	FGF12	NOTEST	3.50E-03	4. 77E-02	3.76859	1	1	no
TCONS_00216855	FGF12	NOTEST	7.41E-07	1.72E-01	17.8241	1	1	no
TCONS_00216860	FGF12	NOTEST	0	3.02E-04	N/A	1	1	no
TCONS_00216861	FGF12	NOTEST	0	1.24E-01	N/A	1	1	no
TCONS_00292398	FGF13	NOTEST	3.51E-02	2.31E-02	-0.606057	1	1	no
TCONS_00292400	FGF13	NOTEST	0	0	0	1	1	no
TCONS_00292401	FGF13	NOTEST	0	0	0	1	1	no
TCONS_00292404	FGF13	NOTEST	0	0	0	1	1	no
TCONS_00292394	FGF13	NOTEST	0	2.23E-07	N/A	1	1	no
TCONS_00292395	FGF13	NOTEST	0	4.58E-04	N/A	1	1	no

TCONS_00292396	FGF13	NOTEST	0	4.01E-04	N/A	1	1	no
TCONS_00292397	FGF13	NOTEST	0	2.36E-05	N/A	1	1	no
TCONS_00292402	FGF13	NOTEST	0	6.51E-02	N/A	1	1	no
TCONS_00092821	FGF14	NOTEST	0	0	0	1	1	no
TCONS_00092822	FGF14	NOTEST	0	0	0	1	1	no
TCONS_00092824	FGF14	NOTEST	0	0	0	1	1	no
TCONS_00092832	FGF14	NOTEST	0	0	0	1	1	no
TCONS_00287112	**FGF16**	**NOTEST**	**6.79E-03**	**0**	**N/A**	**1**	**1**	**no**
TCONS_00266194	**FGF17**	**NOTEST**	**0**	**7.90E-07**	**N/A**	**1**	**1**	**no**
TCONS_00266195	**FGF17**	**NOTEST**	**0**	**6.13E-07**	**N/A**	**1**	**1**	**no**
TCONS_00266196	**FGF17**	**NOTEST**	**0**	**0**	**0**	**1**	**1**	**no**
TCONS_00266197	**FGF17**	**NOTEST**	**0**	**6.54E-03**	**N/A**	**1**	**1**	**no**
TCONS_00266198	**FGF17**	**NOTEST**	**0**	**0**	**0**	**1**	**1**	**no**
TCONS_00233901	**FGF18**	**NOTEST**	**1.64E-02**	**9.91E-02**	**2.5932**	**1**	**1**	**no**

TCONS_00069640	FGF19	NOTEST	0	0	0	1	1	no
TCONS_00270917	**FGF20**	**NOTEST**	**1.88E-02**	**1.13E-02**	**-0.730279**	**1**	**1**	**no**
TCONS_00270918	**FGF20**	**NOTEST**	**2.60E-05**	**3.58E-02**	**10.4267**	**1**	**1**	**no**
TCONS_00270919	**FGF20**	**NOTEST**	**0**	**1.68E-01**	**N/A**	**1**	**1**	**no**
TCONS_00155188	FGF21	NOTEST	0	0	0	1	1	no
TCONS_00155189	FGF21	NOTEST	0	0	0	1	1	no
TCONS_00148688	FGF22	NOTEST	1.25E-01	3.21E-02	-1.95616	1	1	no
TCONS_00148689	FGF22	NOTEST	2.18E-01	9.47E-02	-1.20242	1	1	no
TCONS_00148690	FGF22	NOTEST	1.16E-01	1.98E-02	-2.54258	1	1	no
TCONS_00148691	FGF22	NOTEST	0	1.77E-02	N/A	1	1	no
TCONS_00148692	FGF22	NOTEST	0	9.60E-03	N/A	1	1	no
TCONS_00080898	FGF23	NOTEST	0	0	0	1	1	no

5.4.6.4 MAPK and PI3K pathways dysregulated in FGFR3-KO hTERT MSCs

FGFR3 signalling is known to operate through a number of downstream signalling pathways, with the removal of FGFR3 it can be hypothesised that these pathways may be affected in some manner. The four pathways analysed for these effects were the MAPK, Jak/Stat, PI3K and PLCγ pathways. KegArray was used to examine the effects of knocking out FGFR3 in these pathways, which attributes each transcript to the relevant Kyoto Encyclopedia of Genes and Genomes (KEGG) pathways they are involved in. The software can then be used to provide a signalling pathway map with each differentially regulated transcript highlighted as either upregulated, downregulated or not differentially regulated.

It appeared that the PLCγ pathway was unaffected with very few genes involved in the pathway being differentially regulated. Similarly, although there were transcripts noted as differentially regulated in the Jak/Stat pathways these were not found to be significant by pathway analysis ($p>0.05$). However, the PI3K pathway was found to be significantly upregulated in the FGFR3-KO hTERT MSCs ($p<0.05$) and the pathway is summarised in Figure 5.4.17. The PI3K/Akt pathway is heavily involved in MSC functionality with regulatory roles in MSC proliferation, differentiation and migration (Chen et al., 2013b).

Conversely, the MAPK signalling pathway was found to be enriched in the WT hTERT MSCs by GSEA analysis (Figure 5.4.18). As before, KegArray was used to summarise the MAPK signalling pathway to analyse which features were upregulated and downregulated, as MAPK signalling is known to be a downstream pathway to FGF receptors including FGFR3 (Figure 5.1.1). It is evident that the majority of signalling molecules differentially regulated in the MAPK signalling appear to be downregulated as a response to the removal of FGFR3 signalling.

It is apparent the major downstream signalling pathways from FGFR3 have been impacted in different ways by knocking out FGFR3. Two out of the four pathways appear to be unaffected whilst one is downregulated and another upregulated.

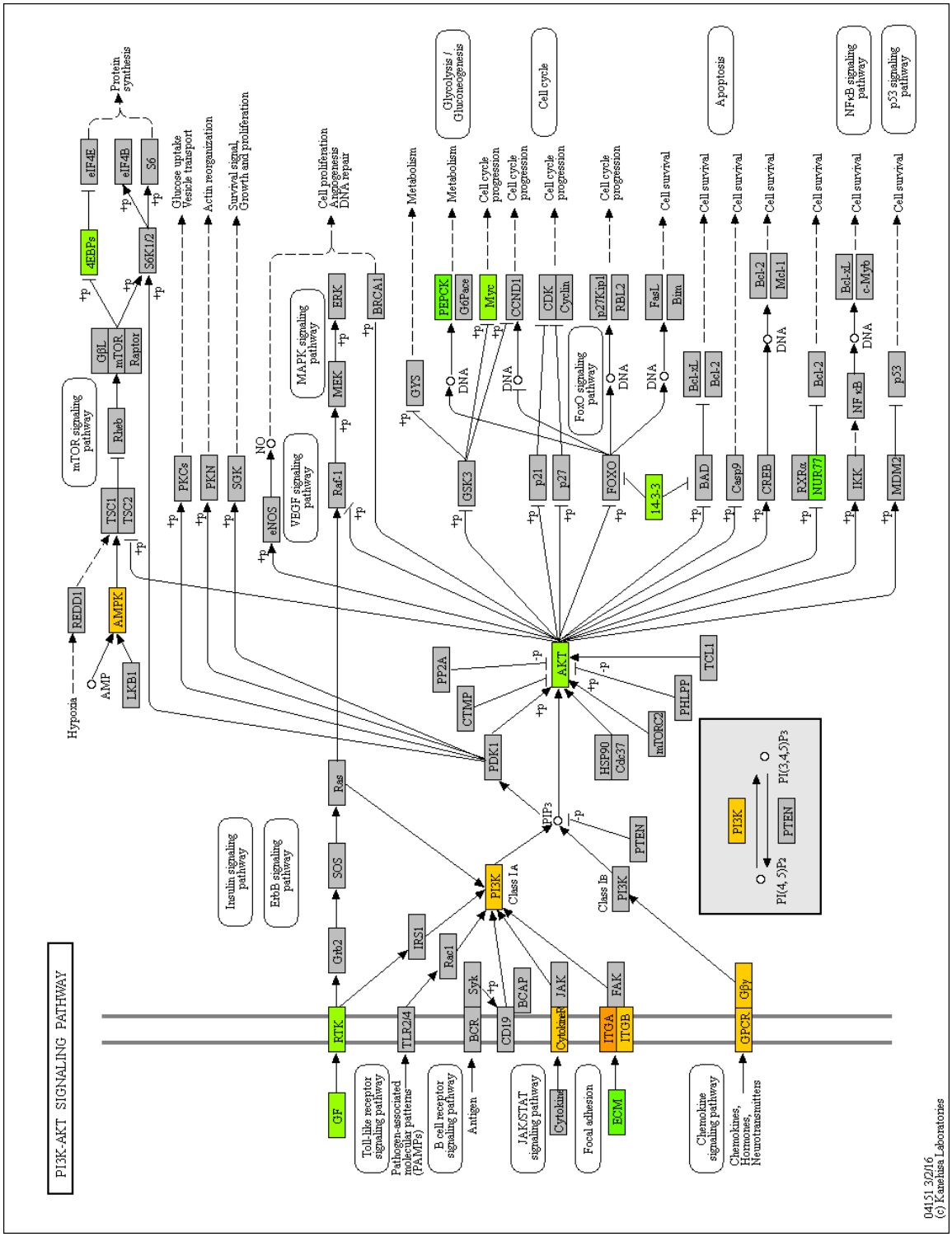

Figure 5.4.17: Overview of significantly differentially regulated transcripts in PI3K-Akt signalling pathway

Summary of PI3K-Akt pathway as found in KegArray with differentially regulated genes highlighted. Downregulate genes are highlighted in green and upregulated genes in orange. Grey indicates no significant changes highlighted by RNA-seq.

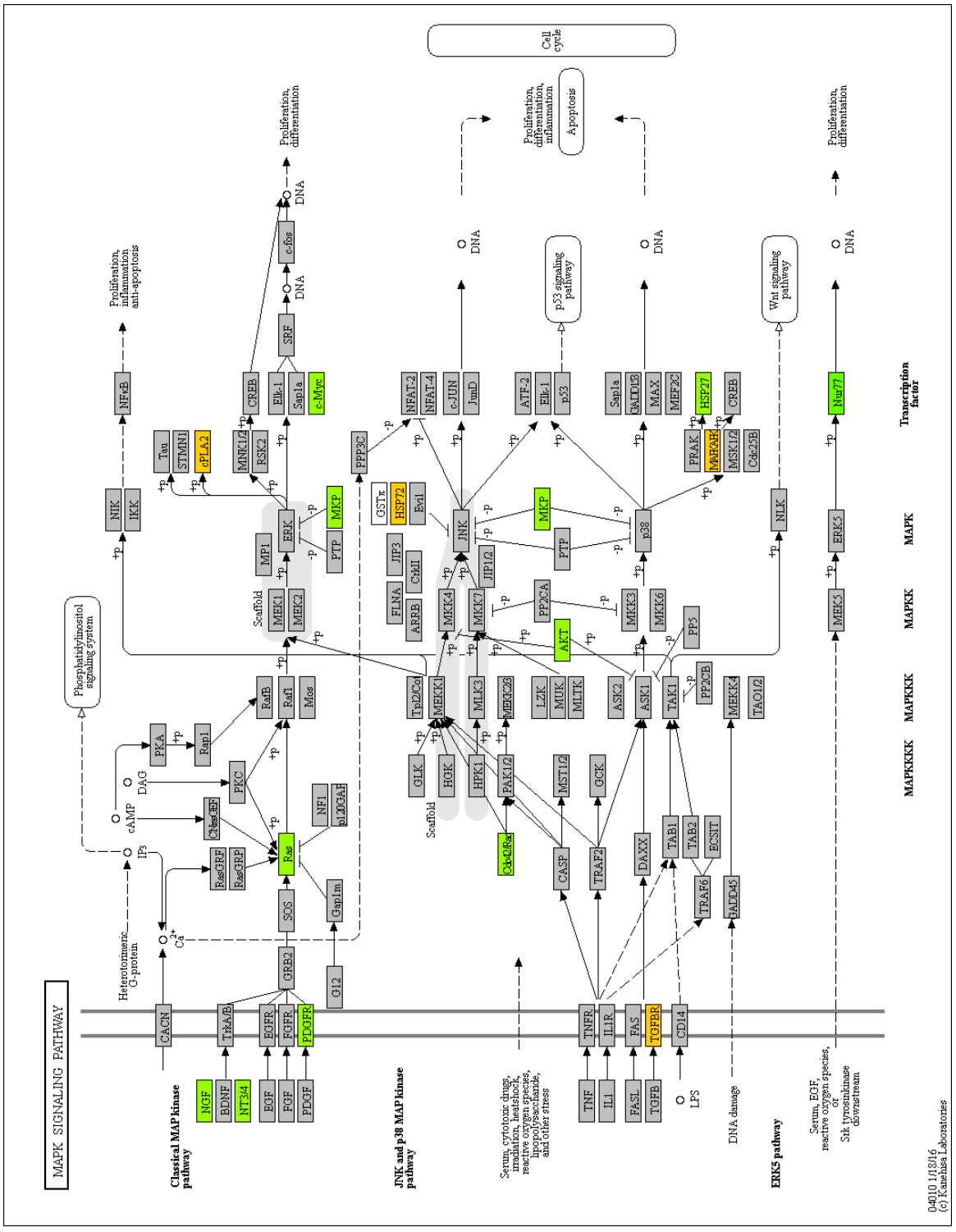

Figure 5.4.18: Overview of significantly differentially regulated transcripts in MAPK signalling pathway

Summary of MAPK pathway as found in KegArray with differentially regulated genes highlighted. Downregulate genes are highlighted in green and upregulated genes in orange. Grey indicates no significant changes highlighted by RNA-seq.

5.4.6.5 Snail1, a transcriptional effector, of FGFR3 is downregulated in FGFR3-KO hTERT MSCs

Figure 5.4.19 lists the 25 most highly upregulated and downregulated transcripts in the FGFR3-KO hTERT MSCs in comparison to the WT hTERT MSCs. One of the genes most downregulated according to this list is Snail1, a transcriptional effector of FGFR3 as previously highlighted. Studies have shown Snail1 to lie downstream of FGFR3 signalling in both chondrocytes and osteoblasts, making it likely that Snail1 also plays a key role in MSC biology. The knockout of FGFR3 would result in no signalling activity through this receptor, reducing the signalling through Snail1 which appears to have reduced the transcript levels in these cells. Typically, this would result in the upregulation of Slug (alternative name Snail2) however, unlike previous studies (Tang et al., 2016) Slug was also downregulated in the FGFR3-KO hTERT MSCs. Slug has previously been shown to have critical regulatory roles for a number of transcription factors involved in MSC differentiation, in addition to MSC migration (Torreggiani et al., 2012).

5.4.6.6 Hedgehog signalling also appears to be differentially regulated as a result of knocking out FGFR3

FGFR3 has previously been linked to Indian hedgehog (IHH) signalling in chondrocytes whereby the reduction of FGFR3 and subsequently FGFR3 signalling resulted in cartilaginous tumours and lesions in *in vivo* studies (Zhou et al., 2015). The FGFR3-KO hTERT MSCs have already presented with an increased proliferative capacity similar to the cells in this study so the IHH signalling pathways were examined in the RNA-seq data to determine if common signalling features were shared by chondrocytes and the hTERT MSCs. IHH was not differentially regulated in the FGFR3-KO hTERT MSCs, however the hedgehog-interacting protein (HHIP) was found to be significantly downregulated. HHIP has previously been shown to repress signalling activity of the hedgehog proteins including IHH, therefore the downregulation of HHIP in the FGFR3-KO hTERT MSCs would suggest an increase in IHH signalling (Chuang and McMahon, 1999). This is further evidenced by the upregulation of parathyroid hormone-like hormone (PTHrP), which has been shown to be upregulated by IHH in chondrocytes (St-Jacques et al., 1999). It would also appear a similar feedback loop is apparent in the hTERT MSCs and the knocking out of FGFR3 has impacted on these pathways earlier in skeletal development than previously thought.

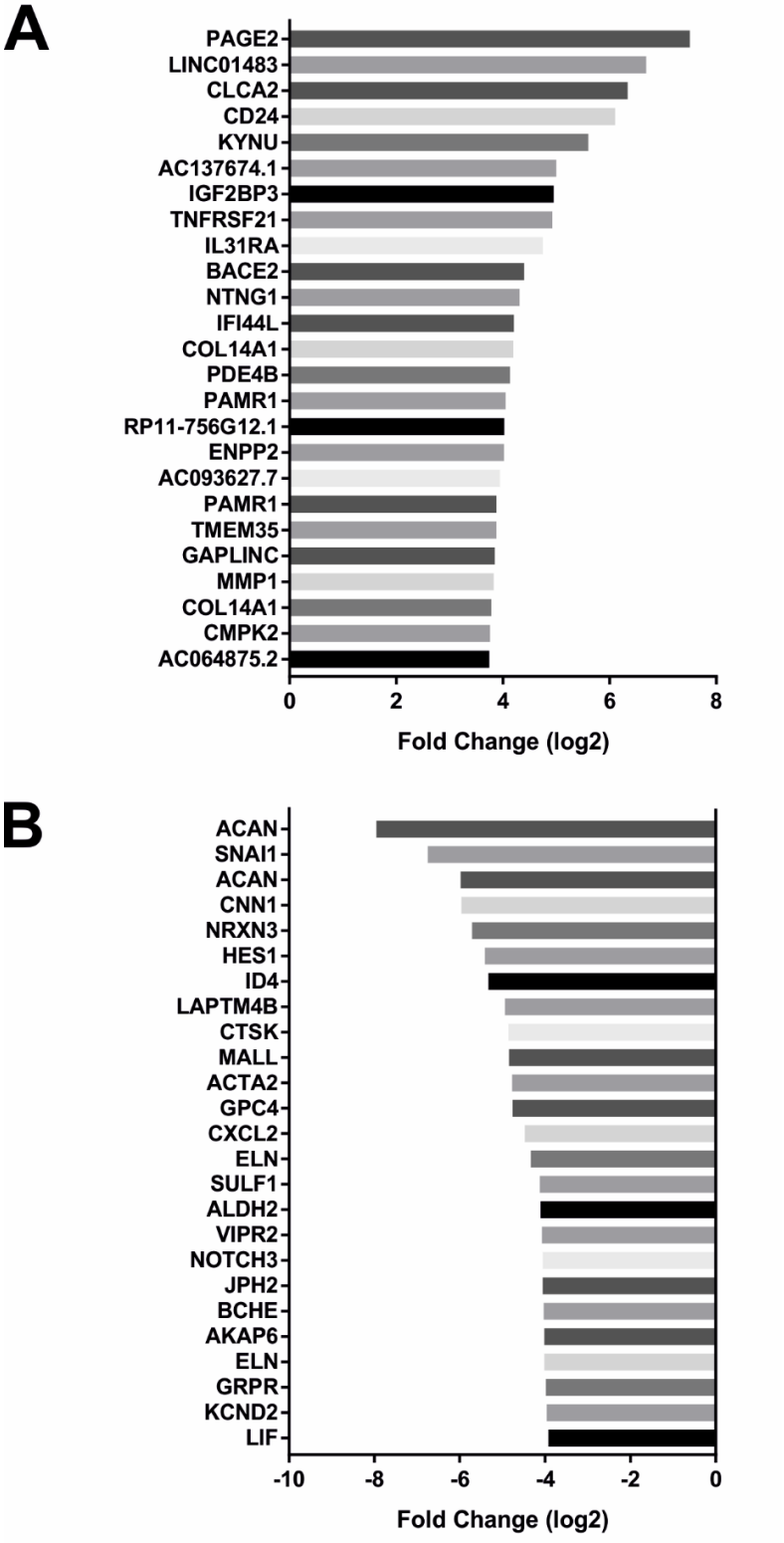

Figure 5.4.19: Significantly upregulated or downregulated transcripts in FGFR3-KO hTERT MSCs compared to WT hTERT MSCs identified by RNA-seq

Top 25 transcripts identified as significantly upregulated (A) or downregulated (B) in the FGFR3-KO hTERT MSCs compared to the WT hTERT MSCs as identified by RNA-seq.

5.4.6.7 Cell adhesion and extracellular matrix interactions downregulated consistently by pathway analysis

Using Enrichr, the differentially regulated transcripts were grouped according to the pathways and functions they were involved in, and these were then analysed to examine the potential effect of removing FGFR3 signalling on the functions of the cells. Figure 5.4.20 shows the top ten statistically significantly downregulated molecular function summarised according to their combined score, as determined by Enrichr. Predominantly these functions were involved in the binding of receptors to a number of targets including growth factors and components of the extracellular matrix, many of which were interlinked and showed similarity to one another.

This trend was continued when downregulated transcripts were grouped and analysed based on the cellular components they were involved in (Figure 5.4.21). The predominant locations where downregulated transcripts were located were the ECM and areas involving adhesion, including the anchoring junction, focal adhesion, cell-substrate adherens junction and the cell-substrate junction. This would suggest the cell-cell interactions and cell-ECM interactions are lessened in the FGFR3-KO hTERT MSCs and that the anchorage between cells has been reduced by the removal of FGFR3.

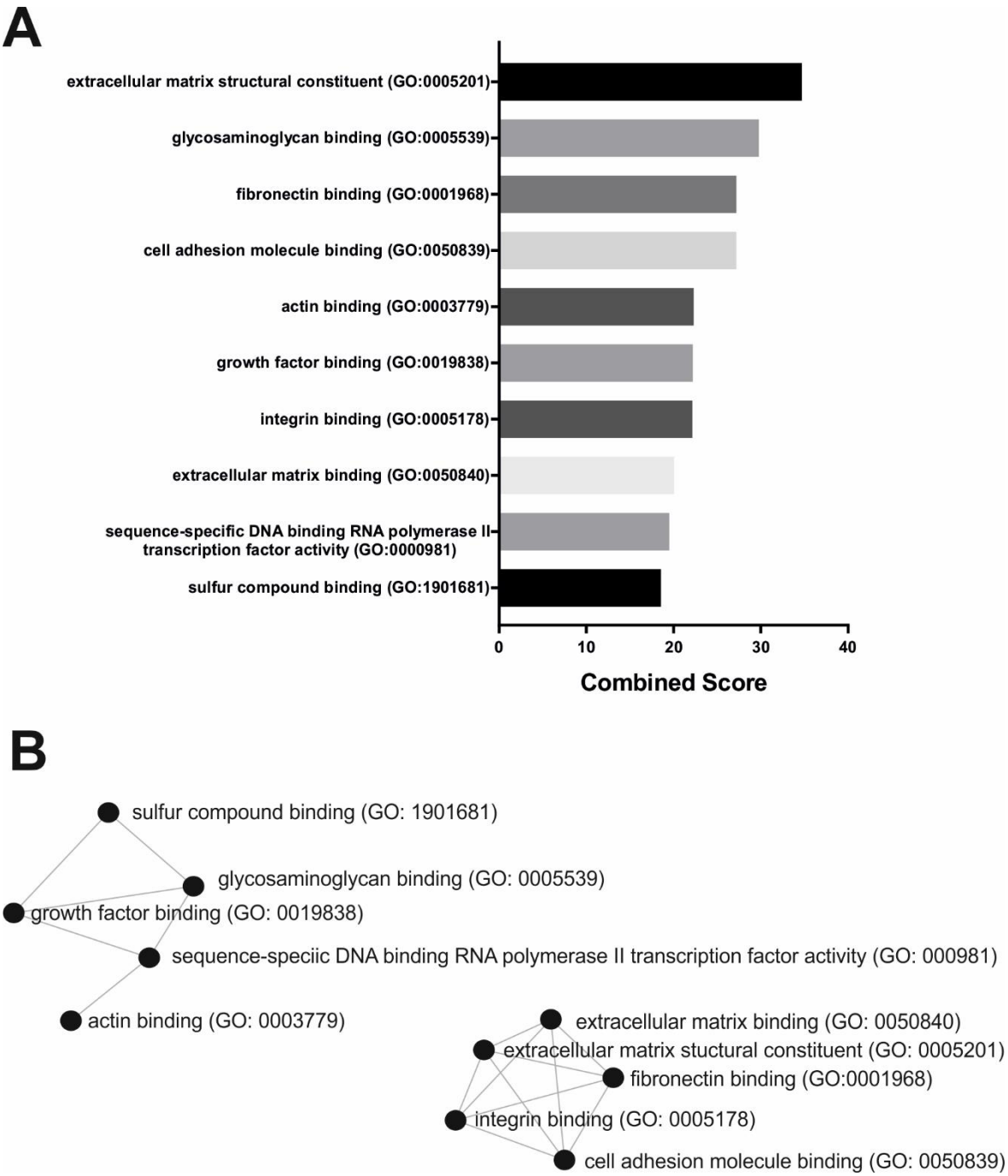

Figure 5.4.20: Top 10 downregulated molecular functions in FGFR3-KO hTERT MSCs

Enrichr analysis showed downregulated molecular functions were typically involved in receptors binding to specific targets. (A) Top 10 downregulated molecular functions and (B) networks showing the links between the processes identified. These were identified using combined score as defined by Enrichr.

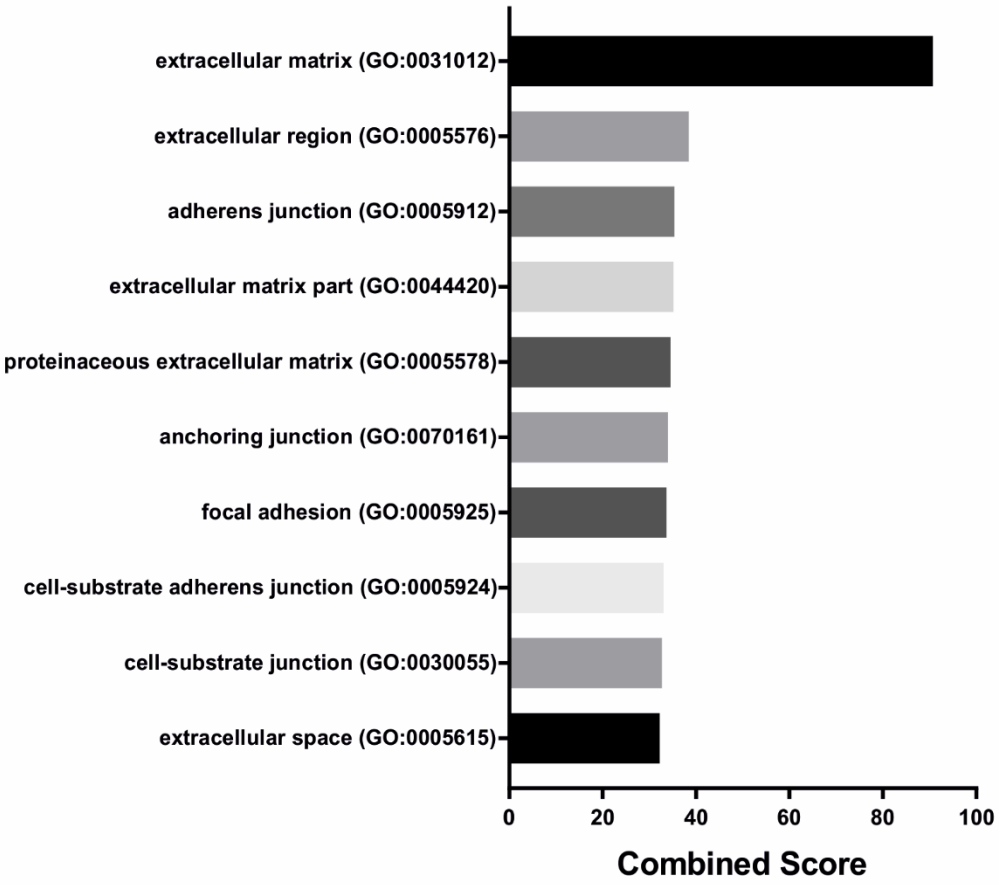

Figure 5.4.21: Top 10 cellular components where downregulated transcripts are found in FGFR3-KO hTERT MSCs

Summary of the cellular components where significantly downregulated transcripts are most likely to be found according to Enrichr analysis. Most are linked to the ECM and cell-cell adhesion.

Pathway analysis using Enrichr, KeggArray and GSEA was then conducted to provide analysis into the KEGG pathways altered in the FGFR3-KO hTERT MSCs. The top ten downregulated KEGG pathways according to Enrichr are summarised in Figure 5.4.22. Both AGE-RAGE signalling and tumour necrosis factor (TNF) signalling were found to be upregulated and again this analysis highlights the downregulation of focal adhesion and also the downregulation of cell adhesion molecules, to examine which features of focal adhesion were upregulated and downregulated. Figure 5.4.23 shows an overview of focal adhesion signalling and highlights the upregulated and downregulated transcripts. As noted previously, the ECM transcripts were notably downregulated, and yet the integrin receptors responsible for interactions between the cytoskeleton and the ECM were found to be upregulated. Specifically, integrin alpha 2, 5, 6 and 11 in addition to integrin beta 8 were found to be upregulated in the FGFR3-KO hTERT MSCs. A number of intermediary signalling molecules were also found to be downregulated in the focal adhesion pathways, including myosin and myosin light chains that interact with the actin cytoskeleton. Anaysis using GSEA for KEGG pathways to identify pathways enriched in either cell type also deemed focal adhesion as being enriched in the WT hTERT MSCs (Figure 5.4.24A).

5.4.6.8 Pathway analysis indicates regulation of actin cytoskeleton altered in FGFR3-KO hTERT MSCs

Pathway analysis also revealed that transcripts relating to the regulation of the actin cytoskeleton was also enriched in the FGFR3-KO hTERT MSCs (Figure 5.4.24B). Focal adhesion and interactions with the ECM have already been noted as downregulated in the FGFR3-KO hTERT MSCs, and the actin cytoskeleton plays critical roles in both of these functions. KEGGarray was used to summarise the pathways involved in the regulation of the actin cytoskeleton where it was found that a number of the receptors involved were upregulated (Figure 5.4.25). Yet, it appeared the majority of differentially regulated mediatory signalling molecules were downregulated. It was also found that α-actinin 1 was downregulated in the FGFR3-KO hTERT MSCs compared to the WT hTERT MSCs. This isoform is predominantly involved in adherens-type junctions in non-muscle cells, connecting the actin to the membrane. It would appear therefore that the actin cytoskeleton of the FGFR3-KO hTERT MSCs may be dysregulated and act differently compared to the WT hTERT MSCs.

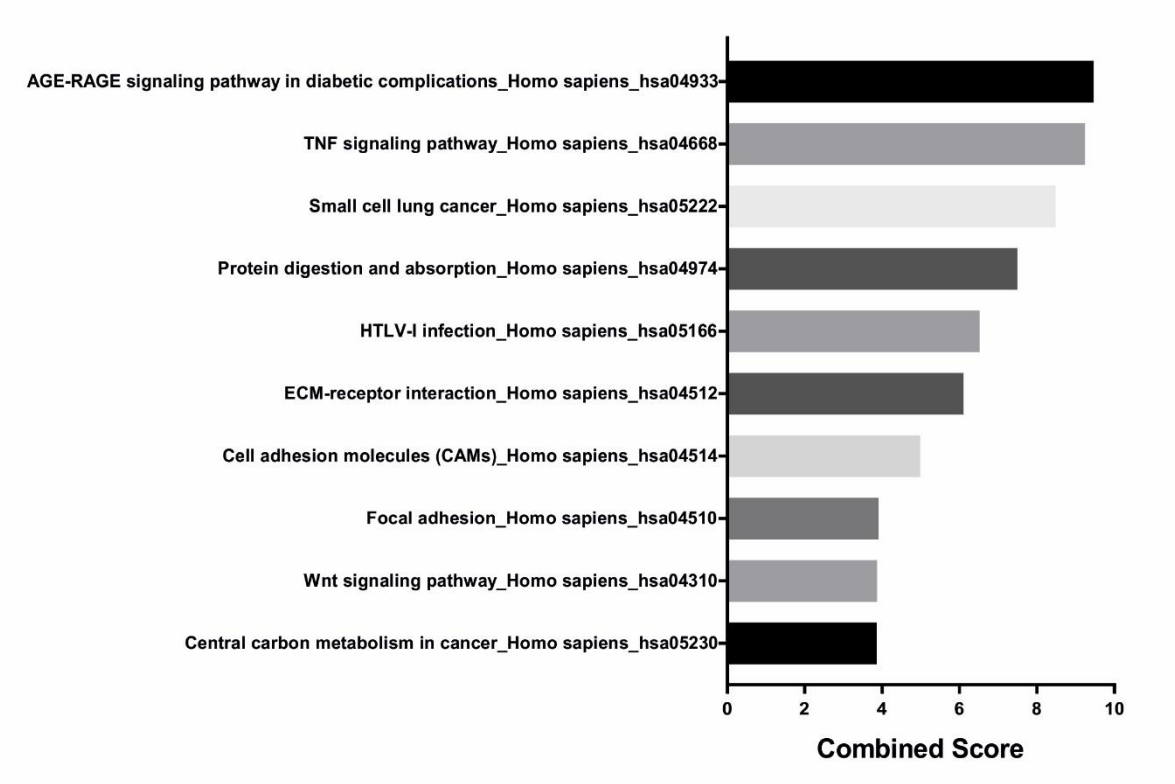

Figure 5.4.22: Top 10 KEGG pathways downregulated in FGFR3-KO hTERT MSCs

Summary of the most downregulated KEGG pathways as found by Enrichr analysis, which include a number of pathways involving cell adhesion and the ECM.

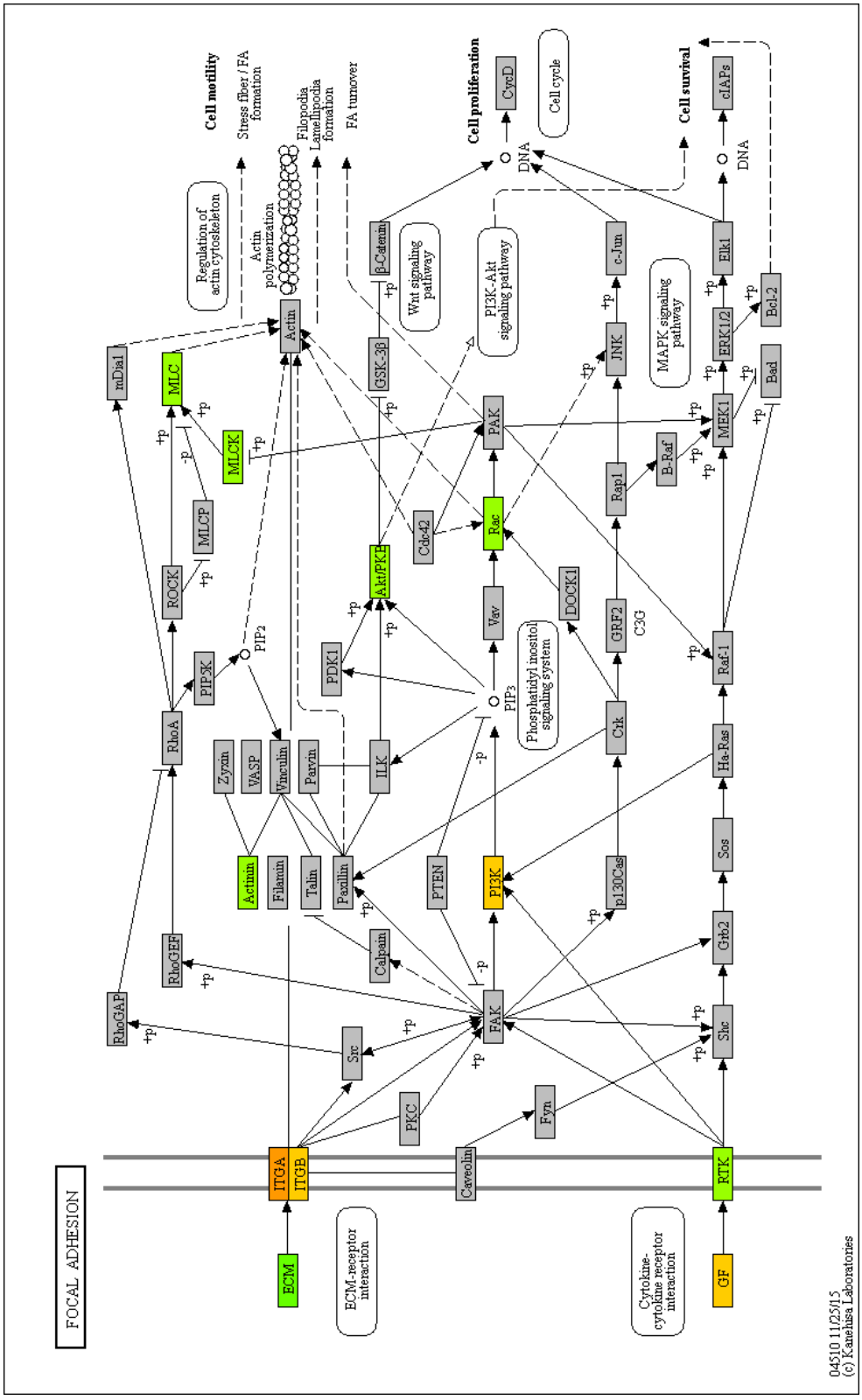

Figure 5.4.23: Overview of significantly differentially regulated transcripts in focal adhesion linked pathways

Summary of focal adhesion linked pathways as found in KegArray with differentially regulated genes highlighted. Downregulate genes are highlighted in green and upregulated genes in orange. Grey indicates no significant changes highlighted by RNA-

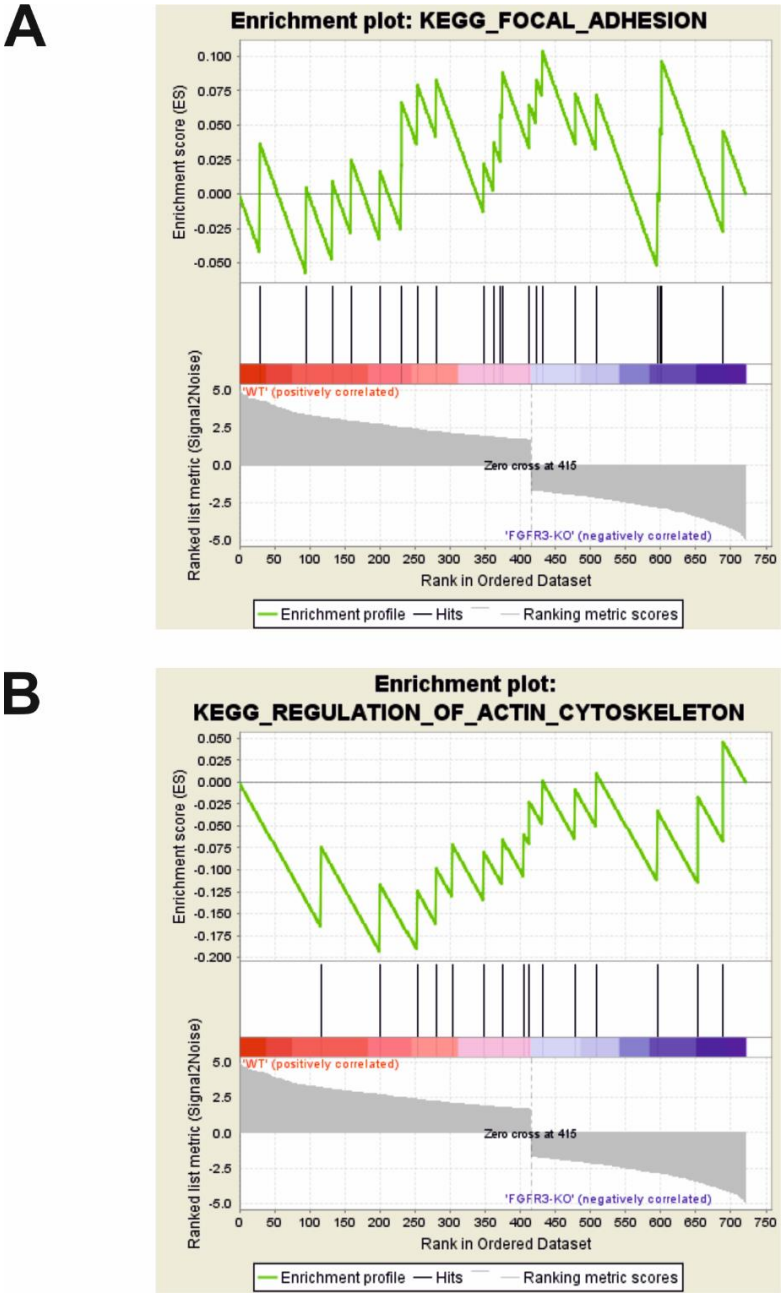

Figure 5.4.24: GSEA enrichment plots of focal adhesion and the regulation of the actin cytoskeleton

GSEA analysis of enrichment of differentially regulated transcripts in the focal adhesion (A) and actin cytoskeleton regulatory (B) KEGG pathways in both WT and FGFR3-KO hTERT MSCs. The top portion of the plot shows the running enrichment score of the transcripts analysed, an overall positive score (A) indicates enrichment in the WT hTERT MSCs and an overall negative score (B) indicates enrichment in the FGFR3-KO hTERT MSCs. The middle portion of the plot indicates where the transcripts identified feature in the overall enrichment ranking of all transcripts. The bottom portion of the plot is not applicable due to the data being provided as a mean of three values.

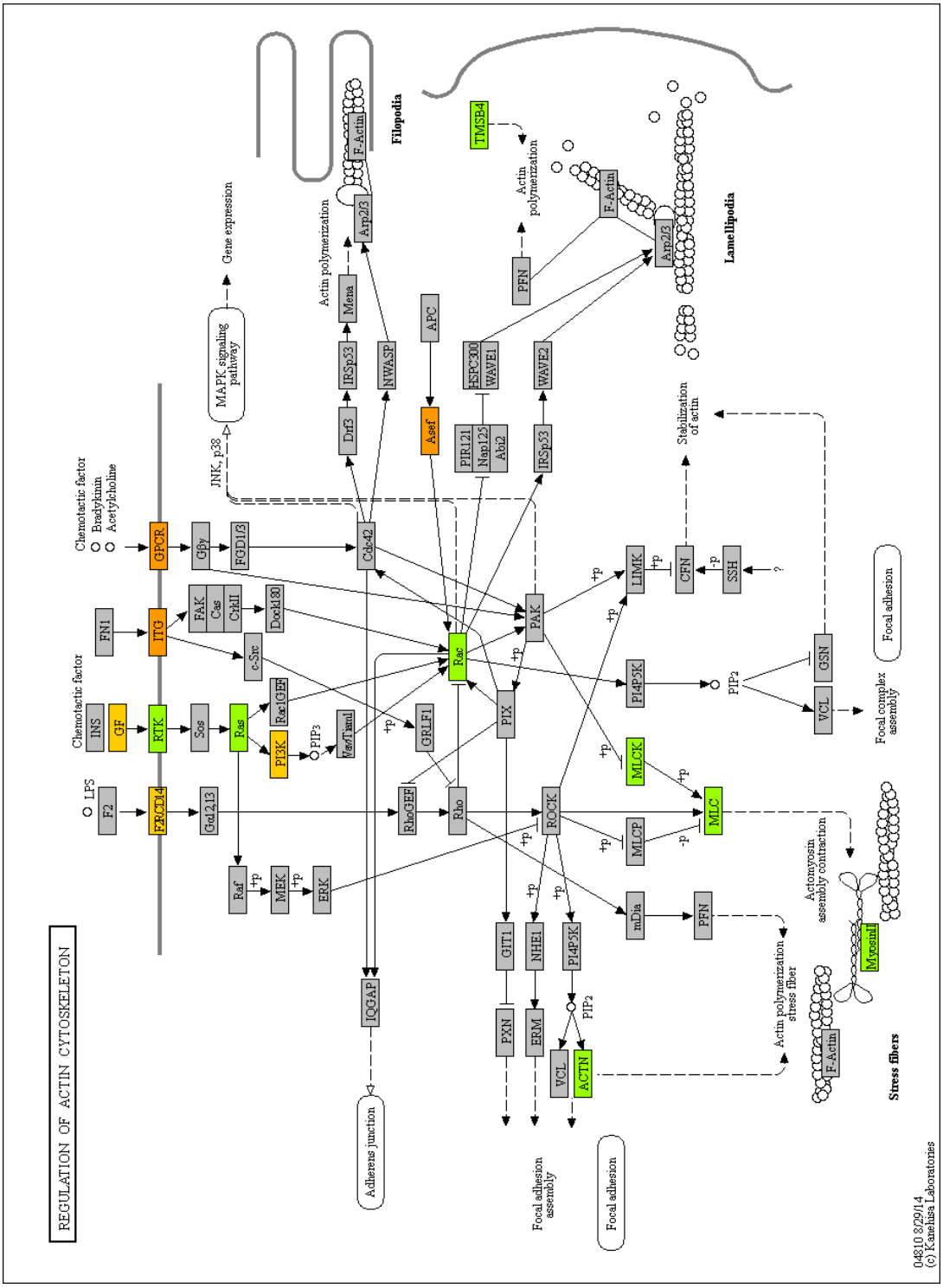

Figure 5.4.25: Overview of significantly differentially regulated transcripts in fthe regulation of the actin cytoskeleton

Summary of actin cytoskeleton regulatory pathways as found in KegArray with differentially regulated genes highlighted. Downregulate genes are highlighted in green and upregulated genes in orange. Grey indicates no significant changes highlighted by RNA-seq.

5.4.6.9 Genes relating to cancer and carcinogenesis upregulated in FGFR3-KO hTERT MSCs

Additionally, a number of genes highly differentially expressed between the WT and FGFR3-KO hTERT MSCs have been associated with various cancers and cancer like behaviours in cells, such as increased proliferation and migration. These characteristics were earlier identified as key phenotypic traits of the FGFR3-KO hTERT MSCs. Overexpressed genes included CD24 (Figure 5.4.19), which has previously been identified as a marker for cancer stem cells in a number of tissues, with raised expression attributed to cells having an increased proliferative capacity and increased invasion and migration (Lee et al., 2008; Yeung et al., 2010; Yang et al., 2014). Additionally, non-coding RNAs such as miR221 were also found to be overexpressed in the FGFR3-KO hTERT MSCs. Micro RNAs are small non-coding RNAs that negatively impact protein expression and miR221 is able to target and negatively regulate genes involved in cell cycle progression and proliferation (Garofalo et al., 2012; Zhu et al., 2015). Cells from osteosarcoma tissues or derived cell lines show upregulation of miR221, which impacts on both proliferation and migration, and the increase of miR221 expression in the FGFR3-KO hTERT MSCs was at a comparable level to literature quoted overexpression in the osteosarcoma samples (Zhu et al., 2015). Finally, c-Myc was upregulated in the FGFR3-KO hTERT MSCs. C-Myc is required for the induction of pluripotent stem cells and is a proto-oncogene that when deregulated has a key role in carcinogenesis (Takahashi et al., 2007; Araki et al., 2011; Dang, 2012). It has previously been linked to proliferation control in MSCs and when overexpressed in combination with retinoblastoma protein in MSCs, results in osteosarcomas in nude mice (Sato et al., 2016; Wang et al., 2016). Whilst the FGFR3-KO hTERT MSCs have not been tested for their transformation ability it appears they may share both phenotypic behaviours in addition to some alterations in gene expression to cancer cells.

This is also reflected in the upregulated pathways in the FGFR3-KO hTERT MSCs whereby pathway analysis of KEGG pathways indicated a number were all involved with cancer.

Additionally, it was noted a number of matrix metalloproteinases (MMPs) were differentially regulated in the FGFR3-KO hTERT MSCs (Table 5.4.4). These proteins are responsible for the degradation of the extracellular matrix and are often highly upregulated in cancers as these then aid the invasion and migration of metastatic cells. MMP1, MMP2 and MMP11 were all found to be upregulated in the FGFR3-KO hTERT MSCs, however MMP15 was found to be downregulated. MMP15 has been reported to be a direct target of Snail1, it is likely therefore that the reduction of Snail1 transcript has also resulted in a reduction of the MMP15 transcript (Tao et al., 2011).

Table 5.4.4: List of matrix metalloproteinases significantly differentially regulated in FGFR3-KO hTERT MSCs

Transcript ID	Gene Name	Status	Y201 WT FPKM	FGFR3-KO FPKM	Log2 Fold Change	P Value	Q Value	Significant?
TCONS_00071136	MMP1	OK	9.6807	137.386	3.82698	9.95274	5.00E-05	0.003863
TCONS_00195651	MMP11	OK	4.01558	10.7522	1.42095	3.07529	5.00E-05	0.003863
TCONS_00117404	MMP2	OK	209.665	424.583	1.01796	2.65787	5.00E-05	0.003863
TCONS_00117917	MMP15	OK	2.54381	0.879735	-1.53185	-3.18428	5.00E-05	0.003863

5.4.7 Alterations in actin cytoskeleton morphologies as a result of FGFR3-KO

RNA-Seq data demonstrated that one of the KEGG pathways altered in these cells was the regulation of the actin cytoskeleton with a number of crucial proteins being dysregulated, additionally, the FGFR3-KO hTERT MSCs have consistently appeared to possess an altered cellular morphology throughout sustained culture. It was therefore decided to visualise the actin cytoskeleton to determine whether any alterations were visible.

Alexa Fluor® tagged Phalloidin was used to selectively label filamentous actin and DAPI was used to counterstain DNA in cells cultured on glass cover slips for 24 hours, single cells were then imaged to analyse the cytoskeleton as seen in Figure 5.4.26A. Positive staining of a number of widely recognised cytoskeletal features were present in the WT hTERT MSCs. Stress fibres, likely to be ventral stress fibres, can be seen running the length of the cell and will be fixed at two focal adhesion points. Additionally, in the bottom panel the WT hTERT MSC appears to have protruding membrane ruffles at the lower edge of the cell with a retracting tail at the top of the panel. These features are typical of fibroblasts with the latter description indicating perhaps the cell was migrating when fixed.

The FGFR3-KO hTERT MSCs on the other hand appear to display some alterations to the conventional actin cytoskeletal morphologies present in the WT hTERT MSCs. The overall shape of the cell appears to more elongated and thinner than the WT hTERT MSC, and these features were quantified using ImageJ. An outline of the imaged cell was created and used to calculate the roundness and the aspect ratio of the cell and these used to compare the FGFR3-KO hTERT MSCs to their WT counterparts. The aspect ratio is a ratio created by dividing the length of the cell by its width, a large aspect ratio indicates the cell is elongated and much longer than it is wide. This initial study analysing a small number of cells demonstrated the FGFR3-KO hTERT MSCs were less rounded and had a higher aspect ratio than the WT hTERT MSCs (Figure 5.4.26), giving evidence to an altered cellular morphology. Furthermore, the stress fibre bundles in the FGFR3-KO hTERT MSCs appear perturbed with reduced staining visible in the cellular bodies. There also appeared to be protrusions of actin extending from the base of the cell making contact with the cover slip the cell was attached to. The positioning of these protrusions was confirmed by false colouring the images collated to form the z-stack, with the images appearing nearest the colour slip coloured white and yellow (Figure 5.4.26B). Additionally, both FGFR3-KO hTERT MSCs featured in this figure appear to possess the migratory morphology with membrane ruffles extending away from the cell. Overall, it appears the actin cytoskeleton in these cells has been altered as a result of the removal of FGFR3.

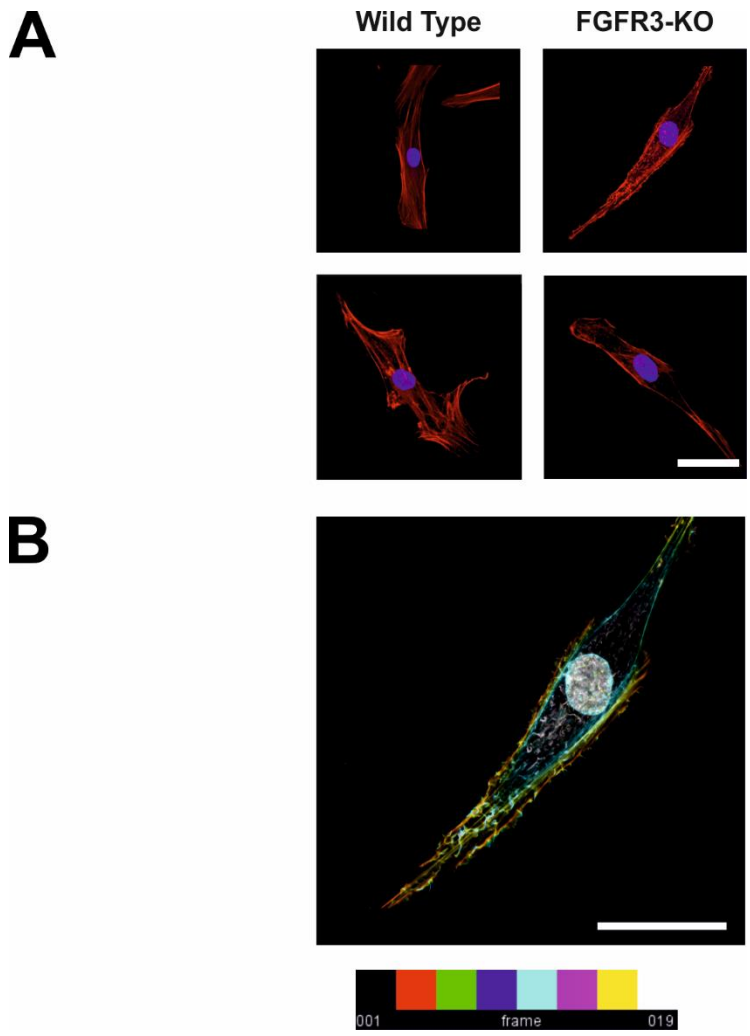

Figure 5.4.26: Staining of hTERT MSCs for the filamentous actin cytoskeleton

Y201 hTERT MSCs or FGFR3-KO hTERT MSCs were seeded onto glass cover slips, allowed to attach and fixed before the actin cytoskeleton was visualised using Alexa Fluor® 647 Phalloidin (red), DNA was counterstained with DAPI (blue) (A). Scale bar represents 50µm. Zeiss imaging software was then used to false colour the images of the z-stack as indicated by the key below the panel. Scale bar = 50µm.

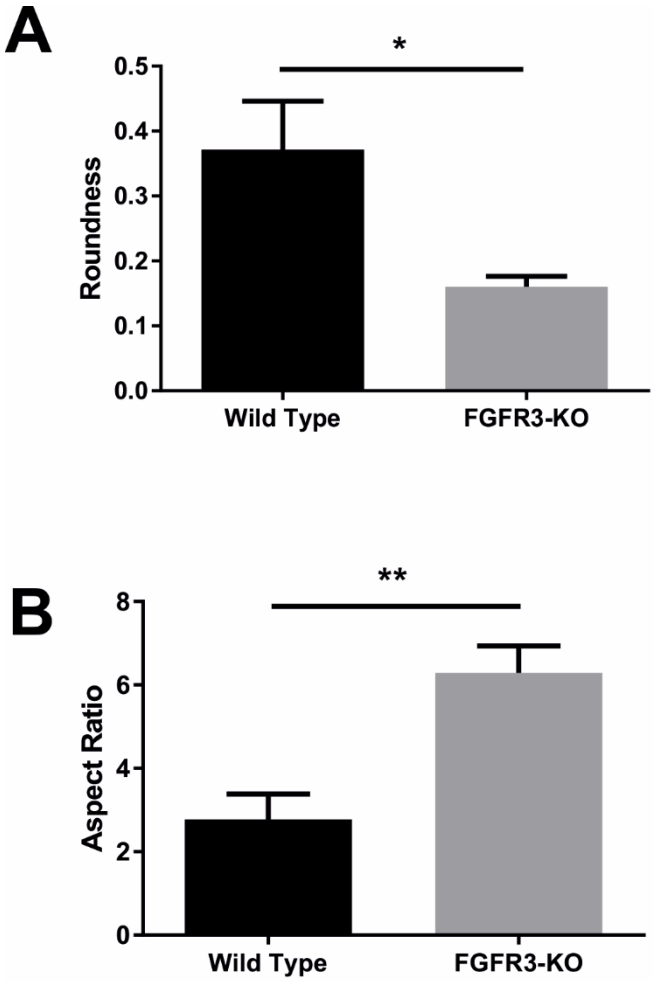

Figure 5.4.27: Morphological analysis of WT and FGFR3-KO hTERT MSCs

ImageJ was used to identify the outline of the cell and the morphology was then quantified according to roundness (A) and aspect ratio (B). Values = mean ± SD, n=3 significance obtained by unpaired t-test with Welch's correction.

5.4.8 FGFR3-KO hTERT MSCs demonstrate increased scratch wound healing capacity in *in vitro* assays possibly due to alterations in population migration

5.4.8.1 FGFR3-KO hTERT MSCs have an increased scratch wound healing capacity in in vitro scratch assays

The RNA-seq data consistently showed pathways involved in cellular adhesions and interactions with the ECM as being downregulated. The actin cytoskeleton was also dysregulated and is critical in the driving of cellular locomotion. Combined with the upregulation of several MMPs and carcinogenic genes, it was hypothesised this may impact on the locomotion and migration of the FGFR3-KO hTERT MSCs. It was therefore decided to explore this further using a scratch wound healing assay to determine whether the cells migratory capacities had indeed been altered by the removal of FGFR3. Initially, cells were seeded at confluency and a wound inflicted in the monolayer which was allowed to heal for 18 hours before the cells were fixed and stained with crystal violet stain. After the 18 hour incubation, the WT hTERT MSCs had migrated successfully into the wound and the area of plastic free from cells had reduced, however, the FGFR3-KO hTERT MSCs had successfully occupied the entirety of the wound in this time. The experiment was therefore repeated with a shorter timecourse of 12 hours to allow for the accurate quantification of the differences in healing capacities. Figure 5.4.28 shows this comparison where on average the WT hTERT MSCs healed 18% of the total wound and the FGFR3-KO hTERT MSCs healed 50% of the wound demonstrating a significant increase in the scratch wound healing capacity of these cells.

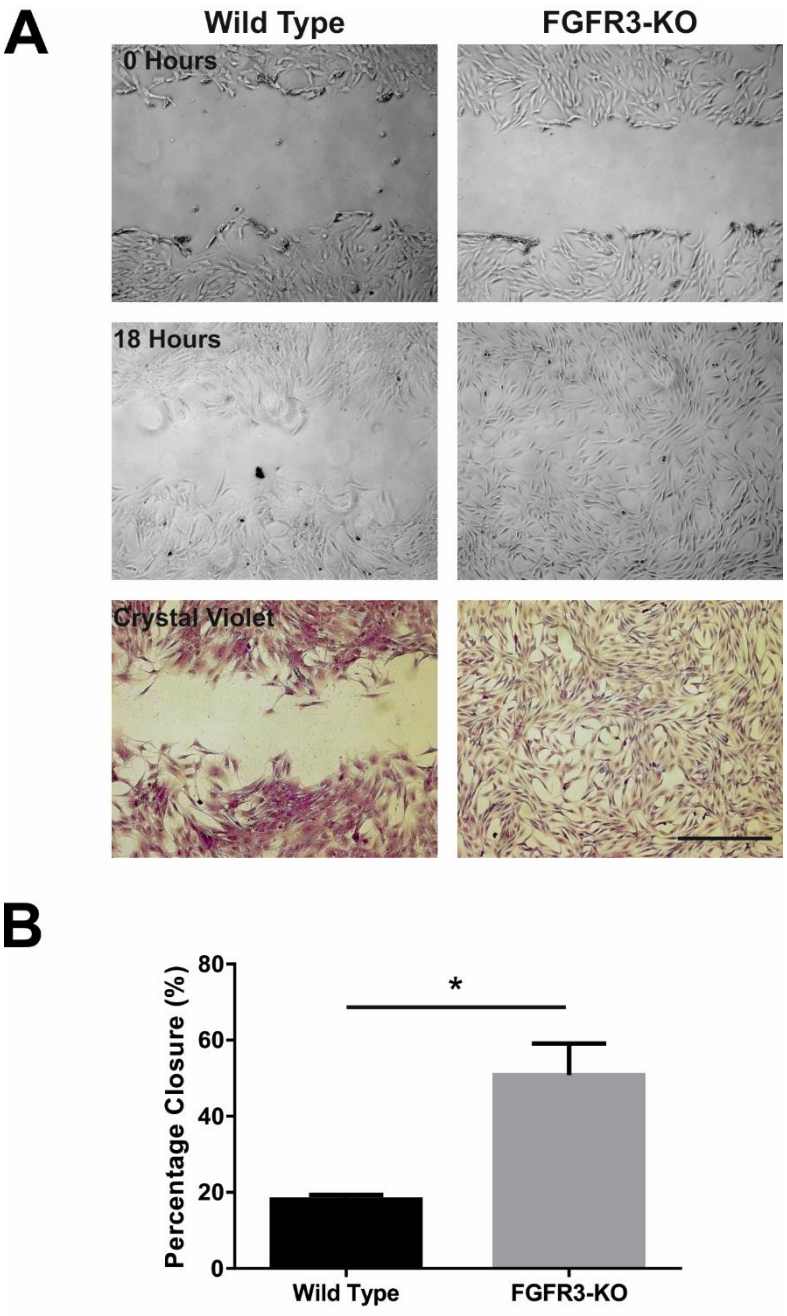

Figure 5.4.28: Analysis of wound healing capacity of WT and FGFR3-KO hTERT MSCs by scratch assay

A confluent monolayer of WT and FGFR3-KO hTERT MSCs were seeded and wounded with a "scratch" and incubated for 18 hours before cells were fixed and stained with crystal violet solution. Scale bar = 500µm (A). A repeat assay was performed for 12 hours and the percentage of the original wound healed was calculated using Corel Draw and ImageJ. Values = mean ± SD, n=3 significance obtained by unpaired t-test with Welch's correction.

Previously, it was described in section 5.4.4 that the FGFR3-KO hTERT MSCs have an increased proliferative capacity compared to the WT hTERT MSCs but this was not evident by MTT/EdU analyses until at least 72 hours had passed. It is therefore unlikely the increased proliferative capacity of these cells influence the wound healing assays but nevertheless it was decided to further determine if any alterations in migration were evident. Additionally, the creation of a wound in a monolayer triggers cues to encourage cell migration to close the newly created gap. Analysis of cells migrating into a gap not created by a scratch wound may give a greater indication as to the migration abilities of the cells.

5.4.8.2 Ptychographic analysis indicates FGFR3-KO hTERT MSCs possess increased migratory capacity due to changes in collective migration but not changes at a single cell level

To provide further information as to the migratory properties of the FGFR3-KO hTERT MSCs, ptychography was used to give a high quality contrast timelapse of individual cells moving into a previously created gap. This gap is not inflicted by a wound but instead is already present in a specially created dish so that migration is not dependent on cues given by a wounded monolayer. Cells were seeded and imaged every 5 minutes for the timecourse and the videos used to provide quantification of the closure of the gap over time and the individual migratory details of each cell. This is possible due to an advanced fuzzy algorithm which allows for the individual labelling of each cell in the video. Figure 5.4.29 shows the beginning and end timepoints of a representative example of a video, with each of the cells labelled by the algorithm. Again it is possible to see that the FGFR3-KO hTERT MSCs are able to close a gap between the cells at an increased rate compared to their WT counterparts.

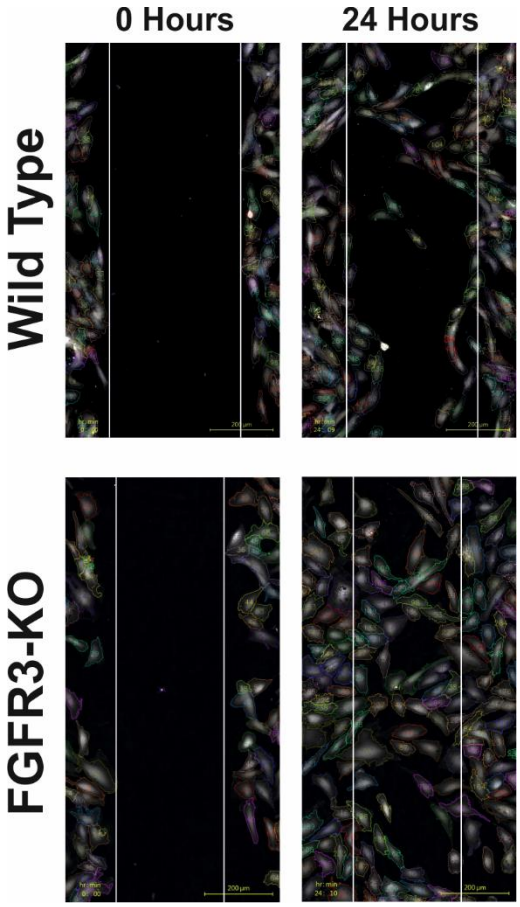

Figure 5.4.29: First and final frames of a hTERT MSC migration timelapse imaged using ptychography

WT and FGFR3-KO hTERT MSCs were plated into Ibidi Culture-Insert dishes and images taken every 5 minutes using pytchography over 24 hours. The first and final frames of one representative timelapse of each cell type are shown here with white lines marking the migratory edge. Each cell has been uniquely labelled during analysis and is also numbered. Scale bar = 200µm.

The timelapses were used to quantify some of the migratory characteristics of each cell type. Cells were chosen so that they were present from the first frame and that continued to migrate within the region of interest throughout the majority of the timelapse. Additionally cells were highlighted that were part of the migratory edge. This allowed for the calculation of the average speed, distance and the migratory index of each relevant cell and these are summarised in Figure 5.4.30. Despite each migratory assay demonstrating an increase in closure by the FGFR3-KO hTERT MSCs there appeared to be no significant differences between any of the migratory properties calculated on a single cell level. FGFR3-KO hTERT MSCs did not migrate faster, further or more directly than their WT counterparts.

However, when the videos were re-examined it appeared apparent that although there were no differences between the migration of the FGFR3-KO and WT hTERT MSCs on a single cell level there may be difference in the migration of the cells on a population level. Many cell types, typically migrate by collective migration that is to say a population of cells migrate through tissues without the disruption of the majority of cell-cell contacts. Cells undergo collective migration by coordinating their actin dynamics allowing cells to follow a migratory leader and so translocate as a whole (reviewed in Rørth, 2009). This typically results in a pattern of migration described as finger-like cell strands which have been highlighted in several frames from a WT hTERT MSC time lapse (Figure 5.4.31). Collective migration follow leader cells can be observed in Supplementary Video 1 of migrating WT hTERT MSCs, whereas the FGFR3-KO hTERT MSCs can be observed to independently migrate (Supplementary Video 2). An overview of all wells analysed in this timecourse is shown in Supplementary Video 3.

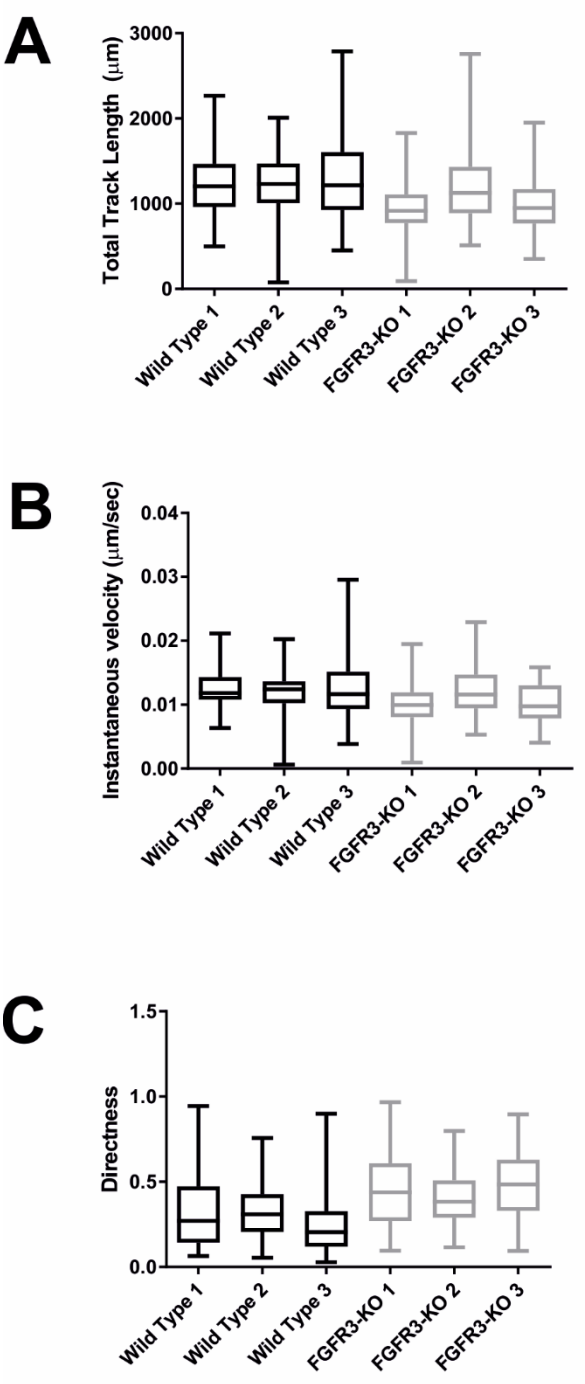

Figure 5.4.30: Quantification of single cell migratory metrics from ptychographic timelapses

Cells were selected from the migratory edge that were visible in frame 1 of the timelapse and migrated within the region of interest for the majority of the experiment. Single cell metrics was then generated from each frame and summarised in box and whisker plots for the distance migrated (A), the instantaneous velocity (B) and the directness of the migration (C). Values = mean of all cells fitting the previously defined parameters and no significance was generated.

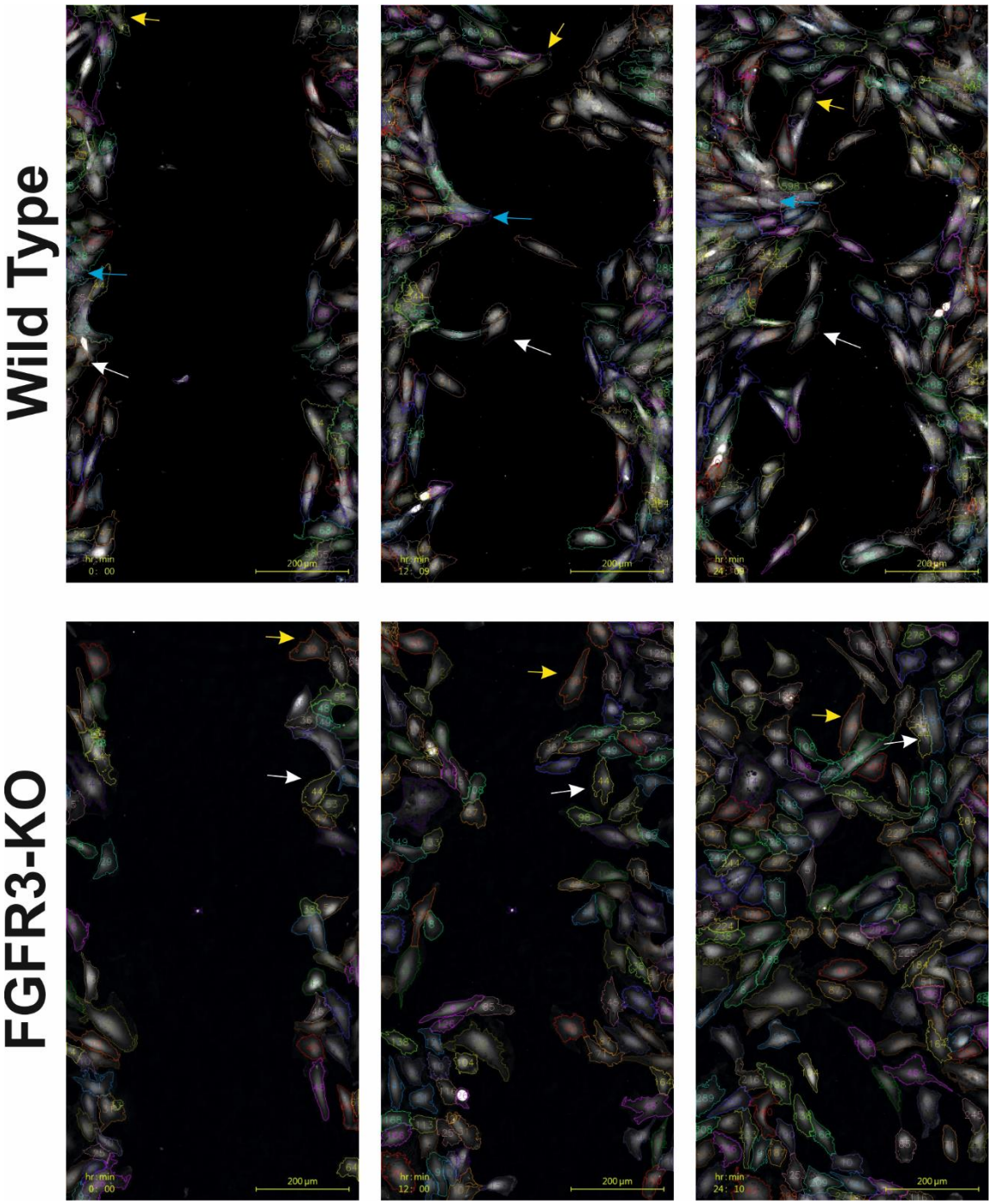

Figure 5.4.31: Evidence of collective migration in WT hTERT MSCs

Three still frame from a ptychography timelapse of WT hTERT MSCs migrating where collective migration can be observed compared to FGFR3-KO hTERT MSCS where independent migration is observed. Coloured arrows in the WT hTERT MSCs mark leader and follower cells tracked through the frames. Arrows in the FGFR3-KO hTERT MSCs show cells independently migration. Further evidence of these migrations patterns can be observed in the Supplementary Videos.

5.5 Discussion

FGFR3 has been shown to be a critical receptor in skeletal development with severe dysplasias occurring upon deregulation of its signalling activity. Activating mutations of FGFR3 cause shortening of the bones and hypertrophic cartilage plates whereas removal of FGFR3 induces vast overgrowth of bones. Much of the work into FGFR3 has been performed either *in vivo* or in chondrocytes, whereas the understanding of how FGFR3 impacts on the behaviour and signalling of MSCs is less well understood. In this chapter, an FGFR3-KO immortalised MSC line was generated using the CRISPR/Cas9 system, developed in Chapter 4, which created a one base insertion resulting in a nonsense mutation that truncates the protein in the extracellular region. This should result in no FGFR3 signalling activity in these cells, providing an avenue to examine the behaviour of MSCs when skeletal elements are formed by endochondral ossification.

5.5.1 Confirmation of FGFR3 knock out status as a result of CRISPR/Cas9 genome editing

One of the issues faced with the analysis of the FGFR3-KO hTERT MSCs was the ability to prove knockout status by non-detection of FGFR3 protein. Despite a clear sequencing trace giving evidence as to the knockout of FGFR3, there was some detectable protein by Western blot. Western blots rely on the specificity of a given antibody to a target, and the FGFR3 antibody in question here did not give a clean single band. Additionally, the antibody was raised against a target deemed commercially sensitive so it was impossible to confirm the antibody was specific to FGFR3 or any potential intracellular protein remaining after genome editing. RNA-seq, a sensitive transcript analysis technique, did not identify any FGFR3 transcripts within the FGFR3-KO hTERT MSCs, and small levels of FGFR3 transcript were detectable in the WT hTERT MSCs. This in combination with the sequencing results and the demonstrable reduction in FGFR3 protein led us to believe the FGFR3-KO hTERT MSCs were likely to have had FGFR3 removed.

To unequivocally demonstrate the phenotype demonstrated by the FGFR3-KO hTERT MSCs is due to CRISPR/Cas9 genome editing, the FGFR3 protein could be introduced back into the cells. By rescuing the phenotype through complementation analysis if the major phenotypic features, such as increased proliferation and reduced differentiation, reverted back to wild type levels it could be concluded FGFR3 was the sole contributor to this phenotype.

5.5.2 Mixed population of FGFR3 CRISPR/Cas9 hTERT MSCs display similar phenotype to FGFR3-KO hTERT MSCs

To provide further evidence that the phenotype presented by the FGFR3-KO hTERT MSCs was due to the removal of FGFR3, and not the introduction of CRISPR/Cas9 or an artefact of single cell colony

derivation, the mixed population isolated by FACS was analysed for some of the key phenotypic features identified (see Appendix). These cells are unlikely to all contain mutations in FGFR3, or if a mutation is present it is unlikely to be the same as identified in the FGFR3-KO hTERT MSCs, but if the CRISPR/Cas9 has a high efficacy then some of the phenotypic features may be observable albeit on a reduced level. The FGFR3-MP hTERT MSCs also demonstrated an increased proliferative capacity and increased wound healing capability, cells were also observable with some of the morphological changes already highlighted. It would therefore appear that this phenotype is likely due to the removal of FGFR3 rather than an artefact of the generation of the cell line.

5.5.3 Removal of FGFR3 results in an increased proliferative capacity

The work presented in this chapter outlines, for the first time, a striking phenotype of FGFR3-KO hTERT MSCs. These cells proliferated at an increased rate in comparison to their WT counterparts, and when plated at clonal density, produced colonies that covered a significantly larger surface area. Null mutations in FGFR3 have previously shown an expansion of the hypertrophic cartilage plate, in addition to elongated bones, which may be partially explained by the cells in these tissues proliferating faster than usual (Deng et al., 1996). It would appear from this study that the restrictive nature of FGFR3 signalling on proliferation rates is also apparent in the hTERT MSCs indicating an impact on skeletal development from its earliest stages.

5.5.4 FGFR3-KO hTERT MSCs demonstrate reduced capacity for differentiation

Additionally, the FGFR3-KO hTERT MSCs appeared to be severely hampered in their ability to differentiate. Histological staining for calcium deposition and lipid droplet formation demonstrated the FGFR3-KO hTERT MSCs had a noticeable reduction in their differentiation capacity. Furthermore, an enzymatic assay for ALP, an early marker of osteogenesis, demonstrated that during early differentiation the FGFR3-KO hTERT MSCs failed to upregulate this important component of bone formation. Early qPCR data suggests that chondrogenesis in the FGFR3-KO hTERT MSCs has been somewhat disrupted, however more repeats of this experiment would be needed to be confident in the dysregulation of chondrogenesis in hTERT MSCs by FGFR3. Previous studies have shown that FGFR3 activation has an impact on chondrocyte differentiation, both in agonistic and antagonistic roles, but the most widely accepted theory is that FGFR3 signalling negatively impacts on chondrocyte differentiation by promoting expansion and proliferation (Murakami et al., 2004; Zhang et al., 2006a). In this study, it would appear that the FGFR3-KO status has also impacted on the ability of the hTERT MSCs to undergo chondrogenesis as the markers analysed did not appear to increase an *in vitro* chondrogenic assay.

5.5.5 RNA-seq analysis determines removal of FGFR3 does not result in compensation in either FGFRs or FGFs

RNA-sequencing was used to determine any changes to the transcriptome caused by the removal of FGFR3 signalling in the FGFR3-KO hTERT MSCs. Similarly to *in vivo* data studying FGFR3-KO mice it would appear no compensation is occurring in the other FGFRs as a result of the removal of FGFR3 (Deng et al., 1996). It would also appear there is little difference in the levels of FGF ligands being expressed, albeit again with subtle differences particularly in the FGF8 and FGF9 subfamilies. Whether the removal of FGFR3 would then heighten activity of the other FGF receptors, namely FGFR1 and FGFR4 in the hTERT MSCs, has yet to be fully explored. This would especially be of keen importance in that the FGF receptors can combine to form heterodimer receptors, and whether the removal of FGFR3 entirely could impact on overstimulation of other signalling networks (Plotnikov et al., 1999; Piccolo et al., 2016).

5.5.6 Removal of FGFR3 signalling appears to impact FGFR3 signalling networks determined by RNA-seq analysis

Notable differences in previously explored FGFR3 signalling networks were detectable at the transcriptome level by RNA-seq, namely in the MAPK and PI3K/Akt pathways. The MAPK signalling pathway has long been known to be an effector of FGFR signalling, and as predicted the pathway was found to be disrupted in the FGFR3-KO hTERT MSCs. In addition, earlier it was shown the FGFR3-KO hTERT MSCs appeared to have a reduction in the sustained phospho-ERK levels, with pERK an effector of the MAPK pathway this reduction is likely a direct result of alterations in this pathway. Typically, the MAPK pathway signalling through ERK is involved in the proliferation rate of mammalian cells with ERK able to translocate to the nucleus and transactivate a number of transcription factors, ultimately impacting on gene expression and cell behaviour (reviewed in Zhang and Liu, 2002). It would be predicted that the non-sustained activation of pERK, in addition to an apparent overall downregulation of the MAPK pathway would result in a slowing of proliferation rate, however the FGFR3-KO hTERT MSCs present with an increased proliferation rate compared to WT hTERT MSCs. This is likely due to a number of other alterations in the transcriptome that counteract against the reduction in the MAPK signalling pathway.

Related to this, the PI3K/Akt pathway was found to be upregulated in the FGFR3-KO hTERT MSCs. This pathway has previously been linked to MSC survival, proliferation, migration and differentiation. Despite the pathway being upregulated in the FGFR3-KO hTERT MSCs, very few of the intermediary signalling molecules were found to have their transcripts upregulated. A number of the signalling pathways require activation of signalling molecules by phosphorylation eventually

resulting in gene expression changes of relevant targets. To understand better the implications of the upregulation of the PI3K/Akt pathway, it would be prudent to perform Western blots specifically looking at the phosphorylation of these signalling molecules to determine whether this upregulation amounts to the cell behaviour changes already described.

It would appear that knocking out FGFR3 also has an impact on the Hedgehog signalling pathway as both HHIP and PTHrP are differentially expressed in the FGFR3-KO hTERT MSCs. HHIP was downregulated which should increase IHH signalling (in addition to Sonic hedgehog and Desert hedgehog) which appears to have upregulated the PTHrP transcript, as IHH and PTHrP exist in a feedback loop. PTHrP has been found to increase chondrocyte proliferation and reduce differentiation when overexpressed in chondrocytes (Minina et al., 2001; Kobayashi et al., 2002). The effect of PTHrP on MSCs is less well explored but appears to inhibit onset chondrogenesis at all stages, but no studies appear to have looked into whether PTHrP also impacts on MSC proliferation in a similar manner to its impact on chrondocytes (Weiss et al., 2010). Knocking out FGFR3 appeared to disrupt chondrogenesis which potentially may be due to this upregulation of PTHrP, however at this stage it is not possible to directly attribute the phenotypic behaviours of the FGFR3-KO hTERT MSCs to a specific alteration in a signalling pathway without further investigation.

Furthermore, Snail1 and Slug were found to be downregulated in the FGFR3-KO hTERT MSCs. Snail has previously been identified as an effector of FGFR3 signalling therefore the downregulation of this protein in response to knocking out FGFR3 is to be expected (de Frutos et al., 2007). However, Slug is typically found to be upregulated in response to the downregulation of Snail1, therefore the downregulation of both factors is unexpected (Torreggiani et al., 2012). Snail1 and Slug have both previously been attributed to regulatory roles of MSC differentiation, with Snail1 having a greater impact on osteogenic and chondrogenic differentiation and Slug on adipogenic differentiation (Pérez-Mancera et al., 2007; Torreggiani et al., 2012). The downregulation of both transcripts would fit with the phenotype presented by the FGFR3-KO hTERT MSCs where the cells do not appear to differentiate in response to biochemical cues. It would also be interesting to determine why Slug is being downregulated, and what signalling occurrences are taking place to cause this effect. Similarly, no reports have been made *in vivo* of a reduction of adipose tissue in FGFR3-KO mice, so whether this phenotype in the hTERT MSCs correlates to a phenotype *in vivo* requires more investigation to conclude.

5.5.7 Removal of FGFR3 results in downregulation of transcripts related to cell-cell adhesion and ECM interactions

FGFF3-KO hTERT MSCs were also found to have a number of processes downregulated that were all to do with cell-cell adhesion and interactions with the ECM. Additionally, a number of MMPs were found to be upregulated, apart from MMP15 which is downstream of Snail1. These results all suggest the FGFR3-KO hTERT MSCs are less adhesive than the WT hTERT MSCs and would suggest of an increased migratory nature. This is typically seen in cancer studies where cells typically upregulate MMPs and downregulate ECM genes in order to promote invasion. However, no studies have yet reported any links between FGFR3 and cell-cell adhesion in mesenchymal cells.

It was shown here that FGFR3 knockout has had an impact on predictable pathways, such as PI3K/Akt and MAPK signalling pathways, yet these transcriptome studies have indicated a number of pathways that have not previously been linked to FGFR3. Further studies to develop the understanding of how FGFR3 impacts on these pathways and through which signalling molecules and transcription factors could aid in the understanding of the phenotype presented by the FGFR3-KO hTERT MSCS. It would also provide further information into the skeletal development of bone and cartilage and the effects aberrant FGFR3 signalling has on these processes.

5.5.8 FGFR3-KO hTERT MSCs demonstrate increased *in vitro* scratch wound healing and disruption of collective cell migration

Migratory studies were undertaken based on the number of pathways and proteins relevant to cellular locomotion were differentially expressed in the FGFR3-KO hTERT MSCS. It was immediately evident that in *in vitro* scratch wound healing assays the FGFR3-KO hTERT MSCs were able to close wounds at an increased rate compared to the WT hTERT MSCs. The further use of ptychography, with a pre-defined gap, created by an insert in a culture dish, allowed for single cell analysis of migratory cells. This technique removes the lack of reproducibility in the scratch assay and the potential damaging of the cells when the wound is created. Ptychographic analysis revealed that although FGFR3-KO hTERT MSCs were able to heal an *in vitro* scratch wound faster than WT hTERT MSCs, on a single cell level there was no significant difference between the two cell types. Instead it appeared that the process of collective cell migration has been disrupted and that cells migrate individually rather than as a population, further discussed in Chapter 7. This is likely due to the disruption of cell-cell interactions and ECM interactions, which are crucial for the proper formation of leader and follower cells (Etienne-Manneville and Hall, 2001; Inaki et al., 2012).

It is also interesting to note that the biological process "epithelial to mesenchymal transition" was repeatedly highlighted in RNA-seq analysis as a pathway significantly altered. This disruption to the migration of cells as a population may again be a reason why overgrowth is observed when FGFR3 signalling is disrupted. Without the cues of other cells to impact on migration it may be that cells are migrating further than they ought during skeletal development. Hypothetically, it might be that this is due to FGFs signalling through FGFR3 to impact on cellular migration, and it would be interesting to determine whether any of the FGFs do impact on the migratory ability of these cells. It would also be interesting to analyse whether these effects also carry to the somatic cells derived from MSCs, which has not been studied in this chapter.

5.5.9 Cytoskeletal morphology impacted as a result of knocking out FGFR3 in hTERT MSCs

Further to the migratory data, the FGFR3-KO hTERT MSCs appeared to have an altered cytoskeleton in that the actin filaments had changes to the typical morphologies expected. The actin cytoskeleton drives the migration of cells by constant turnover and reorganisation, and the FGFR3-KO hTERT MSCs appeared to have both an altered cellular morphology in addition to a reduction in the amount of actin stress fibres. In fact, protrusions were noticeable across the bottom of the cell where the cell is attached to the glass cover slip. It is not certain whether these protrusions are aiding the migration of the cells, but is possibly unlikely due to there being no significant difference in the single cell migration properties observed by ptychography. Additionally, there appeared to be no upregulation of genes relating to cellular migration, nor any identified as important for the upregulation of invasion and migration in cancer. However, previous studies have reported a correlation between the morphology of an MSC and its ability to differentiate, with the trilineage potential retained when cell spreading was restricted (Zhang and Kilian, 2013).

5.5.10 Concluding Remarks

The results in this chapter detail, for the first time, a clear phenotype (summarised in Table 5.5.1) caused by the removal of FGFR3 signalling from hTERT MSCs indicating inactivating FGFR mutations impact on skeletal development right from initiation. Previous studies have focussed on the role of FGFR3 on skeletal development *in vivo* and very limited studies have been performed examining the post-natal role of FGFR3. It would appear that the MSC behaviours upon knocking out FGFR3 closely mirror those of chondrocytes and osteoblasts, and that the effects go further impacting adipogenesis as well as the previously mentioned somatic cell types. RNA-seq data also shows a number of other pathways and targets impacted by the knocking out of FGFR3 which have not previously been discussed. Namely, the upregulation of a number of cancer related protein coding

and non-coding RNAs. Whether this impacts on the carcinogenesis of MSCs and skeletal somatic cells with reduced FGFR3 activity has yet to be determined.

Table 5.5.1: Summary of phenotypic differences between WT and FGFR3-KO hTERT MSCS.

Where a phenotype is more pronounced in one cell type than the other, the increase is marked with a + and the decrease with a -. Where no difference is seen between the two cell types, both are marked with a -.

Phenotype	WT hTERT MSCs	FGFR3-KO hTERT MSCs
Protein Expression Levels		
FGFR3 expression	+	-
pERK expression	At 20 mins + At 6 hours +	At 20 mins + At 6 hours -
Cell morphology		
Cell shape	Fibroblastic	Elongated, extended processes, broad lamellipodia
Actin cytoskeleton	Stress fibres	Protrusions, membrane ruffles
Clonogenic capacity		
Number of colony forming units	-	-
Total surface area covered by colonies	-	+
Average colony surface area	-	+
Proliferation		
EdU	-	+
Differentiation Capacity		
Adipogenesis	+	-
Osteogenesis	+	-

Chondrogenesis	+	-?
Transcriptome analysis		
MAPK	+	-
PI3KT	-	+
Cell adhesion and ECM interactions	+	-
Cancer and carcinogenesis pathways	-	+
Migration and *in vitro* wound healing		
In vitro scratch wound healing capacity	-	+
Collective migration	+	-

Chapter 6 : Analysis of three dimensional *in vitro* spheroid models using hTERT MSCs and CRISPR/Cas9 knock out hTERT MSCs

6.1 Introduction

The creation of genetically modified human cell lines gives a unique insight into the behaviour of cells with mutations without the requirements of patient contact or animal models. However, one of the issues of studying disease in a cell line is the limitation of studying in two dimensions (2D). Human tissues are complex three-dimensional (3D) structures and very rarely, if at all, do cells exist without encountering or interacting with another cell type. Yet, human cells outside of the body are typically cultured in 2D adherent monolayers. More recently, culture techniques have been developed that allow the growth and manipulation of cells in 3D, including the use of cell aggregates known as spheroids (Saleh et al., 2012; Cesarz and Tamama, 2016).

In the body, cells are typically found to be making direct contact with cells from the same, and different, lineages in addition to being surrounded by extracellular matrix (ECM). The cues and signals received from this varied environment impact on cellular behaviour, therefore it is perhaps not surprising that cells in a 3D environment behave differently to the same cells in a 2D monolayer. It has previously been shown that articular chondrocytes removed from their 3D environment lose their inherent properties, and differentiation from MSCs into chondrocytes occurs much more efficiently with the cells in 3D (Von Der Mark et al., 1977; Johnstone et al., 1998). Additionally, in the MSC field, work from our laboratory and other have shown the inherent properties and therapeutic potential of MSCs can be enhanced using 3D culture (Saleh et al., 2011a, 2012; Yamaguchi et al., 2014). Primary MSCs undergo dedifferentiation in a specific environment increasing expression of early mesoderm markers and gaining the ability to form organised tissues when implanted in immunosuppressed mice (Pennock et al., 2015). Publications have also demonstrated MSCs cultured in 3D have increases in Wnt signalling, in addition to an increased osteogenic differentiation, and increased osteoregenerative properties (Wang et al., 2009; Yamaguchi et al., 2014; Saleh et al., 2016; Xu et al., 2016).

The CRISPR/Cas9 genome editing in this thesis has focused on mutations relevant to bone and cartilage, two of the tissues formed by MSCs. These tissues share an interface, termed the

osteochondral interface (reviewed in Hoemann et al., 2012), which is initially derived from an entirely cartilage structure whereupon mineralised bone is formed in a process called endochondral ossification, thus bone and cartilage tissues are interacting from early on in development (Mackie et al., 2008). *In vivo* studies using sodium fluorescein have demonstrated there exists transport pathways in the form of nonmineralised regions allowing the sodium fluorescein to diffuse between the subchondral bone and calcified cartilage (Pan et al., 2009). Moreover *in vitro* systems have demonstrated a number of cellular interactions between chondrocytes, osteocytes, osteoblasts and osteoclasts, including activation and inhibition of major signalling pathways (Zhu et al., 2008, 2009; Blom et al., 2009). There have also been suggestions that the crosstalk between these two tissues can contribute to disease (Westacott et al., 1997).

It is therefore apparent that when studying bone and cartilage tissues it is important to realise the role the osteochondral interface plays in the support, maintenance and repair of these tissues. More recently, models are being made from both tissue types to better understand the osteochondral interface and to determine its relevance for future therapeutics, particularly for diseases such as osteoarthritis (Nukavarapu and Dorcemus, 2013). It was therefore decided to optimise and develop a 3D model which gave a defined osteochondral interface to allow further analysis of the CRISPR/Cas9 hTERT MSCs. In this way it would be possible to determine the effects of the generated mutation on multiple cell types, and also the impact of one of the tissue types having the mutation present and not the other.

6.2 Aims

The aims of this chapter are to develop a 3D spheroid model for the study of the osteochondral interface using pre-differentiated osteogenic and chondrogenic cells including those derived from CRISPR/Cas9 edited hTERT MSCs.

The specific objectives of this chapter are to:

- Test a previously determined 3D spherod methodology developed for primary MSCs in our laboratory using the hTERT MSCs
- Determine the pre-differentiation time required for specific differentiation of hTERT MSCs to continue in mixed osteochondral media
- Use fluorescent labelling techniques to track the cell types within the 3D culture model
- Determine the behaviour differences, if any, of using the FGFR3-KO hTERT MSCs in the developed osteochondral model

6.3 Methods

6.3.1 Cell Culture Methods

6.3.1.1 Pre-differentiation prior to spheroid formation

An appropriate number of cells (Y101, Y201 or FGFR3-KO hTERT MSCs), for the spheroid number required, were seeded into a flask and allowed to attach overnight. Approximately 24 hours after seeding, medium was changed to either osteogenic induction media (described in section 2.1.3.3) or chondrogenic induction media (described in section 5.3.5.2). Cells were incubated in the appropriate media for the pre-differentiation step needed (either 4, 5 or 7 days) before spheroid formation.

6.3.1.2 Pre-differentiation method development

To determine the pre-differentiation step required for the hTERT MSCs, $2x10^4$ cells per cm^2 were seeded into 24 well plates and allowed to adhere overnight. Medium was then aspirated and replaced with either basal medium or, osteogenic or chondrogenic induction media (described in section 2.1.3.3 and section 5.3.5.2 respectively) or up to 7 days. Medium was then aspirated again and either continued in the current differentiation media or replaced with osteochondral differentiation medium (section 6.3.1.3).

Alcian blue staining was performed to stain for glycosaminoglycans. Cells were washed once in PBS before % w/v paraformaldehyde solution for 10 minutes at room temperature. Cells were then washed twice in dH_2O and stained in 1% Alcian BlueGX (pH<1) for 30 minutes. Two further washes with dH_20 were performed before imaging using a brightfield microscope.

6.3.1.3 Osteochondral differentiation media

Osteochondral medium was used to support osteogenic and chondrogenic hTERT MSCs in both 2D monolayer and 3D spheroid culture. This medium consists of DMEM +2% FBS + 1% penicillin-streptomycin + 50 µg/ml ascorbic acid, 5mM β-glycerophosphate, 100nM dexamethasone, 50 µg/ml L-proline and 1% ITS.

6.3.2 Formation of 3D osteochondral interface spheroid models

6.3.2.1 Basal spheroid formation and culture

Spheroids were formed from 30,000 total cells in non-adherent U-bottomed 96-well plates. Basal spheroids were cultured in 100µL DMEM with 0.25% (w/v) methyl-celluose and 1% penicillin-streptomycin leading to the cells aggregating to form spheroids (Saleh et al., 2012). Basal spheroids were maintained in this media for up to 7 days.

6.3.2.2 Osteochondral spheroid formation and culture

Osteochondral spheroids were formed of a 50:50 ratio of osteogenic cells to chondrogenic cells with a total of 30,000 pre-differentiated hTERT MSCs per spheroid. Osteochondral spheroids were maintained in 100µL osteochondral media (section 6.3.1.3) with a final concentration of 0.25% methyl cellulose. A schematic of the model is summarised in Figure 6.4.1.

6.3.2.3 Osteogenic + chondrogenic spheroid formation and culture

Individual osteogenic and chondrogenic spheroids were formed from 30,000 pre-differentiated hTERT MSCs, labelled as required with Cell tracker stain, in individual wells of a U-bottomed well plate. Spheroids were maintained in 100µL osteochondral media (section 6.3.1.3) with a final concentration of 0.25% methyl cellulose also added. 24 hours post spheroid formation, the chondrogenic spheroid was carefully transferred to a well containing a formed osteogenic spheroid. An overview of this model is summarised in Figure 6.4.10.

6.3.2.4 Osteogenic spheroid + chondrogenic suspension 3D model formation and culture

An osteogenic spheroid was formed from 30,000 hTERT MSCs, labelled with cell tracker (described in section 6.3.2.5) as required, and allowed to form in osteochondral media (section 6.3.1.3) for 24 hours. 24 hours post spheroid formation, pre-differentiated chondrogenic cells were trypsinised from the flask, the cell numbers calculated, and then labelled with cell tracker as required. 50µL of media from the osteogenic spheroid wells was removed and discarded. A single cell suspension was then created and 50µL of chondrogenic suspension added to each osteogenic spheroid so that 30,000 chondrogenic cells are present in each well. A schematic of the model is shown in Figure 6.4.15.

6.3.2.5 CellTracker Labelling

To allow visualisation of spheroids and cell tracking, hTERT-MSCs were labelled with either CellTracker green (Life Technologies) or CellTracker red (Life Technologies) prior to spheroid formation as per manufacturer's instructions. The required numbers of cells were aliquoted and centrifuged to remove FBS. Cells were labelled with cell tracker for up to 1 hour and any excess stain neutralised and removed. Osteogenic cells were labelled red and chondrogenic cells labelled green.

6.3.2.6 Cryosectioning

Spheroids to be taken for sectioning and further analysis were carefully removed from the U-bottomed well and transferred to the cap of an Eppendorf. The medium was removed and the spheroid washed with PBS, which was then removed. Tissue-Tek OCT (VWR) was then added to fill the cap and the cap immersed in liquid nitrogen to snap-freeze the spheroid. Spheroids were sectioned at 10µm thickness using a Bright's cryostat (Bright Instruments, UK) and placed onto Superfrost positive microscope slides (Thermo Scientific). The slides were stored at -20^{o}C until required.

6.3.3 Spheroid Imaging and Analysis Methods

6.3.3.1 Imaging spheroids with a multiphoton confocal microscope

Spheroids were imaged using a Zeiss multiphoton inverted microscope with a 37^{o}C incubator attachment and a 95% air, 5% CO_2 supplementation, PBS was added to surrounding wells to minimise evaporation. Spheroids were imaged via Z-stack imaging using a 10x lens and combined to form a 3D image of the spheroid after imaging was complete. Timelapse imaging was set up and images taken every 2 hours of each spheroid, multiple spheroids were imaged at a time by storing spheroid positions. These were readjusted as necessary to ensure the spheroid was kept in the frame of view. Videos were then constructed using Zen lite software. Sections were imaged in the same manner using a 20x lens.

6.3.3.2 Imaging spheroids with a lightsheet microscope

Y101 hTERT MSC osteogenic + chondrogenic spheroids incubated for 10 days were imaged with a Zeiss lightsheet 7.1. Spheroids were visualised with Cell Tracker (Life Technologies) prior to spheroid formation (section 6.3.2.5) and spheroids were then embedded in 1% agarose (w/v)/PBS gel rod using a capillary and a tight-fitting plunger. The agarose was allowed to polymerise and the gel

extruded from the capillary into the chamber filled with PBS. Spheroids were imaged once and then rotated 180^{o} before a second image was taken.

6.3.3.3 Determination of size parameters using ImageJ

Brightfield images were taken on the spheroids to be analysed using a 5x lens. Images were then opened in ImageJ and the diameter measured using the straight line tool across the widest point of the spheroid. An image of a haemocytometer was used to convert the distance measured in pixel to micrometres.

The roundness of the spheroid was measured by altering the threshold of the image so that the entirety of the spheroid was black against the background of the image. The outline of the spheroid was highlighted with the wand tool and the roundness of the resulting image measured.

6.3.3.4 Quantification of Cell tracker labelling in osteogenic and chondrogenic regions of osteochondral sections

Images of osteochondral spheroid sections were opened in ImageJ and separated into the individual colour channels. The appropriate regions were manually defined and the average pixel intensity for each colour quantified in each defined region. Three section images were analysed in this manner and averaged to provide an overview of the amounts of cell tracker present.

6.4 Results

6.4.1 Generation of 3D osteochondral spheroids from pre-differentiated hTERT MSCs

6.4.1.1 hTERT MSCs cannot reproducibly form osteogenic/chondrogenic spheroids using previously developed protocols

Previous work in the laboratory has shown that primary human MSCs pre-differentiated down osteogenic and chondrogenic lineages, by chemical stimulation in 2D, undergo self-organisation once combined in a combined 3D spheroid model (Marshall, 2015). Pre-differentiation in this way followed by a continuation of stimulation via an osteochondral cocktail allowed for the maintenance of differentiation in a 3D setting, enabling interactions between the cell types to occur. In this way, a spheroid has very broad similarities to an early limb bud formation model allowing analysis into the process of endochondral ossification. However, this methodology has not been tested with the hTERT MSCs. The osteochondral spheroid model (summarised in Figure 6.4.1) was therefore tested with the Y101 and Y201 hTERT MSCs to determine whether any spheroid method development would be required before using the GM-hTERT MSCs.

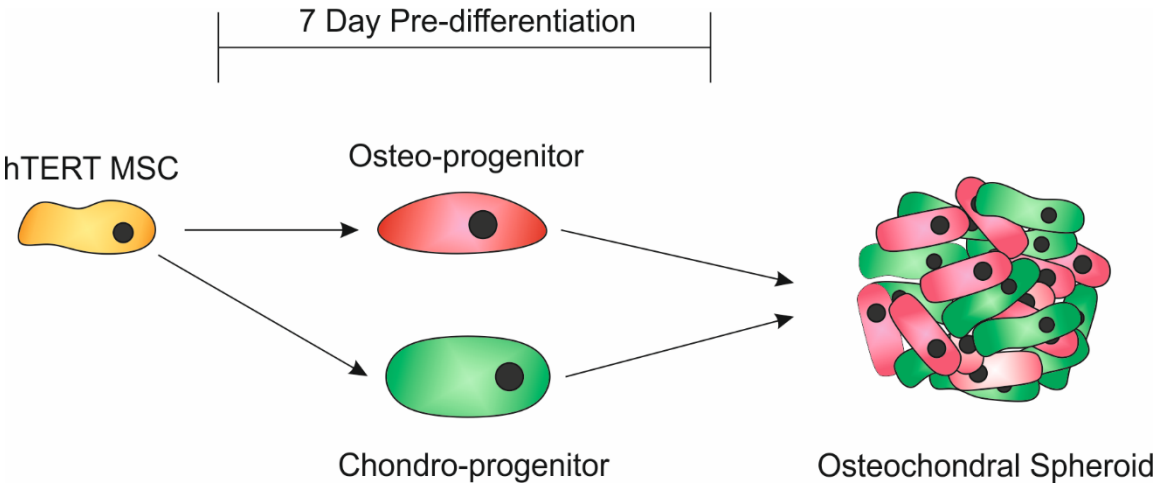

Figure 6.4.1: Overview of methodology used to create osteochondral spheroids

Y101 and Y201 hTERT MSCs are first directed to differentiate down either the osteogenic or chondrogenic lineages for 7 days before these cell populations are fluorescently labelled with Cell-Tracker. Osteo-progenitors are labelled red and chondro-progenitors labelled green. These are then combined in equal proportions to form a spheroid of 30,000 cells.

Y101 and Y201 cells were induced to undergo either osteogenesis or chondrogenesis for 7 days before spheroid formation. These were fluorescently labelled to track progression throughout the timecourse, with osteogenic cells labelled with CellTracker red and chondrogenic cells labelled with CellTracker green. Basal spheroids were also made where half a population of undifferentiated hTERT MSCs were labelled red and the other half green, these were combined similarly to the osteochondral spheroids. Z-stack images were taken at different timepoints throughout a 7 day timecourse to observe spheroid formation and any self-organisation that might be occurring in the spheroids. The first timepoint was delayed until 48 hours post initiation as very little evidence of spheroid formation could be seen at 24 hours, this was unexpected as spheroid formation using primary cells typically takes place within the first 24 hours (results not shown). It became apparent the osteochondral spheroids seemed to have difficulty forming, particularly noticeable in the Y201 hTERT MSCs (Figure 6.4.2). In comparison, the basal controls appeared to have formed spheroids successfully in the majority of cases, as cells formed one spheroid in the well. The osteochondral spheroids instead appeared to have large numbers of cell clumps throughout the well, which was observable in all of the wells. This did not improve throughout the timecourse.

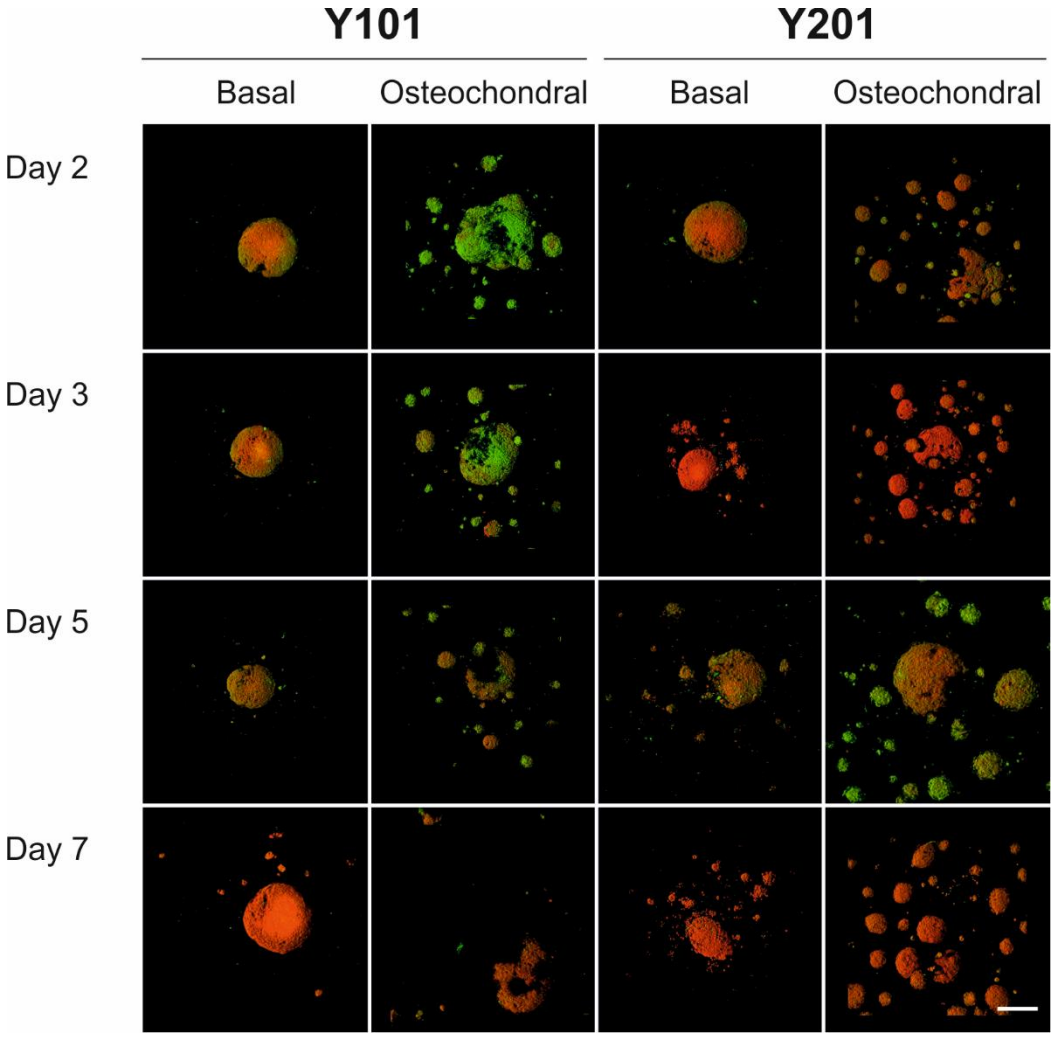

Figure 6.4.2: Z-stack images of osteochondral and basal spheroids formed after 7 days pre-differentiaton

Z-stack images were taken post spheroid formation of basal (B) and osteochondral (OC) spheroids. hTERT MSCs were differentiated for 7 days prior to spheroid formation and compared to basal cells which had not been subjected to any differentiation signals throughout the experiment. Osteogenic cells were labelled with CellTracker red and chondrogenic cells labelled with CellTracker green. Equal proportions of basal hTERT MSCs were labelled red and green. Scale bar = 200µm.

6.4.1.2 Reducing pre-differentiation allows single spheroid formation

As the basal cells were able to form single spheroids successfully, it was hypothesised that the pre-differentiation was preventing the hTERT MSCs from forming spheroids successfully. In order to determine whether this was true hTERT MSCs were pre-differentiated for 4 or 5 days and then induced to form osteochondral spheroids, single differentiation controls were also included to determine which differentiation may be causing the issues. Brightfield images were taken every day over the timecourse. As seen in Figure 6.4.3, both the Y101 and Y201 hTERT MSCs seemed to be able to form spheroids in all conditions tested when pre-differentiated for 4 days. The Y201 hTERT MSCs also seemed to be able to form osteochondral spheroids after 5 days of pre-differentiation however the single differentiation controls seem more fragile and more prone to making smaller spheroids rather than one large spheroid. The Y101 hTERT MSCs were not able to form osteochondral spheroids after 5 days of pre-differentiation with the majority of spheroids having cellular debris present in the well. This appeared to be mostly due to the osteogenic cells as the Y101 chondrogenic spheroids have formed correctly.

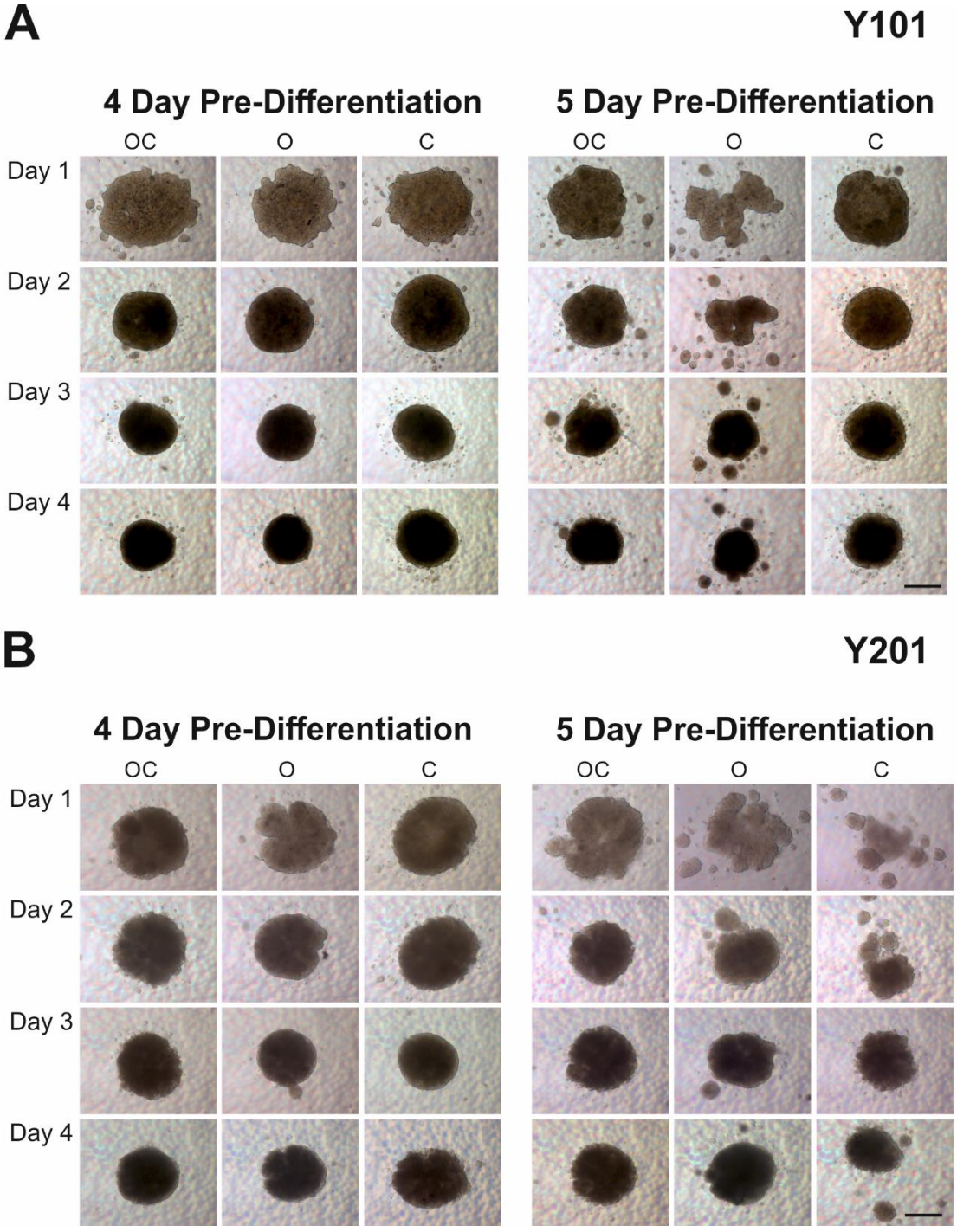

Figure 6.4.3: Brightfield images of spheroids formed from hTERT MSCs differentiated for either 4 or 5 days prior to spheroid formation

hTERT-MSCs were induced to form spheroids after either 4 days or 5 days pre-differentiation. Osteochondral spheroids (OC), comprising of both osteogenic and chondrogenic cells, were made in addition to osteogenic (O) and chondrogenic (C) only spheroids. Scale bar = 200µm.

6.4.1.3 Confirming specific differentiation in 2D

The hTERT MSCs are able to differentiate into each of the three lineages typical of MSCs. There is therefore a risk that when exposed to signals from multiple lineages, such as the osteogenic and chondrogenic signals in the osteochondral media, the hTERT MSCs may not progress down the desired lineage. In order to determine whether 4 days differentiation prior to exposure to both osteogenic and chondrogenic signals was sufficient to maintain the hTERT MSCs down the wanted lineage, a differentiation assay was set up. The assay set up has been summarised in Figure 6.4.4, in brief cells were exposed to either osteogenic or chondrogenic media for 4 days prior to exposure to osteochondral media for 7 days. This was then compared to both positive and negative controls, whereby cells were exposed to either of the differentiation media or sustained in basal medium throughout.

As seen in Figure 6.4.5A, Y101 hTERT-MSCs that had been differentiated in osteogenic media prior to osteochondral maintenance medium had similar levels of Alizarin red staining compared to the osteogenic positive control with negligible Alcian blue staining. Conversely, Y101 hTERT-MSCs differentiated in chondrogenic media prior to osteochondral maintenance medium, showed weak Alizarin red staining and enhanced Alcian blue staining. Additionally the cells appeared to condense during this timeframe, a feature of chondrogenic induction. These findings suggest that 4 days is sufficient for Y101 hTERT-MSCs to be directed down one lineage and exposure to osteochondral differentiation signals after this time maintains differentiation status. However, when the same experiment was performed with the Y201 hTERT MSCs (Figure 6.4.5B) the cells that had been maintained in osteochondral media did not appear to have differentiated specifically as both conditions appeared to have similar low levels of staining for both histological stains. This would suggest 4 days of pre-differentiation is not enough to sustain specific differentiation in osteochondral media for the Y201 hTERT MSCs.

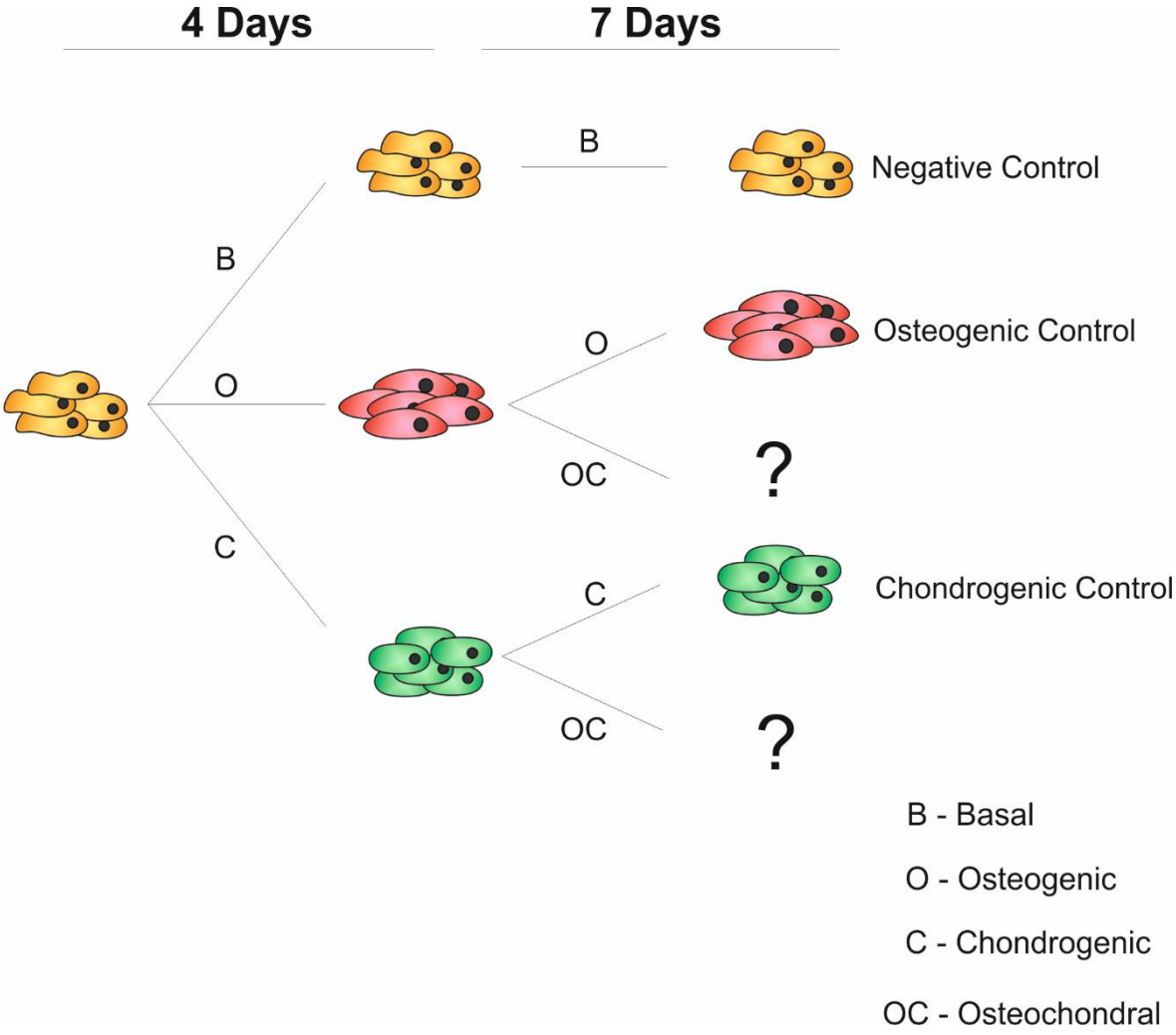

Figure 6.4.4: Schematic summary of 2D differentiation timecourse.

Cells were incubated for 11 days in total, either 11 days in basal media (B), osteogenic (O) or chondrogenic (C) media, or 4 days in osteogenic or chondrogenic media before changing to osteochondral (OC) media for 7 days.

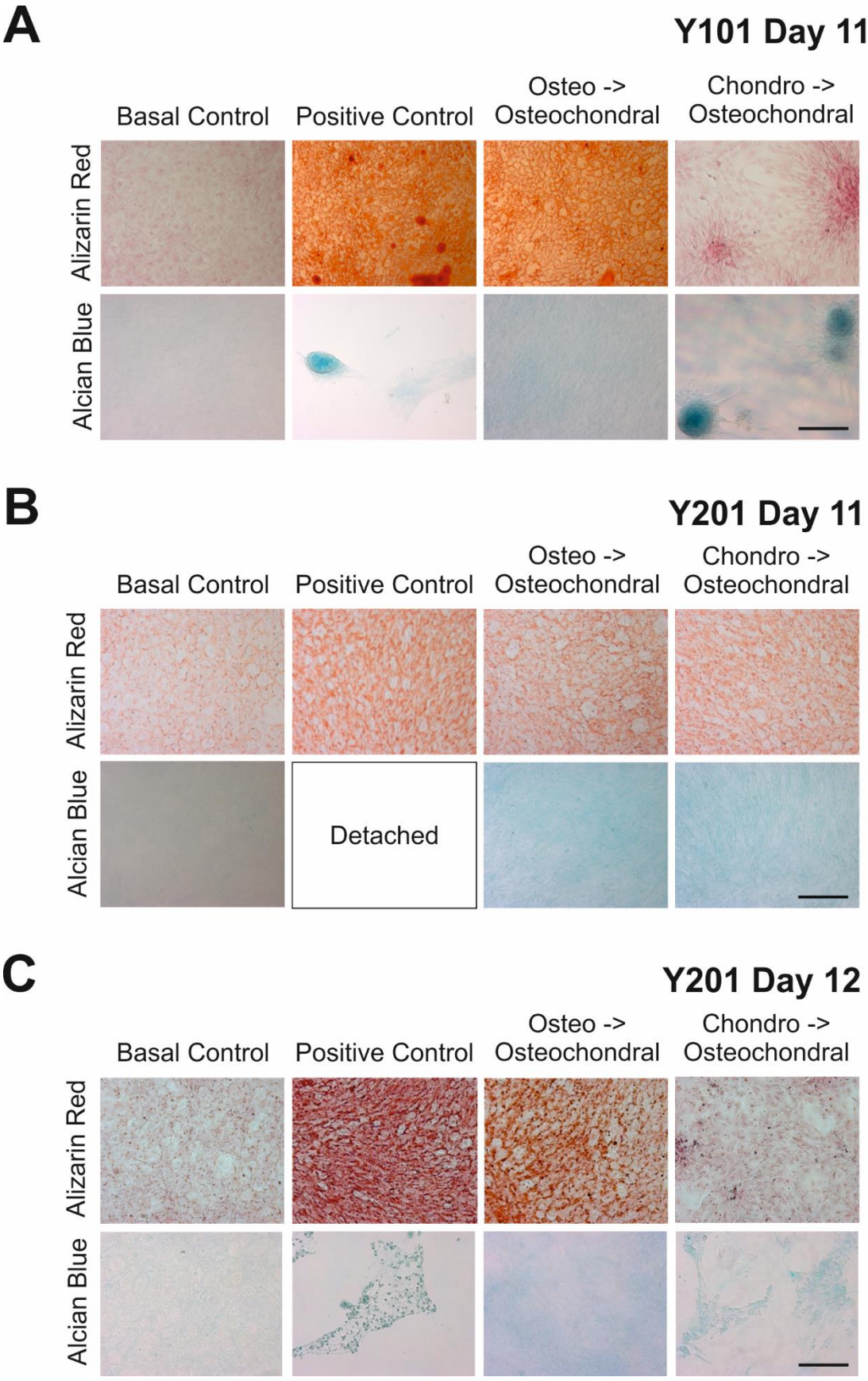
A
Y101 Day 11
Basal Control
Positive Control
Osteo -> Osteochondral
Chondro -> Osteochondral
Alizarin Red
Alcian Blue
B
Y201 Day 11
Basal Control
Positive Control
Osteo -> Osteochondral
Chondro -> Osteochondral
Alizarin Red
Alcian Blue
Detached
C
Y201 Day 12
Basal Control
Positive Control
Osteo -> Osteochondral
Chondro -> Osteochondral
Alizarin Red
Alcian Blue

Figure 6.4.5: Histological staining of partially differentiated Y101 hTERT-MSCs.

Y101 (A) and Y201 (B) hTERT MSCs were incubated for 11 days in total, either 11 days in basal media, osteogenic or chondrogenic media, or 4 days in osteogenic or chondrogenic media before changing to 7 days osteochondral media. Y201 hTERT MSCs had this process repeated with a 5 day pre-differentiation, followed by 7 days incubation in osteochondral media for a total of a 12 day timecourse. Cells were stained with Alizarin red to identify calcium deposition or with Alcian blue for glycosaminoglycans. Scale bar = 200μm

The experiment was then repeated with a 5 day pre-differentiation step in specific differentiation cues to determine whether this would be sufficient to retain specific differentiation in the mixed media. Figure 6.4.5C shows the staining levels of Y201 hTERT MSCs with this extended timecourse. The differentiation achieved in the osteochondral media appeared to be much more specific than when the cells were incubated for 4 days in the specific differentiation cues. An increased level of Alizarin Red staining was seen in the osteogenic cells that have been exposed to the osteochondral media, with levels similar to those seen in the positive control, conversely the Alcian blue staining of this sample is relatively low. The Y201 hTERT MSCs differentiated in chondrgenic media appeared to have potentially begun condensation and the levels of Alcian blue in the cells that were later differentiated in the mixed media are at a similar level to the positive control. Overall, it appears that the Y201 hTERT MSCs require an extended differentiation step in specific differentiation media than the Y101 hTERT MSCs to retain specific differentiation in a mixed media.

6.4.1.4 Y101 hTERT MSCs predifferentiated for 4 days reliably form osteochondral spheroids and demonstrate self-organisation

With the confirmation that the hTERT MSCs could form osteochondral spheroids with a reduced pre-differentiation step, and that differentiation would retain specificity both the Y101 and Y201 hTERT MSCs were differentiated and induced to form spheroids. Figure 6.4.6 shows the osteochondral spheroids formed by the Y101 hTERT MSCs and Y201 hTERT MSCs. The Y101 hTERT MSCs successfully form individual spheroids that appeared to begin to shrink and become more regular in shape throughout the timecourse and these were cultured for up to 7 days. Conversely, the Y201 hTERT MSCs failed to reproducibly form spheroids using this methodology with a number of cells forming multiple smaller spheroid like masses throughout the well. It would appear that a further method development would be required for analysing osteogenic and chondrogenic Y201 hTERT MSCs in a 3D model.

The Y101 hTERT MSCs successfully formed osteochondral spheroids and these were further analysed. Initially the size and shape of the spheroids was analysed throughout the timecourse. Figure 6.4.7A shows the Y101 osteochondral spheroids do shrink over the timecourse, and Figure 6.4.7B shows that as the spheroids shrink they become increasingly round.

To observe any internal organisation of the osteogenic and chondrogenic cells in the spheroids, the spheroids were sectioned, and resulting sections imaged (Figure 6.4.8). There appeared to be a level of separation of the osteogenic (red) and chondrogenic (green) cells in the later stages of the timecourse, with sections typically possessing portions with increased presence of red fluorescence or green fluorescence. These have been highlighted in Figure 6.4.8B. The amounts of red and green fluorescence in these regions was quantified which showed the fluorescence levels of each colour did not appear to correlate with the regions highlighted (Figure 6.4.9). It would perhaps be more beneficial to have a clearer osteochondral interface than this model can provide, therefore alternatives were sought.

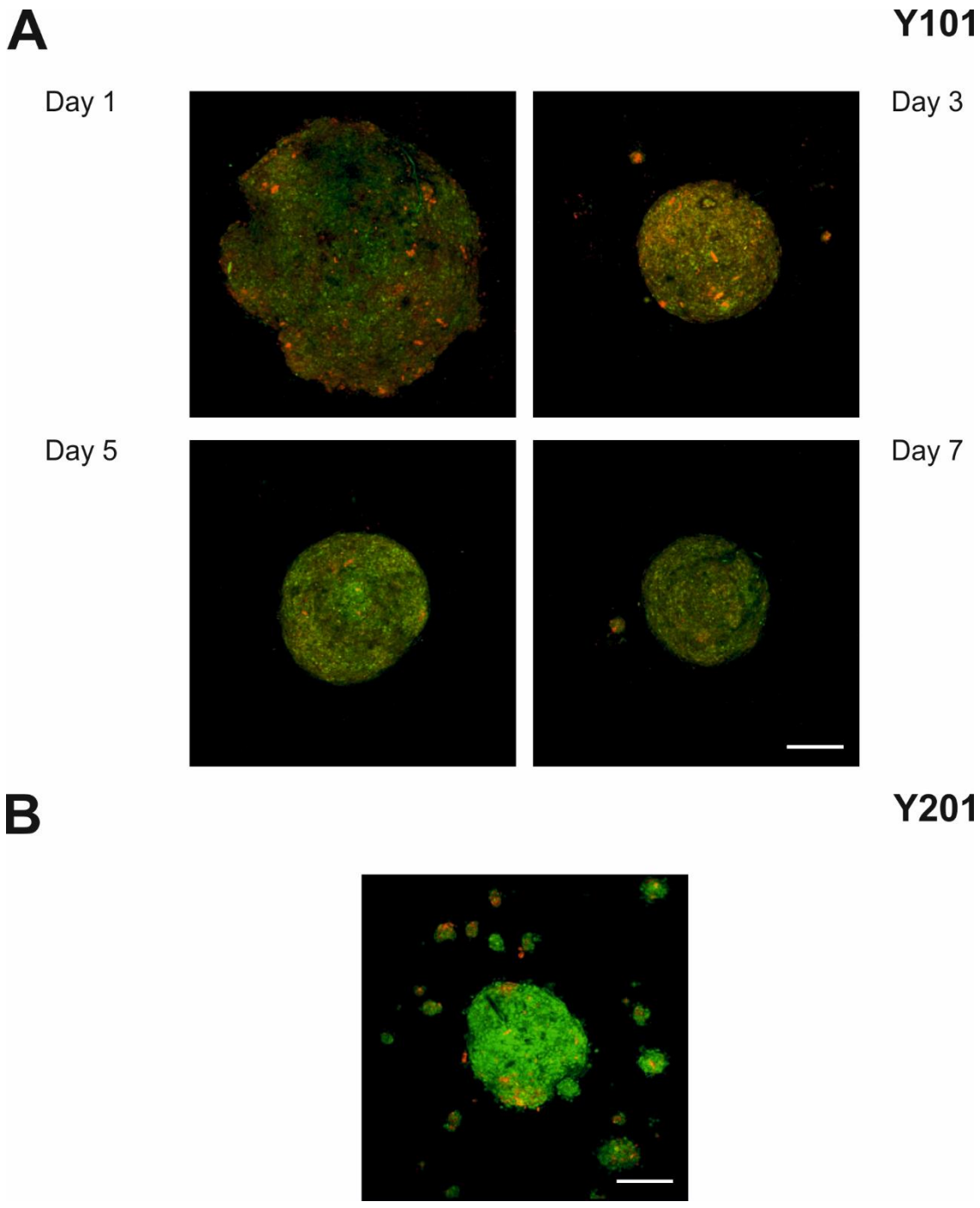

Figure 6.4.6: Fluorescent microscopy of osteochondral spheroids.

Z-stack images were taken post spheroid formation of pre-differentiated Y101 hTERT MSCs (A) and Y201 hTERT MSCs (B) with osteogenic cells labelled red and chondrogenic cells labelled green. Scale bar = 200µm

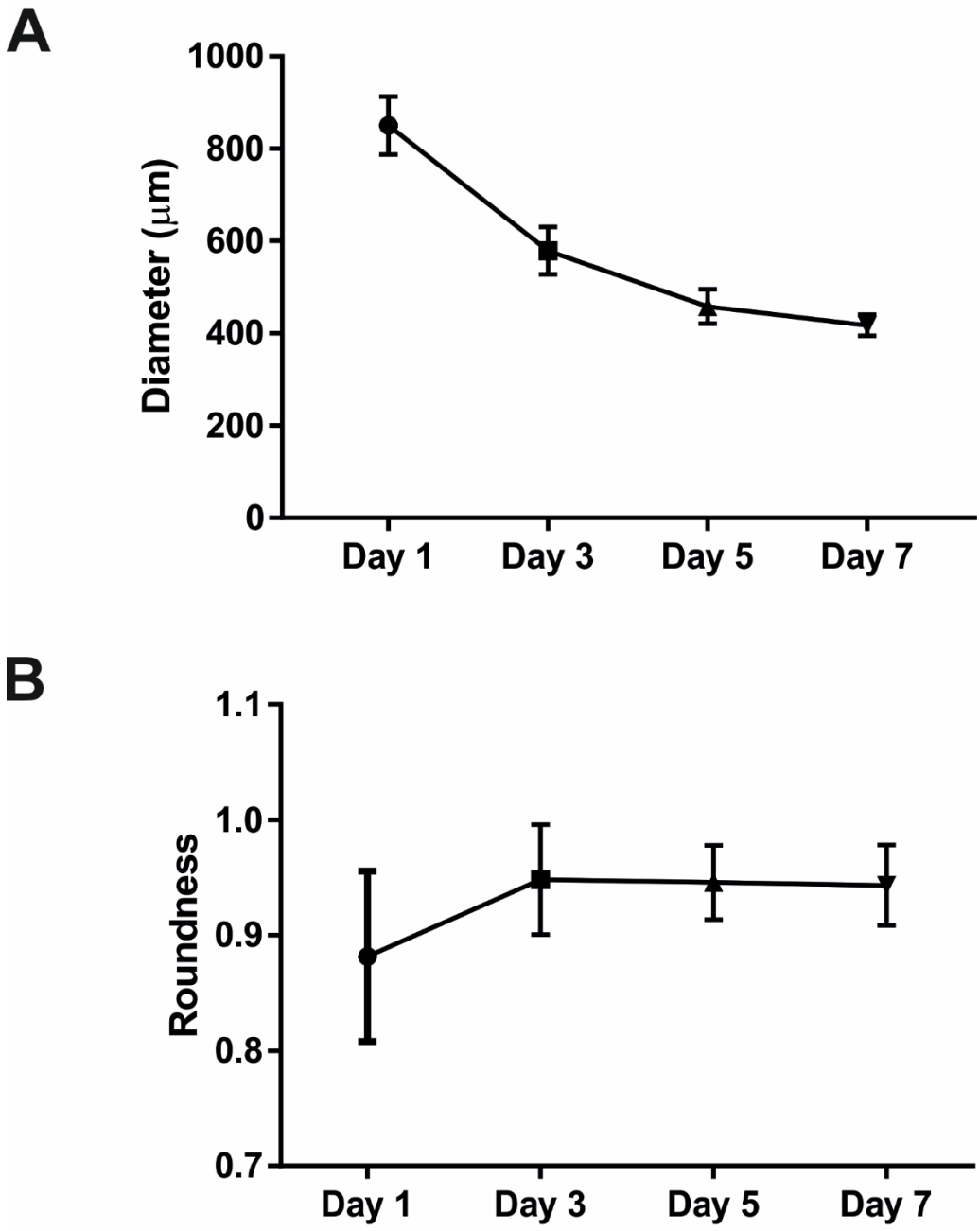

Figure 6.4.7: Shape analysis of Y101 osteochondral spheroids

Brightfield images of Y101 ostoechondral spheroids were taken and analysed for diameter (A) and roundness (B) using ImageJ. Values = mean ± SD, n=6

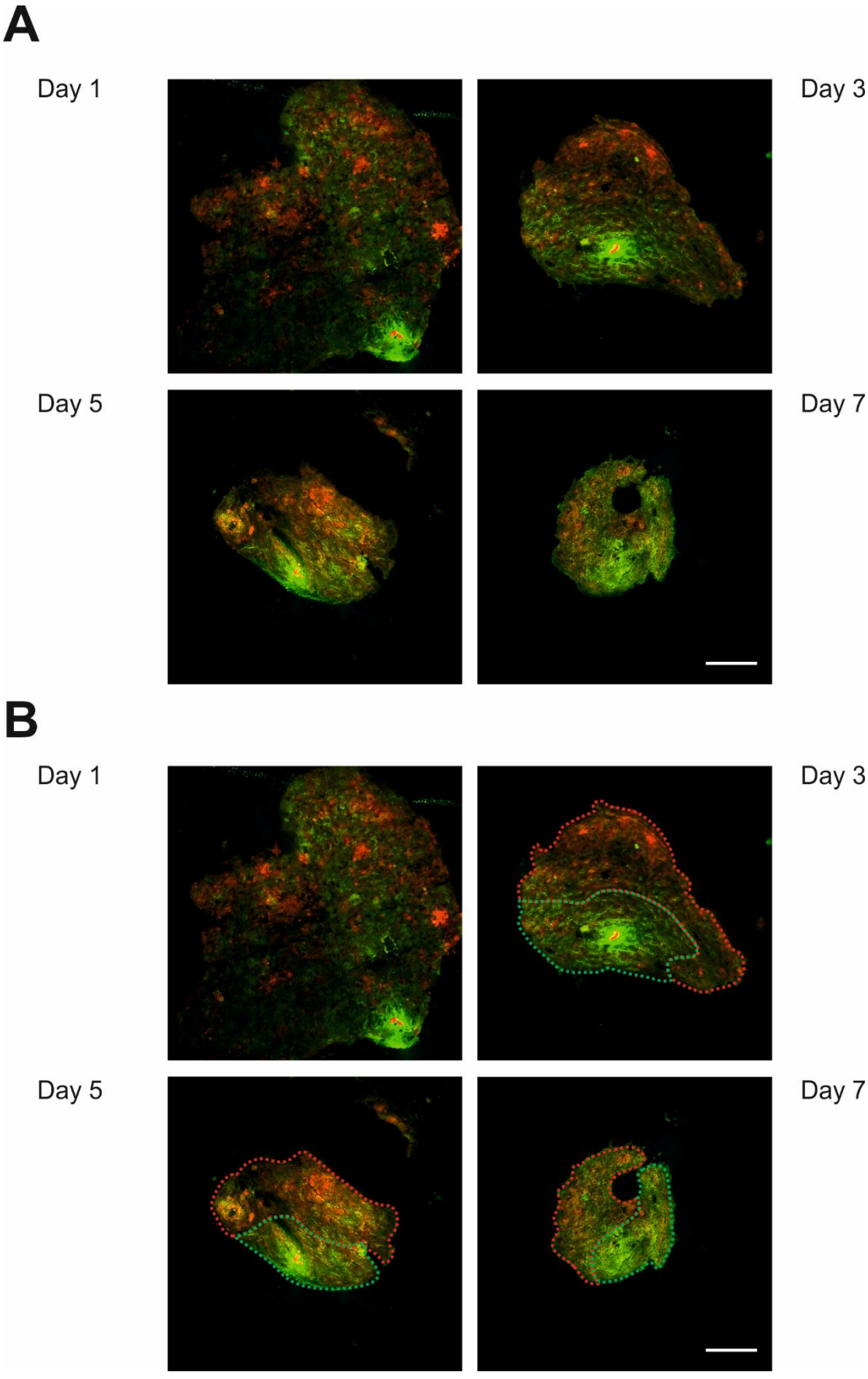
A
Day 1
Day 3
Day 5
Day 7
B
Day 1
Day 3
Day 5
Day 7

Figure 6.4.8: Fluorescent microscopy of sectioned Y101 hTERT MSC osteochondral spheroids.

Fluorescent images were taken of sections of Y101 hTERT MSCs osteochondral spheroids to observe internal organisation (A) and internal organisation of osteogenic and chondrogenic cells highlighted (B). Osteogenic cells labelled red and chondrogenic cells labelled green. Scale bar = 200µm

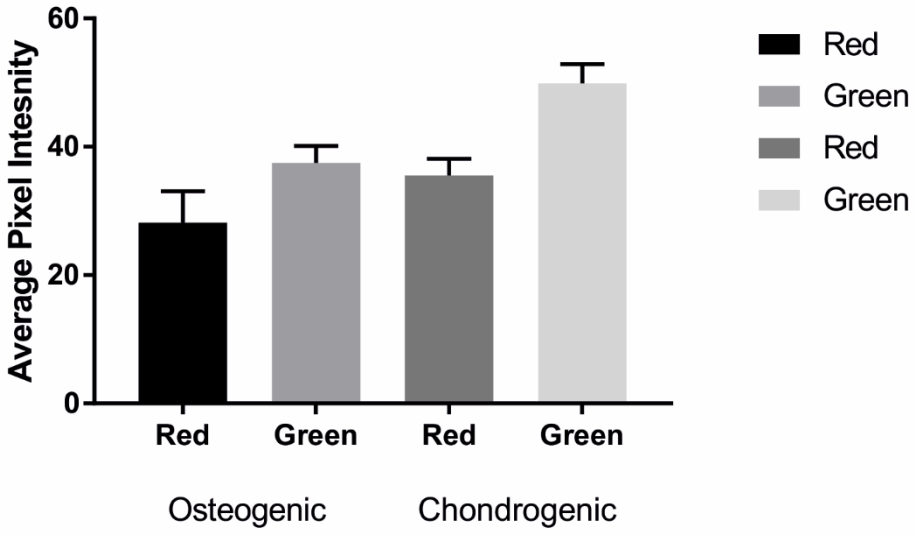

Figure 6.4.9: Section analysis of osteochondral spheroids of osteogenic and chondrogenic regions

Sections from day 7 osteochondral spheroids were analysed for red and green pixel intensity using ImageJ based on regions as highlighted in the previous figure. Regions identified as having more red pixels visually were termed osteogenic and those with more green pixels termed chondrogenic for the purpose of this analysis. It was clear however that the average pixel intensity of these regions did not correlate with the regions identified.

6.4.2 Osteogenic and chondrogenic spheroids combine in culture to form osteochondral interface

The osteochondral spheroids analysed previously demonstrate a level of self-organisation but an interface between the two cell types may be easier to analyse interactions between cells. Additionally, the Y201 hTERT MSCs did not reliably form osteochondral spheroids, and these are the hTERT MSCs previously successfully used for genome editing with CRISPR/Cas9 therefore additional work was needed to find a reliable spheroid model for these cells. Figure 6.4.10 shows a schematic of how an osteochondral interface may be generated using a different approach by creating two individual spheroids and allowing them to combine in a single well, which has previously been demonstrated with primary MSCs in the Genever group.

Y101 and Y201 hTERT MSCs were pre-differentiated for 4/5 days respectively before being induced to form individual osteogenic and chondrogenic spheroids. 24 hours after spheroid formation was initiated, the spheroids were placed into the same well and incubated for up to 7 days. The combination of spheroids is here on referred to as “osteogenic + chondrogenic” spheroids. Figure 6.4.11 shows the osteogenic + chondrogenic spheroids formed from Y101 hTERT MSCs, similarly to the osteochondral spheroids, the Y201 hTERT MSCs could not reliably form chondrogenic spheroids rendering it impossible to combine the osteogenic and chondrogenic spheroids as planned.

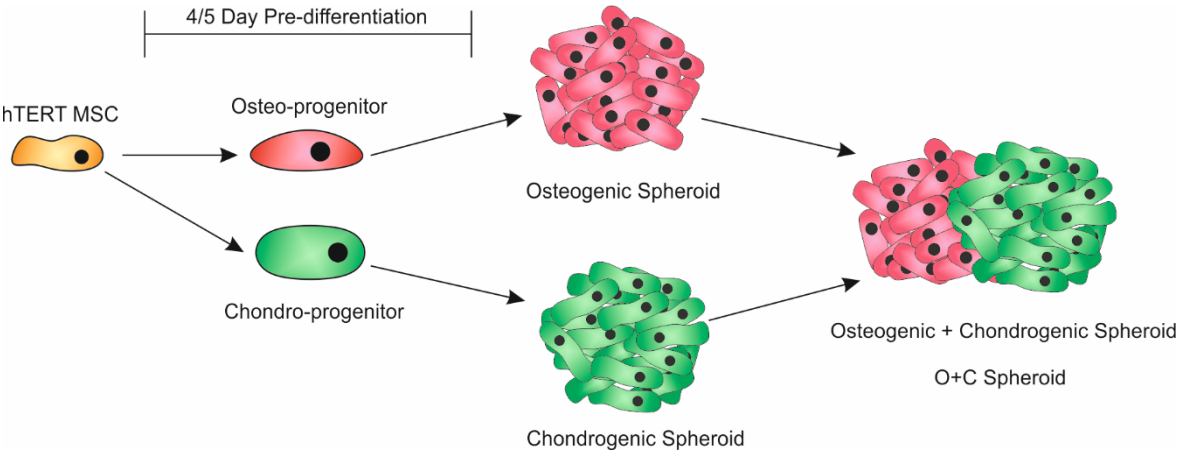

Figure 6.4.10: Overview of methodology used to create osteogenic + chondrogenic spheroids

Y101 and Y201 hTERT MSCs are first directed to differentiate down either the osteogenic or chondrogenic lineages for 4/5 days respectively before being fluorescently labelled with Cell-Tracker. Osteo-progenitors are labelled red and chondro-progenitors labelled green. 30,000 cells are used to create each spheroid which are then allowed to form for 24 hours before being combined in a single well.

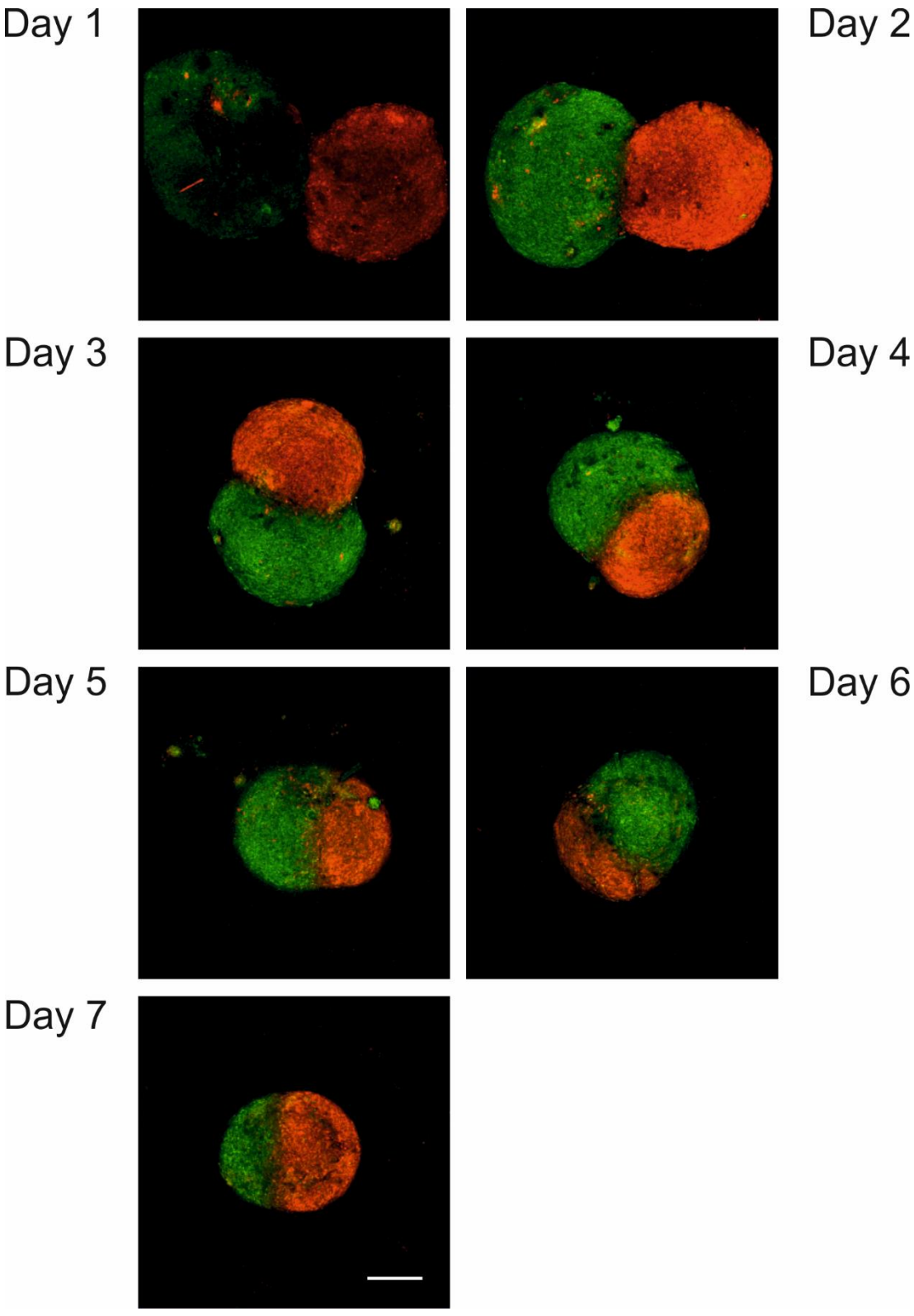

Figure 6.4.11: Fluorescent microscopy of osteogenic + chondrogenic spheroids.

Z-stack images were taken after osteogenic (red) and chondrogenic (green) spheroids formed from 30,000 Y101 hTERT MSCs were combined up to 7 days. Scale bar = 200µm

The two Y101 hTERT MSC spheroids can be seen to be joined after 24 hours before merging to form a single spheroid by day 4, but throughout the timecourse red/green regions remain distinct. The shape and size of these spheroids were analysed as before, and showed that the merging spheroids become more compact and more round with time in culture (Figure 6.4.12). This gives an indication that the spheroids are merging and condensing to form one individual spheroid.

These spheroids were then sectioned to observe internal organisation, with the earliest timepoint being day 2 to allow the spheroids to form a connection that might be sustained throughout sectioning (Figure 6.4.13). The spheroids were still clearly separate entities at days 2 and 3, however by day 5 have merged into one spheroid. The red and green regions were clearly distinct throughout the timecourse but an integrated boundary of the two spheroids was also visible when osteogenic and chondrogenic cells are forming an interface. These have been magnified and displayed in Figure 6.4.13B.

To examine further the behaviour of the osteogenic + chondrogenic spheroids the timecourse was extended to a 10 day timecourse, and the spheroids imaged using a lightsheet microscope. This microscope embeds the spheroid in agarose and suspends it within a chamber allowing for the spheroid to be rotated and images taken of multiple angles. Initially, the osteogenic + chondrogenic spheroids were imaged with the multi photon microscope which confirmed the usual behaviour of spheroid merging (Figure 6.4.14A). Additionally, at day 10 it appeared the osteogenic spheroid may be overlapping and almost engulfing the chondrogenic spheroid. The osteogenic + chondrogenic spheroids were then imaged on the lightsheet microscope and images taken of opposite sides of the spheroid, i.e. the spheroid was rotated 180^{o} between images. Figure 6.4.14B shows two osteogenic + chondrogenic spheroids imaged in this way. Although the green fluorescence was not as well defined in these images it again appeared that the osteogenic spheroid was beginning to wrap around the chondrogenic spheroid at this later timepoint.

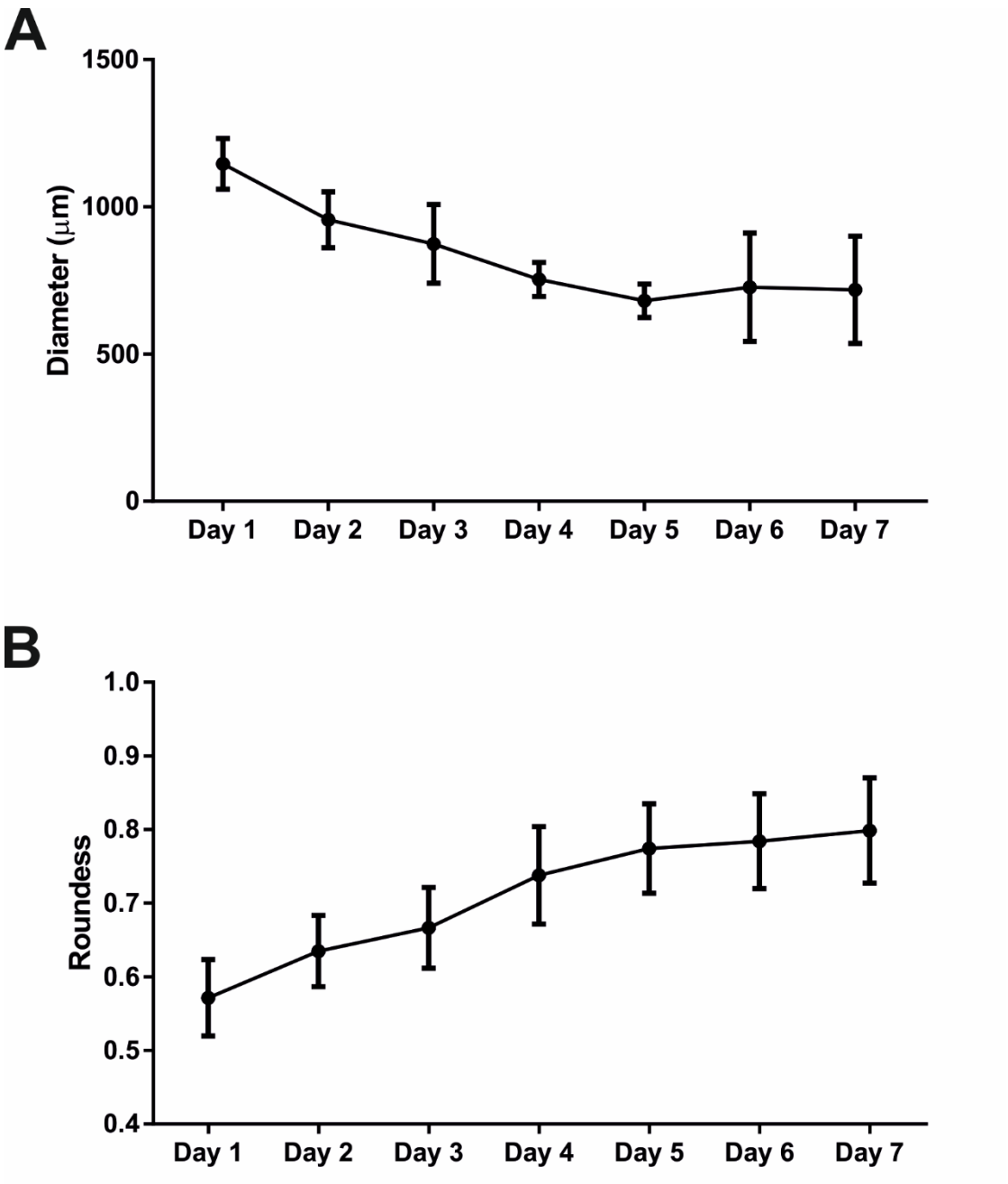

Figure 6.4.12: Shape analysis of Y101 osteogenic + chondrogenic spheroids

Brightfield images of Y101 osteogenic + chondrogenic spheroids were taken and analysed for diameter (A) and roundness (B) using ImageJ. The decrease in diameter and increase in roundness would suggest the spheroids are combining and merging in culture. Values = mean ± SD, n=6 (n=5 for days 6 and 7)

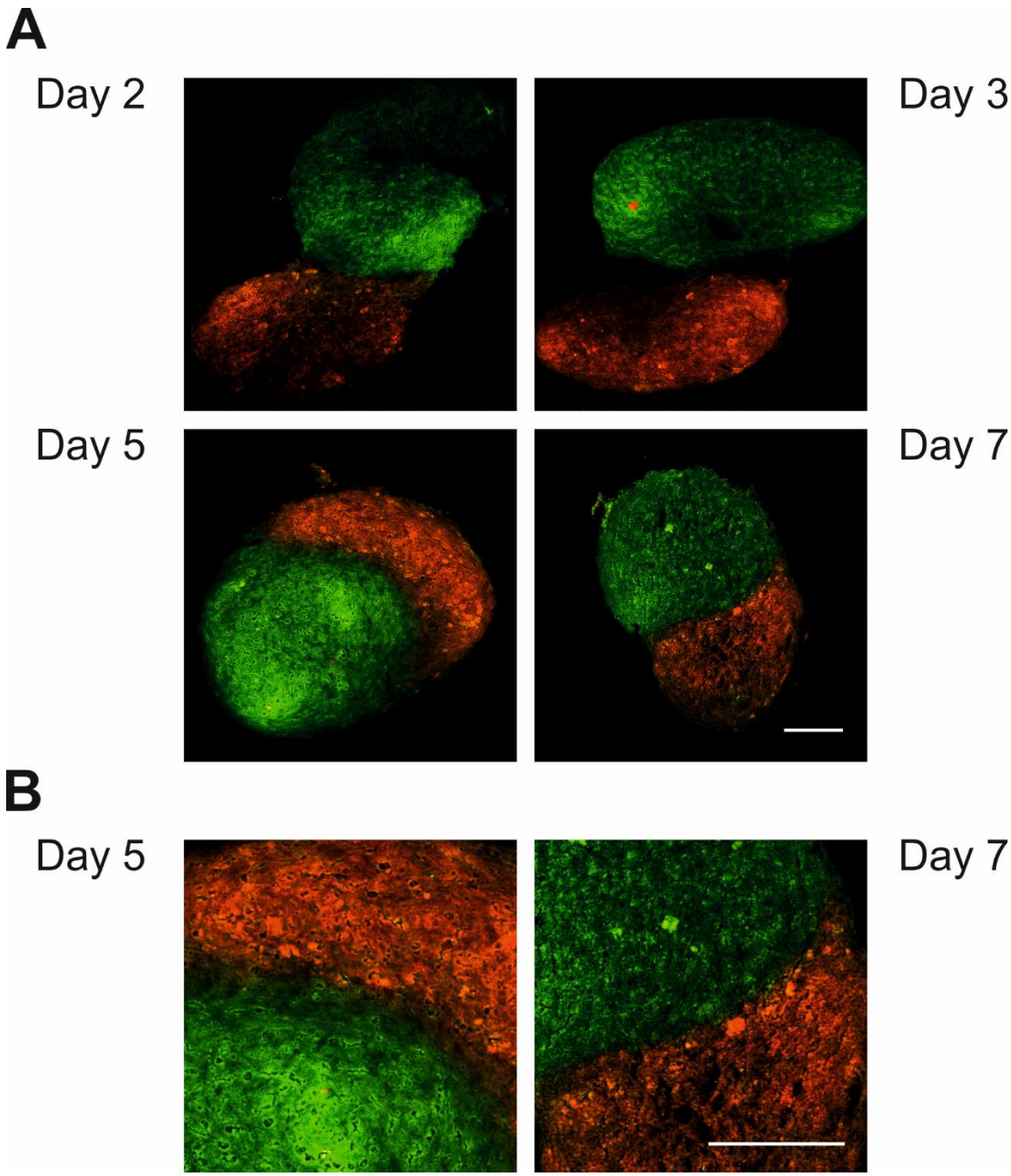

Figure 6.4.13: Fluorescent microscopy of sectioned Y101 hTERT MSC osteogenic + chondrogenic spheroids.

Fluorescent Images were taken of sections of Y101 hTERT MSCs osteogenic + chondrogenic spheroids to observe internal organisation (A). The osteochondral interface where the two cell types meet and could interact are magnified for the later timepoints (B). Osteogenic spheroids labelled red and chondrogenic spheroids labelled green. Scale bar = 200µm

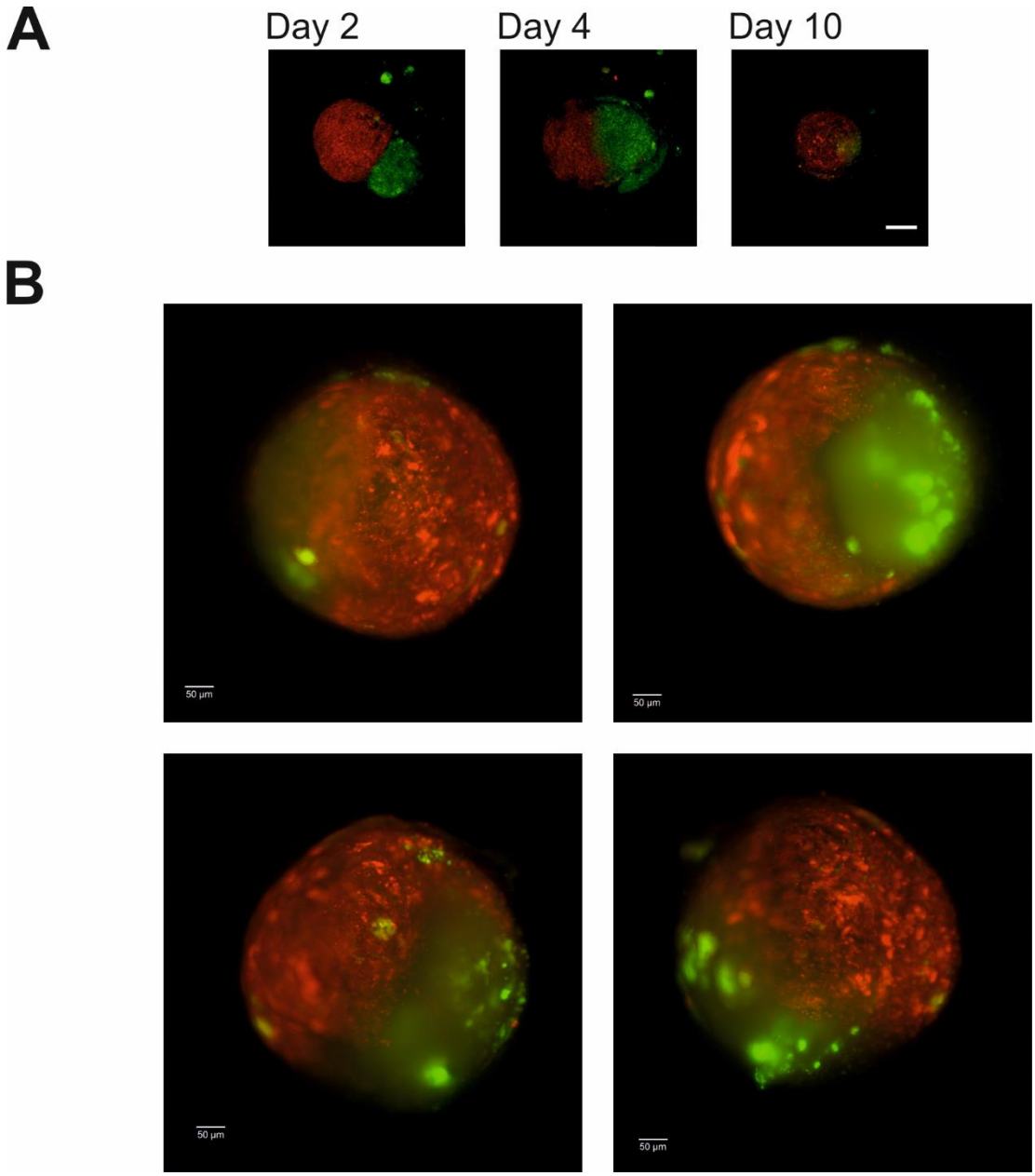

Figure 6.4.14: Fluorescent microscopy using both a multiphoton and a lightsheet microscpe to image Y101 hTERT MSC osteogenic + chondrogenic spheroids.

Fluorescent images were taken of osteogenic (red) + chondrogenic (green) spheroids formed from Y101 hTERT MSCs using either a multiphoton microscope (A) or a lightsheet microscope to observe spheroid merging at later timepoints. Lighsheet images were taken 10 days post spheroid combination with two individual spheroids imaged twice at 0° (left panels) and at 180° (right panels). Scale bar = 200µm (A) or 50µm (B)

6.4.3 Combining an osteogenic spheroid and chondrogenic suspension formed from pre-differentiated Y201 hTERT MSCs results in lateral self-organisation

Currently neither of the tested spheroid models were compatible with the Y201 hTERT MSCs as the chondrogenic cells appeared to have difficulties forming reliable and consistent individual spheroids in culture. However, the osteogenic spheroids consistently formed. It was therefore decided to add the chondrogenic cells as a suspension to a pre-formed osteogenic spheroid (Figure 6.4.15). This could allow for the formation of an osteochondral interface between the two cell types if the chondrogenic cells interact with the osteogenic spheroid.

Figure 6.4.16 shows a timecourse of this "osteogenic spheroid + chondrogenic suspension" model beginning 24 hours after the chondrogenic suspension had been added to the well. At day 1 the chondrogenic suspension very clearly is making interactions with the osteogenic spheroid, with the suspension surrounding the spheroid. At later timepoints though, the resulting spheroid appears to show self-organisation with two distinct regions observable, one red and one green, not unlike the osteogenic + chondrogenic spheroid model described above to in this chapter.

To determine if the self-organisation was also observable on the inside of the resultant spheroid, the osteogenic spheroid + chondrogenic suspension spheroids were sectioned and the sections imaged (Figure 6.4.17A). Sections were first taken at day 2 to allow for the osteogenic spheroid + chondrogenic suspension to form a stable interaction that might last throughout the sectioning process. This again indicated there was a level of self-organisation present, as distinct red and green regions were observable. The sections also appeared to have a green outline throughout the timecourse, which maybe as a result of the chondrogenic suspension surrounding the osteogenic spheroid. An osteochondral interface was clearly seen in each timepount, although perhaps not as well defined as the oteogenic + chondrogenic spheroid interface observed earlier, and has been magnified and presented in Figure 6.4.17B.

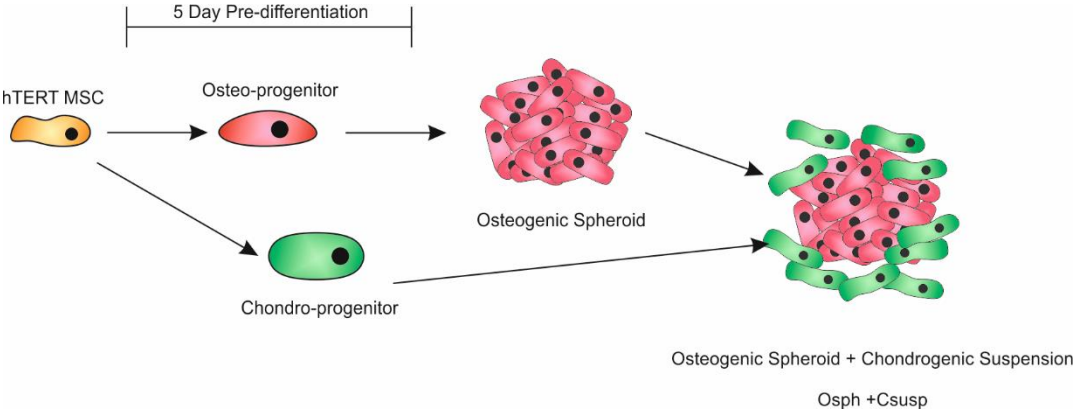

Figure 6.4.15: Schematic overview of osteogenic spheroid + chondrogenic suspension model

Y201 hTERT MSCs are differentiated for 5 days into either osteogenic progenitors or chondrogenic progenitors, with chondrogenic induction occurring 24 hours after osteogenic induction. Osteogenic cells are then labelled in red and induced to form spheroids. 24 hours post spheroid formation, chondrogenic cells are labelled green and added to the osteogenic spheroid.

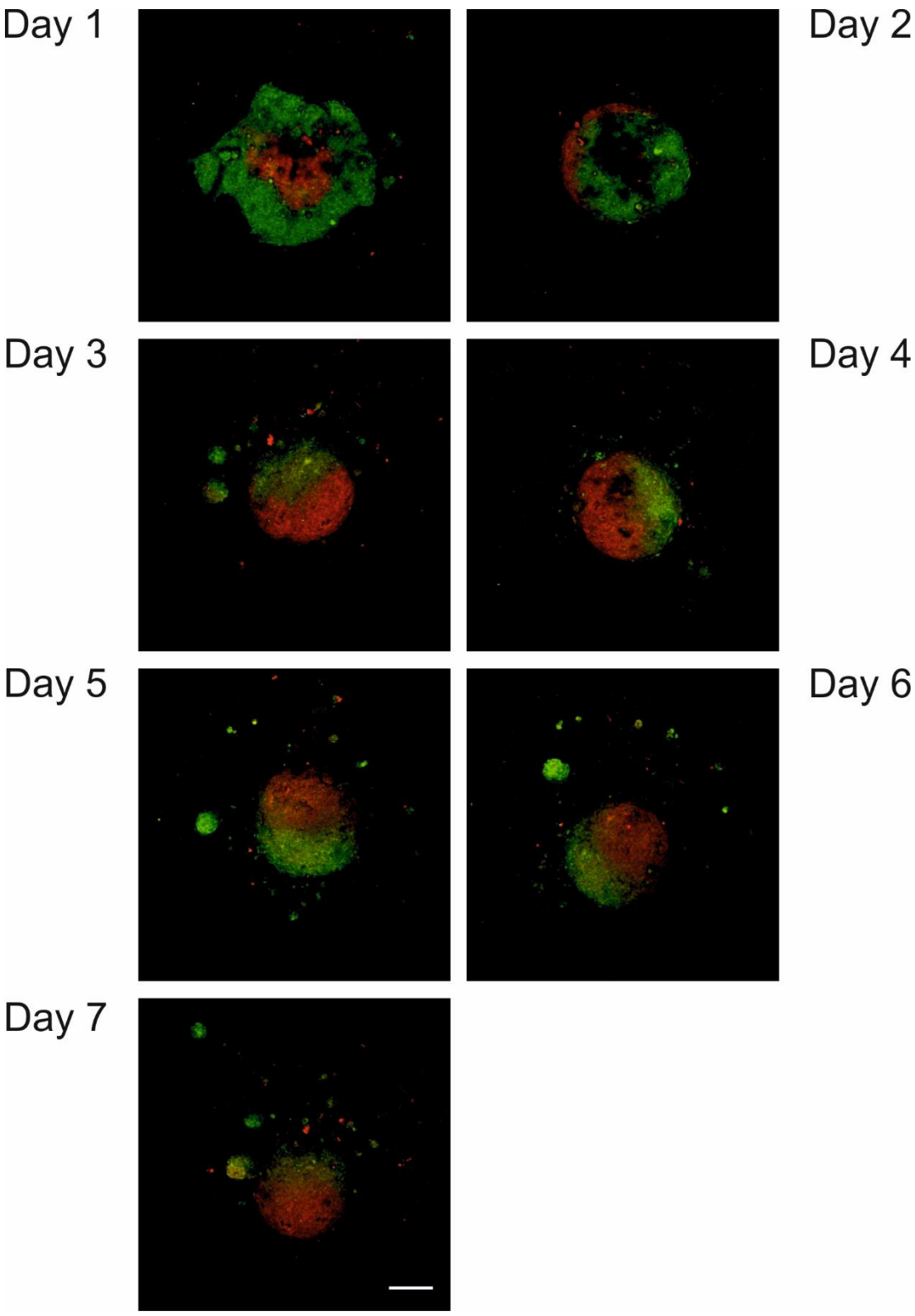

Figure 6.4.16: Fluorescent microscopy of osteogenic spheroids + chondrogenic suspension

Chondrogenic (green) suspension is added 24 hours post osteogenic (red) spheroid formation and z-stack fluorescent images taken 48 hours post spheroid formation to observe interactions between the osteogenic spheroid and chondrogenic suspension. Scale bar = 200µm

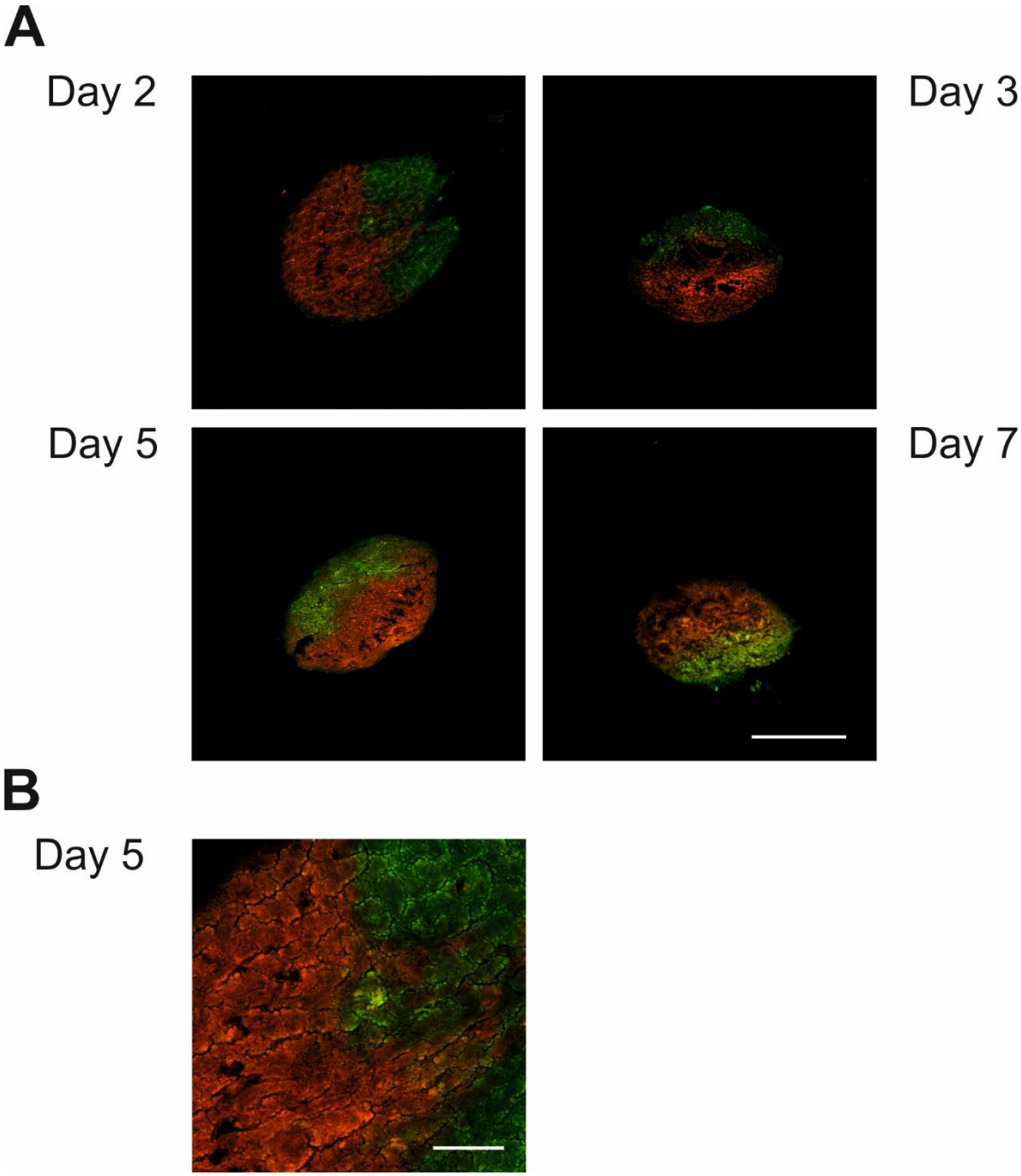

Figure 6.4.17: Fluorescent microscopy of sectioned Y201 hTERT MSC osteogenic spheroid + chondrogenic suspension model.

Fluorescent Images were taken of sections of Y201 hTERT MSCs osteogenic spheroids + chondrogenic suspension to observe internal organisation (A). An osteochondral interface where the two cell types meet and could interact is magnified (B). Osteogenic spheroids labelled red and chondrogenic suspension labelled green. Scale bar = 200µm

6.4.4 Combining CRISPR/Cas9 with 3D spheroid models – analysis of FGFR3-KO hTERT MSC spheroids

The aim of this study was to generate a spheroid model that could be used to study CRISPR/Cas9 modified hTERT MSCs in a 3D environment. The FGFR3-KO hTERT MSCs had a clear distinctive phenotype, described in Chapter 5, and presented with very little differentiation capabilities. It was therefore decided to determine how these phenotypic alterations would affect cell behaviour in a 3D osteogenic/chondrogenic spheroid model.

6.4.4.1 FGFR3-KO hTERT MSCs form basal spheroids with similar behaviours to WT hTERT MSCs but are also able to form both osteogenic and chondrogenic spheroids

Initially, the FGFR3-KO hTERT MSCs were induced to form basal spheroids, without any differentiation cues, and compared to the Y201 hTERT MSCs (referred to as WT hTERT MSCs). This would confirm that the FGFR3-KO hTERT MSCs were able to form spheroids and determine whether the increased proliferative/migratory capacities would impact on spheroid formation and behaviour. Figure 6.4.18 shows brightfield images of a timecourse analysing FGFR3-KO hTERT MSC basal spheroids and comparing them to WT hTERT MSC spheroids. FGFR3-KO hTERT MSCs formed basal spheroids successfully and reliably in each case. The spheroids also appeared to behave similarly to the WT hTERT MSCS as similar spheroid shapes were formed and the diameter appeared to reduce with time in culture. This was quantified and is summarised in Figure 6.4.19. The reduction in diameter of both spheroid types seemed to peak around days 4 and 5 with both spheroid types reaching a similar minimum of diameter at this point.

-

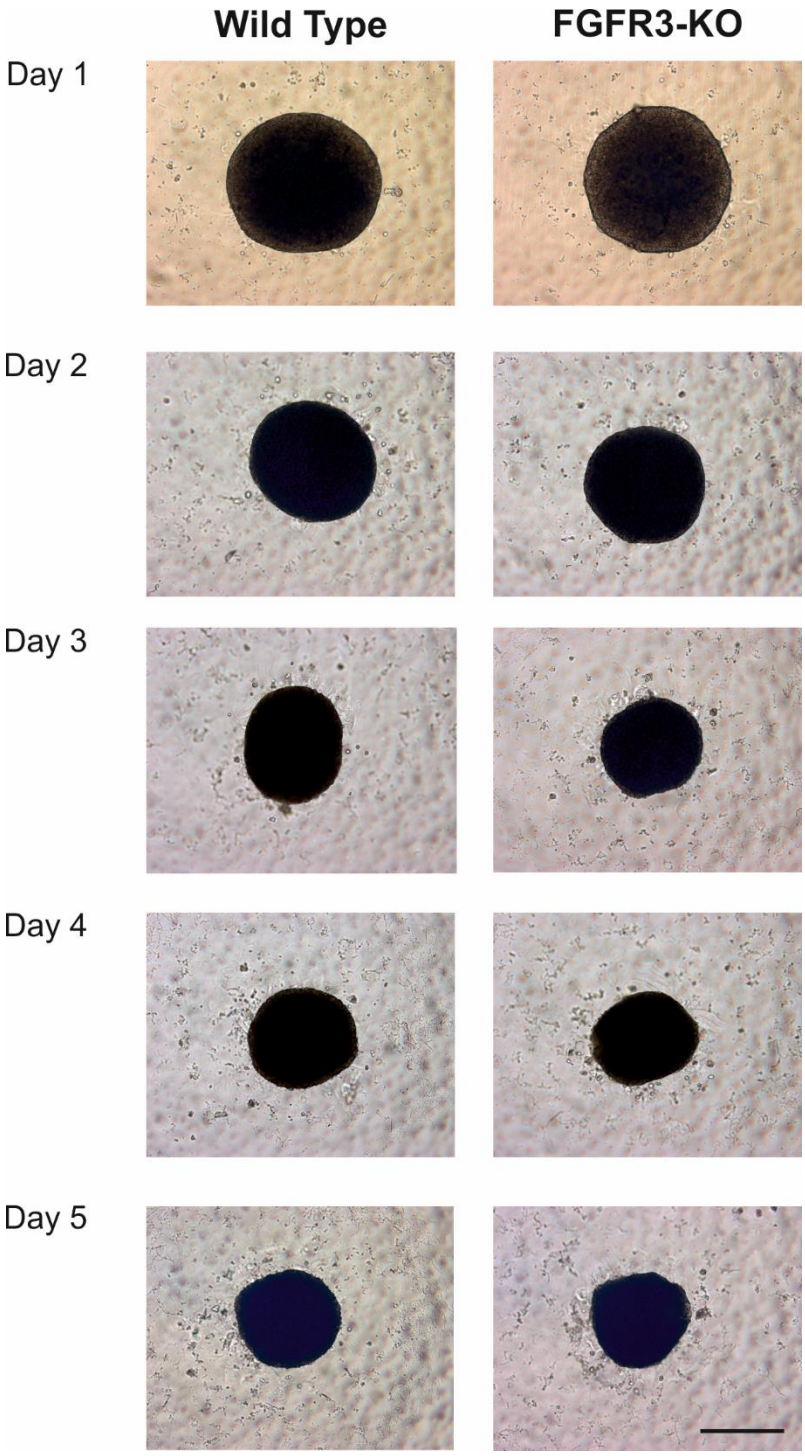

Figure 6.4.18: Comparison of basal spheroids formed from FGFR3-KO hTERT MSCs or WT hTERT MSCs

Brightfield images were taken of spheroids formed from 30,000 FGFR3-KO hTERT MSCs and compared to spheroids formed from WT hTERT MSCs. Scale bar = 200µm

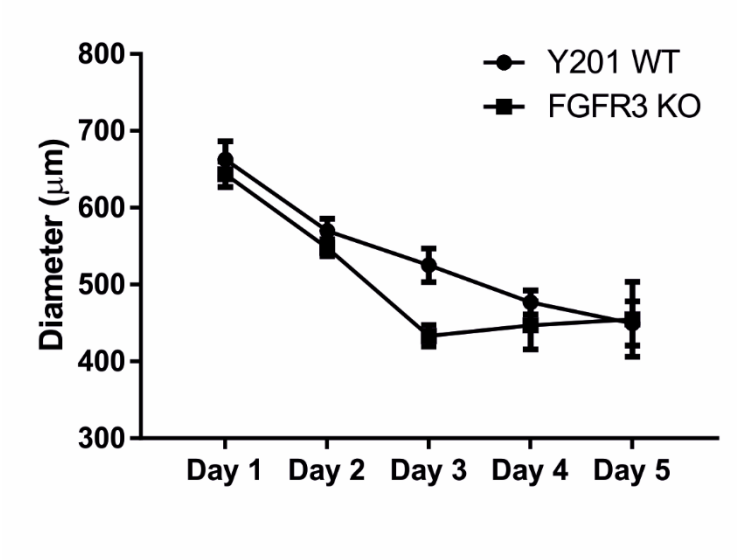

Figure 6.4.19: Size analysis of FGFR3-KO basal spheroids compared to WT hTERT MSC basal spheroids

Brightfield images of Y101 osteogenic + chondrogenic spheroids were taken and analysed for diameter using ImageJ. The FGFR3-KO hTERT MSCs seem to behave similarly to WT hTERT MSCs with spheroids shrinking overtime in culture. Values = mean ± SD, n=6

Finally before using the FGFR3-KO hTERT MSCs in the osteogenic spheroids + chondrogenic suspension model, the ability of the FGFR3-KO hTERT MSCs to form osteogenic and chondrogenic spheroids was tested. FGFR3-KO hTERT MSCs were differentiated down either the osteogenic or chondrogenic lineage and induced to form spheroids. 24 hours post spheroid induction, brightfield images were taken of the resultant spheroids (Figure 6.4.20). It was evident that the issues with formation of chondrogenic spheroids by the WT hTERT MSCs were not shared by the FGFR3-KO hTERT MSCs. The FGFR3-KO hTERT MSCs were able to form both osteogenic and chondrogenic spheroids successfully and reliably in every case. This may be due to the inability of the FGFR3-KO hTERT MSCs to differentiate effectively, therefore these spheroids may not be very different to the basal spheroids.

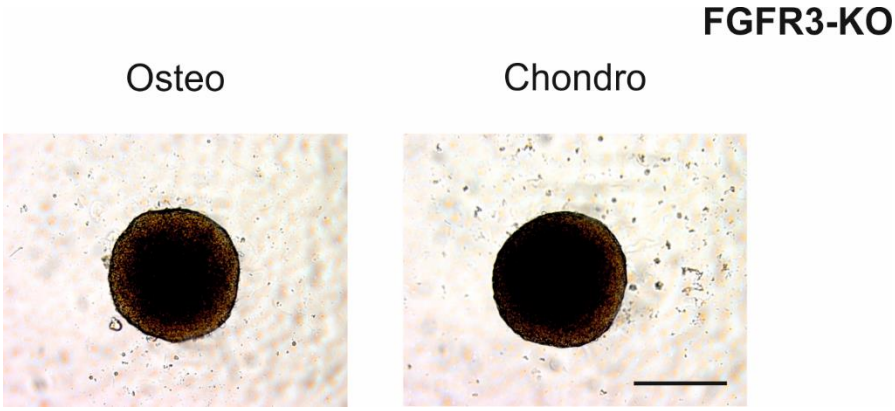

Figure 6.4.20: Brightfield images of osteogenic and chondrogenic spheroids formed from FGFR3-KO hTERT MSCs

FGFR3-KO hTERT MSCs were pre-differentiated for 5 days in either osteogenic or chondrogenic media before spheroid formation. Brightfield images were then taken of spheroids formed from 30,000 FGFR3-KO hTERT MSCs. Scale bar = 200µm

6.4.4.2 Osteogenic spheroid + chondrogenic suspension 3D model with FGFR3-KO hTERT MSCs results in apparent self-organisation but formation appears different to WT hTERT MSCs

After determining that the FGFR3-KO hTERT MSCs were capable of making spheroids, including osteogenic and chondrogenic spheroids, the osteogenic spheroid + chondrogenic suspension model was used to analyse these cells. A level of self-organisation was evident when the WT hTERT MSCs were used in this model, and since the FGFR3-KO hTERT MSCs are unable to differentiate it will be interesting to determine whether this self-organisation is still present. The FGFR3-KO hTERT MSCs were therefore pre-differentiated and the osteo-progenitors used to form an osteogenic spheroid, with the chondrogenic suspension added 24 hours post spheroid formation. Representative fluorescent images from this timecourse are presented in Figure 6.4.21. Initially, it would appear the FGFR3-KO hTERT MSCs are forming similar spheroids to the WT hTERT MSC. The chondrogenic suspension interacted with the osteogenic spheroid, and it appeared there was a level of self-organisation, particularly when the resulting spheroid is sectioned (Figure 6.4.21B). However, the combined spheroid + suspension did not appear to be shrinking and merging as observed with the WT hTERT MSCs (Figure 6.4.16). The diameter of the WT hTERT MSC spheroids decreases over time in culture whilst the roundness increases, but the FGFR3-KO hTERT MSCs appeared to maintain diameter and decrease slightly in roundness (Figure 6.4.22). Additionally, whereas the WT hTERT MSCs appeared to surround the osteogenic spheroid before self-organisation occurred, the FGFR3-KO hTERT MSCs appeared to attach to the osteogenic spheroid, giving the appearance of self-organisation. It was also noted that out of 25 spheroids formed in this way 4 failed to interact entirely, something which was never seen in the WT hTERT MSCs (results not shown). There appeared to be subtle differences between the behaviours of the WT hTERT MSCs and the FGFR3-KO hTERT MSCs in this osteochondral model.

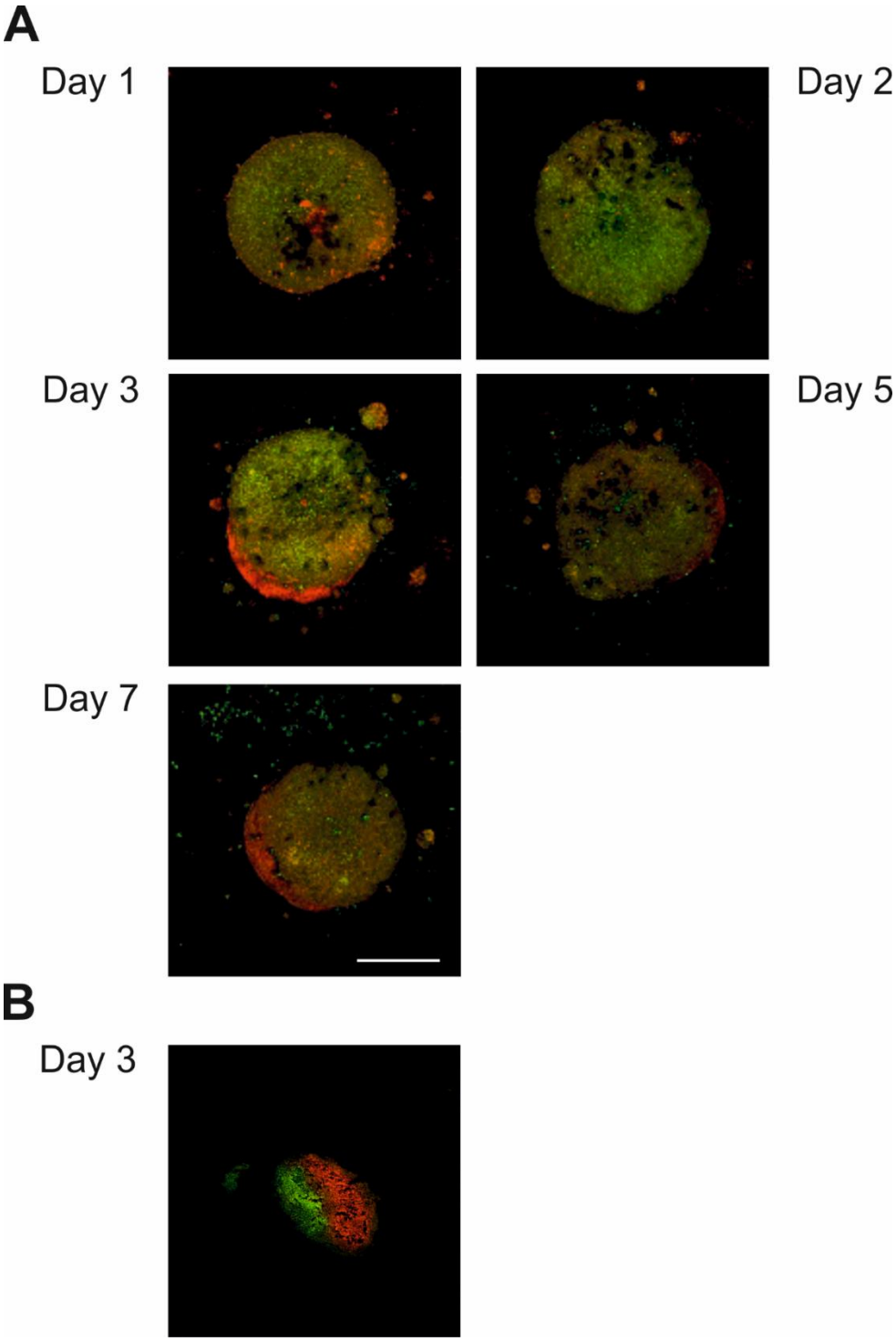

Figure 6.4.21: Timecourse of FGFR3-KO hTERT MSC osteogenic spheroid + chondrogenic suspension

Chondrogenic (green) suspension formed from pre-differentiated FGFR3-KO hTERT MSCs is added 24 hours post osteogenic (red) spheroid formation and z-stack fluorescent images taken 48 hours post spheroid formation to observe interactions between the osteogenic spheroid and chondrogenic suspension. Scale bar = 200µm (A) Sectional analysis of a day 3 spheroid + suspension revealing a defined osteochondral interface between the two cell types. (B)

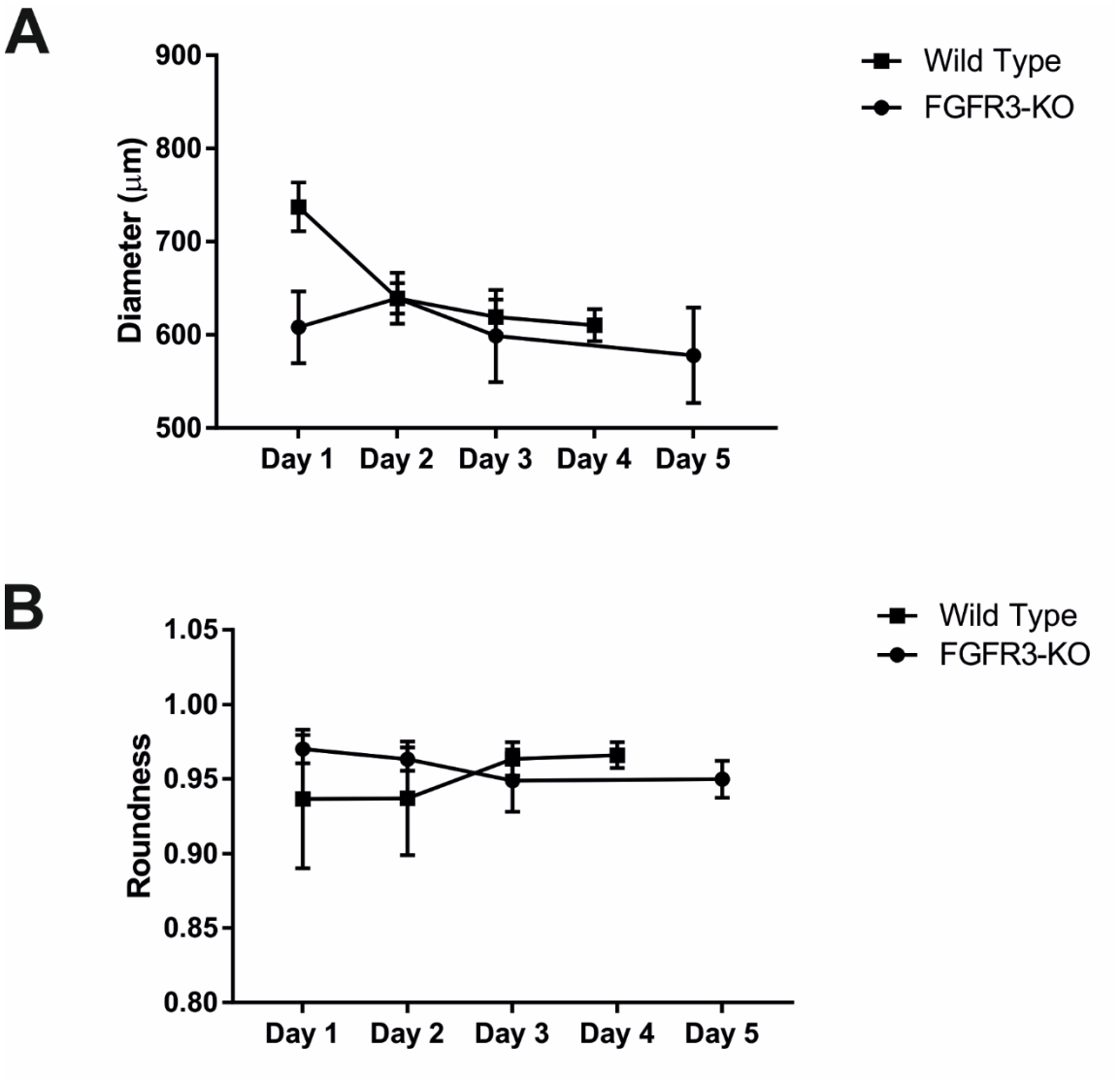

Figure 6.4.22: Shape analysis of WT and FGFR3-KO hTERT MSC osteogenic spheroid + chondrogenic suspension models

ImageJ was used to quantify the diameter (A) and roundness (B) of the WT and FGFR3-KO osteogenic spheroid + chondrogenic suspension models which were imaged using a brightfield microscope.

To examine further any differences between the FGFR3-KO hTERT MSCs and the WT hTERT MSCs in the osteogenic spheroid + chondrogenic suspension model, timelapses were set up to analyse the formation of the spheroids. After applying the fluorescently labelled chondrogenic suspension, the forming spheroids were imaged and analysed using the multi photon microscope, with images taken every 2 hours. Figure 6.4.23 shows still images taken of spheroids forming in this way, and the complete timelapse for three WT hTERT MSC spheroids and three FGFR3-KO hTERT MSC spheroids is supplied in Supplementary Videos 4-9. The WT hTERT chondrogenic suspension always appears to interact with the osteogenic spheroid as two out of three WT hTERT MSC chondrogenic suspensions entirely wrap the osteogenic spheroid, this behaviour was also observed in the day 1 still image in Figure 6.4.16. However, despite the FGFR3-KO hTERT chondrogenic suspension shrinking over time, it does not appear to always interact with the osteogenic spheroid and never completely surrounds the spheroid in the same manner as the WT hTERT chondrogenic suspension.

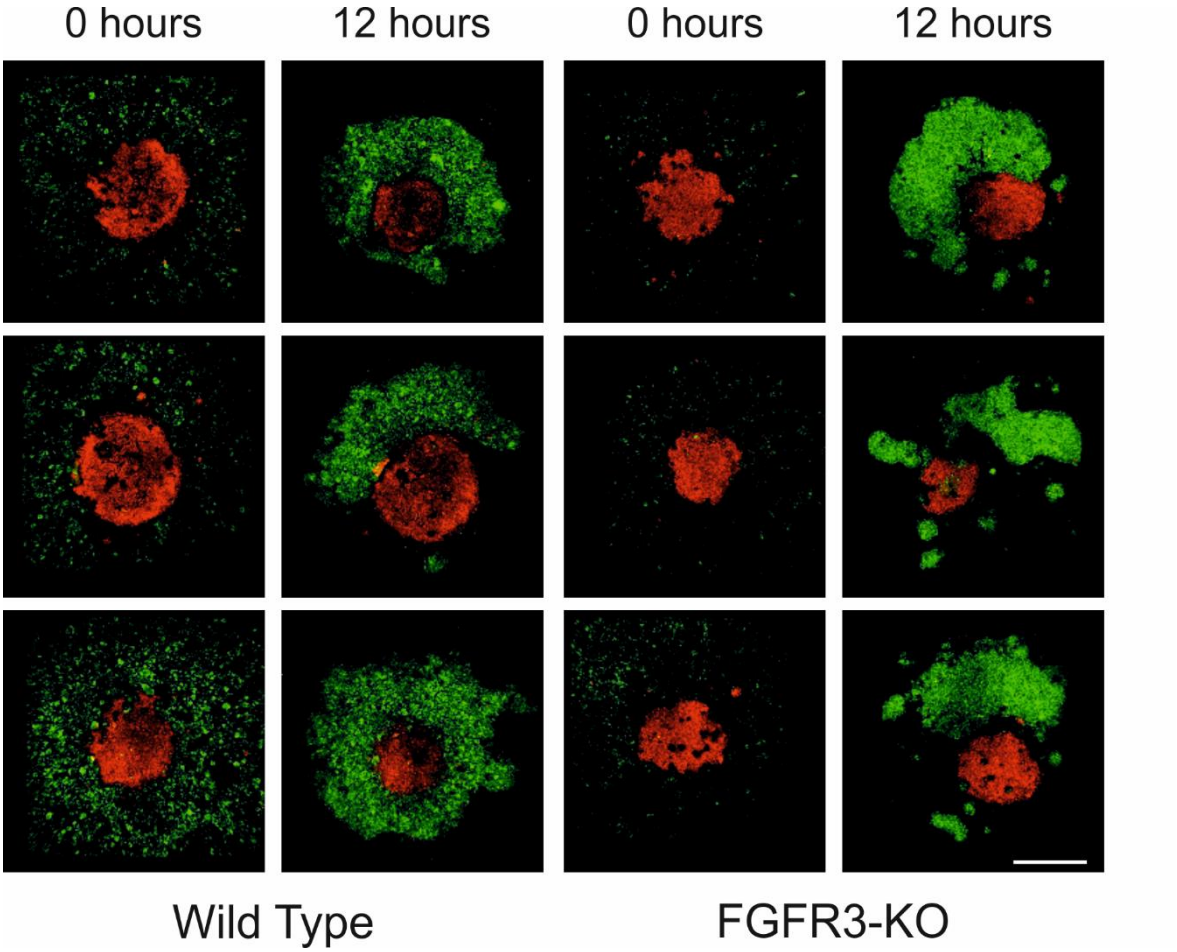

Figure 6.4.23: Still frames from timelapse imaging of WT and FGFR3-KO hTERT MSC osteogenic spheroid + chondrogenic suspension models

Fluorescent imaging of WT (left panels) and FGFR3-KO (right panels) models during timelapse imaging of interaction of chondrogenic suspension (green) with osteogenic spheroids (red). After 12 hours it appeared the WT hTERT MSC chondrogenic suspension was interacting with the osteogenic spheroid in each instance, whereas this did not appear to be the case with the FGFR3-KO hTERT MSC cells. Scale bar = 200µm

6.5 Discussion

The aim of this chapter was to develop a 3D spheroid model suitable for analysing the effects of mutations generated by CRISPR/Cas9 genome editing, on an osteochondral interface. To this end multiple 3D spheroid models were formed from pre-differentiated osteogenic and chondrogenic hTERT MSCs and the resulting osteochondral interface examined.

6.5.1 Length of pre-differentiation of hTERT MSCs impacts spheroid formation

It was observed that the pre-differentiation of hTERT MSCs before spheroid assembly can impact on spheroid formation, which may be due to the laying down of ECM by MSCs during differentiation. This was further evidenced by the ability of the FGFR3-KO hTERT MSCs to form chondrogenic spheroids after pre-differentiation whereas the WT Y201 hTERT MSCs could not. The FGFR3-KO hTERT MSCs have a very limited capacity for differentiation and therefore not likely to be laying down the same amounts of ECM as WT cells, particularly as FGFR3 has previously been linked to the matrix production of chondrocytes (Davidson et al., 2005). The formation of spheroids using different cell types has been shown to be dependent on cell-cell interactions via cadherins, whereas the actomyosin skeleton is critical for spheroid compaction (Tsai et al., 2015; Yeh et al., 2012; Lee et al., 2012). The FGFR3-KO hTERT MSCs were able to form spheroids, which compacted successfully, despite the changes observed in the actin cytoskeleton previously. It has also been shown that MSCs lifted thermally before spheroid formation accelerates the process in comparison to cells that had been trypsinised (Kim and Ma, 2013). The rate of spheroid formation was not analysed for the basal spheroids, however it would be interesting to determine whether this was decreased in the FGFR3-KO hTERT MSCs, as RNA-seq previously demonstrated a decrease in ECM related proteins.

6.5.2 hTERT MSC spheroids can be used for analysis of osteochondral interface without a scaffold or matrix

Furthermore, the models developed in this chapter do not rely on a scaffold or other matrix, but are constructed solely from cells. The addition of a scaffold adds increased complexity to an experiment, and often multiple scaffold materials need to be refined to stimulate the desired differentiation and cellular behaviours. Many studies analysing the osteochondral interface rely on scaffolds and are typically focussed on the creation of grafts for the treatment of osteoarthritis and other diseases which damage the osteochondral interface (Cheng et al., 2011; Khanarian et al., 2012; Nukavarapu and Dorcemus, 2013). Spheroid models have also been implanted into an osteochondral defect, with subsequent repair as a result (Murata et al., 2015). This is likely as a result of the spheroid environment, which has been shown to improve MSC survival and trophic

factor secretion leading to a preservation of osteogenic capacity (Murphy et al., 2016). The results in this chapter give further evidence of the ability to study the osteochondral interface without the need of a scaffold providing a simple model for analysis of the osteochondral interface. It would be interesting to further this work by extending the periods the spheroids were cultured for, and to determine whether Collagen X (a marker of chondrocyte hypertrophy) and deposits of calcium can be found how these compared with previously published models.

6.5.3 Applying the differential adhesion hypothesis to hTERT MSC spheroids

Cell population arrangements from within a mixture of cell types have been proposed to behave similarly to a mixture of immiscibly liquids through the differential adhesion hypothesis (DAH). This hypothesis states that when two liquids (or mobile cells) with varying surface tension are mixed, they will spontaneously arrange to maximise mutual adhesive bonding (Steinberg, 2007). This thermodynamic principle was first attributed to the spontaneous arrangement of tissues developing from ESCs. MSCs share these attributes with ESCs, both being a liquid-like cell and able to self-assemble into spheroids. The DAH states a cell aggregate with a lower surface tension will envelope an aggregate of a higher surface tension and the surface tension of an aggregate has been shown to be linearly correlated with cell surface cadherin expression (Foty and Steinberg, 2005). When Y101 hTERT MSCs were analysed using the osteogenic + chondrogenic spheroid model, the osteogenic spheroid was seen to overlap and engulf the chondrogenic spheroid, suggesting in this instance that, according to the DAH, the osteogenic spheroid had the lower surface tension. It would be interesting to determine whether if the osteogenic spheroid + chondrogenic suspension model, used with the Y201 hTERT MSCs, also displayed this behaviour if maintained for longer periods in culture. This could then be compared to the FGFR3-KO hTERT MSCs, where very little self-organisation seemed to be present in this 3D model, which would suggest the cadherin expression profiles of the differentiated FGFR3-KO hTERT MSCs were dissimilar to those of the differentiated WT cells.

6.5.4 Time lapse imaging of spheroid formation can provide key insights into cellular phenotypes

It was initially unclear whether the FGFR3-KO hTERT MSCs behaved similarly to the WT hTERT MSCs when analysed in the osteogenic spheroid + chondrogenic suspension model as both cell types formed an osteochondral interface through apparent self-organisation. However, by analysing the formation of the spheroid through time lapse imaging, it became apparent that this may not be the case. This experiment highlights the importance of spheroid formation as well as the behaviours of the formed spheroid. Studies examining the use of 3D culture rarely examine the formation of the

spheroid, but as previously mentioned, spheroid formation gives insight into the cell surface protein expression on the cells in addition to the presence and composition of ECM (Kim and Ma, 2013). Additionally, it was observed that the FGFR3-KO hTERT chondrogenic suspension does not appear to interact with the osteogenic spheroid in every instance, whereas the WT hTERT chondrogenic suspension does.

6.5.5 Concluding Remarks

Overall the results in this chapter demonstrate the possibility of studying the osteochondral interface with a cellular model. The model can be altered depending on whether the formation of the interface is of interest or not as it was found that an osteochondral interface can be created in a number of ways, whether by lateral self-organisation over time, or a forced interaction through spheroid combination. This creates a number of potential analyses possible from one technique. Additionally, the methods developed in this chapter require minimal numbers of cells and a short pre-differentiation step prior to a simple spheroid formation. Combining these 3D spheroid models with Cell Tracker labelling allows for the analysis of the formation of the osteochondral interface over time and space. Collectively, the results from this chapter indicate it is possible to create an osteochondral interface within a spheroid, suitable for the analysis of WT and GM hTERT MSC behaviours.

Chapter 7 : Discussion

The work presented in this thesis provides a complete methodology for the use of the CRISPR/Cas9 genome editing system with immortalised MSC cell lines. Immortalised MSCs were genetically modified in this study to demonstrate the ability to generate isogenic human disease cell line models. Proof of concept was demonstrated using Runx2 and Sox9, two critical transcription factors of MSC differentiation and both the genotype and phenotype of cells was analysed. The CRISPR/Cas9 system was then subsequently used to generate an FGFR3-KO hTERT MSC line which models CATSHL syndrome in humans. This cell line was then analysed providing novel insights into the cellular mechanisms behind this syndrome. Typically, cells are cultured *in vitro* in a 2D monolayer and supplemented with serum containing media. Finally, alternative methods in studying hTERT MSCs *in vitro* were explored by using pre-differentiated cells in a 3D self-forming spheroid model to analyse an osteochondral interface. Additionally, serum was severely reduced in media and the resultant cellular behaviours analysed. This provides insight into how the study of human cell line models may be improved to better represent *in vivo* cellular behaviour.

7.1.1 The use of genome edited MSCS for skeletal disease modelling

The study of human disease, focussing on those with a genetic element, typically relies on the identification of the causative gene mutation. Experimental modelling, be it with animal models or human cells, allows for the identification of underlying cellular and molecular mechanisms of the disease. It also enables the development of therapeutics in order to treat diseases. The conservation of the genome between vertebrates allows for the modelling of human diseases in a number of animal models, and these have been (and remain to be) an invaluable tool in the understanding of human disease. However, there are a number of reasons why it is advantageous for biomedical research to be conducted in a human setting. Stem cells provide the ability to study diseases in this context, with an extended capacity for self-renewal and an ability to differentiate into a multitude of lineages. The combination of stem cells with engineered nucleases, such as the CRISPR/Cas9 system, would appear to be the gold standard for creating disease relevant cell lines for the modelling of human disease. Although many studies have detailed the use of the CRISPR/Cas9 system with ESC cell lines and iPSCs, no studies could be found detailing the use of CRISPR/Cas9 with MSCs (Ebert et al., 2012; Avior et al., 2016). This is likely due to either the reduced differentiation potential of MSCs, compared to ESCs and iPSCs, or due to the requirement of an

immortalised cell line. Nevertheless, the creation of GM MSCs would allow greater insight into the impact of skeletal diseases on native bone marrow cells. Additionally, the maintenance of immortalised MSCs is far simpler than that of ESCs/iPSCs and therefore may prove a more accessible technology to many laboratories.

7.1.2 Proof of concept – using CRISPR/Cas9 to knock out master transcription regulators in hTERT MSCs

The work summarised in Chapter 4 details a reproducible method for the genetic modification of the hTERT MSCs. In particular, the FGFR3 modified cells that were produced displayed specific traits indicative that the resultant phenotypes are likely not to be a result of the CRISPR/Cas9 genome editing process, but caused as a result of the modifications to the relevant genes. Both the Runx2 and Sox9 targeted hTERT MSCs require further evidence to confirm their knockout status but each demonstrated alterations in their proliferation and differentiation capacities as shown in section 4.4. These proof of concept studies are the first of their kind to demonstrate the possibility of using CRISPR/Cas9 in immortalised MSCs. Despite Runx2 being attributed as the master transcription regulator of osteogenesis, it was found that each of the clonal lines developed increased calcium deposition in response to osteogenic cues. It is known that Runx2 is less crucial in committed osteoblasts, but in this study it appeared Runx2 may also be less critical in adult progenitor stem cells (Takarada et al., 2013). In addition, the *in vitro* differentiation of MSCs uses chemical stimuli not present *in vivo*, which instead relies on the stimulation of differentiation via morphogens and other factors. Whether chemical stimuli such as these are able to positively influence the osteogenic differentiation of MSCs without the presence of Runx2, perhaps by the stimulation of signalling components critical to differentiation such as ALP, would be an interesting hypothesis to explore further.

7.1.3 Creating an *in vitro* skeletal disease model with hTERT MSCs and CRISPR/Cas9

The study of skeletal disease typically occurs within animal models, particularly in mice as evidenced in section 1.7 where an overview of some of the more prevalent genetic disease indicated a lack of human cellular models. It was also apparent that the consideration of the role of MSCs in the development of various skeletal diseases and their pathophysiology was often neglected. Studies of human cells typically focussed on somatic cell types, namely osteoblasts, osteoclasts and chondrocytes. Yet, the bone and bone marrow are inextricably linked and share vasculature (Del Fattore et al., 2010). It is likely that diseases of the skeleton will also result in alterations to MSC behaviour, and studies into these changes may grant better understanding of the cellular and molecular mechanisms of the disease.

Results presented in Chapter 5 demonstrate the power of creating a disease model using this system in MSCs, whereby FGFR3-KO hTERT MSCs were generated as a disease model for CATSHL syndrome. This syndrome results in extensively overgrown bones, those formed by endochondral ossification, and expanded hypertrophic growth plates (Toydemir et al., 2006; Escobar et al., 2016). Many studies have demonstrated the effects of MSCs on chondrocytes and the role of FGFR3 in the proliferation/differentiation of chondrocytes, but to my knowledge, no studies have been conducted on the role of FGFR3 in MSCs (Sahni et al., 1999; Benoist-Lasselin et al., 2007). The results presented in Chapter 5 demonstrate unequivocally that FGFR3 plays a critical role in MSC biology, with functions in almost every behaviour of MSCs, including migration, differentiation and proliferation. Overall, it would appear the behaviour of MSCs is shifted towards an increased proliferative and migratory phenotype at the expense of differentiation.

7.1.4 FGFR3 has a potential role in MSC migration

Furthermore, the development of the FGFR3-KO hTERT MSCs created implications for the role of FGFR3 in skeletal tissues that had not previously been considered. Namely, that of migration. Although FGFRs have been previously implicated in cellular migration of other cell types, as of writing, there have been no studies analysing the effects of FGFR3 (Xian et al., 2007; Nguyen et al., 2013). And yet, in section 5.4.8 it is apparent that MSC migration is directly linked to FGFR3. Namely, the process of collective migration appears to be affected. Collective migration is a critical process for tissue morphogenesis in development and shares common basic mechanisms with single cell migration in that both the actin cytoskeleton and organisation of membrane trafficking are polarised, and the underlying molecules driving polarisation feature in particular RAC and CDC42 (Rørth, 2009). However, collective migration relies on the leader cells interactions with the ECM and cell-cell interactions with follower cells to drive migration in a single direction (reviewed in Mayor and Etienne-Manneville, 2016). The FGFR3-KO hTERT MSCs were repeatedly demonstrated, by RNA-seq summarised in 5.4.6, to have downregulated transcripts in pathways involving ECM interactions, cell-cell interactions and focal adhesions. Additionally, it was found that transcripts from the PI3K pathway were enriched in the FGFR3-KO hTERT MSCs, and publications have previously shown that Ras and Rho family GTPases influence the activity of each other in pathways not fully understood. This would suggest that the dysregulation of FGFR3 signalling has increased PI3K signalling which is activating the GTPases required for cellular migration. However, without the directional signalling from interactions with the ECM, in addition to the increased expression of MMPs degrading the ECM, and without the typical cell-cell interactions seen in collective migration, the FGFR3-KO hTERT MSCs independently migrate. Without this regulation of migration, it would

appear that bone morphogenesis is dysregulated thus leading to the overgrowth of long bones observed in CATSHL syndrome.

7.1.5 The impact of removing FGFR3 on FGF signalling

The observed apparent increase in PI3K signalling yet decrease in MAPK signalling, would at first appear unusual as one might predict that all signalling through FGFR3 is decreased. However, the FGF signalling family is pleiotropic with many of the FGF ligands able to bind multiple receptors, albeit at differing affinities (Zhang et al., 2006c; Ornitz and Itoh, 2015). The removal of FGFR3, despite no significant differences in FGFR expression visible as a result of the knockout, would still alter the FGFR landscape. FGF ligands, such as FGF18, which show preferential binding to the splice variants of FGFR3 would instead be activating other receptors. Additionally, since the publication of the crystal structure of a homodimer of FGFR1 with FGF2 bound, it has been realised that receptor-receptor interactions thermodynamically allow for the heterodimerisation of FGFR receptors (Plotnikov et al., 1999). This has been further analysed using Fluorescence Resonance Energy Transfer (FRET), which again demonstrated the formation of FGFR heterodimers. The removal of FGFR3 therefore not only impacts on the signals generated by FGFR3 homodimers, but the signals received by these heterodimers as well (Piccolo et al., 2016). With this predicted difference in the output signals generated through the FGF signalling pathway in the absence of FGFR3, it might be postulated that the cytosolic signalling output of the family as a whole has been altered thus resulting in increased signalling through the PI3K pathway but a decreased signalling through the MAPK pathway.

7.1.6 FGFR3-KO hTERT MSC phenotype resembles a cancerous cell

The phenotype of the FGFR3-KO hTERT MSCs resembles that of a cancerous cell in many ways, with an increased affinity for both proliferation and migration. Additionally, a number of transcripts were found to be upregulated that have previously been identified as important in carcinogenesis including both protein coding and non-coding RNAs. FGFR3 has been linked to cancers previously acting as both an oncogene and a tumour suppressor depending on the cellular origin (Lafitte et al., 2013). Further studies would be required to determine whether the FGFR3-KO hTERT MSCs were cancerous, or if in fact less mutations would be required for the cells to become cancerous. It would also be interesting to note whether FGFR3 inactivation mutations resulted in a predisposition to cancerous growths both in mouse and in human. No studies were performed in this thesis to determine whether the FGFR3-KO hTERT MSCs were cancerous, as no *in vivo* work was undertaken.

7.1.7 Skeletal disease modelling in 3D *in vitro* spheroid models

The combination of genetically modified hTERT MSCs and 3D spheroid models adds a further layer of complexity to the study, and is an attractive research option. The advantages of working *in vitro*, with cell lines and established differentiation protocols, are accessible yet the complexity of *in vivo* tissues can also be mimicked. The results in Chapter 6 demonstrate a number of 3D spheroid models suitable for the analysis of both osteogenic and chondrogenic differentiating MSCs and a defined osteochondral interface to analyse interactions between the cell types. Furthermore, these 3D models were also shown to be suitable for the study of GM-hTERT MSCs and revealed yet more cellular mechanisms that could not be gleamed with *in vivo* data. It was shown in section 6.4.4, that whilst FGFR3-KO hTERT MSCs were able to form the various spheroids tested, the formation of these osteochondral models appeared to differ to that of the WT hTERT MSCs. Combined with the knowledge from RNA-seq data that transcripts from pathways involving ECM interactions and cell-cell signalling pathways these processes are critical for signalling between cells and their environment, and although the molecular mechanisms converting the mechanical stimuli experienced within the bone to biochemical signals are unknown, it can be postulated that signalling within the environment of the cell is crucial (Tamura et al., 2001; Biggs and Dalby, 2010; Eleniste and Bruzzaniti, 2012). I would propose that the loss of FGFR3 function has severely hampered the ability of MSCs to respond to signals from other cells and their environment leading to cells no longer acting synonymously. It would be interesting to determine whether these findings transpire to also be true within osteoblasts and chondrocytes thus leading to the decoupling of cell signalling within a tissue, potentially indicating that signalling across the osteochondral interface is also impacted with reduced FGFR3 signalling.

7.1.8 Limitations of *in vitro* modelling with regards to serum

Despite the benefits of studying human diseases in a human setting there are also a number of drawbacks due to research being performed *in vitro*. Firstly, the wide use of serum in culture as a supplementation for cell growth results in an undefined media that may not be the best buffer to replicate physiology. This should be a consideration during biomedical research due to the impact of serum on a multitude of cellular behaviours, for example in stem cells, serum is known to affect both proliferation and differentiation (Morris and Warburton, 1994; Tateishi et al., 2008; Gong et al., 2009). Results from Chapter 3 concur with this evaluation, as various properties of the hTERT MSCs were found to be altered when serum was reduced in culture conditions. Ideally, serum would be removed entirely and defined supplementation, such as BSA or ITS, would be used but it was not feasible to establish these culture conditions within the time frame of this thesis. Regardless, the hTERT MSCs did demonstrate a reduced proliferative capacity and increased osteogenic

capabilities. In fact, RNA-seq showed the metabolism of the cells had altered as a response, with cells upregulating a number of pathways relating to the metabolism of lipids. Indeed, this replicates the behaviour of osteoblasts *in vivo* as these cells require an almost constant energy supply, indicating the potential for the reduction of serum to create a culture condition that more directly replicates the conditions MSCs would exist in *in vivo* (Shapiro and Haselgrove, 1991). The recapitulation of physiological conditions *in vitro* allows for a more direct comparison of data gained *in vivo* compared to the traditional artificial culture methods typically used, both in regards to serum and 2D monolayer culture. The ability of cells to respond to environmental cues is a complex field but it is clear that to best understand human biology, *in vitro* culture conditions must be developed with biomimicry in mind. In this way, it is possible to develop increasingly effective cellular therapies due to our increased understanding of cell behaviour *in vivo.*

7.2 Future Directions

The work presented in this thesis demonstrates the proof-of-concept that the understanding of differentiation and regeneration of post-natal progenitor MSCs can be furthered by genome editing techniques targeting relevant genes. Furthermore, human skeletal diseases can be modelled using a combination of CRISPR/Cas9 and hTERT MSCs. It would be interesting to determine the effects of knocking out Runx2 and Sox9 on the formation and patterning observed with the osteochondral spheroid models. Particularly as the FGFR3-KO hTERT MSCs, which were unable to differentiate properly, displayed alterations in these models. The combination of the 3D spheroid models and the GM-hTERT MSCs adds a layer of complexity to the studies allowing for studies of interactions between cell types. It is well known that bone and cartilage tissues interact with each other and impact on differentiation of the tissues. The alteration of the signalling pathways and interactions as a result of various gene modifications could be determined using the osteochondral interface developed in this thesis. This work could be further developed by introducing vasculature into the osteochondral model perhaps using human umbilical vein endothelial cells (HUVECS) which have been previously shown to self-organise within MSC spheroids (Saleh et al., 2011a, 2011b).

The FGFR3-KO hTERT MSC line showed an alteration to the collective migration ability of these cells, potentially contributing to the overgrowth of bones seen in CATSHL syndrome. It would be beneficial to these studies to understand the impact of increased FGFR3 signalling, perhaps through inducing an activating mutation with CRISPR/Cas9, and how this impacts on the proliferation and migration of the hTERT MSCs. This could benefit our understanding of how the length of bones is determined and whether this process could be targeted to improve therapeutics for various skeletal diseases.

7.3 Concluding Remarks

The work in this thesis lends itself to an enormous potential now possible with the combination of hTERT MSCs with CRISPR/Cas9 genome editing, it would in theory be possible to use the methodology developed to edit almost any gene of interest. Yet, the study of human biology in *in vitro* systems possesses a number of disadvantages due to cell culture techniques ubiquitously used throughout biomedical research. The technologies investigated in this thesis, used in combination, would enable sophisticated studies of a serum-free human 3D culture system where targeted mutations could be introduced to further our understanding of post-natal development in a biologically relevant context. Additionally, there has been a rise in the use of 3D cellular spheroids in drug discovery due to recent advancements in high throughput screening technologies suitable for use with 3D cell cultures. With the development of the CRISPR/Cas9 methodology in this thesis, and the differentiated 3D spheroid models, high throughput screening of potential drug compounds is possible with generated disease relevant mutations in MSCs and differentiated daughter cells. It would therefore be possible to determine the effects of these compounds on each element of the bone, cartilage and marrow, in addition to combinations thereof and to confirm no impact on the signalling between these cell types. All whilst the cells were maintained in a physiologically relevant buffer. Whilst *in vitro* technologies many never fully recapitulate the complexity of human tissues, the ability to study cell-cell interactions in an environment approximating human physiology, in both health and disease, cannot be underestimated.

Appendix: Analysis of a mixed population of FGFR3 targeted GM-hTERT MSCs

Mixed population of FGFR3 CRISPR/Cas9 hTERT MSCs display behaviours similar to FGFR3-KO hTERT MSCs

As previously discussed, the CRISPR/Cas9 system does not introduce the same mutation into each cell that has a DSB successfully inserted. However, if a particular sgRNA is efficient many cells should have mutations present, it could then be possible to perform phenotypic studies on these cells and see behaviours already identified in individual cell lines. To provide further evidence that the phenotype of the FGFR3-KO hTERT MSCs described in this chapter can be attributed to the removal of FGFR3, analysis of some of the key features was performed on the FGFR3-MP hTERT MSCs. Figure A.1 shows a monolayer of sub-confluent FGFR3-MP hTERT MSCs both by phase microscopy and stained with crystal violet to show the morphology of the cells. The majority of the cells show a typical fibroblastic profile similar to the WT hTERT MSCs shown earlier, however a number of cells have an elongated morphology and these have been highlighted in the figure with arrows. This elongated morphology appears more similar to the morphology seen in the FGFR3-KO hTERT MSCs discussed earlier. Furthermore, the FGFR3-MP hTERT MSCs have an increased proliferative capacity compared to the WT hTERT MSCs as shown by EdU staining in Figure A.2A. Cells that have cycled and incorporated EdU during S phase have stained and are fluorescently labelled in green, DAPI has been used as a counterstain to highlight all nuclei. By comparing the numbers of labelled and unlabelled nuclei it is apparent that during the 72 hours EdU incubation, significantly more of the FGFR3-MP hTERT MSCs have completed a cell cycle (Figure A.2B). Again, this is a phenotypic characteristic identified in the FGFR3-KO hTERT MSCs in earlier results.

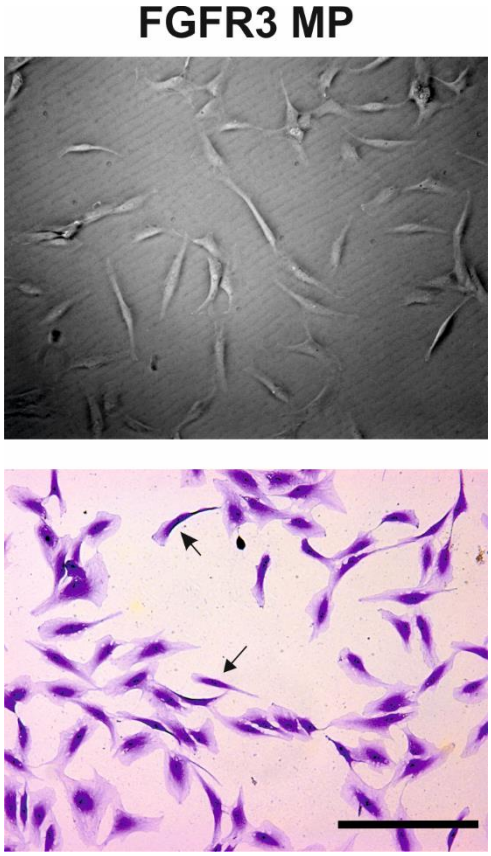

Figure A.1: Qualitative analysis of FGFR3-MP hTERT MSC morphology by microscopy

FGFR3-MP hTERT MSCs were seeded at subconfluency and imaged using phase microscopy (top panel) or fixed and stained with crystal violet (bottom panel) to highlight the morphology of these cells. Scale bar = 200μm.

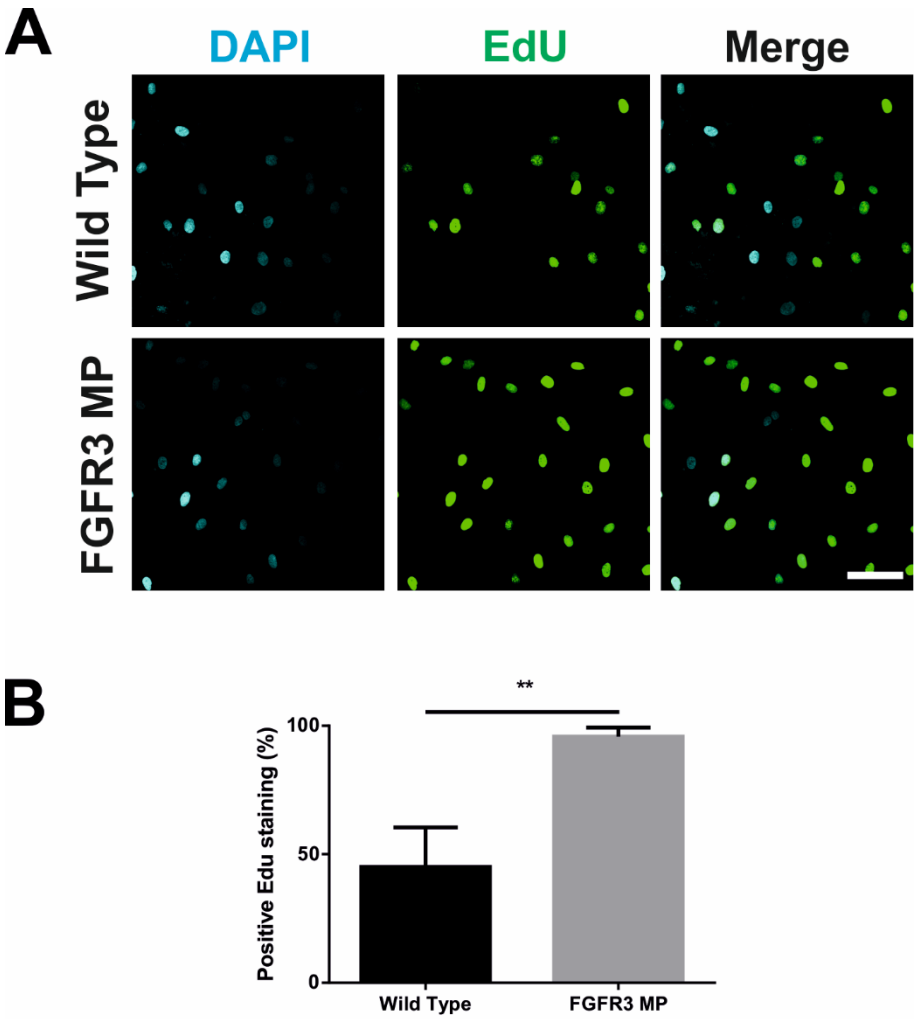

Figure A.2: EdU staining of FGFR3-MP hTERT MSCs compared to WT hTERT MSCs

WT hTERT MSCs and FGFR3-MP hTERT MSCs were synchronised by serum starvation and supplemented with EdU over 72 hours. Cells were counterstained with DAPI and imaged by confocal microscopy to quantify fluorescent cells, green staining = EdU and blue staining = DAPI (A) The results were then summarised in a bar chart (B). Values = mean ± SD, n=3 significance obtained by unpaired t-test with Welch's correction.

Finally, the FGFR3-MP hTERT MSCs were seeded in a confluent monolayer, a scratch wound created and the resultant healing monitored over time (Figure A.3). After 18 hours it was apparent the FGFR3-MP hTERT MSCs had a greater wound healing capacity compared to the WT hTERT MSCs as on average the FGFR3-MP hTERT MSCs healed nearly 50% more of wound during the timecourse. Over 18 hours the FGFR3-KO hTERT MSCs were able to completely heal a wound created in a similar fashion demonstrating again the similarities of the phenotypic behaviours between the FGFR3-KO hTERT MSCs and the FGFR3-MP hTERT MSCs.

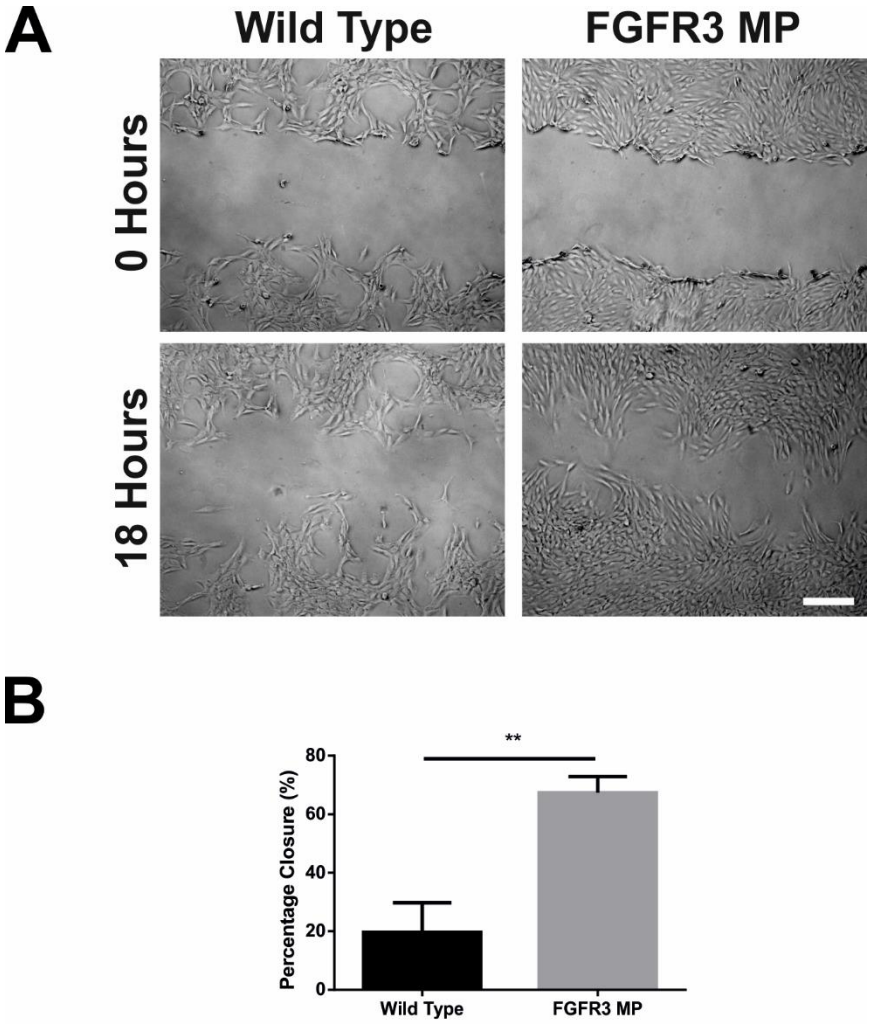

Figure A.3: Scratch assay of FGFR3-MP hTERT MSCs compared to WT hTERT MSCs

A confluent monolayer of FGFR3-MP and WT hTERT MSCs was wounded by a "scratch" and imaged by phase microscopy (A). The wound was then allowed to heal for 18 hours following which the percentage closure was calculated and summarised in a bar chart (B). Scale bar = 200µm. Values = mean ± SD, n=3 significance obtained by unpaired t-test with Welch's correction.

List of Abbreviations

3D	Three dimensional
ALP	Alkaline phosphatase
BMP	Bone morphogenic protein
bp	Base pair
BSA	Bovine serum albumin
cAMP	Cyclic adenosine monophosphate
CATSHL	Camptodactyly, tall stature, scoliosis, and hearing loss
CFU-f	Colony forming unit - fibroblast
CMV	Cytomegalovirus
CPC	Cetylpyridinium chloride
CRISPR	Clustered regularly interspaced short palindromic repeats
crRNA	CRISPR RNA
DMEM	Dulbecco's Modified Eagle Medium
DMSO	Dimethylsulfoxide
DSB	Double stranded break
ECCs	Embryonal carcinoma cells
ECM	Extracellular matrix
EDTA	Ethylenediaminetetraacetic acid
ESCs	Embryonic stem cells
FA	Fatty acid

FACS	Fluorescent-activated cell sorting
FBS	Foetal bovine serum
FDA	Food and Drug Administration
FDR	False discovery rate
FGF	Fibroblast growth factor
FGFR	Fibroblast growth factor receptor
FOP	Fibrodysplasia ossificans progressiva
FPKM	Fragments per kilobase of transcript per million mapped reads
(e)GFP	(Enhanced) green fluorescent protein
GAPDH	Glyceraldehyde 3-phosphate dehydrogenase
GM	Genetically modified
GSEA	Gene set enrichment analysis
hTERT	Human telomerase
HEK293FT	Human embryonic kidney 293 FT
HHIP	Hedgehog interacting protein
IBMX	3-isobutyl-1-methylxanthine
Indel	Small insertion or deletion of DNA
IHH	Indian hedgehog
iPSCs	Induced pluripotent stem cells
ITS	Insulin-Transferrin-Selenium
KEGG	Kyoto Encyclopedia of Genes and Genomes
KO	Knockout
miRNA	Micro RNA
MM	Mismatch
MMP	Matrix metalloproteinases

MP	Mixed population
MSCs	Mesenchymal stem/stromal cells
MTT	3-(4,5-Dimethylthiazol-2-yl)-2,5-Diphenyltetrazolium Bromide
OI	Osteogenesis imperfecta
oim	Osteogenesis imperfecta murine
NHEJ	Non homologous end joining
PAM	Protospacer adjacent motif
PBS	Phosphate buffered saline
PFA	Paraformaldehyde
pre-crRNA	Precursor CRISPR RNA
RPKM	Reads per kilobase of transcript per million mapped reads
Runx2	Runt-related transcript factor 2
SADDAN	Severe achondroplasia with developmental delay and acanthosis nigricans
SD	Standard deviation
sgRNA	single guide RNA
Sox9	Sex-determining region box 9
ssODN	Single stranded oligonucleotide
TALE(N)s	Transcription activator-like effector (nuclease)s
tracrRNA	Trans-activating CRISPR RNA
WT	Wild type
wt/vol	weight / volume
ZFNs	Zinc fingers

References

Abremski, K., and Hoess, R. (1984). Bacteriophage P1 site-specific recombination. Purification and properties of the Cre recombinase protein. J. Biol. Chem. *259*, 1509–1514.

Adamek, G., Felix, R., Guenther, H.L., and Fleisch, H. (1987). Fatty acid oxidation in bone tissue and bone cells in culture. Characterization and hormonal influences. Biochem. J. *248*, 129–137.

Akiyama, H., Chaboissier, M.-C., Martin, J.F., Schedl, A., and de Crombrugghe, B. (2002). The transcription factor Sox9 has essential roles in successive steps of the chondrocyte differentiation pathway and is required for expression of Sox5 and Sox6. Genes Dev. *16*, 2813–2828.

Akune, T., Ohba, S., Kamekura, S., Yamaguchi, M., Chung, U.-I., Kubota, N., Terauchi, Y., Harada, Y., Azuma, Y., Nakamura, K., et al. (2004). PPARgamma insufficiency enhances osteogenesis through osteoblast formation from bone marrow progenitors. J. Clin. Invest. *113*, 846–855.

Altman, J., and Das, G.D. (1965). Autoradiographic and histological evidence of postnatal hippocampal neurogenesis in rats. J. Comp. Neurol. *124*, 319–335.

Araki, R., Hoki, Y., Uda, M., Nakamura, M., Jincho, Y., Tamura, C., Sunayama, M., Ando, S., Sugiura, M., Yoshida, M.A., et al. (2011). Crucial role of c-Myc in the generation of induced pluripotent stem cells. Stem Cells Dayt. Ohio *29*, 1362–1370.

Asharani, P.V., Keupp, K., Semler, O., Wang, W., Li, Y., Thiele, H., Yigit, G., Pohl, E., Becker, J., Frommolt, P., et al. (2012). Attenuated BMP1 function compromises osteogenesis, leading to bone fragility in humans and zebrafish. Am. J. Hum. Genet. *90*, 661–674.

Austin, C.P., Battey, J.F., Bradley, A., Bucan, M., Capecchi, M., Collins, F.S., Dove, W.F., Duyk, G., Dymecki, S., Eppig, J.T., et al. (2004). The Knockout Mouse Project. Nat. Genet. *36*, 921–924.

Avior, Y., Sagi, I., and Benvenisty, N. (2016). Pluripotent stem cells in disease modelling and drug discovery. Nat. Rev. Mol. Cell Biol. *17*, 170–182.

Ayache, S., Panelli, M.C., Byrne, K.M., Slezak, S., Leitman, S.F., Marincola, F.M., and Stroncek, D.F. (2006). Comparison of proteomic profiles of serum, plasma, and modified media supplements used for cell culture and expansion. J. Transl. Med. *4*, 40.

Barak, Y., Nelson, M.C., Ong, E.S., Jones, Y.Z., Ruiz-Lozano, P., Chien, K.R., Koder, A., and Evans, R.M. (1999). PPAR gamma is required for placental, cardiac, and adipose tissue development. Mol. Cell *4*, 585–595.

Barrangou, R., Fremaux, C., Deveau, H., Richards, M., Boyaval, P., Moineau, S., Romero, D.A., and Horvath, P. (2007). CRISPR Provides Acquired Resistance Against Viruses in Prokaryotes. Science *315*, 1709–1712.

Baxter, M.A., Wynn, R.F., Jowitt, S.N., Wraith, J.E., Fairbairn, L.J., and Bellantuono, I. (2004). Study of Telomere Length Reveals Rapid Aging of Human Marrow Stromal Cells following In Vitro Expansion. STEM CELLS *22*, 675–682.

Benoist-Lasselin, C., Gibbs, L., Heuertz, S., Odent, T., Munnich, A., and Legeai-Mallet, L. (2007). Human immortalized chondrocytes carrying heterozygous FGFR3 mutations: An in vitro model to study chondrodysplasias. FEBS Lett. *581*, 2593–2598.

Bibikova, M., Golic, M., Golic, K.G., and Carroll, D. (2002). Targeted chromosomal cleavage and mutagenesis in Drosophila using zinc-finger nucleases. Genetics *161*, 1169–1175.

Biggs, M.J.., and Dalby, M.. (2010). Focal adhesions in osteoneogenesis. Proc. Inst. Mech. Eng. [H] *224*, 1441–1453.

Binder, B.Y.K., Sagun, J.E., and Leach, J.K. (2015). Reduced serum and hypoxic culture conditions enhance the osteogenic potential of human mesenchymal stem cells. Stem Cell Rev. *11*, 387–393.

Bitinaite, J., Wah, D.A., Aggarwal, A.K., and Schildkraut, I. (1998). FokI dimerization is required for DNA cleavage. Proc. Natl. Acad. Sci. *95*, 10570–10575.

Blom, A.B., Brockbank, S.M., van Lent, P.L., van Beuningen, H.M., Geurts, J., Takahashi, N., van der Kraan, P.M., van de Loo, F.A., Schreurs, B.W., Clements, K., et al. (2009). Involvement of the Wnt signaling pathway in experimental and human osteoarthritis: Prominent role of Wnt-induced signaling protein 1. Arthritis Rheum. *60*, 501–512.

Boch, J., Scholze, H., Schornack, S., Landgraf, A., Hahn, S., Kay, S., Lahaye, T., Nickstadt, A., and Bonas, U. (2009). Breaking the code of DNA binding specificity of TAL-type III effectors. Science *326*, 1509–1512.

Böker, W., Yin, Z., Drosse, I., Haasters, F., Rossmann, O., Wierer, M., Popov, C., Locher, M., Mutschler, W., Docheva, D., et al. (2008). Introducing a single-cell-derived human mesenchymal stem cell line expressing hTERT after lentiviral gene transfer. J. Cell. Mol. Med. *12*, 1347–1359.

Bornes, T.D., Adesida, A.B., and Jomha, N.M. (2014). Mesenchymal stem cells in the treatment of traumatic articular cartilage defects: a comprehensive review. Arthritis Res. Ther. *16*, 432.

Bradley, A., Evans, M., Kaufman, M.H., and Robertson, E. (1984). Formation of germ-line chimaeras from embryo-derived teratocarcinoma cell lines. Nature *309*, 255–256.

Campbell, B.G., Wootton, J.A., Krook, L., DeMarco, J., and Minor, R.R. (1997). Clinical signs and diagnosis of osteogenesis imperfecta in three dogs. J. Am. Vet. Med. Assoc. *211*, 183–187.

Campbell, B.G., Wootton, J.A., MacLeod, J.N., and Minor, R.R. (2000). Sequence of normal canine COL1A1 cDNA and identification of a heterozygous alpha1(I) collagen Gly208Ala mutation in a severe case of canine osteogenesis imperfecta. Arch. Biochem. Biophys. *384*, 37–46.

Caplan, A.I., and Dennis, J.E. (2006). Mesenchymal stem cells as trophic mediators. J. Cell. Biochem. *98*, 1076–1084.

Carroll, D. (2011). Genome Engineering With Zinc-Finger Nucleases. Genetics *188*, 773–782.

Carstairs, A., and Genever, P. (2014). Stem cell treatment for musculoskeletal disease. Curr. Opin. Pharmacol. *16*, 1–6.

Cermak, T., Doyle, E.L., Christian, M., Wang, L., Zhang, Y., Schmidt, C., Baller, J.A., Somia, N.V., Bogdanove, A.J., and Voytas, D.F. (2011). Efficient design and assembly of custom TALEN and other TAL effector-based constructs for DNA targeting. Nucleic Acids Res. *39*, e82.

Cesarz, Z., and Tamama, K. (2016). Spheroid Culture of Mesenchymal Stem Cells. Stem Cells Int. *2016*.

Chakkalakal, S.A., Zhang, D., Culbert, A.L., Convente, M.R., Caron, R.J., Wright, A.C., Maidment, A.D.A., Kaplan, F.S., and Shore, E.M. (2012). An Acvr1 R206H knock-in mouse has fibrodysplasia ossificans progressiva. J. Bone Miner. Res. Off. J. Am. Soc. Bone Miner. Res. *27*, 1746–1756.

Chanda, D., Kumar, S., and Ponnazhagan, S. (2010). Therapeutic potential of adult bone marrow-derived mesenchymal stem cells in diseases of the skeleton. J. Cell. Biochem. *111*, 249–257.

Chase, L.G., Lakshmipathy, U., Solchaga, L.A., Rao, M.S., and Vemuri, M.C. (2010). A novel serum-free medium for the expansion of human mesenchymal stem cells. Stem Cell Res. Ther. *1*, 8.

Chen, Y., and Gridley, T. (2013). Compensatory regulation of the Snai1 and Snai2 genes during chondrogenesis. J. Bone Miner. Res. *28*, 1412–1421.

Chen, E.Y., Tan, C.M., Kou, Y., Duan, Q., Wang, Z., Meirelles, G.V., Clark, N.R., and Ma'ayan, A. (2013a). Enrichr: interactive and collaborative HTML5 gene list enrichment analysis tool. BMC Bioinformatics *14*, 128.

Chen, J., Crawford, R., Chen, C., and Xiao, Y. (2013b). The key regulatory roles of the PI3K/Akt signaling pathway in the functionalities of mesenchymal stem cells and applications in tissue regeneration. Tissue Eng. Part B Rev. *19*, 516–528.

Chen, L., Adar, R., Yang, X., Monsonego, E.O., Li, C., Hauschka, P.V., Yayon, A., and Deng, C.-X. (1999). Gly369Cys mutation in mouse FGFR3 causes achondroplasia by affecting both chondrogenesis and osteogenesis. J. Clin. Invest. *104*, 1517–1525.

Chen, M., Przyborowski, M., and Berthiaume, F. (2009). Stem Cells for Skin Tissue Engineering and Wound Healing. Crit. Rev. Biomed. Eng. *37*, 399–421.

Cheng, H., Luk, K.D.K., Cheung, K.M.C., and Chan, B.P. (2011). In vitro generation of an osteochondral interface from mesenchymal stem cell–collagen microspheres. Biomaterials *32*, 1526–1535.

Chipman, S.D., Sweet, H.O., Mcbride, D.J., Davisson, M.T., Marks, S.C., Shuldiner, A.R., Wenstrup, R.J., Rowe, D.W., and Shapiro, J.R. (1993). Defective proα2(I) collagen synthesis in a recessive mutation in mice: A model of human osteogenesis imperfecta. Proc. Natl. Acad. Sci. U. S. A. *90*, 1701–1705.

Cho, S.Y., and Jin, D.-K. (2015). Guidelines for genetic skeletal dysplasias for pediatricians. Ann. Pediatr. Endocrinol. Metab. *20*, 187–191.

Cho, S.W., Kim, S., Kim, Y., Kweon, J., Kim, H.S., Bae, S., and Kim, J.-S. (2013). Analysis of off-target effects of CRISPR/Cas-derived RNA-guided endonucleases and nickases. Genome Res.

Christian, M., Cermak, T., Doyle, E.L., Schmidt, C., Zhang, F., Hummel, A., Bogdanove, A.J., and Voytas, D.F. (2010). Targeting DNA double-strand breaks with TAL effector nucleases. Genetics *186*, 757–761.

Chuang, P.-T., and McMahon, A.P. (1999). Vertebrate Hedgehog signalling modulated by induction of a Hedgehog-binding protein. Nature *397*, 617–621.

Cinelli, R.A., Ferrari, A., Pellegrini, V., Tyagi, M., Giacca, M., and Beltram, F. (2000). The enhanced green fluorescent protein as a tool for the analysis of protein dynamics and localization: local fluorescence study at the single-molecule level. Photochem. Photobiol. *71*, 771–776.

Colvin, J.S., Bohne, B.A., Harding, G.W., McEwen, D.G., and Ornitz, D.M. (1996). Skeletal overgrowth and deafness in mice lacking fibroblast growth factor receptor 3. Nat. Genet. *12*, 390–397.

Cong, L., Ran, F.A., Cox, D., Lin, S., Barretto, R., Habib, N., Hsu, P.D., Wu, X., Jiang, W., Marraffini, L.A., et al. (2013). Multiplex Genome Engineering Using CRISPR/Cas Systems. Science *339*, 819–823.

Copelan, E.A. (2006). Hematopoietic stem-cell transplantation. N. Engl. J. Med. *354*, 1813–1826.

Crisan, M., Yap, S., Casteilla, L., Chen, C.-W., Corselli, M., Park, T.S., Andriolo, G., Sun, B., Zheng, B., Zhang, L., et al. (2008). A perivascular origin for mesenchymal stem cells in multiple human organs. Cell Stem Cell *3*, 301–313.

Dang, C.V. (2012). MYC on the Path to Cancer. Cell *149*, 22–35.

Davidson, D., Blanc, A., Filion, D., Wang, H., Plut, P., Pfeffer, G., Buschmann, M.D., and Henderson, J.E. (2005). Fibroblast Growth Factor (FGF) 18 Signals through FGF Receptor 3 to Promote Chondrogenesis. J. Biol. Chem. *280*, 20509–20515.

De Bari, C., Dell'Accio, F., Tylzanowski, P., and Luyten, F.P. (2001). Multipotent mesenchymal stem cells from adult human synovial membrane. Arthritis Rheum. *44*, 1928–1942.

De Paepe, C., Krivega, M., Cauffman, G., Geens, M., and Van de Velde, H. (2014). Totipotency and lineage segregation in the human embryo. MHR Basic Sci. Reprod. Med. *20*, 599–618.

Del Fattore, A., Capannolo, M., and Rucci, N. (2010). Bone and bone marrow: The same organ. Arch. Biochem. Biophys. *503*, 28–34.

Delezoide, A.-L., Benoist-Lasselin, C., Legeai-Mallet, L., Le Merrer, M., Munnich, A., Vekemans, M., and Bonaventure, J. (1998). Spatio-temporal expression of FGFR 1, 2 and 3 genes during human embryo-fetal ossification. Mech. Dev. *77*, 19–30.

Deltcheva, E., Chylinski, K., Sharma, C.M., Gonzales, K., Chao, Y., Pirzada, Z.A., Eckert, M.R., Vogel, J., and Charpentier, E. (2011). CRISPR RNA maturation by trans-encoded small RNA and host factor RNase III. Nature *471*, 602–607.

Deng, C., Wynshaw-Boris, A., Zhou, F., Kuo, A., and Leder, P. (1996). Fibroblast growth factor receptor 3 is a negative regulator of bone growth. Cell *84*, 911–921.

Diascro, D.D., Vogel, R.L., Johnson, T.E., Witherup, K.M., Pitzenberger, S.M., Rutledge, S.J., Prescott, D.J., Rodan, G.A., and Schmidt, A. (1998). High fatty acid content in rabbit serum is responsible for the differentiation of osteoblasts into adipocyte-like cells. J. Bone Miner. Res. Off. J. Am. Soc. Bone Miner. Res. *13*, 96–106.

Ding, Q., Lee, Y.-K., Schaefer, E.A.K., Peters, D.T., Veres, A., Kim, K., Kuperwasser, N., Motola, D.L., Meissner, T.B., Hendriks, W.T., et al. (2013). A TALEN Genome-Editing System for Generating Human Stem Cell-Based Disease Models. Cell Stem Cell *12*, 238–251.

Dominici, M., Le Blanc, K., Mueller, I., Slaper-Cortenbach, I., Marini, F., Krause, D., Deans, R., Keating, A., Prockop, D., and Horwitz, E. (2006). Minimal criteria for defining multipotent mesenchymal stromal cells. The International Society for Cellular Therapy position statement. Cytotherapy *8*, 315–317.

Doudna, J.A., and Charpentier, E. (2014). The new frontier of genome engineering with CRISPR-Cas9. Science *346*, 1258096.

Doyon, Y., Vo, T.D., Mendel, M.C., Greenberg, S.G., Wang, J., Xia, D.F., Miller, J.C., Urnov, F.D., Gregory, P.D., and Holmes, M.C. (2011). Enhancing zinc-finger-nuclease activity with improved obligate heterodimeric architectures. Nat. Methods *8*, 74–79.

Drögemüller, C., Becker, D., Brunner, A., Haase, B., Kircher, P., Seeliger, F., Fehr, M., Baumann, U., Lindblad-Toh, K., and Leeb, T. (2009). A Missense Mutation in the SERPINH1 Gene in Dachshunds with Osteogenesis Imperfecta. PLOS Genet. *5*, e1000579.

Ducy, P., Zhang, R., Geoffroy, V., Ridall, A.L., and Karsenty, G. (1997). Osf2/Cbfa1: a transcriptional activator of osteoblast differentiation. Cell *89*, 747–754.

Eagle, H. (1955). Nutrition needs of mammalian cells in tissue culture. Science *122*, 501–514.

Ebert, A.D., Liang, P., and Wu, J.C. (2012). Induced Pluripotent Stem Cells as a Disease Modeling and Drug Screening Platform. J. Cardiovasc. Pharmacol. *60*, 408–416.

Eggan, K., and Jaenisch, R. (2003). Differentiation of F1 embryonic stem cells into viable male and female mice by tetraploid embryo complementation. Methods Enzymol. *365*, 25–39.

Eleniste, P.P., and Bruzzaniti, A. (2012). Focal Adhesion Kinases in Adhesion Structures and Disease. J. Signal Transduct. *2012*, e296450.

Ellsworth, J.L., Berry, J., Bukowski, T., Claus, J., Feldhaus, A., Holderman, S., Holdren, M.S., Lum, K.D., Moore, E.E., Raymond, F., et al. (2002). Fibroblast growth factor-18 is a trophic factor for mature chondrocytes and their progenitors. Osteoarthritis Cartilage *10*, 308–320.

Enderli, T.A., Burtch, S.R., Templet, J.N., and Carriero, A. (2016). Animal models of osteogenesis imperfecta: applications in clinical research.

Enomoto, H., Furuichi, T., Zanma, A., Yamana, K., Yoshida, C., Sumitani, S., Yamamoto, H., Enomoto-Iwamoto, M., Iwamoto, M., and Komori, T. (2004). Runx2 deficiency in chondrocytes causes adipogenic changes in vitro. J. Cell Sci. *117*, 417–425.

Escobar, L.F., Tucker, M., and Bamshad, M. (2016). A second family with CATSHL syndrome: Confirmatory report of another unique FGFR3 syndrome. Am. J. Med. Genet. A. *170*, 1908–1911.

Etienne-Manneville, S., and Hall, A. (2001). Integrin-mediated activation of Cdc42 controls cell polarity in migrating astrocytes through PKCzeta. Cell *106*, 489–498.

European Commission Workshop (2010). Of mice and men – are mice relevant models for human disease (London, UK).

Evans, M.J., and Kaufman, M.H. (1981). Establishment in culture of pluripotential cells from mouse embryos. Nature *292*, 154–156.

Fisher, S., Jagadeeswaran, P., and Halpern, M.E. (2003). Radiographic analysis of zebrafish skeletal defects. Dev. Biol. *264*, 64–76.

Foty, R.A., and Steinberg, M.S. (2005). The differential adhesion hypothesis: a direct evaluation. Dev. Biol. *278*, 255–263.

Friedenstein, A.J., Piatetzky-Shapiro, I.I., and Petrakova, K.V. (1966). Osteogenesis in transplants of bone marrow cells. Development *16*, 381–390.

Froud, S.J. (1999). The development, benefits and disadvantages of serum-free media. Dev. Biol. Stand. *99*, 157–166.

de Frutos, C.A., Vega, S., Manzanares, M., Flores, J.M., Huertas, H., Martínez-Frías, M.L., and Nieto, M.A. (2007). Snail1 is a transcriptional effector of FGFR3 signaling during chondrogenesis and achondroplasias. Dev. Cell *13*, 872–883.

Fu, Y., Foden, J.A., Khayter, C., Maeder, M.L., Reyon, D., Joung, J.K., and Sander, J.D. (2013). High-frequency off-target mutagenesis induced by CRISPR-Cas nucleases in human cells. Nat. Biotechnol. *31*, 822–826.

Fu, Y., Sander, J.D., Reyon, D., Cascio, V.M., and Joung, J.K. (2014). Improving CRISPR-Cas nuclease specificity using truncated guide RNAs. Nat. Biotechnol. *32*, 279–284.

Fukuchi, Y., Nakajima, H., Sugiyama, D., Hirose, I., Kitamura, T., and Tsuji, K. (2004). Human placenta-derived cells have mesenchymal stem/progenitor cell potential. Stem Cells Dayt. Ohio *22*, 649–658.

Galindo, M., Pratap, J., Young, D.W., Hovhannisyan, H., Im, H.-J., Choi, J.-Y., Lian, J.B., Stein, J.L., Stein, G.S., and van Wijnen, A.J. (2005). The bone-specific expression of Runx2 oscillates during the cell cycle to support a G1-related antiproliferative function in osteoblasts. J. Biol. Chem. *280*, 20274–20285.

Galindo, M., Kahler, R.A., Teplyuk, N.M., Stein, J.L., Lian, J.B., Stein, G.S., Westendorf, J.J., and Wijnen, A.J. van (2007). Cell cycle related modulations in Runx2 protein levels are independent of lymphocyte enhancer-binding factor 1 (Lef1) in proliferating osteoblasts. J. Mol. Histol. *38*, 501–506.

Garofalo, M., Quintavalle, C., Romano, G., Croce, C.M., and Condorelli, G. (2012). miR221/222 in Cancer: Their Role in Tumor Progression and Response to Therapy. Curr. Mol. Med. *12*, 27–33.

Gasiunas, G., Barrangou, R., Horvath, P., and Siksnys, V. (2012). Cas9–crRNA ribonucleoprotein complex mediates specific DNA cleavage for adaptive immunity in bacteria. Proc. Natl. Acad. Sci. *109*, E2579–E2586.

Gimble, J.M., Zvonic, S., Floyd, Z.E., Kassem, M., and Nuttall, M.E. (2006). Playing with bone and fat. J. Cell. Biochem. *98*, 251–266.

Gómez-Barrena, E., Rosset, P., Lozano, D., Stanovici, J., Ermthaller, C., and Gerbhard, F. (2015). Bone fracture healing: Cell therapy in delayed unions and nonunions. Bone *70*, 93–101.

Gong, Z., Calkins, G., Cheng, E., Krause, D., and Niklason, L.E. (2009). Influence of culture medium on smooth muscle cell differentiation from human bone marrow-derived mesenchymal stem cells. Tissue Eng. Part A *15*, 319–330.

Gottipamula, S., Muttigi, M.S., Kolkundkar, U., and Seetharam, R.N. (2013). Serum-free media for the production of human mesenchymal stromal cells: a review. Cell Prolif. *46*, 608–627.

Gronthos, S., Mankani, M., Brahim, J., Robey, P.G., and Shi, S. (2000). Postnatal human dental pulp stem cells (DPSCs) in vitro and in vivo. Proc. Natl. Acad. Sci. U. S. A. *97*, 13625–13630.

Gstraunthaler, G. (2003). Alternatives to the use of fetal bovine serum: serum-free cell culture. ALTEX *20*, 275–281.

Guo, J., Gaj, T., and Barbas, C.F. (2010). Directed evolution of an enhanced and highly efficient FokI cleavage domain for Zinc Finger Nucleases. J. Mol. Biol. *400*, 96–107.

Hall, B., Limaye, A., and Kulkarni, A.B. (2009). Overview: Generation of Gene Knockout Mice. Curr. Protoc. Cell Biol. Editor. Board Juan Bonifacino Al *CHAPTER*, Unit-19.1217.

Hayflick, L. (1965). THE LIMITED IN VITRO LIFETIME OF HUMAN DIPLOID CELL STRAINS. Exp. Cell Res. *37*, 614–636.

Hermida-Gómez, T., Fuentes-Boquete, I., Gimeno-Longas, M.J., Muiños-López, E., Díaz-Prado, S., de Toro, F.J., and Blanco, F.J. (2011). Quantification of cells expressing mesenchymal stem cell markers in healthy and osteoarthritic synovial membranes. J. Rheumatol. *38*, 339–349.

Hockemeyer, D., Soldner, F., Beard, C., Gao, Q., Mitalipova, M., DeKelver, R.C., Katibah, G.E., Amora, R., Boydston, E.A., Zeitler, B., et al. (2009). Efficient targeting of expressed and silent genes in human ESCs and iPSCs using zinc-finger nucleases. Nat. Biotechnol. *27*, 851–857.

Hockemeyer, D., Wang, H., Kiani, S., Lai, C.S., Gao, Q., Cassady, J.P., Cost, G.J., Zhang, L., Santiago, Y., Miller, J.C., et al. (2011b). Genetic engineering of human ES and iPS cells using TALE nucleases. Nat. Biotechnol. *29*, 731–734.

Hockemeyer, D., Wang, H., Kiani, S., Lai, C.S., Gao, Q., Cassady, J.P., Cost, G.J., Zhang, L., Santiago, Y., Miller, J.C., et al. (2011a). Genetic engineering of human pluripotent cells using TALE nucleases. Nat. Biotechnol. *29*, 731–734.

Hoemann, C.D., Lafantaisie-Favreau, C.-H., Lascau-Coman, V., Chen, G., and Guzmán-Morales, J. (2012). The cartilage-bone interface. J. Knee Surg. *25*, 85–97.

Home Office (2013). Annual Statistics of Scientific Procedures on Living Animals Great Britain 2012.

Home Office (2016). Annual Statistics of Scientific Procedures on Living Animals Great Britain 2015.

Horwitz, E.M., Gordon, P.L., Koo, W.K.K., Marx, J.C., Neel, M.D., McNall, R.Y., Muul, L., and Hofmann, T. (2002). Isolated allogeneic bone marrow-derived mesenchymal cells engraft and stimulate growth in children with osteogenesis imperfecta: Implications for cell therapy of bone. Proc. Natl. Acad. Sci. *99*, 8932–8937.

Horwitz, E.M., Le Blanc, K., Dominici, M., Mueller, I., Slaper-Cortenbach, I., Marini, F.C., Deans, R.J., Krause, D.S., Keating, A., and International Society for Cellular Therapy (2005). Clarification of the nomenclature for MSC: The International Society for Cellular Therapy position statement. Cytotherapy *7*, 393–395.

Hulbert, A.J. (2008). The links between membrane composition, metabolic rate and lifespan. Comp. Biochem. Physiol. A. Mol. Integr. Physiol. *150*, 196–203.

Inaki, M., Vishnu, S., Cliffe, A., and Rørth, P. (2012). Effective guidance of collective migration based on differences in cell states. Proc. Natl. Acad. Sci. U. S. A. *109*, 2027–2032.

Iredale, J.P. (1999). Demystified ... gene knockouts. Mol. Pathol. *52*, 111–116.

Ishino, Y., Shinagawa, H., Makino, K., Amemura, M., and Nakata, A. (1987). Nucleotide sequence of the iap gene, responsible for alkaline phosphatase isozyme conversion in Escherichia coli, and identification of the gene product. J. Bacteriol. *169*, 5429–5433.

Jaiswal, N., Haynesworth, S.E., Caplan, A.I., and Bruder, S.P. (1997). Osteogenic differentiation of purified, culture-expanded human mesenchymal stem cells in vitro. J. Cell. Biochem. *64*, 295–312.

James, A.W. (2013). Review of Signaling Pathways Governing MSC Osteogenic and Adipogenic Differentiation. Scientifica *2013*, e684736.

James, S., Fox, J., Afsari, F., Lee, J., Clough, S., Knight, C., Ashmore, J., Ashton, P., Preham, O., Hoogduijn, M., et al. (2015). Multiparameter Analysis of Human Bone Marrow Stromal Cells Identifies Distinct Immunomodulatory and Differentiation-Competent Subtypes. Stem Cell Rep. *4*, 1004–1015.

Jansen, R., Embden, J.D.A. van, Gaastra, W., and Schouls, L.M. (2002). Identification of genes that are associated with DNA repeats in prokaryotes. Mol. Microbiol. *43*, 1565–1575.

Jinek, M., Chylinski, K., Fonfara, I., Hauer, M., Doudna, J.A., and Charpentier, E. (2012). A Programmable Dual-RNA–Guided DNA Endonuclease in Adaptive Bacterial Immunity. Science *337*, 816–821.

Johnstone, B., Hering, T.M., Caplan, A.I., Goldberg, V.M., and Yoo, J.U. (1998). In vitro chondrogenesis of bone marrow-derived mesenchymal progenitor cells. Exp. Cell Res. *238*, 265–272.

Jones, E.A., Kinsey, S.E., English, A., Jones, R.A., Straszynski, L., Meredith, D.M., Markham, A.F., Jack, A., Emery, P., and McGonagle, D. (2002). Isolation and characterization of bone marrow multipotential mesenchymal progenitor cells. Arthritis Rheum. *46*, 3349–3360.

Jungers, W.L. (1986). Scaling. Why is animal size so important? By K. Schmidt-Nielsen. New York: Cambridge University Press. 1984. xi + 241 pp., figures, tables, appendices, references, index. $29.95 (cloth), $9.95 (paper). Am. J. Phys. Anthropol. *69*, 129–130.

Justesen, J., Stenderup, K., Ebbesen, E.N., Mosekilde, L., Steiniche, T., and Kassem, M. (2001). Adipocyte tissue volume in bone marrow is increased with aging and in patients with osteoporosis. Biogerontology *2*, 165–171.

Kajstura, J., Leri, A., Finato, N., Di Loreto, C., Beltrami, C.A., and Anversa, P. (1998). Myocyte proliferation in end-stage cardiac failure in humans. Proc. Natl. Acad. Sci. U. S. A. *95*, 8801–8805.

Kania, M.A., Bonner, A.S., Duffy, J.B., and Gergen, J.P. (1990). The Drosophila segmentation gene runt encodes a novel nuclear regulatory protein that is also expressed in the developing nervous system. Genes Dev. *4*, 1701–1713.

Kansara, M., and Thomas, D.M. (2007). Molecular pathogenesis of osteosarcoma. DNA Cell Biol. *26*, 1–18.

Kaplan, F.S., Le Merrer, M., Glaser, D.L., Pignolo, R.J., Goldsby, R., Kitterman, J.A., Groppe, J., and Shore, E.M. (2008). Fibrodysplasia ossificans progressiva. Best Pract. Res. Clin. Rheumatol. *22*, 191–205.

Kay, S., Hahn, S., Marois, E., Hause, G., and Bonas, U. (2007). A Bacterial Effector Acts as a Plant Transcription Factor and Induces a Cell Size Regulator. Science *318*, 648–651.

Khanarian, N.T., Jiang, J., Wan, L.Q., Mow, V.C., and Lu, H.H. (2012). A hydrogel-mineral composite scaffold for osteochondral interface tissue engineering. Tissue Eng. Part A *18*, 533–545.

Kiani, C., Chen, L., Wu, Y.J., Yee, A.J., and Yang, B.B. (2002). Structure and function of aggrecan. Cell Res. *12*, 19–32.

Kim, H., and Kim, J.-S. (2014). A guide to genome engineering with programmable nucleases. Nat. Rev. Genet. *15*, 321–334.

Kim, J., and Ma, T. (2013). Endogenous extracellular matrices enhance human mesenchymal stem cell aggregate formation and survival. Biotechnol. Prog. *29*, 441–451.

Kim, H.J., Lee, H.J., Kim, H., Cho, S.W., and Kim, J.-S. (2009). Targeted genome editing in human cells with zinc finger nucleases constructed via modular assembly. Genome Res. *19*, 1279–1288.

Kleinsmith, L.J., and Pierce, G.B. (1964). MULTIPOTENTIALITY OF SINGLE EMBRYONAL CARCINOMA CELLS. Cancer Res. *24*, 1544–1551.

Klemm, D.J., Leitner, J.W., Watson, P., Nesterova, A., Reusch, J.E.-B., Goalstone, M.L., and Draznin, B. (2001). Insulin-induced Adipocyte Differentiation ACTIVATION OF CREB RESCUES ADIPOGENESIS FROM THE ARREST CAUSED BY INHIBITION OF PRENYLATION. J. Biol. Chem. *276*, 28430–28435.

Kobayashi, T., Chung, U.-I., Schipani, E., Starbuck, M., Karsenty, G., Katagiri, T., Goad, D.L., Lanske, B., and Kronenberg, H.M. (2002). PTHrP and Indian hedgehog control differentiation of growth plate chondrocytes at multiple steps. Dev. Camb. Engl. *129*, 2977–2986.

Komori, T., Yagi, H., Nomura, S., Yamaguchi, A., Sasaki, K., Deguchi, K., Shimizu, Y., Bronson, R.T., Gao, Y.H., Inada, M., et al. (1997). Targeted disruption of Cbfa1 results in a complete lack of bone formation owing to maturational arrest of osteoblasts. Cell *89*, 755–764.

Krakow, D., and Rimoin, D.L. (2010). The skeletal dysplasias. Genet. Med. *12*, 327–341.

Kuhn, H.G., Dickinson-Anson, H., and Gage, F.H. (1996). Neurogenesis in the dentate gyrus of the adult rat: age-related decrease of neuronal progenitor proliferation. J. Neurosci. Off. J. Soc. Neurosci. *16*, 2027–2033.

Kuleshov, M.V., Jones, M.R., Rouillard, A.D., Fernandez, N.F., Duan, Q., Wang, Z., Koplev, S., Jenkins, S.L., Jagodnik, K.M., Lachmann, A., et al. (2016). Enrichr: a comprehensive gene set enrichment analysis web server 2016 update. Nucleic Acids Res. *44*, W90-97.

Kwok, C., Weller, P.A., Guioli, S., Foster, J.W., Mansour, S., Zuffardi, O., Punnett, H.H., Dominguez-Steglich, M.A., Brook, J.D., Young, I.D., et al. (1995). Mutations in SOX9, the Gene Responsible for Campomelic Dysplasia and Autosomal Sex Reversal. Am. J. Hum. Genet. *57*, 1028–1036.

Lafitte, M., Moranvillier, I., Garcia, S., Peuchant, E., Iovanna, J., Rousseau, B., Dubus, P., Guyonnet-Dupérat, V., Belleannée, G., Ramos, J., et al. (2013). FGFR3 has tumor suppressor properties in cells with epithelial phenotype. Mol. Cancer *12*, 83.

Lai, R.C., Arslan, F., Lee, M.M., Sze, N.S.K., Choo, A., Chen, T.S., Salto-Tellez, M., Timmers, L., Lee, C.N., El Oakley, R.M., et al. (2010). Exosome secreted by MSC reduces myocardial ischemia/reperfusion injury. Stem Cell Res. *4*, 214–222.

Langenbach, F., and Handschel, J. (2013). Effects of dexamethasone, ascorbic acid and β-glycerophosphate on the osteogenic differentiation of stem cells in vitro. Stem Cell Res. Ther. *4*, 117.

Launey, M.E., Buehler, M.J., and Ritchie, R.O. (2010). On the Mechanistic Origins of Toughness in Bone. Annual Review of Materials Research *40*, 25–3.

Le Blanc, K., Tammik, L., Sundberg, B., Haynesworth, S.E., and Ringdén, O. (2003). Mesenchymal Stem Cells Inhibit and Stimulate Mixed Lymphocyte Cultures and Mitogenic Responses Independently of the Major Histocompatibility Complex. Scand. J. Immunol. *57*, 11–20.

Lee, C.J., Dosch, J., and Simeone, D.M. (2008). Pancreatic Cancer Stem Cells. J. Clin. Oncol. *26*, 2806–2812.

Lee, E.J., Park, S.J., Kang, S.K., Kim, G.-H., Kang, H.-J., Lee, S.-W., Jeon, H.B., and Kim, H.-S. (2012). Spherical bullet formation via E-cadherin promotes therapeutic potency of mesenchymal stem cells derived from human umbilical cord blood for myocardial infarction. Mol. Ther. J. Am. Soc. Gene Ther. *20*, 1424–1433.

Li, C., Chen, L., Iwata, T., Kitagawa, M., Fu, X.-Y., and Deng, C.-X. (1999). A Lys644Glu Substitution in Fibroblast Growth Factor Receptor 3 (FGFR3) Causes Dwarfism in Mice by Activation of STATs and Ink4 Cell Cycle Inhibitors. Hum. Mol. Genet. *8*, 35–44.

Lin, H.-T., Tarng, Y.-W., Chen, Y.-C., Kao, C.-L., Hsu, C.-J., Shyr, Y.-M., Ku, H.-H., and Chiou, S.H. (2005). Using Human Plasma Supplemented Medium to Cultivate Human Bone Marrow–Derived Mesenchymal Stem Cell and Evaluation of Its Multiple-Lineage Potential. Transplant. Proc. *37*, 4504–4505.

Liu, Q., Segal, D.J., Ghiara, J.B., and Barbas, C.F. (1997). Design of polydactyl zinc-finger proteins for unique addressing within complex genomes. Proc. Natl. Acad. Sci. U. S. A. *94*, 5525–5530.

Lv, F.-J., Tuan, R.S., Cheung, K.M.C., and Leung, V.Y.L. (2014). Concise review: the surface markers and identity of human mesenchymal stem cells. Stem Cells Dayt. Ohio *32*, 1408–1419.

Mackay, A.M., Beck, S.C., Murphy, J.M., Barry, F.P., Chichester, C.O., and Pittenger, M.F. (1998). Chondrogenic Differentiation of Cultured Human Mesenchymal Stem Cells from Marrow. Tissue Eng. *4*, 415–428.

Mackie, E.J., Ahmed, Y.A., Tatarczuch, L., Chen, K.-S., and Mirams, M. (2008). Endochondral ossification: How cartilage is converted into bone in the developing skeleton. Int. J. Biochem. Cell Biol. *40*, 46–62.

Makrythanasis, P., Temtamy, S., Aglan, M.S., Otaify, G.A., Hamamy, H., and Antonarakis, S.E. (2014). A novel homozygous mutation in FGFR3 causes tall stature, severe lateral tibial deviation, scoliosis, hearing impairment, camptodactyly, and arachnodactyly. Hum. Mutat. *35*, 959–963.

Mali, P., Aach, J., Stranges, P.B., Esvelt, K.M., Moosburner, M., Kosuri, S., Yang, L., and Church, G.M. (2013a). CAS9 transcriptional activators for target specificity screening and paired nickases for cooperative genome engineering. Nat. Biotechnol. *31*, 833–838.

Mali, P., Yang, L., Esvelt, K.M., Aach, J., Guell, M., DiCarlo, J.E., Norville, J.E., and Church, G.M. (2013b). RNA-Guided Human Genome Engineering via Cas9. Science *339*, 823–826.

Mark, P., Kleinsorge, M., Gaebel, R., Lux, C.A., Toelk, A., Pittermann, E., David, R., Steinhoff, G., and Ma, N. (2013). Human Mesenchymal Stem Cells Display Reduced Expression of CD105 after Culture in Serum-Free Medium. Stem Cells Int. *2013*, e698076.

Marshall, J. (2015). Analysis of 3D in vitro models using mesenchymal stromal cells. University of York.

Martin, G.R. (1981). Isolation of a pluripotent cell line from early mouse embryos cultured in medium conditioned by teratocarcinoma stem cells. Proc. Natl. Acad. Sci. *78*, 7634–7638.

Marx, V. (2014). Gene editing: how to stay on-target with CRISPR. Nat. Methods *11*, 1021–1026.

Mayor, R., and Etienne-Manneville, S. (2016). The front and rear of collective cell migration. Nat. Rev. Mol. Cell Biol. *17*, 97–109.

Mendicino, M., Bailey, A.M., Wonnacott, K., Puri, R.K., and Bauer, S.R. (2014). MSC-Based Product Characterization for Clinical Trials: An FDA Perspective. Cell Stem Cell *14*, 141–145.

Meunier, P., Courpron, P., Edouard, C., Bernard, J., Bringuier, J., and Vignon, G. (1973). Physiological senile involution and pathological rarefaction of bone. Quantitative and comparative histological data. Clin. Endocrinol. Metab. *2*, 239–256.

Miller, J., McLachlan, A.D., and Klug, A. (1985). Repetitive zinc-binding domains in the protein transcription factor IIIA from Xenopus oocytes. EMBO J. *4*, 1609–1614.

Miller, J.C., Holmes, M.C., Wang, J., Guschin, D.Y., Lee, Y.-L., Rupniewski, I., Beausejour, C.M., Waite, A.J., Wang, N.S., Kim, K.A., et al. (2007). An improved zinc-finger nuclease architecture for highly specific genome editing. Nat. Biotechnol. *25*, 778–785.

Miller, J.C., Tan, S., Qiao, G., Barlow, K.A., Wang, J., Xia, D.F., Meng, X., Paschon, D.E., Leung, E., Hinkley, S.J., et al. (2011). A TALE nuclease architecture for efficient genome editing. Nat. Biotechnol. *29*, 143–148.

Minaire, P., Edouard, C., Arlot, M., and Meunier, P.J. (1984). Marrow changes in paraplegic patients. Calcif. Tissue Int. *36*, 338–340.

Minina, E., Wenzel, H.M., Kreschel, C., Karp, S., Gaffield, W., McMahon, A.P., and Vortkamp, A. (2001). BMP and Ihh/PTHrP signaling interact to coordinate chondrocyte proliferation and differentiation. Dev. Camb. Engl. *128*, 4523–4534.

Mojica, F.J.M., Díez-Villaseñor, C., García-Martínez, J., and Almendros, C. (2009). Short motif sequences determine the targets of the prokaryotic CRISPR defence system. Microbiology *155*, 733–740.

Morris, C.B., and Warburton, S. (1994). Serum-screening and selection. In Cell & Tissue Culture: Laboratory Procedures, A. Doyle, J.B. Griffiths, and D.G. Newell, eds. (Wiley), p. 2B 1.1-2B 1.5.

Moscou, M.J., and Bogdanove, A.J. (2009). A simple cipher governs DNA recognition by TAL effectors. Science *326*, 1501.

Muraglia, A., Cancedda, R., and Quarto, R. (2000). Clonal mesenchymal progenitors from human bone marrow differentiate in vitro according to a hierarchical model. J. Cell Sci. *113 (Pt 7)*, 1161–1166.

Murakami, S., Balmes, G., McKinney, S., Zhang, Z., Givol, D., and Crombrugghe, B. de (2004). Constitutive activation of MEK1 in chondrocytes causes Stat1-independent achondroplasia-like dwarfism and rescues the Fgfr3-deficient mouse phenotype. Genes Dev. *18*, 290–305.

Murata, D., Tokunaga, S., Tamura, T., Kawaguchi, H., Miyoshi, N., Fujiki, M., Nakayama, K., and Misumi, K. (2015). A preliminary study of osteochondral regeneration using a scaffold-free three-dimensional construct of porcine adipose tissue-derived mesenchymal stem cells. J. Orthop. Surg. *10*, 35.

Murphy, K.C., Hoch, A.I., Harvestine, J.N., Zhou, D., and Leach, J.K. (2016). Mesenchymal Stem Cell Spheroids Retain Osteogenic Phenotype Through α2β1 Signaling. STEM CELLS Transl. Med. *5*, 1229–1237.

Musunuru, K. (2013). Genome editing of human pluripotent stem cells to generate human cellular disease models. Dis. Model. Mech. *6*, 896–904.

Narayanan, R., Huang, C.-C., and Ravindran, S. (2016). Hijacking the Cellular Mail: Exosome Mediated Differentiation of Mesenchymal Stem Cells. Stem Cells Int. *2016*.

Nguyen, P.T., Tsunematsu, T., Yanagisawa, S., Kudo, Y., Miyauchi, M., Kamata, N., and Takata, T. (2013). The FGFR1 inhibitor PD173074 induces mesenchymal–epithelial transition through the transcription factor AP-1. Br. J. Cancer *109*, 2248–2258.

Nukavarapu, S.P., and Dorcemus, D.L. (2013). Osteochondral tissue engineering: Current strategies and challenges. Biotechnol. Adv. *31*, 706–721.

Oleykowski, C.A., Bronson Mullins, C.R., Godwin, A.K., and Yeung, A.T. (1998). Mutation detection using a novel plant endonuclease. Nucleic Acids Res. *26*, 4597–4602.

Ornitz, D.M., and Itoh, N. (2015). The Fibroblast Growth Factor signaling pathway. Wiley Interdiscip. Rev. Dev. Biol. *4*, 215–266.

Otto, F., Thornell, A.P., Crompton, T., Denzel, A., Gilmour, K.C., Rosewell, I.R., Stamp, G.W., Beddington, R.S., Mundlos, S., Olsen, B.R., et al. (1997). Cbfa1, a candidate gene for cleidocranial dysplasia syndrome, is essential for osteoblast differentiation and bone development. Cell *89*, 765–771.

Pan, J., Zhou, X., Li, W., Novotny, J.E., Doty, S.B., and Wang, L. (2009). In situ measurement of transport between subchondral bone and articular cartilage. J. Orthop. Res. *27*, 1347–1352.

Park, Y.-K., and Ge, K. (2016). Glucocorticoid receptor accelerates, but is dispensable for, adipogenesis. Mol. Cell. Biol. MCB.00260-16.

Pattanayak, V., Lin, S., Guilinger, J.P., Ma, E., Doudna, J.A., and Liu, D.R. (2013). High-throughput profiling of off-target DNA cleavage reveals RNA-programmed Cas9 nuclease specificity. Nat. Biotechnol. *31*, 839–843.

Pauli, R.M. (1993). Achondroplasia. In GeneReviews(®), R.A. Pagon, M.P. Adam, H.H. Ardinger, S.E. Wallace, A. Amemiya, L.J. Bean, T.D. Bird, N. Ledbetter, H.C. Mefford, R.J. Smith, et al., eds. (Seattle (WA): University of Washington, Seattle), p.

Pennock, R., Bray, E., Pryor, P., James, S., McKeegan, P., Sturmey, R., and Genever, P. (2015). Human cell dedifferentiation in mesenchymal condensates through controlled autophagy. Sci. Rep. *5*, 13113.

Pérez-Mancera, P.A., Bermejo-Rodríguez, C., González-Herrero, I., Herranz, M., Flores, T., Jiménez, R., and Sánchez-García, I. (2007). Adipose tissue mass is modulated by SLUG (SNAI2). Hum. Mol. Genet. *16*, 2972–2986.

Perlman, R.L. (2016). Mouse models of human disease. Evol. Med. Public Health *2016*, 170–176.

Peters, K., Ornitz, D., Werner, S., and Williams, L. (1993). Unique Expression Pattern of the FGF Receptor 3 Gene during Mouse Organogenesis. Dev. Biol. *155*, 423–430.

Piccolo, N.D., Sarabipour, S., and Hristova, K. (2016). A New Method to Study Heterodimerization of Membrane Proteins and its Application to Fibroblast Growth Factor Receptors. J. Biol. Chem. jbc.M116.755777.

Pittenger, M.F., Mackay, A.M., Beck, S.C., Jaiswal, R.K., Douglas, R., Mosca, J.D., Moorman, M.A., Simonetti, D.W., Craig, S., and Marshak, D.R. (1999). Multilineage potential of adult human mesenchymal stem cells. Science *284*, 143–147.

Plotnikov, A.N., Schlessinger, J., Hubbard, S.R., and Mohammadi, M. (1999). Structural Basis for FGF Receptor Dimerization and Activation. Cell *98*, 641–650.

van Poll, D., Parekkadan, B., Cho, C.H., Berthiaume, F., Nahmias, Y., Tilles, A.W., and Yarmush, M.L. (2008). Mesenchymal stem cell-derived molecules directly modulate hepatocellular death and regeneration in vitro and in vivo. Hepatol. Baltim. Md *47*, 1634–1643.

Pratap, J., Galindo, M., Zaidi, S.K., Vradii, D., Bhat, B.M., Robinson, J.A., Choi, J.-Y., Komori, T., Stein, J.L., Lian, J.B., et al. (2003). Cell Growth Regulatory Role of Runx2 during Proliferative Expansion of Preosteoblasts. Cancer Res. *63*, 5357–5362.

Qi, L.S., Larson, M.H., Gilbert, L.A., Doudna, J.A., Weissman, J.S., Arkin, A.P., and Lim, W.A. (2013). Repurposing CRISPR as an RNA-Guided Platform for Sequence-Specific Control of Gene Expression. Cell *152*, 1173–1183.

Ran, F.A., Hsu, P.D., Lin, C.-Y., Gootenberg, J.S., Konermann, S., Trevino, A.E., Scott, D.A., Inoue, A., Matoba, S., Zhang, Y., et al. (2013). Double Nicking by RNA-Guided CRISPR Cas9 for Enhanced Genome Editing Specificity. Cell *154*, 1380–1389.

Renkawitz, J., Lademann, C.A., and Jentsch, S. (2014). Mechanisms and principles of homology search during recombination. Nat. Rev. Mol. Cell Biol. *15*, 369–383.

Reyon, D., Tsai, S.Q., Khayter, C., Foden, J.A., Sander, J.D., and Joung, J.K. (2012). FLASH assembly of TALENs for high-throughput genome editing. Nat. Biotechnol. *30*, 460–465.

Riminucci, M., Remoli, C., Robey, P.G., and Bianco, P. (2015). Stem cells and bone diseases: New tools, new perspective. Bone *70*, 55–61.

Rørth, P. (2009). Collective cell migration. Annu. Rev. Cell Dev. Biol. *25*, 407–429.

Rosset, P., Hernigou, P., Gebhard, F., Ehrnthaller, C., Baldini, N., Gomez Barrena, E., and Layrolle, P. (2016). Expanded autologous MSCs and biomaterials in non-unions: a European clinical trial. (Montréal, Canada), p.

Rouet, P., Smih, F., and Jasin, M. (1994). Introduction of double-strand breaks into the genome of mouse cells by expression of a rare-cutting endonuclease. Mol. Cell. Biol. *14*, 8096–8106.

Rumyantsev, P.P., and Borisov, A. (1987). DNA synthesis in myocytes from different myocardial compartments of young rats in norm, after experimental infarction and in vitro. Biomed. Biochim. Acta *46*, S610-615.

Sahni, M., Ambrosetti, D.-C., Mansukhani, A., Gertner, R., Levy, D., and Basilico, C. (1999). FGF signaling inhibits chondrocyte proliferation and regulates bone development through the STAT-1 pathway. Genes Dev. *13*, 1361–1366.

Saleh, F., Carstairs, A., Etheridge, S.L., and Genever, P. (2016). Real-Time Analysis of Endogenous Wnt Signalling in 3D Mesenchymal Stromal Cells. Stem Cells Int. *2016*, 7132529.

Saleh, F.A., Whyte, M., and Genever, P.G. (2011a). Effects of endothelial cells on human mesenchymal stem cell activity in a three-dimensional in vitro model. Eur. Cell. Mater. *22*, 242–257; discussion 257.

Saleh, F.A., Whyte, M., Ashton, P., and Genever, P.G. (2011b). Regulation of mesenchymal stem cell activity by endothelial cells. Stem Cells Dev. *20*, 391–403.

Saleh, F.A., Frith, J.E., Lee, J.A., and Genever, P.G. (2012). Three-dimensional in vitro culture techniques for mesenchymal stem cells. Methods Mol. Biol. Clifton NJ *916*, 31–45.

Sarugaser, R., Lickorish, D., Baksh, D., Hosseini, M.M., and Davies, J.E. (2005). Human umbilical cord perivascular (HUCPV) cells: a source of mesenchymal progenitors. Stem Cells Dayt. Ohio *23*, 220–229.

Sato, Y., Mabuchi, Y., Miyamoto, K., Araki, D., Niibe, K., Houlihan, D.D., Morikawa, S., Nakagawa, T., Nakajima, T., Akazawa, C., et al. (2016). Notch2 Signaling Regulates the Proliferation of Murine Bone Marrow-Derived Mesenchymal Stem/Stromal Cells via c-Myc Expression. PLoS ONE *11*.

Sauer, B. (1998). Inducible gene targeting in mice using the Cre/lox system. Methods San Diego Calif *14*, 381–392.

Schroeder, T.M., Jensen, E.D., and Westendorf, J.J. (2005). Runx2: A master organizer of gene transcription in developing and maturing osteoblasts. Birth Defects Res. Part C Embryo Today Rev. *75*, 213–225.

Seeliger, F., Leeb, T., Peters, M., Brugmann, M., Fehr, M., and Hewicker-Trautwein, M. (2003). Osteogenesis imperfecta in two litters of dachshunds. Vet. Pathol. *40*, 530–539.

Seo, B.-M., Miura, M., Gronthos, S., Bartold, P.M., Batouli, S., Brahim, J., Young, M., Robey, P.G., Wang, C.Y., and Shi, S. (2004). Investigation of multipotent postnatal stem cells from human periodontal ligament. The Lancet *364*, 149–155.

Shapiro, I.M., and Haselgrove, J.C. (1991). Energy metabolism in bone. In Bone: A Treatise, B.K. Hall, ed. (CRC Press), pp. 99–140.

Shen, B., Zhang, W., Zhang, J., Zhou, J., Wang, J., Chen, L., Wang, L., Hodgkins, A., Iyer, V., Huang, X., et al. (2014). Efficient genome modification by CRISPR-Cas9 nickase with minimal off-target effects. Nat. Methods *11*, 399–402.

Shiang, R., Thompson, L.M., Zhu, Y.-Z., Church, D.M., Fielder, T.J., Bocian, M., Winokur, S.T., and Wasmuth, J.J. (1994). Mutations in the transmembrane domain of FGFR3 cause the most common genetic form of dwarfism, achondroplasia. Cell *78*, 335–342.

Shore, E.M., Xu, M., Feldman, G.J., Fenstermacher, D.A., Cho, T.-J., Choi, I.H., Connor, J.M., Delai, P., Glaser, D.L., LeMerrer, M., et al. (2006). A recurrent mutation in the BMP type I receptor ACVR1 causes inherited and sporadic fibrodysplasia ossificans progressiva. Nat. Genet. *38*, 525–527.

Spangrude, G.J., Heimfeld, S., and Weissman, I.L. (1988). Purification and characterization of mouse hematopoietic stem cells. Science *241*, 58–62.

Spees, J.L., Gregory, C.A., Singh, H., Tucker, H.A., Peister, A., Lynch, P.J., Hsu, S.-C., Smith, J., and Prockop, D.J. (2004). Internalized Antigens Must Be Removed to Prepare Hypoimmunogenic Mesenchymal Stem Cells for Cell and Gene Therapy*. Mol. Ther. *9*, 747–756.

Steinberg, M.S. (2007). Differential adhesion in morphogenesis: a modern view. Curr. Opin. Genet. Dev. *17*, 281–286.

Stevens, L.C., and Little, C.C. (1954). Spontaneous Testicular Teratomas in an Inbred Strain of Mice. Proc. Natl. Acad. Sci. U. S. A. *40*, 1080–1087.

St-Jacques, B., Hammerschmidt, M., and McMahon, A.P. (1999). Indian hedgehog signaling regulates proliferation and differentiation of chondrocytes and is essential for bone formation. Genes Dev. *13*, 2072–2086.

Stöckl, S., Bauer, R.J., Bosserhoff, A.K., Göttl, C., Grifka, J., and Grässel, S. (2013). Sox9 modulates cell survival and adipogenic differentiation of multipotent adult rat mesenchymal stem cells. J. Cell Sci. *126*, 2890–2902.

Su, N., Sun, Q., Li, C., Lu, X., Qi, H., Chen, S., Yang, J., Du, X., Zhao, L., He, Q., et al. (2010). Gain-of-function mutation in FGFR3 in mice leads to decreased bone mass by affecting both osteoblastogenesis and osteoclastogenesis. Hum. Mol. Genet. *19*, 1199–1210.

Su, N., Jin, M., and Chen, L. (2014). Role of FGF/FGFR signaling in skeletal development and homeostasis: learning from mouse models. Bone Res. *2*.

Su, W.-C.S., Kitagawa, M., Xue, N., Xie, B., Garofalo, S., Cho, J., Deng, C., Horton, W.A., and Fu, X.-Y. (1997). Activation of Statl by mutant fibroblast growth-factor receptor in thanatophoric dysplasia type II dwarfism. Nature *386*, 288–292.

Subramanian, A., Tamayo, P., Mootha, V.K., Mukherjee, S., Ebert, B.L., Gillette, M.A., Paulovich, A., Pomeroy, S.L., Golub, T.R., Lander, E.S., et al. (2005). Gene set enrichment analysis: A knowledge-based approach for interpreting genome-wide expression profiles. Proc. Natl. Acad. Sci. *102*, 15545–15550.

Swamynathan, P., Venugopal, P., Kannan, S., Thej, C., Kolkundar, U., Bhagwat, S., Ta, M., Majumdar, A.S., and Balasubramanian, S. (2014). Are serum-free and xeno-free culture conditions ideal for large scale clinical grade expansion of Wharton's jelly derived mesenchymal stem cells? A comparative study. Stem Cell Res. Ther. *5*, 88.

Szczepek, M., Brondani, V., Büchel, J., Serrano, L., Segal, D.J., and Cathomen, T. (2007). Structure-based redesign of the dimerization interface reduces the toxicity of zinc-finger nucleases. Nat. Biotechnol. *25*, 786–793.

Szymczak, A.L., Workman, C.J., Wang, Y., Vignali, K.M., Dilioglou, S., Vanin, E.F., and Vignali, D.A.A. (2004). Correction of multi-gene deficiency in vivo using a single "self-cleaving" 2A peptide–based retroviral vector. Nat. Biotechnol. *22*, 589–594.

Takahashi, K., and Yamanaka, S. (2006). Induction of pluripotent stem cells from mouse embryonic and adult fibroblast cultures by defined factors. Cell *126*, 663–676.

Takahashi, K., Tanabe, K., Ohnuki, M., Narita, M., Ichisaka, T., Tomoda, K., and Yamanaka, S. (2007). Induction of pluripotent stem cells from adult human fibroblasts by defined factors. Cell *131*, 861–872.

Takarada, T., Hinoi, E., Nakazato, R., Ochi, H., Xu, C., Tsuchikane, A., Takeda, S., Karsenty, G., Abe, T., Kiyonari, H., et al. (2013). An analysis of skeletal development in osteoblast-specific and chondrocyte-specific runt-related transcription factor-2 (Runx2) knockout mice. J. Bone Miner. Res. *28*, 2064–2069.

Tamura, Y., Takeuchi, Y., Suzawa, M., Fukumoto, S., Kato, M., Miyazono, K., and Fujita, T. (2001). Focal adhesion kinase activity is required for bone morphogenetic protein--Smad1 signaling and osteoblastic differentiation in murine MC3T3-E1 cells. J. Bone Miner. Res. Off. J. Am. Soc. Bone Miner. Res. *16*, 1772–1779.

Tang, Y., Feinberg, T., Keller, E.T., Li, X.-Y., and Weiss, S.J. (2016). Snail/Slug binding interactions with YAP/TAZ control skeletal stem cell self-renewal and differentiation. Nat. Cell Biol. *18*, 917–929.

Tao, G., Levay, A.K., Gridley, T., and Lincoln, J. (2011). Mmp15 is a direct target of Snai1 during endothelial to mesenchymal transformation and endocardial cushion development. Dev. Biol. *359*, 209–221.

Tateishi, K., Ando, W., Higuchi, C., Hart, D.A., Hashimoto, J., Nakata, K., Yoshikawa, H., and Nakamura, N. (2008). Comparison of human serum with fetal bovine serum for expansion and differentiation of human synovial MSC: potential feasibility for clinical applications. Cell Transplant. *17*, 549–557.

Teven, C.M., Farina, E.M., Rivas, J., and Reid, R.R. (2014). Fibroblast growth factor (FGF) signaling in development and skeletal diseases. Genes Dis. *1*, 199–213.

Thomson, J.A., Itskovitz-Eldor, J., Shapiro, S.S., Waknitz, M.A., Swiergiel, J.J., Marshall, V.S., and Jones, J.M. (1998). Embryonic stem cell lines derived from human blastocysts. Science *282*, 1145–1147.

Torreggiani, E., Lisignoli, G., Manferdini, C., Lambertini, E., Penolazzi, L., Vecchiatini, R., Gabusi, E., Chieco, P., Facchini, A., Gambari, R., et al. (2012). Role of Slug transcription factor in human mesenchymal stem cells. J. Cell. Mol. Med. *16*, 740–751.

Toydemir, R.M., Brassington, A.E., Bayrak-Toydemir, P., Krakowiak, P.A., Jorde, L.B., Whitby, F.G., Longo, N., Viskochil, D.H., Carey, J.C., and Bamshad, M.J. (2006). A Novel Mutation in FGFR3 Causes Camptodactyly, Tall Stature, and Hearing Loss (CATSHL) Syndrome. Am. J. Hum. Genet. *79*, 935–941.

Tsai, A.-C., Liu, Y., Yuan, X., and Ma, T. (2015). Compaction, fusion, and functional activation of three-dimensional human mesenchymal stem cell aggregate. Tissue Eng. Part A *21*, 1705–1719.

Tu, Q., Zhang, J., Paz, J., Wade, K., Yang, P., and Chen, J. (2008). Haploinsufficiency of Runx2 results in bone formation decrease and different BSP expression pattern changes in two transgenic mouse models. J. Cell. Physiol. *217*, 40.

Turner, N., and Grose, R. (2010). Fibroblast growth factor signalling: from development to cancer. Nat. Rev. Cancer *10*, 116–129.

Valverde-Franco, G., Liu, H., Davidson, D., Chai, S., Valderrama-Carvajal, H., Goltzman, D., Ornitz, D.M., and Henderson, J.E. (2004). Defective bone mineralization and osteopenia in young adult FGFR3−/− mice. Hum. Mol. Genet. *13*, 271–284.

Von Der Mark, K., Gauss, V., Von Der Mark, H., and Müller, P. (1977). Relationship between cell shape and type of collagen synthesised as chondrocytes lose their cartilage phenotype in culture. Nature *267*, 531–532.

Wagers, A.J., and Weissman, I.L. (2004). Plasticity of Adult Stem Cells. Cell *116*, 639–648.

Wagner, W., and Ho, A.D. (2007). Mesenchymal stem cell preparations--comparing apples and oranges. Stem Cell Rev. *3*, 239–248.

Wagner, W., Horn, P., Castoldi, M., Diehlmann, A., Bork, S., Saffrich, R., Benes, V., Blake, J., Pfister, S., Eckstein, V., et al. (2008). Replicative senescence of mesenchymal stem cells: a continuous and organized process. PloS One *3*, e2213.

Wang, J.-Y., Wu, P.-Q., Chen, P.C.-H., Lee, C.-W., Chen, W.-M., and Hung, S.-C. (2016). Generation of Osteosarcomas From a Combination of Rb Silencing and c-Myc Overexpression in Human Mesenchymal Stem Cells. Stem Cells Transl. Med. sctm.2015-0226.

Wang, W., Itaka, K., Ohba, S., Nishiyama, N., Chung, U., Yamasaki, Y., and Kataoka, K. (2009). 3D spheroid culture system on micropatterned substrates for improved differentiation efficiency of multipotent mesenchymal stem cells. Biomaterials *30*, 2705–2715.

Wang, Y., Spatz, M.K., Kannan, K., Hayk, H., Avivi, A., Gorivodsky, M., Pines, M., Yayon, A., Lonai, P., and Givol, D. (1999). A mouse model for achondroplasia produced by targeting fibroblast growth factor receptor 3. Proc. Natl. Acad. Sci. U. S. A. *96*, 4455–4460.

Weiss, S., Hennig, T., Bock, R., Steck, E., and Richter, W. (2010). Impact of growth factors and PTHrP on early and late chondrogenic differentiation of human mesenchymal stem cells. J. Cell. Physiol. *223*, 84–93.

Westacott, C.I., Webb, G.R., Warnock, M.G., Sims, J.V., and Elson, C.J. (1997). Alteration of cartilage metabolism by cells from osteoarthritic bone. Arthritis Rheum. *40*, 1282–1291.

Wojtowicz, A.M., Templeman, K.L., Hutmacher, D.W., Guldberg, R.E., and García, A.J. (2010). Runx2 overexpression in bone marrow stromal cells accelerates bone formation in critical-sized femoral defects. Tissue Eng. Part A *16*, 2795–2808.

Xian, W., Schwertfeger, K.L., and Rosen, J.M. (2007). Distinct roles of fibroblast growth factor receptor 1 and 2 in regulating cell survival and epithelial-mesenchymal transition. Mol. Endocrinol. Baltim. Md *21*, 987–1000.

Xu, W. ’an, Chen, Q., Liu, C., Chen, J., Xiong, F., and Wu, B. (2017). A novel, complex RUNX2 gene mutation causes cleidocranial dysplasia. BMC Med. Genet. *18*, 13.

Xu, Y., Shi, T., Xu, A., and Zhang, L. (2016). 3D spheroid culture enhances survival and therapeutic capacities of MSCs injected into ischemic kidney. J. Cell. Mol. Med. *20*, 1203–1213.

Yamaguchi, Y., Ohno, J., Sato, A., Kido, H., and Fukushima, T. (2014). Mesenchymal stem cell spheroids exhibit enhanced in-vitro and in-vivo osteoregenerative potential. BMC Biotechnol. *14*, 105.

Yang, C.-H., Wang, H.-L., Lin, Y.-S., Kumar, K.P.S., Lin, H.-C., Chang, C.-J., Lu, C.-C., Huang, T.-T., Martel, J., Ojcius, D.M., et al. (2014). Identification of CD24 as a Cancer Stem Cell Marker in Human Nasopharyngeal Carcinoma. PLOS ONE *9*, e99412.

Yeh, H.-Y., Liu, B.-H., and Hsu, S.-H. (2012). The calcium-dependent regulation of spheroid formation and cardiomyogenic differentiation for MSCs on chitosan membranes. Biomaterials *33*, 8943–8954.

Yeung, T.M., Gandhi, S.C., Wilding, J.L., Muschel, R., and Bodmer, W.F. (2010). Cancer stem cells from colorectal cancer-derived cell lines. Proc. Natl. Acad. Sci. U. S. A. *107*, 3722–3727.

Young, H.E., and Black, A.C. (2004). Adult stem cells. Anat. Rec. A. Discov. Mol. Cell. Evol. Biol. *276*, 75–102.

Young, D.W., Hassan, M.Q., Yang, X.-Q., Galindo, M., Javed, A., Zaidi, S.K., Furcinitti, P., Lapointe, D., Montecino, M., Lian, J.B., et al. (2007). Mitotic retention of gene expression patterns by the cell fate-determining transcription factor Runx2. Proc. Natl. Acad. Sci. U. S. A. *104*, 3189–3194.

Zarjou, A., Kim, J., Traylor, A.M., Sanders, P.W., Balla, J., Agarwal, A., and Curtis, L.M. (2011). Paracrine effects of mesenchymal stem cells in cisplatin-induced renal injury require heme oxygenase-1. Am. J. Physiol. - Ren. Physiol. *300*, F254–F262.

Zhang, D., and Kilian, K.A. (2013). The effect of mesenchymal stem cell shape on the maintenance of multipotency. Biomaterials *34*, 3962–3969.

Zhang, W., and Liu, H.T. (2002). MAPK signal pathways in the regulation of cell proliferation in mammalian cells. Cell Res. *12*, 9–18.

Zhang, R., Murakami, S., Coustry, F., Wang, Y., and Crombrugghe, B. de (2006a). Constitutive activation of MKK6 in chondrocytes of transgenic mice inhibits proliferation and delays endochondral bone formation. Proc. Natl. Acad. Sci. U. S. A. *103*, 365–370.

Zhang, X., Yang, M., Lin, L., Chen, P., Ma, K.T., Zhou, C.Y., and Ao, Y.F. (2006b). Runx2 overexpression enhances osteoblastic differentiation and mineralization in adipose--derived stem cells in vitro and in vivo. Calcif. Tissue Int. *79*, 169–178.

Zhang, X., Ibrahimi, O.A., Olsen, S.K., Umemori, H., Mohammadi, M., and Ornitz, D.M. (2006c). Receptor Specificity of the Fibroblast Growth Factor Family THE COMPLETE MAMMALIAN FGF FAMILY. J. Biol. Chem. *281*, 15694–15700.

Zhang, Y., Li, X., Qian, S., Guo, L., Huang, H., He, Q., Liu, Y., Ma, C., and Tang, Q.-Q. (2012). Down-regulation of type I Runx2 mediated by dexamethasone is required for 3T3-L1 adipogenesis. Mol. Endocrinol. Baltim. Md *26*, 798–808.

Zhao, Q., Ren, H., and Han, Z. (2016). Mesenchymal stem cells: Immunomodulatory capability and clinical potential in immune diseases. J. Cell. Immunother. *2*, 3–20.

Zhou, S., Xie, Y., Tang, J., Huang, J., Huang, Q., Xu, W., Wang, Z., Luo, F., Wang, Q., Chen, H., et al. (2015). FGFR3 Deficiency Causes Multiple Chondroma-like Lesions by Upregulating Hedgehog Signaling. PLOS Genet. *11*, e1005214.

Zhu, J., Liu, F., Wu, Q., and Liu, X. (2015). miR-221 increases osteosarcoma cell proliferation, invasion and migration partly through the downregulation of PTEN. Int. J. Mol. Med. *36*, 1377–1383.

Zhu, M., Chen, M., Zuscik, M., Wu, Q., Wang, Y.-J., Rosier, R.N., O'Keefe, R.J., and Chen, D. (2008). Inhibition of β-catenin signaling in articular chondrocytes results in articular cartilage destruction. Arthritis Rheum. *58*, 2053–2064.

Zhu, M., Tang, D., Wu, Q., Hao, S., Chen, M., Xie, C., Rosier, R.N., O'Keefe, R.J., Zuscik, M., and Chen, D. (2009). Activation of β-Catenin Signaling in Articular Chondrocytes Leads to Osteoarthritis-Like Phenotype in Adult β-Catenin Conditional Activation Mice. J. Bone Miner. Res. *24*, 12–21.

Zuk, P.A., Zhu, M., Mizuno, H., Huang, J., Futrell, J.W., Katz, A.J., Benhaim, P., Lorenz, H.P., and Hedrick, M.H. (2001). Multilineage Cells from Human Adipose Tissue: Implications for Cell-Based Therapies. Tissue Eng. *7*, 211–228.